Immunomodulatory Properties of IgG Glycosylation and The Anti-Inflammatory Mechanism of Intravenous Immunoglobulin

Xiaojie Yu

A thesis submitted for the degree of *Doctor of Philosophy*

St Peter's College

Department of Biochemistry

University of Oxford

Trinity 2013

Table of contents

Immunomodulatory properties of IgG glycosylation and the anti-inflammatory mechanism of intravenous immunoglobulin

Xiaojie (Ben) Yu

St Peter's College and the Department of Biochemistry

Abstract

The IgG Fc domain mediates a range of antibody effector functions, including antibody dependent cell-mediated cytotoxicity (ADCC), complement activation, phagocytosis, and the recently emerged general anti-inflammatory effect of immunoglobulin therapy (IVIg). The conserved *N*-glycan attached to Fc N297 maintains the Fc structural integrity for the effector functions, while its glycoform is known to modulate the affinity for the Fc γ-receptors (FcγRs), complement, and the C-type lectin DC-SIGN. IgG Fc exhibits protein-directed glycosylation characterized by a series of biantennary complex type glycoforms, with a small population of sialylated species. The sialylated Fc has been proposed to bind DC-SIGN and initiate an anti-inflammatory signalling pathway. The restricted Fc glycan processing is partially attributed to the hydrophobic interaction between Fc glycan and the hydrophobic Fc protein backbone. Mutations within the hydrophobic Fc protein-glycan interface dramatically increases Fc glycan processing, while concomitantly decreases Fc affinity for the FcγRs. However, it is unclear whether this disrupted Fc-FcγR interaction was due to the increased terminal glycan processing, or the perturbed Fc protein-glycan interface. Here, the integrity of the Fc protein-glycan interface was demonstrated to be important in maintaining the productive Fc-FcγR interaction independently of glycoform. This glycoform-independent effect was exploited to generate novel inhibitory Fc variants. In addition, the interaction between sialylated IgG and the putative IVIg receptor DC-SIGN was re-evaluated. Analysis shows that IVIg binds DC-SIGN in a glycan-independent, Fab-mediated manner. Furthermore, the effect of IVIg sialylation on human antigen presenting cells was examined; evidence presented here indicate that IVIg deglycosylation, not desialylation, has an anti-inflammatory effect on human dendritic cells (DCs). These data suggest the need for a general re-evaluation of the current mechanistic model of anti-inflammatory IVIg.

List of Publications

The work performed during the duration of the D.Phil resulted in the following publications:

Bowden, T. A., Baruah, K., Coles, C. H., Harvey, D. J., **Yu, X.**, Song, B. D., Stuart, D. I., Aricescu, A. R., Scanlan, C. N., Jones, E. Y. & Crispin, M. (2012). Chemical and Structural Analysis of an Antibody Folding Intermediate Trapped during Glycan Biosynthesis. *J Am Chem Soc* **134**, 17554-63.

Lux, A., **Yu, X.**, Scanlan, C. N. & Nimmerjahn, F. (2013). Impact of immune complex size and glycosylation on IgG binding to human FcgammaRs. *J Immunol* **190**, 4315-23.

Yu, X., Vasiljevic, S., Mitchell, D. A., Crispin, M. & Scanlan, C. N. (2013). Dissecting the molecular mechanism of IVIg therapy: the interaction between serum IgG and DC-SIGN is independent of antibody glycoform or Fc domain. *J Mol Biol* **425**, 1253-8.

Ackerman, M. E., Crispin, M., **Yu, X.**, Baruah, K., Boesch, A. W., Harvey, D. J., Dugast, A. S., Heizen, E. L., Ercan, A., Choi, I., Streeck, H., Nigrovic, P. A., Bailey-Kellogg, C., Scanlan, C. & Alter, G. (2013). Natural variation in Fc glycosylation of HIV-specific antibodies impacts antiviral activity. *J Clin Invest* **123**, 2183-92.

Yu, X., Baruah, K., Harvey, D. J., Vasiljevic, S., Alonzi, D. S., Song, B. D., Higgins, M. K., Bowden, T. A., Scanlan, C. N. & Crispin, M. (2013). Engineering hydrophobic protein-carbohydrate interactions to fine-tune monoclonal antibodies. *J Am Chem Soc*. **135**, 9723-32.

Crispin, M., **Yu, X.**, Bowden, T. A. (2013). Crystal structure of sialylated IgG Fc: Implications for the mechanism of IVIg therapy. *Proc Natl Acad Sci U S A*. **DOI:10.1073**

Acknowledgement

First, I would like to thank my parents for the opportunity to experience life and education in England. I am certain that the benefits will last for a lifetime.

I am very grateful to both Dr Chris Scanlan and Dr Max Crispin, for their incredible kindness, encouragement and intellectual engagements, from which I have learned much about glycobiology as well as lessons outside of science. The laissez-faire spirit and the fearless venture into new scientific territories at the lab have been, and will continue to be, a constant inspiration for me. I am also grateful to Prof. Raymond Dwek, for his support and encouragement.

I would like to thank members of the lab for their generous help. Snezana, thank you for teaching me all these techniques and your general wisdom, I am sure that it is a matter of time before a handsome Italian joins the lab☺. Kavitha, thank you for the all the help on the bench and your insights into Fc. Camille, thanks for all the free gp120s and useful Siglec discussions. Martin, thank you for all the scientific and arty conversations, it is a shame that I never got to phage display. David, thank you for teaching me mass spectrometry and the tremendous effort for the 241 paper. I owe much thanks to many past and present members of the lab, for their support and wonderful company.

Finally, I would like to thank the collaborators: Dr Daniel Mitchell for DC-SIGN, Dr Amin Moghaddam for the DC assay, Dr Thomas Bowden for X-ray crystallography work and Dr Amanda Unsworth for phlebotomy.

This thesis is dedicated to my supervisor Dr Christopher N. Scanlan (10.8.77-04.05.13).

Chapter 1

Introduction

1. Introduction

1.1. Human Antibodies

1.1.1. Overview of Structure and Function

The immunoglobulins (Ig), also called the antibodies, form an important part of the human immune system. Multiple types of antibodies (also called isotypes) exist, and the number of isotypes varies between different animal species, from seven in horses to only one in rabbits. Most known classes of antibodies are made of heavy and light chains, except those of sharks and camels, which consist of only heavy chains [1]. Human antibodies are classified into five isotypes based on their distinctive structure, function and site of activity: IgA, IgD, IgE, IgG, and IgM (the heavy chain of which is called α, δ, ε, γ and μ respectively)[2; 3]. IgG is the most studied and thus most well-characterized isotype to date[2; 4], and its monomeric form represents the prototypical antibody structure. IgG is a relatively large glycoprotein with an overall Y-shaped structure comprised of two heavy chains, each weighted approximately 50 kDa, and two light chains, each weighted approximately 25 kDa[2; 3; 5; 6; 7] (Fig. 1.1). While the heavy chain is classified into five groups that determine the antibody isotype, the light chain is classified into two types, either kappa (κ) or lamda (λ)[2]. Together, the heavy and light chains form three distinctive features of an antibody: the antigen binding domain (Fab), the crystallisable domain (Fc), and the hinge domain[3; 5; 6; 8] (Fig. 1.1).

The Fab domain binds to a specific antigen with high affinity, commonly seen as a part of the innate immunity, and the Fc binds to the Fc receptors (FcRs) as well as components of the complement system, thus bridging the innate and adaptive immunity[2; 9]. The hinge region links the Fab and Fc regions and regulates the flexibility of these two domains[5; 8]. There are two well-established functions for antibodies. First, the Fab-mediated antigen binding results in the formation of immune complex, which leads to antigen clearance. Second, the Fc

mediates the engagement of immune complex with Fc receptors, and triggers cellular and complement responses[2; 9]. In addition to these well-known functions, novel functions of antibodies, such as Fc-mediated anti-inflammation[10], have been uncovered.

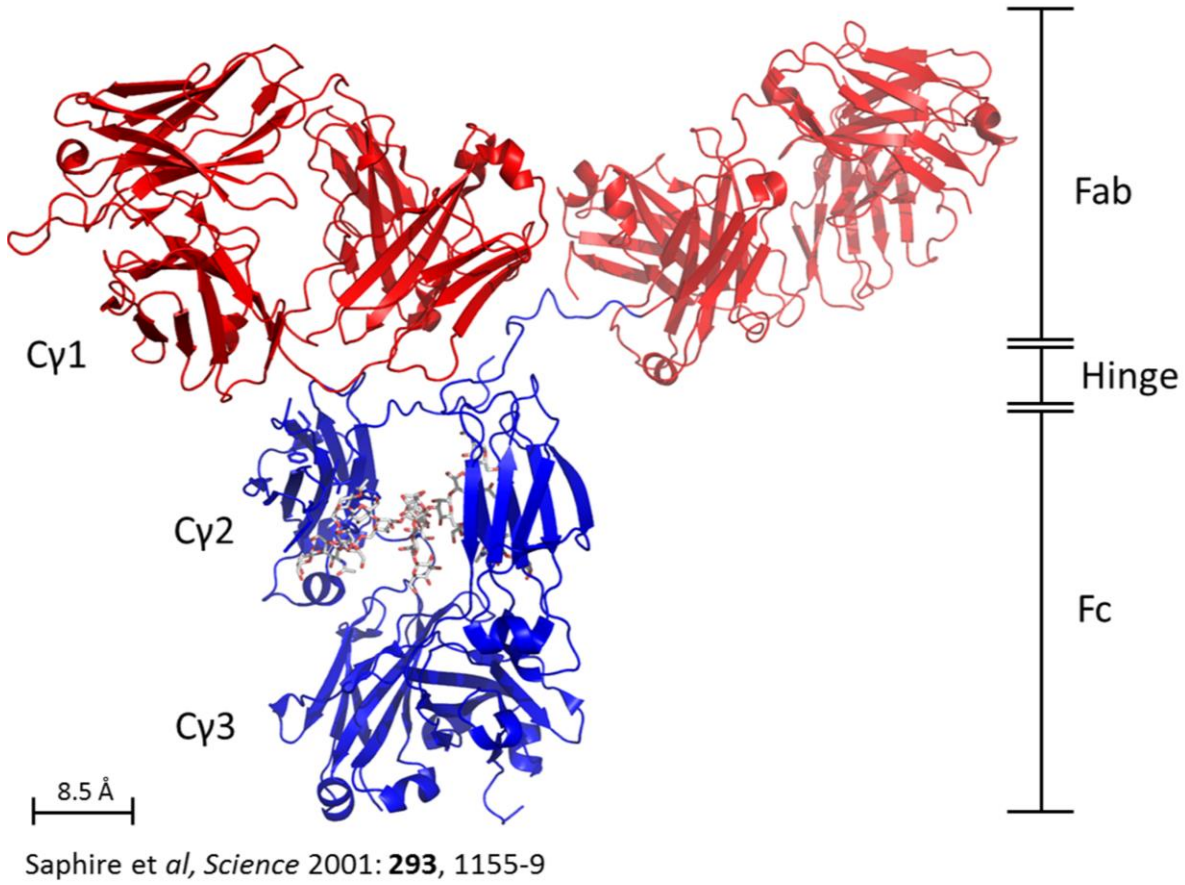

Figure 1.1. Crystal structure of full length human IgG1 antibody. The IgG1 b12 antibody is shown as cartoon diagram. It consists of two identical Fab regions (red), a hinge region and an Fc region (blue). Each heavy chain has three constant domains: Cγ1, Cγ2 and Cγ3 domains. The *N*-linked glycans attached to the Cγ2 domains are shown as stick representation in grey. This crystal structure (PDB ID: 1HZH) is adopted from Saphire *et al*, 2001[11] and the image is generated using Pymol Molecular Graphics System, DeLano Scientific LLC.

1.1.2. Antibody Isotypes

Different antibody isotypes, which mediate distinct functions, are produced at different stages of an immune response under different stimulatory milieus, via a regulated isotype switching mechanism in B cells[12]. By default, B cells produce IgM without previous exposure to an antigen. IgM circulates in the human serum at about 1-2.5 mg/mL, and its typical pentameric form is a potent activator of the complement pathway through interaction with C1q[4]. IgG represents the most abundant isotype in human serum, circulating at around 12 mg/mL, and is the main isotype produced in response to active vaccination[4]. IgE is known to bind large pathogens such as parasites; and it is unique in that its monomeric form binds to the high affinity IgE receptor FcεRI on mast cells and basophils during the steady-state and is responsible for causing hypersensitivity including the commonly known allergic reactions[4; 13]. IgA is present in human serum at about 2.5 mg/mL in its monomeric form and is predominately dimeric (linked by a J-chain) on the mucosal surfaces, which prevents antigens such as bacteria breaching the musical system[14; 15]. IgD is an ancient antibody preserved in most jawed vertebrates; although its precise function remains unclear due to a lack of investigation[16], some evidence indicates a role in maintaining peripheral B cell homeostasis[17; 18].

Apart from the distinct structural and functional features, different antibody isotypes are differentially glycosylated, among which IgG glycosylation is the most investigated and is discussed in detail in section 1.3. While IgG has only one conserved *N*-glycosylation site, other antibody isotypes contain multiple conserved *N*-glycosylation sites[4]. IgA has two conserved *N*-glycosylation sites: N263 and N459, which exhibits differential glycosylation depending on its oligomeric state. For example, the majority of *N*-glycan on serum IgA is biantennary complex type and predominantly terminal sialylated[19]. In contrast, the dimeric secretory IgA contains approximately 50% *N*-Acetylglucosamine (GlcNAc)-terminating

glycans and 10% oligomannose glycans[19]. IgD also contains multiple conserved *N*-glycosylation sites: N445 and N496 are occupied with sialylated biantennary complex type glycans, while N354 is occupied exclusively by oligomannose type glycans and is required for IgD assembly and secretion[4; 20]. IgE is the most heavily glycosylated isotype, with seven *N*-glycosylation sites that account for approximately 12% of its molecular weight[20]. While most of the sites are occupied by sialylated biantennary complex type glycans, the N394 is exclusively occupied by oligomannose structures[20]. IgM has five *N*-glycosylation sites, three of which (N171, N332 and N395) are occupied by mainly sialylated biantennary complex type glycans, and two of which (N402 and N563) are occupied by oligomannose glycans[4; 21]. Although the N297 *N*-glycosylation site is conserved across all the isotypes, with the glycan buried in the Fc domain apart from IgA[22], its function varies among different isotypes[4]. Apart from *N*-glycosylation, IgD and IgA also contain *O*-glycosylation sites that impart structural integrity to these isotypes[4]. The glycosylation and its functional implications for IgA, IgD, IgE and IgM will not be discussed further as they are beyond the scope of this thesis.

1.1.3. IgG Subclasses

Human IgG is further divided into four subclasses called IgG1, IgG2, IgG3 and IgG4, and the number indicates their relative abundance in serum[23; 24]. Each IgG subclass is elicited by different antigens. For example, IgG2 is mainly induced carbohydrate antigens[25], and IgG4 is only induced by prolonged immunization with protein antigens[26]. Different IgG subclasses differ in their Fc domain sequences; sequence alignment of the constant domain (Cγ1, hinge, Cγ2, and Cγ3) of each subclass shows that the different IgG subclasses are relatively conserved in sequence and differ mainly in their hinge region (Table. 1.1, Fig. 1.2). The hinge region of each subclass differs in their length, flexibility and sequence. IgG1 and IgG3 have similar hinge flexibility despite that IgG3 has many more residues at the hinge, including 21 proline residues[8; 27]. IgG2 hinge lacks a glycine residue that is conserved in

other subclasses, which reduces its relative flexibility[28]. A large of fraction of IgG4 lacks the interchain disulphide bonds, which is thought to be due to a key residue difference upstream of the second cysteine that normally forms the interchain disulphide bond[26]. The lack of interchain disulphide bonds might provide a basis for bispecific IgG4 generation[26]. In summary, the degree of IgG subclass flexibility conferred by the hinge region follows: IgG3 > IgG1 > IgG4 > IgG2[29].

Table 1.1. Constant region of IgG1, IgG2, IgG3 and IgG4.

IgG Subclass	Cγ1	Hinge	Cγ2	Cγ3
IgG1	1-98	99-110	111-223	224-330
IgG2	1-98	99-110	111-219	220-326
IgG3	1-98	99-160	161-270	271-376
IgG4	1-98	99-110	111-220	221-327

The residue position of Cγ1, hinge, Cγ2, and Cγ3 regions of human IgG1 (Accession number: P01857), IgG2 (Accession number: P01859), IgG3 (Accession number: P01860) and IgG4 (Accession number: P01861). Numbering according to the respective accession codes.

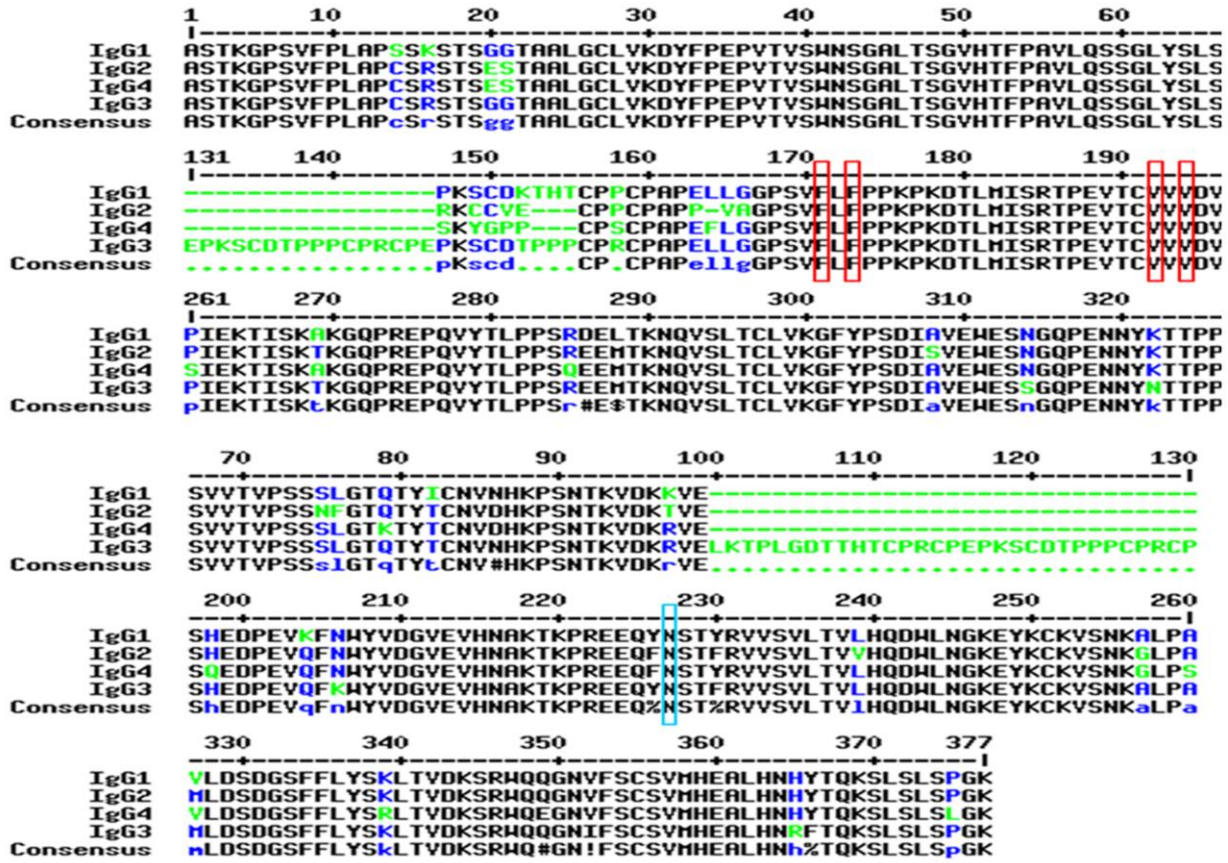

Figure 1.2. Sequence alignment of Cγ1, hinge, Cγ2, and Cγ3 regions of human IgG1 (Accession number: P01857), IgG2 (Accession number: P01859), IgG3 (Accession number: P01860) and IgG4 (Accession number: P01861). The hydrophobic residues in the Cγ2 domain: F241, F243, V262, and V264, are highlighted by red boxes. The *N*-glycosylation site N297 is highlighted by a cyan box. Sequence alignment was carried out using Multalin.

1.2. Human IgG1 Fc

1.2.1. Structure

The human IgG1 Fc domain consists of well-defined Ig domains. For example, the Cγ2 domain exhibits a typical Greek-key β-barrel, mainly composed of two β-sheets; and each β-sheet consists of three and four anti-parallel β-strands respectively (Fig. 1.3). Moreover, the β-strands are connected by loops and helices (Fig. 1.3). The Fc domain exhibits a well-defined horseshoe-like structure (Fig. 1.4) that mediates a range of effector functions including ADCC, CDC, phagocytosis, and general anti-inflammation[4; 10; 23]. The Fc fragment is a homodimer comprised of the constant region of the heavy chains. The Cγ2 and Cγ3 domains of each heavy chain are linked by two interchain disulphide bonds located at the Cγ2 domains where a conserved *N*-linked glycan is also attached to the N297 (Fig. 1.4)[4; 5]. While the two opposing Cγ2 domains sit relatively apart from each other, partly due to the steric hindrance of the *N*-glycans, the two opposing Cγ3 domains form extensive hydrophobic interactions that involve more than 20 residues on each chain[5] (Fig. 1.4). Together, the Cγ2 and Cγ3 domains form the binding site for various Fc binding proteins. For example, the FcγRs and complement molecule C1q interact with the Cγ2 domain and the lower hinge region[30; 31], while protein A and the neonatal Fc receptor (FcRn) bind to the interface of Cγ2 and Cγ3 domains[30; 32; 33]. The Fc *N*-glycan has been shown to influence the horseshoe structure and modulate the Fc affinity for the FcγRs and C1q[4; 34]. For example, deglycosylated Fc displays increased disorder at the C'E loop that contains the N297 (Fig. 1.3), and exhibits significantly decreased affinity for the FcγRs[35; 36]. The effect of differential glycosylation on Fc structure is discussed in more detail in section 1.4.

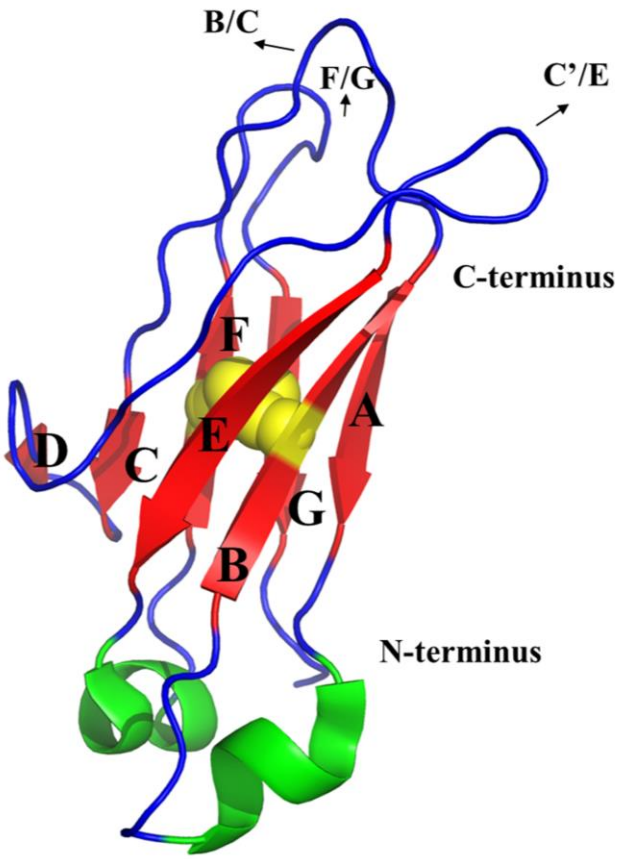

Structural motif	Residue number
β-strand A	V240-F243
A/B loop #1	P244-K246
Helice #1	P247-L251
A/B loop #2	M252-P257
β-strand B	E258-V264
B/C loop	D265-N276
β-strand C	W277-V279
C/D loop	D280-G281
β-strand D	V282-Q283
C/C' loop	V284-Q294
C'/E loop	Q295-T299
β-strand E	Y300-T307
Helice #2	L309-D315
E/F loop	G316-E318
β-strand F	Y319-V323
F/G loop	S324-P331
β-strand G	I332-I336

Figure 1.3. Structure and organization of the human IgG1 Fc Cγ2 domain. The structure of human IgG1 Fc Cγ2 domain is shown in cartoon representation, showing a Greek-key β-barrel. The β-strands are shown in red, the α-helices are shown green, loops are shown in blue, the conserved disulphide bond is shown in yellow. Each β-strand is labelled with letters A to F. The structure was made from, and residue numbers follow PDB ID 1H3Y. The image is generated using Pymol Molecular Graphics System, DeLano Scientific LLC.

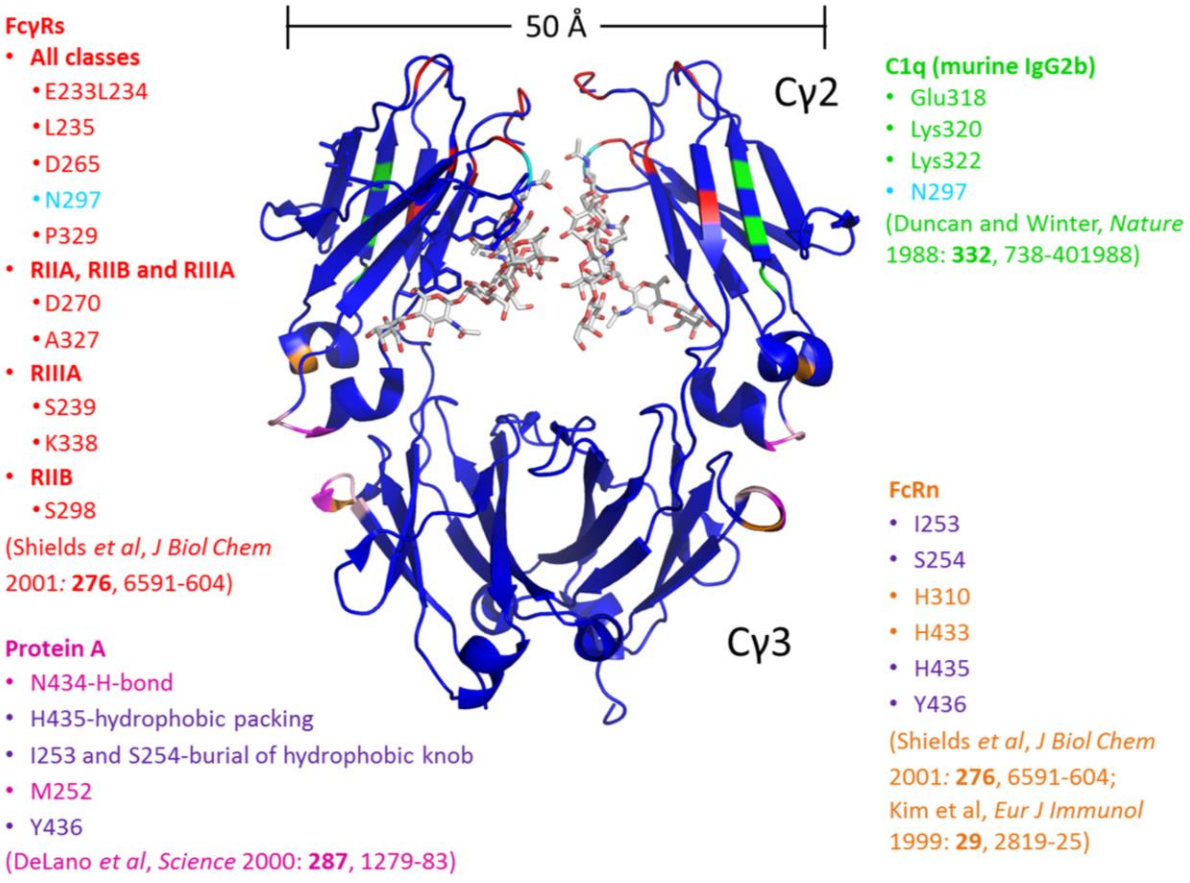

Figure 1.4. Crystal structure of a human IgG1 Fc. The Fc region of IgG1 b12 antibody, comprised of the lower hinge region, Cγ2 and Cγ3 domainsd, is shown as blue cartoon representation. The *N*-linked glycan attached to the Cγ2 domain is shown as grey stick representation. Amino acid residues important for various Fc receptors/ligands interactions are highlighted in different colors: red, FcγRs; green, C1q; pink, ProteinA; orange, FcRn; cyan, FcγRs and C1q; purple, Protein A and FcRn. This Fc crystal structure is cropped from the full length IgG1 structure (PDB ID: 1HZH) reported by Saphire *et al*, 2001[11]; and the image is generated using Pymol Molecular Graphics System, DeLano Scientific LLC.

1.2.2. Function Through Fc Receptors

IgG Fc mediates antibody effector functions by engaging with a range of Fc receptors present on the cell surface or in solution. These IgG Fc receptors include the FcγRs[9], the complement molecule C1q[31] and the FcRn[37; 38]. Areas of Fc important for productive engagement with various Fc receptors are highlighted in Fig. 1.4. Recently, the C-type lectin, dendritic cell-Specific intercellular adhesion molecule-3-grabbing non-integrin (DC-SIGN), has been proposed to be a ligand of an sialylated IgG Fc glycoform (sFc), and the binding initiates a

novel anti-inflammatory signalling pathway[39; 40]. This interaction between sFc and DC-SIGN is discussed in more detail in section 1.7. The FcγRs are a more established family of type 1 single transmembrane proteins, and six human FcγRs have been cloned: FcγRIA, FcγRIIA, FcγRIIB, FcγRIIC, FcγRIIIA, and FcγRIIIB [9] (Fig. 1.5). These receptors are classified into either activatory or inhibitory depending on their associated intracellular signalling components. The activatory FcγRs, which include the FcγRIA, FcγRIIA, FcγRIIC and FcγRIIIA, usually associate with a signalling component containing the putative activatory immunoreceptor tyrosine-based activation motif (ITAM)[9]. For the FcγRIA and FcγRIIIA, their intracellular domain non-covalently associates with the ITAM-containing signalling component called the γ-chain[9]; while the intracellular domain of FcγRIIA and FcγRIIC contain an intrinsic ITAM motif that could signal independently of the γ-chain[9; 41; 42; 43] (Fig. 1.5). The FcγRIIIB, which is 99% homologous with the FcγRIIIA, is a GPI anchored receptor and only found to be expressed on neutrophils[44; 45]. Although the role of FcγRIIIB remains unclear, it has been shown to play an important role in neutrophil response to immune complexes[46; 47].

In contrast to the existence of multiple activatory FcγRs, the FcγRIIB is the only known inhibitory receptor in humans, containing the inhibitory immunoreceptor tyrosine-based inhibition motif (ITIM) at its intracellular domain[9; 44] (Fig. 1.5). The immunosuppressive effect of FcγRIIB has been shown to be critical in maintaining immune homeostasis, by increasing the activation threshold of B cells and other FcγRIIB-expressing immune cells[48]. Its immunosuppressive role manifests in FcγRIIB-deficient mice that exhibits increased tendency to develop voluntary inflammatory conditions[49; 50; 51], whereas the induction of FcγRIIB expression in autoimmune mouse models could ameliorate inflammatory pathologies[52; 53]. The emerging importance of FcγRIIB in immunomodulation has triggered interests in engineering both FcγRIIB and Fc for immunosuppressive therapies[54]. For

example, antibody variants engineered to bind FcγRIIB with higher affinity have been shown to significantly inhibit B cell receptor (BCR)-induced human B cell activation, by simultaneously engaging the BCR and FcγRIIB[55], and such antibody has been shown to suppress humoral immunity in mouse[56]. Furthermore, recent data showed that the FcγRIIB is essential for the function of immunomodulatory monoclonal antibodies against tumour necrosis factor receptors such as CD40, and such antibodies, when engineered to have enhanced affinity for FcγRIIB, were able to significantly increase potency of an immune response during vaccination[57; 58]. In addition, the soluble variants of FcγRIIB have emerged as a viable therapeutics for immune-complex-mediated inflammation, by inhibiting Fc-FcγR interactions, and some variants have recently entered clinical trial for treating inflammation[54; 59]. Similar immunosuppressive effects of other soluble FcγR variants have also been demonstrated[60; 61; 62; 63]. Section 4.2.4 of this thesis presents the generation of novel FcγRIIB-selective Fc variants that present as potential therapeutic agents.

Usually, immune cells express multiple classes of FcγRs, both activatory and inhibitory, to regulate the threshold of cellular activation[9; 44; 54]. The cell surface expression of the FcγRs on various immune cells is summarized in Fig. 1.5. Some immune cells, such as myeloid derived DCs and macrophages are found to express multiple classes of FcγRs[44; 64; 65; 66]. In contrast, certain cell types express only one type of FcγR. For example, B cells only express the FcγRIIB on their cell surface, while NK cells express predominantly the FcγRIIIA on which its ADCC function largely depends[44; 48]. The crystal structures of a number of FcγRs have been determined: the FcγRIA[67], FcγRIIA[42], FcγRIIB[68], FcγRIIIA[69] and FcγRIIIB[70]. These crystal structures demonstrate conserved structural motifs among human FcγRs (Fig. 1.6); for example, they contain two Ig-like extracellular domains named D1 and D2, except FcγRIA that has an additional D3 domain[71]. Each domain is comprised of 1 five-stranded β-sheet and 1 three-stranded β-sheet[71].

The molecular mechanism of Fc-FcγR interaction has been solved by the crystal structure of the Fc-FcγRIIIA complex[69; 72] (Fig. 1.6), and more recently, the Fc-FcγRIIB complex[73] (PDB ID not yet published upon this thesis submission). The crystal structure shows 1:1 molar ratio of Fc-FcγR interaction, and that the interdomain angle of the FcγRIIIA opens by about 10 degrees upon Fc binding[69; 70]. Concomitantly, the Fc adopts an asymmetric opening of the horseshoe structure between the Cγ2 domains at the N-terminal tip[69; 70]. The Cγ2 domains and the lower hinge region of Fc form the binding site for the FcγRs[30; 71]. Based on this structure, mutagenesis of the IgG1 Fc backbone has been carried out to determine the residues essential for Fc-FcγR interaction[30]. As expected, due to the structural homology among these FcγRs, a common panel of Fc amino acid mutations affected all FcγRs binding[30]. Furthermore, selective Fc residues that affect Fc binding to certain FcγRs were also identified[30]. Identification of Fc residues important for FcγRs binding has enabled the engineering of Fc with desired effector functions, which is discussed in more detail in section 1.6.

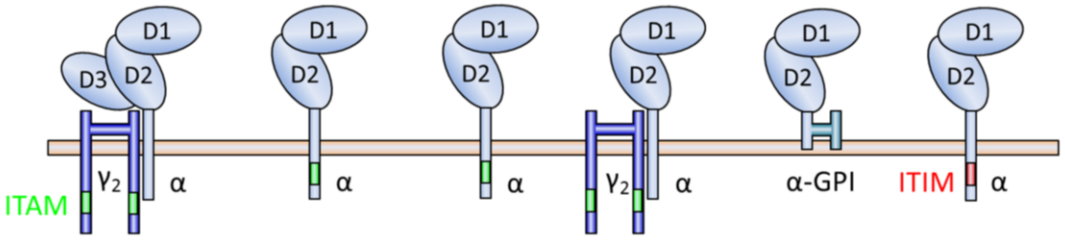

Name	FcγRI (CD64)	FcγRIIA^{131H} (CD32a)	FcγRIIC (CD32c)	FcγRIIIA^{158V} (CD16a)	FcγRIIIB (CD16b)	FcγRIIB^{232I} (CD32b)
Affinity (Kd)	High (15 nM)	Low (0.2 µM)	Low (8.3 µM)	Low (0.5 µM)	Low (5 µM)	Low (8.3 µM)
Subclass preference	IgG1>3>4	IgG1≫3>2>4	IgG4>3>1>2	IgG3≫1>4>2	IgG3>1	IgG4>3>1>2
Alleles	---	131H, 131R	---	158V, 158F	---	232I, 232T
Murine orthologue	FcγRI	---	---	FcγRIII FcγRIV	---	FcγRIIB
B cell	---	---	---	---	---	+
T cell	---	---	---	---	---	---
NK cell	---	---	+	+	---	+/-
Monocyte	+	+	+	+	---	+/-
Macrophage	+	+	+	+	---	+/-
DC	+	+	---	---	---	+
Basophil	---	+	---	---	+/-	+
Neutrophil	(+)	+	+	---	+	+/-
Mast cell	(+)	+	---	---	---	---
Eosinophil	---	+	---	---	---	---

Figure 1.5. Human FcγRs. Schematic representation of human FcγRIA, FcγRIIA, FcγRIIB, FcγRIIC, FcγRIIIA, and FcγRIIIB, embedded in the cell membrane (light salmon), are shown associated or not with the FcRγ chain (purple). The intracellular signalling motifs include the activatory ITAM (green box) and inhibitory ITIM (red box). FcγRIIIB is anchored to the membrane via a GPI anchor. Various FcγRs properties, ligand specificity and cellular expression are shown, below the schematic representation. The FcγRs affinity for IgG1 Fc, subclass preference, and cellular expression are adopted from Bruhns, 2012[74]. For FcγRIIA, the affinity shown corresponds to the 131H variant (affinity for 131R variant is 0.3 µM); for FcγRIIIA, the affinity shown corresponds to the 158V variant (affinity for F158 variant is 0.85 µM); for FcγRIIB, the affinity shown corresponds to the 232I variant (affinity for 232T is very similar to 232I variant[75]). The different FcγR alleles and their murine orthologue are derived from Nimmerjahn and Ravetch, 2008[44]. (---, none or no expression; +, cell surface expression detected; +/-, cell surface expression detected on very low percentage or rare subset of cells; (+), inducible cell surface expression)

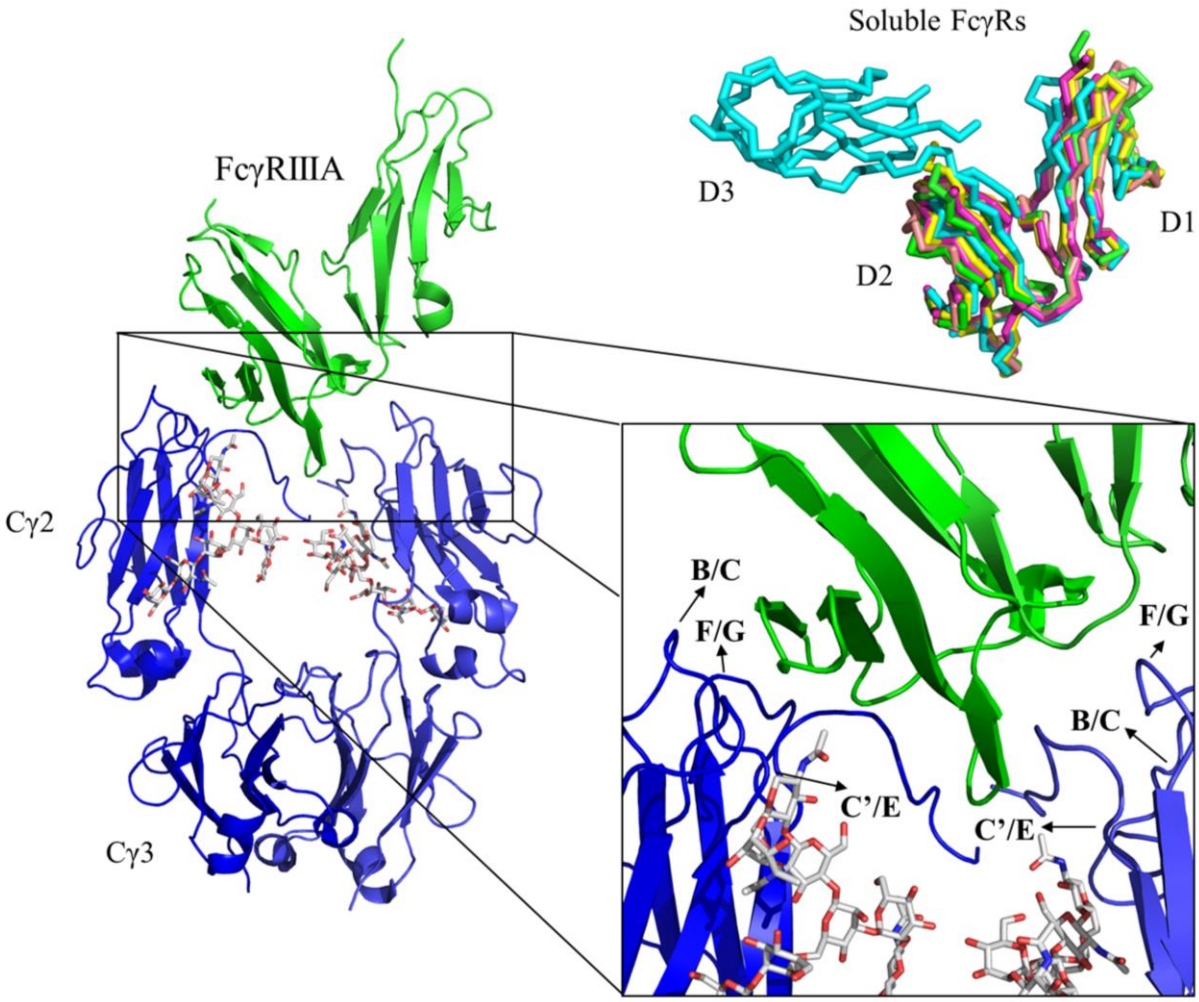

Figure 1.6. Structure of the human IgG1 Fc-FcγR complex. The overall structure of the Fc-FcγR shown in cartoon representation on the left, and the *N*-linked glycan on Fc is shown in grey sticks. The detailed view of Fc-FcγR binding interface is shown on the right bottom (PDB ID 3SGJ). The overlay of the extracellular domain of FcγRIA (cyan, PDB ID 3RJD), FcγRIIA (pink, PDB ID 1FCG), FcγRIIB (yellow, PDB ID 2FCB), FcγRIIIA (green, PDB ID 3SGJ) and FcγRIIIB (salmon-pink, PDB ID 1T83), using Pymol Molecular Graphics System, DeLano Scientific LLC, is shown on the right top as ribbon representation. The image is generated using Pymol Molecular Graphics System, DeLano Scientific LLC.

1.3. Human IgG Fc Glycosylation

1.3.1. Overview

All human immunoglobulins are glycosylated, albeit to different extends[4; 76]. IgG glycosylation accounts for 2-3% of total IgG molecular weight, which is relatively low compared with the 12-14% for IgM, IgD and IgE[4; 76]. IgG Fc has a conserved *N*-glycosylation site at N297 across all subclasses[4; 76] (Fig. 1.2), while no conserved glycosylation sites on the Fab region was found. However, sequence analysis indicates that about 20% of human IgG Fab regions are glycosylated[4; 77]; and these *N*-glycosylation consensus sequences on Fab result from somatic mutations, indicating that glycosylation is positively selected during antibody biogenesis[24; 77]. Indeed, most Fab glycosylation occur on exposed loop regions and have been shown to significantly modulate antigen binding[4]; however, oligomannose glycans has also been detected in narrow antigen-binding grooves[78]. Like other glycoproteins, natural IgG *N*-glycosylation occurs in the endoplasmic reticulum and the Golgi apparatus of a B cell, in a well-defined eukaryotic *N*-glycosylation pathway[79] (Fig. 1.7A).

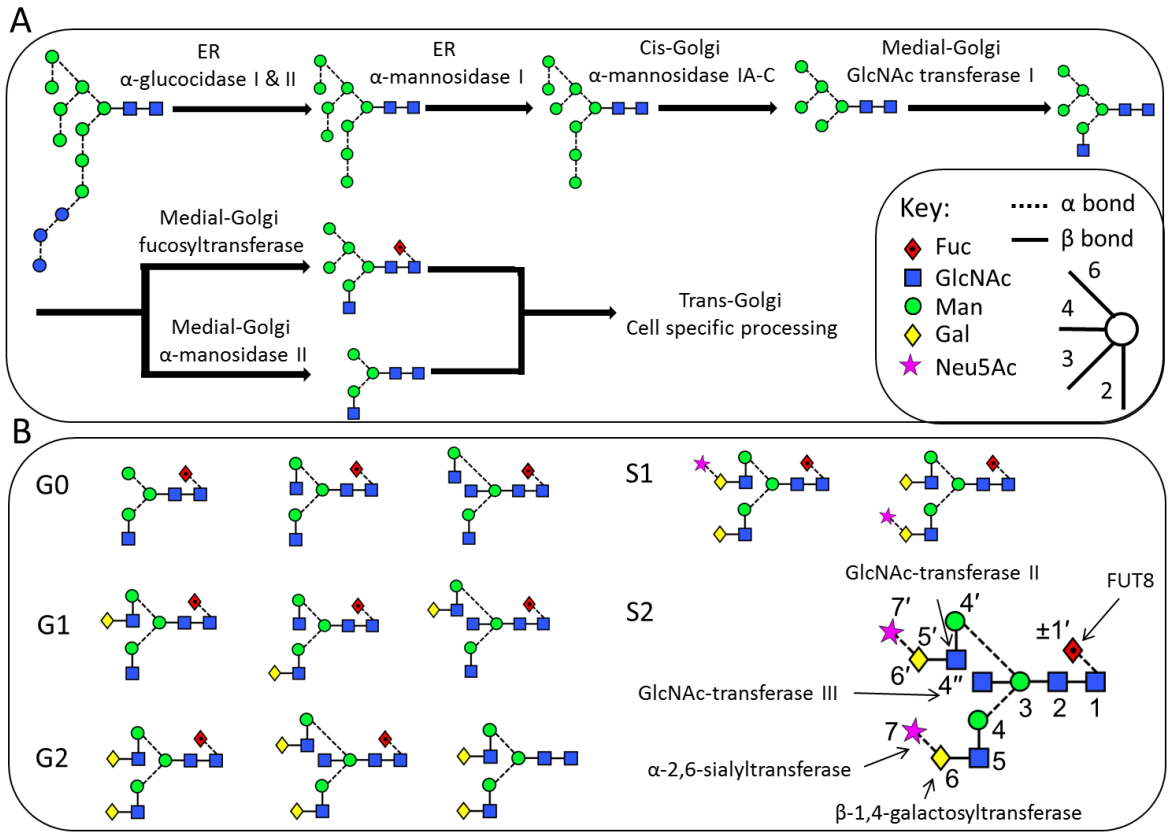

Figure 1.7. Mammalian *N*-glycosylation pathway. (A) The conserved eukaryotic *N*-glycosylation pathway, from early processing in the endoplasmic reticulum, to late Golgi apparatus modifications, is shown in schematic representation. (B) Commonly detected IgG Fc *N*-glycan species. G0, without terminal galactose; G1, with one terminal galactose; G2, with two terminal galactoses; S1, monosialylated; S2, disialylated. The symbolic representation of glycans follows that of Harvey *et al*, 2009[80], with residues in both the schematic diagrams and molecular graphics following the color scheme of the Centre for Functional Glycomics. The linkage position is shown by the angle of the lines linking the sugar residues (vertical line = 2-link, forward slash = 3-link, horizontal line = 4-link, back slash = 6-link). Anomericity is indicated by full lines for β-bonds and broken lines for α-bonds. Oligosaccharide nomenclature follows that of Bowden et al, 2012[81]. Residue labelling follows that of Vliegenhart et al, 1983[82] with the additional modifications of **7** for sialic acid, **1'** for α1→6-linked core fucose. These residue labels are in bold-face throughout the thesis.

1.3.2. Serum IgG Glycosylation

Human serum IgG from healthy individuals exhibits predominantly biantennary complex type glycans, of which neutral glycoforms represent approximately 82%, with agalactosylated (G0), mono-galactosylated (G1) and di-galactosylated (G2) biantennary complex type glycans accounting for approximately 26%, 38%, and 18% respectively. Sialylated structures accounts for the remaining 19%[83] (Table 1.2). Furthermore, approximately 15% of IgG

glycan have bisecting *N*-acetylglucosamine (GlcNAc) attached to the β-mannose, and between 80%-92% of IgG glycan are core-fucosylated[4; 77; 83; 84] (Table 1.2). Although as many as over 32 different types of glycans have been detected on IgG Fc, several commonly detected glycans predominate[77] (Fig. 1.7B). The glycosylation of Fc and Fab differ significantly, mainly in levels of terminal sialylation and bisection, whilst the level of core-fucosylation and the ratio between G0, G1 and G2 are similar[83] (Table 1.2). As much as 74% of Fab glycan could be sialylated whereas only about 13% of Fc glycan is sialylated[77]. Moreover, Fc contains about three times less bisected glycoform than Fab[83] (Table 1.1). Interestingly, the presence of tri-antennary and larger glycans has not been found in healthy people, even on the exposed Fab glycosylation sites[4; 76]. This is in contrast to other glycoproteins such as fetuine and the FcγRs, which have been shown to contain a large proportion of tri-antennary and tetra-antennary oligosaccharides on their solvent exposed glycosylation sites[85; 86]. The disparity suggests that either the glycosylation sites on Fab region are not sufficiently exposed or the B cell glycosyltransferase expression is insufficient for generating multi-antennary oligosaccharide.

Table 1.2. Relative proportions of different *N*-glycan species detected on human IgG.

%	G0	G1	G2	Mono-sial	Di-sial	Fucose	Bisection
IgG	26	38	18	12	7	92	15
Fab	8	12	5	42	32	90	36
Fc	26	41	20	9	4	92	12

Numbers are calculated from Holland *et al*, 2006[83], and represents the average results from six people. *N*-linked glycan were released from human serum IgG by Peptide-*N*-Glycosidase F (PNGase F).

1.4. Fc Protein-Glycan Interaction

1.4.1. Crystallographic Comparison of Different Fc Glycoforms

The limited Fc glycan processing was shown to be due to restricted access of Golgi-resident glycosyltransferases as a result of limited glycan flexibility imposed by the unusually prolific glycan-protein interaction at the Cγ2 region[4; 87]. Early crystal structures of Fc show that the twin Fc glycans are positioned in the Fc horseshoe structure in a precisely defined fashion[34; 81; 88] (Fig. 1.4). Each glycan lies close to a number of amino acid residues on the Cγ2 domain to which the glycan is attached, and forms a number of non-covalent interactions dominated by hydrophobic and electrostatic interactions[35; 88] (Fig. 1.8). Moreover, the extent of twin Fc terminal glycan processing has been shown to regulate the distance between the two opposing Cγ2 domains[34]; for example, the successive removal of monosaccharide residues from the reducing end of Fc glycan by exoglycosidases narrows the gap between the two Cγ2 domains, whilst the Cγ3 domains remain unaffected[34; 35; 89]. Removal of the two terminal GlcNAc residues and the core mannoses further decreases the distance between the Cγ2 domains and lowers the Fc melting temperature, an indication of structural instability[35; 90].

Contrary to the reported positive effect of Fc glycosylation on Cγ2 domain spacing, comparison of a deglycosylated human Fc crystal structure with several glycosylated Fc structures reveals that deglycosylated Fc is also able to adopt a similarly open conformation[36], a conclusion supported by structural data collected from Fc glyco-variants in solution-phase[36]. Moreover, the crystallographic study of a Fc mutant that has native glycosylation shows that the Cγ2 domains of natively glycosylated Fc could assume a more open conformation compared with natively glycosylated, unmutated, Fc structures[91]. This observation raises the question of whether the observed, glycan-dependent, Cγ2 domain spacing is a genuine trend

or a crystallographic artefact. The impact of different Fc glycoforms on Fc effector functions is discussed in section 1.5.

Crystal structures of a series of human IgG1 Fc glycoforms have been obtained, these include: $Man_9GlcNAc_2$[92], hybrid[81], $Gal_2GlcNAc_2Man_3GlcNAc_2Fuc$[11], $GlcNAc_2Man_3GlcNAc_2Fuc$[88], $Man_3GlcNAc_2Fuc$[35], $ManGlcNAc_2Fuc$[35], sialylated[93] and deglycosylated[35]. These structures capture Fc glycoforms at different stages of glycan biogenesis, from the early oligomannose structures to the mature complex type glycans, and provide structural insights into the differential Fc glycan-protein packing. A comparison of these crystal structures reveals that regardless of the glycoform, the interaction between the core pentassacharide ($Man_3GlcNAc_2$) and the Fc protein backbone is conserved[81] (Fig. 1.8). One of the major changes in protein-glycan packing during Fc glycan biogenesis occurs during the transition from hybrid type to complex type. During this transition, the GlcNAc**5'** is transferred to the 6-arm core mannose (Man**4**) by the *N*-acetylglucosaminyltransferase II, which allows the formation of stacking interaction between the GlcNAc**5'** and the hydrophobic residue F243[81] (Fig. 1.9). This stacking interaction has been shown to increase Fc stability while suppress subsequent enzymatic processing of Fc glycan[81; 94].

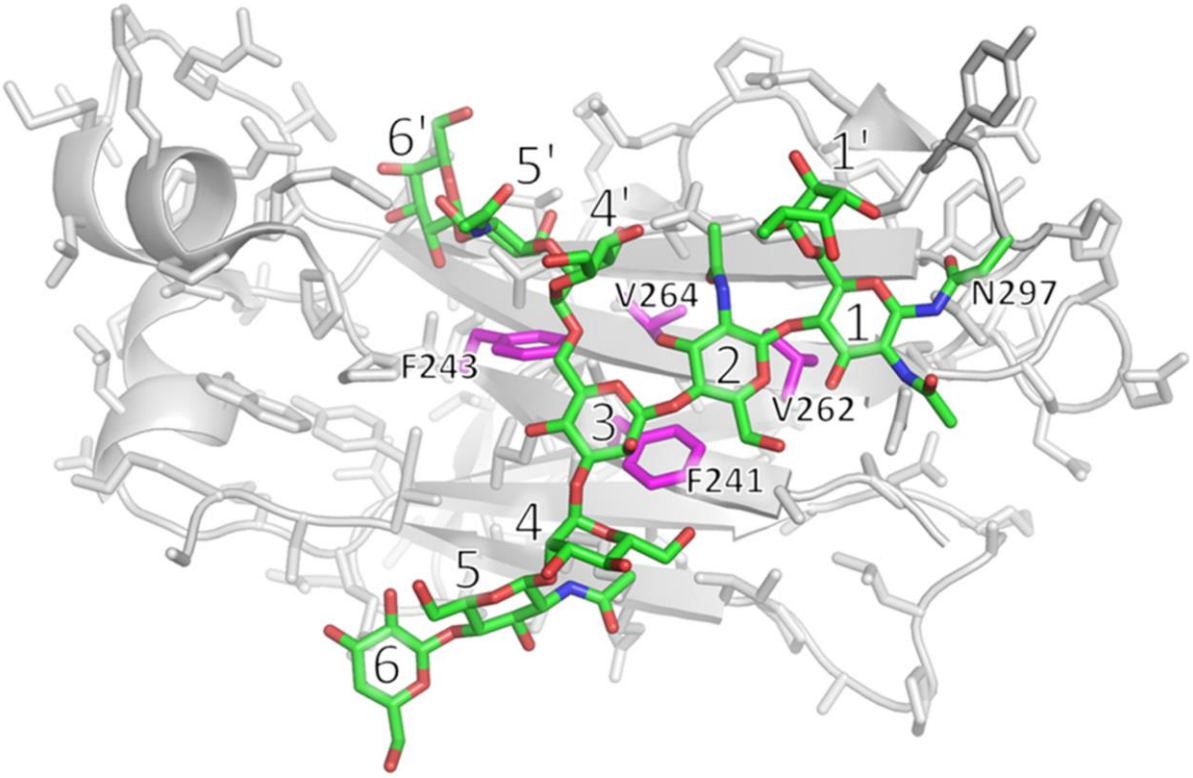

Figure 1.8. Packing of a biantennary complex type *N*-glycan (sticks in green) to the protein surface (cartoon in grey) of human IgG1 Fc Cγ2 domain (PDB ID: 3AVE). Four hydrophobic residues on the protein–glycan interface are highlighted in pink (sticks). The image is generated using Pymol Molecular Graphics System, DeLano Scientific LLC.

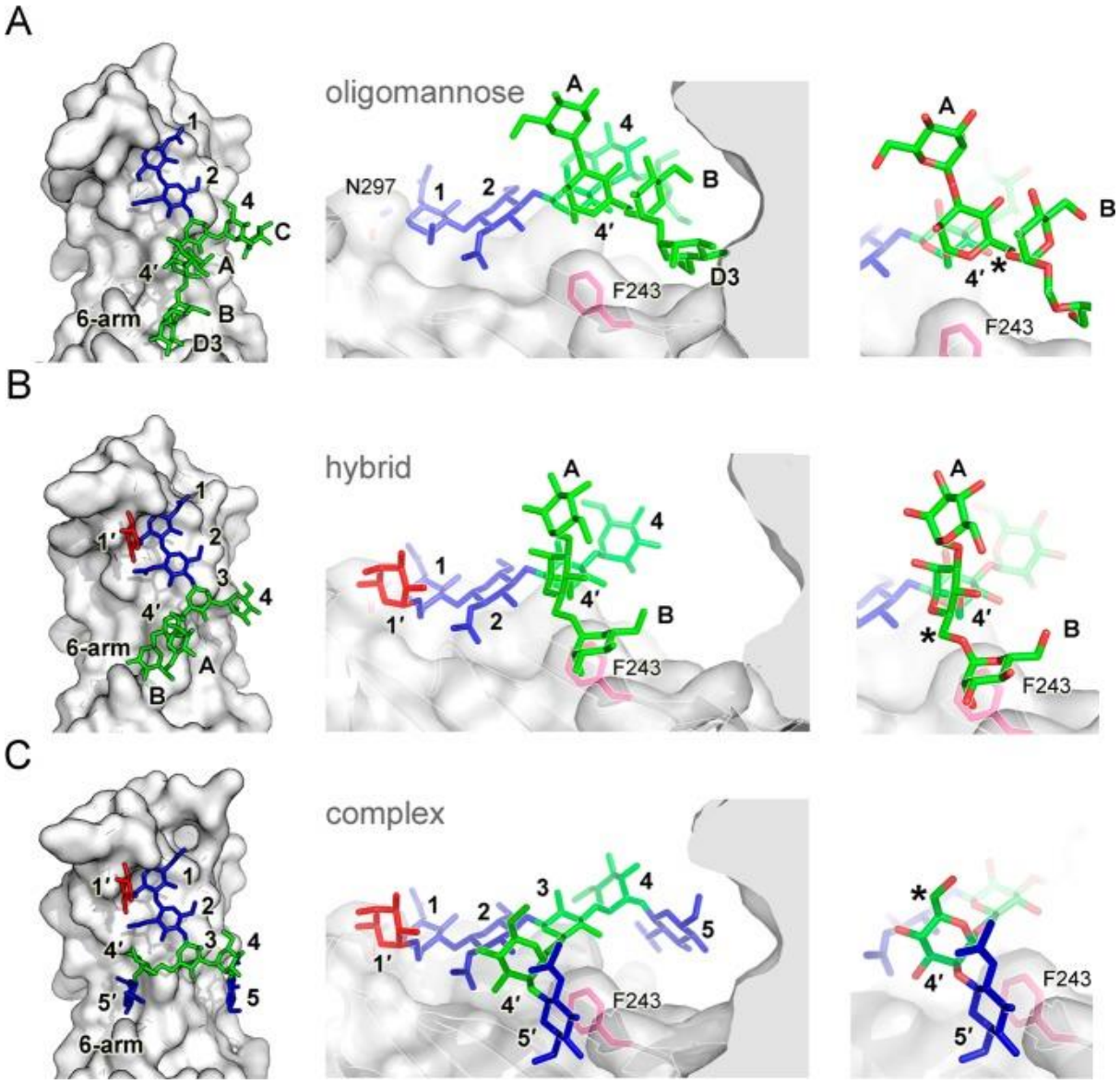

Figure 1.9. Structural transitions of IgG1 Fc glycans between (A) oligomannose-type (PDB ID 2WAH), (B) hybrid-type (PDB ID 4B7I, the 3-arm GlcNAc is not built due to a lack of electron density), and (C) complex-type glycosylation (PDB ID 3AVE), as observed by X-ray crystallography. The left-hand column displays the glycan packing against the Cγ2 domain. The central column shows a view with the 6-arm in the foreground. The right-hand column is a close-up and shows the conformational changes occurring within the 6-arm; an asterix indicates the location of the C6 carbon of the Man**4′** residue. The protein surface is colored gray, the F243 side-chain is colored pink. Fucose is coloured in red, GlcNAc is coloured in blue, and mannose is coloured in green. Figure reproduced from Bowden *et al*, 2012[81]. The image is generated using Pymol Molecular Graphics System, DeLano Scientific LLC.

1.4.2. Fc Hydrophobic Protein Ladder

Apart from F243, which only forms significant protein-glycan interactions in complex type Fc glycoforms, a series of hydrophobic residues, comprised of F241, V262, and V264, readily form van der Waals interactions with the core pentasaccharide, regardless of the Fc glycoform[87; 88] (Fig. 1.8). Together, F241, F243, V262, and V264, which are in close proximity, form a ladder of hydrophobic residues crucial for maintaining the Fc protein-glycan interactions. In addition to the hydrophobic interactions, significant electrostatic interactions occur between the positively charged E265 and R301 residues and the hydroxyl groups projecting from sugar hexoses at the reducing end of the oligosaccharide[87; 88]. These hydrophobic and electrostatic interactions collectively limit the Fc glycan flexibility and results in reduced terminal galactosylation and sialylation due to restricted access of Golgi-resident glycosyltransferases. Abolition of these Fc glycan-protein interactions, realized by the mutagenesis of the hydrophobic and charged residues, dramatically increased Fc terminal glycan galactosylation and sialylation, accompanied by decreased Fc-mediated cytotoxicity[87; 95; 96; 97]. Several potential mechanisms have been proposed to explain this decreased Fc effector function. One possibility is that the increased Fc terminal glycan processing, particularly terminal sialylation, could alter the Fc tertiary structure to result in decreased FcγR binding. Moreover, it could be due to the putatively increased Fc glycan flexibility, as a result of reduced Fc protein-glycan interactions. In addition, a decreased glycosylation site occupancy, as observed in the hydrophobic mutants[87], could lead to a larger fraction of aglycosylated Fc that is known to cause decreased effector functions[30; 98]. In this thesis, the role of Fc protein-glycan interface on Fc-FcγR interaction is explored in Chapter 4.

1.4.3. Terminal Galactose

Besides the interaction between the Fc hydrophobic ladder and the core pentasaccharide of the Fc glycan, terminal galactoses have been shown to interact with the Fc protein backbone and further restrict Fc glycan flexibility. The 6-arm of Fc glycan has been shown to exhibit similar mobility as the Fc protein backbone[99], an indication of the 6-arm glycan immobility. Consistent with a role in stabilizing the protein-glycan interactions, removal of the Gal**6'** significantly increases Fc glycan flexibility[99]. More recent NMR data show that the 6-arm of Fc glycan has both bound and free states from the protein backbone[100], potentially permitting access to terminal glycosyltransferases. In contrast, some reported that the Gal**6** on the 3-arm is more mobile than the Fc backbone[101].

1.5. Fc Glycosylation and Their Associated Effector Functions

1.5.1. Deglycosylation

The structural impact of deglycosylation on Fc has been discussed in section 1.4.1. While the reported effects of deglycosylation on the openness of Fc Cγ2 domains vary from report to report[35; 36], the increased flexibility at the C'E loop of the Cγ2 domains upon deglycoslylation has been consistently observed (Fig. 1.10), a motif shown to disrupt Fc-FcγR interactions[35; 36; 102]. The Fc glycan has been shown to be essential for stabilizing the Fc structure[35; 81; 89], and deglycosylation abrogates Fc binding to all FcγRs[30; 103]. This is explored by the bacterial secreted Endoglycosidase S, which cleaves the IgG Fc glycan between the GlcNAc**1** and GlcNAc**2** residues to abolishes Fc binding for FcγRs except the high affinity FcγRIA[104; 105]. Moreover, mutations at the *N*-glycosylation sequon, which leads to the generation of aglycosylated Fc, significantly reduces Fc binding for all FcγRs[98]. However, a recent study shows that, while deglycosylated monomeric IgG exhibits minimal binding to FcγRs in isolation, significant binding could be detected between deglycosylated IgG-coated immune

complexes and FcγRs expressed on CHO cells, an effect dependent on the size of the immune complex and the IgG subclass[106]. On the other hand, a combination of mutations have been shown to be able to restore aglycosylated Fc binding to selective FcγRs including FcγRIA, FcγRIIA and FcγRIIB, albeit to different extents relative to the wild type[98; 107]. The minimal Fc glycan required for Fc structural stability and effector function measured by FcγRI-mediated superoxide assay is found to be the core trisaccharide[89]. More recently, a novel, antigen-specificity-independent, anti-inflammatory effect of Fc-deglycosylated IgG has been reported in a mouse model of immune complex-mediated rheumatoid arthritis (RA); and the mechanism was shown to be via deglycosylated Fc-mediated immune complex disruption[108]. Nevertheless, the mechanism of Fc-mediated immune complex disruption remains unclear. The immunosuppressive effect of deglycosylated IgG is discussed in the context of data presented in Chapter 6.

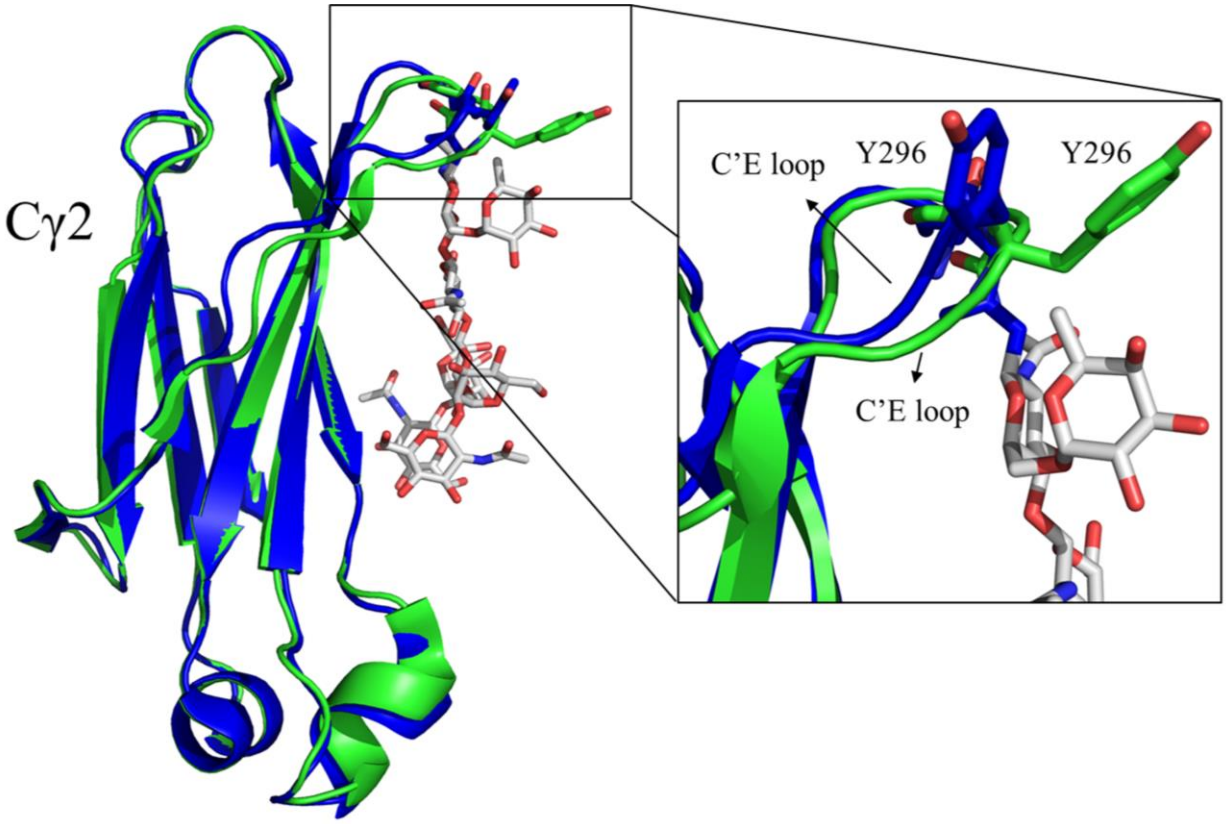

Figure 1.10. Overlay of glycosylated and aglycosylated human IgG1 Fc Cγ2 domains. Glycosylated Fc (PDB ID 3AVE) is coloured in blue, and aglycosylated Fc (PDB ID 3S7G) is coloured in green. The *N*-glycan attached to N297 of glycosylated Fc is coloured in grey. The C'E loop is enlarged on the right. The image is generated using Pymol Molecular Graphics System, DeLano Scientific LLC.

1.5.2. Core Fucosylation

The α1,6-linked core fucose of Fc glycan has been established to reduce Fc binding affinity for the activatory FcγRIIIA[109; 110; 111; 112; 113]. Defucosylation of Fc glycan increases the Fc binding affinity for the FcγRIIIA by about 27 fold[109], an effect referred to as the "fucose effect". A comparison of crystal structures of the FcγRIIIA in complex with either fucosylated or defucosylated Fc permits a molecular explanation for the fucose effect[109; 110] (Fig. 1.11). These structures illustrate for the first time that the *N*-glycan attached to the N162 of FcγRIIIA interacts directly with the core pentasaccharide of the Fc glycan, and

defucosylated Fc glycan interacts more favourably with the N162 glycan of FcγRIIIA than its fucosylated counterpart, which explains the fucose effect (Fig. 1.11). Consistently, previous studies showed that FcγRIIIA deglycosylation at N162 abrogates the fucose effect[85; 109; 114]. In addition to the N162 glycan, the *N*-glycan attached to N45 in FcγRIIIA has been shown to hinder the high affinity interaction between nonfucosylated Fc and FcγRIIIA, possibly via steric hindrance[85].

In line with the enhanced affinity for the FcγRIIIA, defucosylated IgG Fc has been found to mediate more potent ADCC[115; 116; 117; 118]. The level of fucosylation of normal human serum IgG Fc glycan varies from 80% to 92%[4; 83]; while *in vitro* generated recombinant IgG, expressed in Chinese hamster ovary (CHO) cells or human embryonic kidney (HEK 293) cells, consistently exceeds 90%[118], suggesting fucoyslation as a natural point of immune regulation. However, natural variations in the level of fucosylated serum IgG in healthy or immune compromised individuals have not been reported to date, although elevated levels of fucosylated serum IgG were observed in association with fetal maternal allotype thrombocytopenia[119].

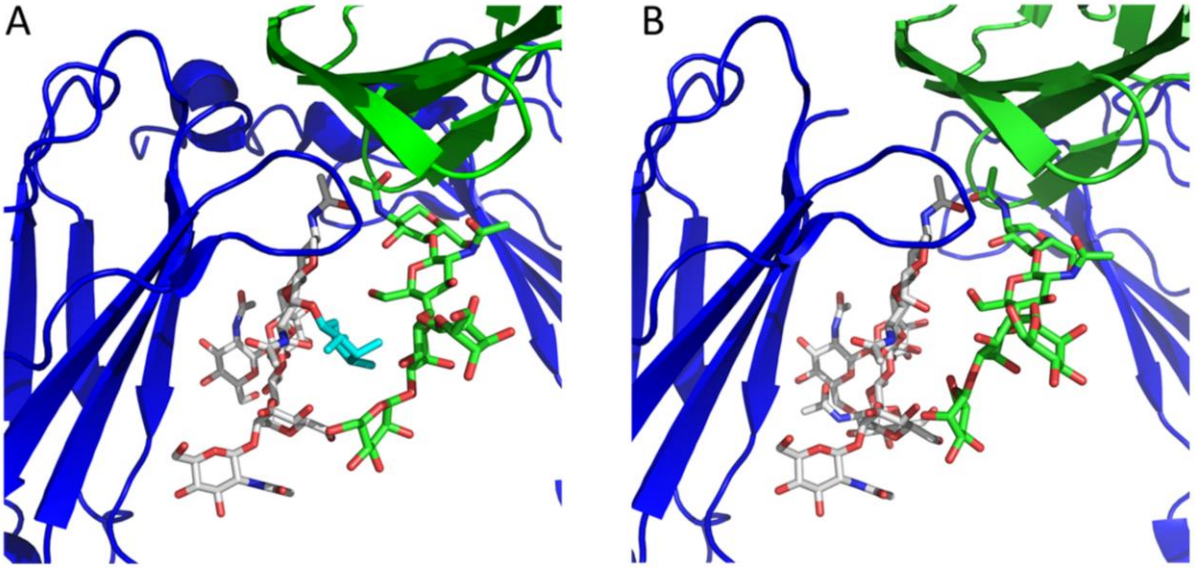

Figure 1.11. Comparison of the interface of FcγRIIIA in complex with fucosylated Fc or afucosylated Fc. The protein backbone of Fc and FcγRIIIA are shown in blue and green cartoon representation respectively. The Fc glycan is shown in grey and the FcγRIIIA N162 glycan is shown in green. Schematic representation of interaction between FcγRIIIA glycan with the glycan of (A) Fucosylated Fc (PDB ID 3SGJ), with the Fc α1,6-core fucose shown in cyan. (B) Nonfucosylated Fc (PDB ID 3SGK). The image is generated using Pymol Molecular Graphics System, DeLano Scientific LLC.

1.5.3. Terminal Galactosylation

Terminal galactosylated Fc account for about 63% of all Fc glycoforms[83] and has been shown to affect Fc affinity for the FcγRs. For example, hypergalactosylation of Fc terminal glycan has been shown to increase Fc affinity for the FcγRIIIA by 3 folds, presumably due to increased structural rigidity of the Fc Cγ2 domains[120]. In contrast, other reports suggest that hypogalactosylated Fc has increased affinity for the FcγRs[121]. The level of Fc galactosylation has been shown to change with age[122], and agalactosylation is found to be associated with inflammatory conditions such as RA[121]. Patients with RA have been found to have elevated levels of agalactosylated serum IgG[123], with increases of as much as 117% in serum IgG G0 glycoform detected[123]. Further examination reveals that the IgG Fc is hypogalactosylated whereas the Fab galactosylation level remains normal[83]. A similar study found that an increase in IgG G0 glycoform is also present in a small number of other inflammatory

diseases, including tuberculosis and Crohn's disease[124]. Interestingly, pregnant RA women, who normally experience disease remission, show increased IgG galactosylation before reverting back to hypogalactosylation after giving birth[125]. The cellular mechanism behind this increased IgG G0 level has been found to be due to lower galactosyltransferase activities in B cells[126; 127]; however, this does not fully explain the selective agalactosylation of the Fc region. A suggested pro-inflammatory mechanism of RA, mediated by the G0 glycoform, involves the binding of a cluster of Fc G0 glycoform to the mannose binding lectin (MBL), which subsequently activates the alternative complement pathway and leads to inflammation[128]. However, a study using MBL-deficient mice showed that MBL does not affect the pathogenesis of RA[129], indicating that observed *in vitro* interaction between Fc G0 glycoform and MBL might not be relevant under physiological conditions.

In contrast to its pro-inflammatory roles, a more recent study reveals an anti-inflammatory pathway that requires Fc galactosylation. In this newly proposed anti-inflammatory pathway, immune complex formed by IgG1 with high level of Fc galactosylation promotes the potential association of the inhibitory FcγRIIB and dectin-1, a C-type lectin, which subsequently triggers an inhibitory signalling cascade[130]. While the 3-arm galactose is entirely solvent exposed, the 6-arm galactose could form multiple electrostatic interactions with amino acid residues within the Cγ2 domain[99]. A comparison of the galactoses on different Fc crystal structures reveals the existence of two galacotose conformations (Fig. 1.12). In one conformation, the oxygen within the galactose ring points towards the Fc Cγ2 protein surface (Fig. 1.12A); however, the conformation of this galactose deviates from the putative galactose conformation, indicating a potential misconstruction of this particular monosaccharide. In the other conformation, the oxygen within the galactose ring points away from the Cγ2 protein surface (Fig. 1.12B); interestingly, this galactose conformation is

associated with α2,6-sialylation (sialic acid not shown in Fig. 1.12B for clarity). The functional significance of the multiple conformations awaits elucidation.

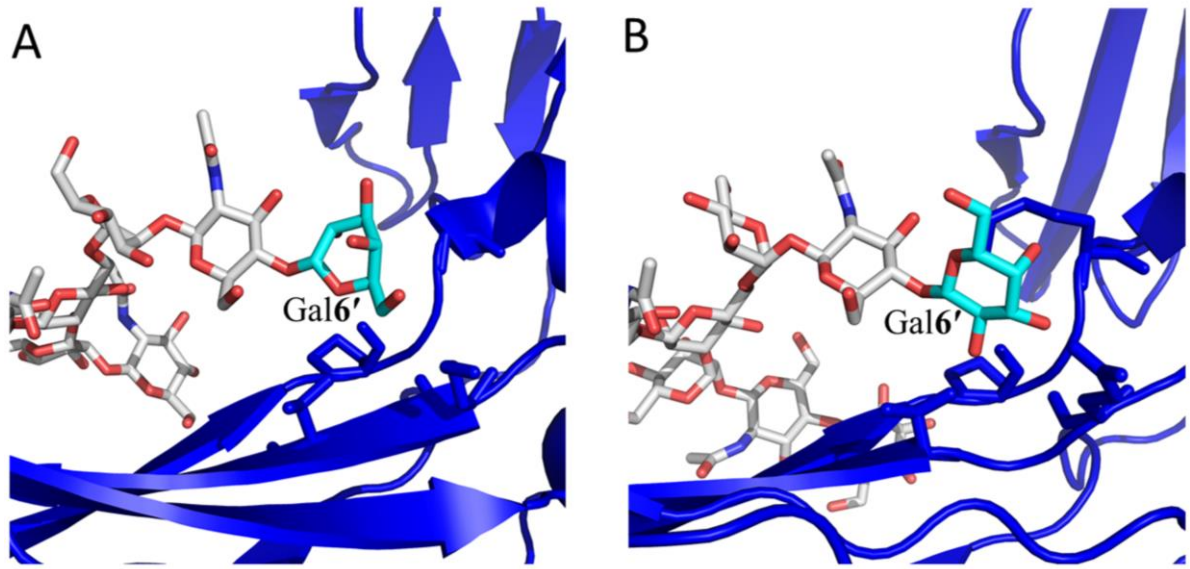

Figure 1.12. Multiple orientations of the 6-arm galactose. The IgG1 Fc Cγ2 domain protein backbone is shown in blue cartoon representation. The *N*-glycan is shown in grey stick representation, while the 6-arm galactose (Gal**6′**) is shown in cyan. Selective residues close to the Gal**6′** is shown in blue stick representation. (A) Snapshot of Cγ2 domain with Gal**6′** pointing towards Cγ2 domain protein surface (PDB ID 1H3Y). (B) Snapshot of Cγ2 domain with Gal**6′** pointing away from Cγ2 domain protein surface (PDB ID unavailable, manuscript containing this sFc structure submitted in May 2013). The image is generated using Pymol Molecular Graphics System, DeLano Scientific LLC.

1.5.4. Terminal Sialylation

Terminal sialylation occurs in about 10% of serum IgG Fc glycan[4; 83], normally in α2,6-linkage[131]. It has been shown that, sialylation, regardless of linkage type has been shown to decrease Fc binding affinity for the human FcγRIIIA[132], and the murine FcγRIIB, FcγRIII and FcγRIV by at least 10 folds[133]. This decreased binding affinity correlates with decreased *in vivo* activities of hypersialylated monoclonal antibodies[132; 133]. It has been speculated that the addition of a bulky sialic acid residue at glycan terminus might impact the structure of the

Fc hinge that modulates FcγRs binding[132; 134; 135]. IgG Fc terminal glycan sialylation is regulated by the immune system. For example, active immunization was found to decrease the level of antigen-specific IgG Fc sialylation by 40%, an effect restricted to IgG but not IgM[133]. Moreover, a pro-inflammatory milieu during immunization favors the generation of antigen specific IgG with lower Fc sialylation and vice versa[136]. However, this immunization-mediated decrease in antigen specific IgG Fc sialylation, observed in mouse models, does not seem to translate into human trials[137]. In addition to modulating Fc binding to FcγRs, Fc sialylation, in an α2,6-linkage-specific manner, has been shown to exert anti-inflammatory properties in mice[23; 133; 138]. In fact, the α2,6-sialylated Fc fraction has been determined to be the active component of the IVIg[133], a common therapeutic used to treat a range of autoimmune conditions[139]. Moreover, recombinant hyper-α2,6 sialylated IgG Fc (sFc), at a 10-fold less dose than the clinical IVIg, has been shown to recapitulate the therapeutic effect of IVIg in autoimmune mouse models[138].

1.5.5. Terminal Mannose

Oligomannose glycoforms form a small fraction of total IgG Fc glycoforms. Some high mannose glycoforms, including $Man_5GlcNAc_2$, generated using the GlcNAc Transferase I (GnTI-deficient) HEK 293S cell line, and $Man_9GlcNAc_2$, generated by adding the α-mannosidase inhibitor Kifunensine to cell culture, have been shown to enhance Fc affinity for the FcγRIIIA but decrease Fc affinity for the FcγRIIB compared with native complex type glycoforms[140; 141]. The increased affinity for the FcγRIIIA is mainly attributed to the lack of core fucose on high mannose Fc glycoforms[140], a property known to dramatically increase Fc affinity for the FcγRIIIA[110]. Moreover, the $Man_9GlcNAc_2$ glycoform has been shown to bind FcγRIIIA with approximately 20% higher affinity than $Man_5GlcNAc_2$ glycoform, indicating a role of the outer branch α1,2-linked mannose in modulating Fc-FcγR interaction[140].

In addition, oligomannose glycoforms have been shown to increase Fc clearance in the serum[142; 143], possibly through increased interaction with mannose binding receptors on cell surfaces. On the other hand, contradictory data show that the observed faster clearance of the oligomannose Fc glycoform is due to trimming of the oligomannose by serum mannosidases, a phenomenon captured by incubating oligomannose Fc glycoform in human serum[144]. Studies using radiolabelled antibodies show that oligomannose Fc glycoforms have similar clearance rate with other glycoforms; however, terminal mannose, as well as terminal galactose, increase the amount of Fc catabolized in the liver, an observation that has not been reported before[145].

1.5.6. Complement Activation

Fc glycosylation has been shown to be indispensable for the effective binding of Fc to C1q and complement activation[31; 89; 103]. Various Fc glycoforms exhibit different affinities for C1q and differential efficacy in activating complement dependent cytotoxicity[140]. Complex type glycoforms, regardless of their fucosylation status, activate the complement pathway more efficiently than hybrid or oligomannose glycoforms[140]. Moreover, terminal galactosylation has been found to increase C1q binding[146]. Fc glycan forms extensive hydrophobic and electrostatic interactions with the Fc protein backbone[87; 95; 118]. When this hydrophobic interaction is disrupted by mutating one of the hydrophobic residues, a significant increase in terminal galactosylation and sialylation was observed[87; 95]. The increased terminal processing was accompanied by decreased Fc affinity for the C1q, and reduced Fc mediated complement activation[87]. However, this impaired, Fc-mediated complement activation, could not be reproduced in another study using the murine IgG2a[147], compared with human chimeric IgG3 used in the previous report[87]. These contradictory results might be due to the different species origins of IgG used, and the different types of sialic acid, *N*-acetylneuraminic (Neu5Ac) acid or *N*-glycolylneuraminic acid, present on Fc glycan. Thus, further investigation is needed to

confirm the influence of increased glycan flexibility and terminal sialylation on Fc-C1q interactions. Besides directly influencing Fc binding to C1q, the Fc terminal GlcNAc**5** and GlcNAc**5'** residues have been shown to bind the MBL and indirectly activate the alternative complement cascade, a mechanism proposed to explain the inflammatory RA associated with decreased Fc galactosylation[148; 149]. However, as discussed in section 1.5.3, the *in vivo* effect of this agalactosylated Fc-MBL interaction might be insignificant[129].

1.6. Fc Glycoengineering to Modulate IgG Effector Functions

1.6.1. Defucosylation

The correlation identified between Fc glycoforms and their effector functions enables the design and generation of Fc variants with desired functions. Post-translational modification of Fc glycan by enzymatic treatment presents a convenient method to generate different glycoforms. In addition, genetically engineered cell lines have proven to be the most efficient platform. For example, the recently described yeast strain *Pichia pastoris,* whose *N*-glycosylation pathway has been heavily genetically modified, proves a promising new platform for the generation of precisely defined Fc glycoforms[150].

Defucosylation has generated much interest in the therapeutic area due to its ADCC-enhancing effect. A number of approaches have been used to generate defucosylated antibodies[24; 77; 115; 117; 118; 151]. To date, the most efficient method utilizes the FUT8 CHO cell line, which produces 100% defucosylated antibodies[151; 152]. A number of defucosylated therapeutic monoclonal antibodies, whose natural biantennary complex glycoforms are approved for medical uses in humans, have been generated to increase the efficacy of their Fc dependent-functions. For example, defucosylated 2G12, an anti-human immunodeficiency virus (HIV1) antibody, exhibits enhanced antiviral activity *in vitro*[115]. Moreover, the defucosylated version of rituximab, an anti-CD20 monoclonal antibody used for treatment of

B cell lymphoma via ADCC, exhibits greater than 100-fold enhanced cytotoxicity against a human $CD20^+$ B lymphoma cell line[153]. Furthermore, the defucosylated anti-Her2 monoclonal antibody trastuzumab, also known as Herceptin, showed 10-fold increase in cytotoxicity against a breast cancer cell line *in vitro*[112]. Both defucosylated rituximab and trastuzumab were generated in the FUT8 deficient CHO cell line. In addition to modulating the level of core fucose, various other glycoforms, which normally constitute a minor fraction of IgG glycan pool, could be generated using both genetic engineering and *in vitro* modulation of the cell culture medium as mentioned in section 1.4. For example, overexpressing the GlcNAc Transferase III, which adds the bisecting GlcNAc to the central β-mannose, in HEK 293-EBNA cells, allowed the production of highly bisected Fc glycoform with increased ADCC resulting from decreased core-fucosylation[109; 154]. Among these approaches, defucosylated monoclonal antibodies show most promise in improving some clinical therapeutics in the immediate future.

1.6.2. Deglycosylation

The deglycosylation-mediated abolition of Fc-mediated effector functions has been explored therapeutically in treating antibody-mediated autoimmune diseases. One such strategy involves the competitive antigen binding between a recombinant deglycosylated monoclonal antibody and an endogenous autoimmune antibody that share the same antigen specificity. As the antigen specificity and serum half-life are generally unaffected by Fc deglycosylation, the deglycosylated monoclonal antibody could thus reduce the effective concentration of endogenous autoimmune antibodies; this concept has been proven in murine disease models including antibody-mediated platelet depletion[155] and Aβ-mediated Alzheimer's disease[156]. In addition, a recent report showed that the selective deglycosylation of serum IgG Fc, by treatment with endoglycosidase S (EndoS), could significant enhance the binding of an antigen-specific, EndoS-resistant, monoclonal antibody to the FcγRIIIA in an *in vitro* assay

that mimics the serum environment[104]. This selective deactivation of serum IgG Fc could potentially enhance the efficacy of therapeutic monoclonal antibodies whose effector functions are mediated through FcγRs.

Following the pioneering research on the Fc protein-glycan interface, led by Lund and colleagues in 1996[87], part of this thesis continues to explore the role of hydrophobic residues on the protein-glycan interface at the IgG1 Fc Cγ2 domain. In addition to the known increased glycan terminal processing, the role of the hydrophobic protein-glycan interface in Fc-FcγRs interaction is examined.

1.7. Molecular Mechanism of Anti-inflammatory IVIg

1.7.1. Overview

IVIg consists of pooled human serum IgG and has been used as a primary means of treating various autoimmune conditions including multiple sclerosis, RA, chronic inflammatory demyelinating polyneuropathies, immune thrombocytopenia (ITP) and Kawasaki syndrome[23; 157; 158; 159; 160]. This anti-inflammatory property emerges as a relatively novel and distinctive property of IgG. In contrast to the well-established Fab-mediated antigen binding and Fc-mediated effector functions, the mechanism behind the anti-inflammatory IVIg remains controversial and elusive despite being used as a therapeutic agent since 1981[161]. Several components of the immune system to which IgG interact with, including the complement molecules and various Fc receptors, along with different parts of the IgG molecule, including the Fab and Fc domains, have been examined for their roles in the IVIg-mediated anti-inflammation.

1.7.2. Complement System

The complement system is an important component of the innate immune system, and IVIg has been found to bind certain complement molecules[23]. Indeed, IVIg has been shown to improve dermatomyositis, a syndrome partially mediated by the complement deposition of C5b-C9, through interaction with C3b[162]. Moreover, IVIg has been shown to inhibit deposition of early complement components C4b and C3b onto cell surfaces[163], which would serve to pre-empt complement-mediated inflammation. Despite these interactions between IVIg and the complement molecules, the complement system is not essential in the pathogenesis of all known murine autoimmune diseases including ITP and RA[23]. Moreover, the inactivation of the complement system, either via deletion of the complement receptors or depletion of complement molecules, has no impact on IVIg activity improving ITP in mouse[10; 164; 165]. Therefore, the anti-inflammatory IVIg is unlikely to act through the complement system.

1.7.3. FcRn Saturation by IVIg

The FcRn is a cell surface receptor expressed on a range of tissues including myeloid-derived antigen presenting cells. FcRn binds and recycles serum IgG to prevent IgG degradation, which explains the extended half-life of serum IgG compared with other isotypes[38]. In normal healthy individuals, serum IgG circulates at approximately 12 mg/mL; the injection of IVIg, used at 2-3 grams per kilogram body weight[23], would effectively increase the total serum IgG concentration by approximately 2 folds. Therefore, one hypothesis of the anti-inflammatory mechanism of IVIg is that the high level of exogenous IVIg saturates the FcRn and decreases the half-life of endogenous serum IgG, which would include the pathogenic autoantibodies, to reduce pathology[166; 167; 168]. For example, in a rat ITP model, induced using the anti-platelet monoclonal antibody 7E3, IVIg dose-dependently increases the clearance rate of this

monoclonal antibody *in vivo*, shown not to be due to direct IVIg-7E3 interaction[166], but as a result of IVIg-mediated FcRn saturation[167]. The increased clearance rate of pathogenic antibody post-IVIg injection was also recapitulated in murine models of autoantibody mediated cutaneous bullous diseases (autoimmune skin blistering diseases)[168]. Moreover, IVIg does not provide additional protection if these mouse models used were FcRn deficient[168]. For some animal models, the FcRn is essential for the induction antibody-mediated autoimmunity, such as a murine model of serum transfer RA[169]. However, some argue that FcRn deficient mouse would result in a faster clearance of the IVIg as well pathogenic antibody, thus under-estimating the apparent IVIg dose injected[23]. While these mouse models support an FcRn-dependent mechanism of IVIg, a number of reports present contradictory results. For example, aglycosylated IVIg, known not to affect IgG-FcRn interaction[30], does not confer protection in the RA mouse model[133; 170], which suggests that IVIg-mediated FcRn saturation is not sufficient for the anti-inflammatory IVIg effect. In addition, FcRn was shown to be redundant in an IVIg-mediated amelioration of mouse ITP model[171]. The same group demonstrates that the amount of exogenous anti-platelet antibody bound to platelets in the FcRn deficient mouse remains virtually the same compared with the wild type, and the presence of IVIg does not affect this binding[171]. Taking all these experiments into consideration, FcRn might not be involved in IVIg-mediated anti-inflammation; however, more animal models and methodologies need to be examined before any conclusion could be made.

1.7.4. Fab Mediated Self-Antigen Binding

The IVIg has been shown to bind numerous self-antigens including cell adhesion molecules[172], Deoxyribonucleic acid (DNA)[173; 174], the death receptor CD95[175], the sialic acid-binding immunoglobulin-type lectins 9 (siglec9)[176], anti-idiotype antibodies[177; 178] and various others[23; 179; 180]. This polyclonality suggests a potential role of Fab-mediated

autoreactivity in the anti-inflammatory IVIg. Some of these antigen-specific antibodies have been evaluated for their contribution towards anti-inflammation. The most well-established study involves the anti-CD95 antibody present in IVIg preparations. The death receptor CD95, also known as Fas, is present on the keratinocytes, and binding of Fas to its soluble Fas ligand induces keratinocyte apoptosis[181], which is also the underlying cause for the toxic epidermal necrolysis. The anti-CD95 antibodies found in IVIg have been shown to reverse the disease progression of patients with toxic epidermal necrolysis[175]. Moreover, IVIg depleted of CD95-specific antibodies could not ameliorate Fas-mediated keratinocyte apoptosis[175]. Another *in vitro* experiment supporting the requirement of Fab shows that Fab fragments, derived from IVIg, inhibit the toll-like receptors (TLR-4) mediated human DC activation as efficiently as whole IVIg[182]. Despite the identification of various self-reactive antibodies in IVIg, the cellular and *in vivo* effects of each self-reactive antibody require further investigation in order to determine their contribution to the anti-inflammatory effect of IVIg.

1.7.5. Fc Mediated Activatory FcγRs Blockade and Inhibitory FcγRIIB Upregulation

The Fc region of IVIg has been proposed to saturate the activatory FcγRs and block induction of antibody Fc-mediated autoimmune diseases. Several FcγRs have been identified to be central for disease induction in various autoimmune disease models. For example, the FcγRIII is essential for disease induction in mouse ITP and inflammatory RA[10; 164; 183; 184]. In humans, ITP pathogenesis also requires FcγRIII[185; 186]. In constrast, the high affinity FcγRIA seems to be dispensable for the ITP pathogenesis in both humans and mice[23]. While the FcγRs-blocking hypothesis seems to be plausible, the fact that monomeric IgG, which accounts for 97% of IVIg preparations[23], does not normally bind low affinity FcγRs counts against it[9] . It is well established that only in the form of immune complex could IgG bind and activate low affinity FcγRs[9]. Nevertheless, it is possible that the small fraction of

multimeric IgG in IVIg preparation contain anti-inflammatory activity[23]. Previous reports showed that aged IVIg preparations, which contains about 10% dimeric IVIg, is more effective in ameliorating ITP in mouse than fresh IVIg preparations, although the interaction between dimeric IVIg and FcγRs was not accessed in that study[164]. Moreover, multimeric IgG generated *in vitro*, by crosslinking IgG Fc domains, could protect mouse from ITP at one seventh of the dose of normal IVIg[187]. Remarkably, the injection of *in vitro* derived ovalbumin-IgG immune complex could dose-dependently protect mouse from ITP, to a similar level as the IVIg control[165]. This therapeutic effect of exogenous immune complex could be extended to albumin-IgG and transferrin-IgG immune complexes[165]. While it is unclear whether the soluble immune complex-mediated amelioration of autoimmune diseases share the same molecular pathway as the anti-inflammatory IVIg, the immune complex formed between IgG and soluble antigens represents a novel anti-inflammatory therapy [188; 189]. In the light of this finding, various multimeric IgG Fc constructs, generated by protein engineering, have been developed and shown to ameliorate murine RA, ITP and inflammatory neuropathy[190; 191].

While several activatory FcγRs exist, the FcγRIIB is the only inhibitory FcγR in both humans and mice[9]. Therefore, upregulating FcγRIIB will contribute towards an anti-inflammatory state. Indeed, the FcγRIIB has been shown to be essential for the IVIg-mediated protection in the ITP[10; 192], RA[40; 169; 184], and nephrotoxic nephritis[193]. Moreover, IVIg treatment increases the expression of FcγRIIB by 60% on splenic macrophages in a mouse ITP model[10] and 170% in a mouse RA model[184]. However, a direct interaction between IVIg and the FcγRIIB is unlikely due to its low affinity for the monomeric IgG.

1.7.6. Fc Glycan-dependence of Anti-inflammatory IVIg

The Fc domain, but not the Fab domain, of IVIg, has been shown to retain the anti-inflammatory activity of IVIg in human ITP[194] and murine models of ITP, RA and nephrotoxic nephritis[10; 133; 184; 193]. Furthermore, the *N*-linked Fc glycan has been shown to be indispensable for the IVIg effect, as deglycosylation of Fc abrogates the anti-inflammatory IVIg[133; 195]. Further glycan analysis identifies sFc to be the active component of IVIg in mouse models of ITP and RA, and neuraminidase treatment of IVIg abrogates its activity[133; 170; 196]. In addition, the type of linkage that confers IVIg efficacy is restricted to the α2,6-linkage, as IVIg enriched for the α2,3-linked sialic acid does not show any IVIg efficacy[133; 138]. IVIg enriched for the α2,6-sialylation, using the α2,6-Neu5Ac-specific lectin, *Sambucus nigra* (SNA), has been shown to achieve the same protection from RA in mice as non-enriched IVIg, at just one tenth of the dose[133]. A recombinant hypersialylated IgG Fc, generated by *in vitro* galactosylation and sialylation, has been shown to recapitulate the anti-inflammatory IVIg effect in RA mouse model[40; 138], which represents an improved form of traditional IVIg preparation. Despite the *in vivo* activity of the SNA-enriched α2,6-sialylated IVIg, several reports show that the SNA selectively enriches IVIg with α2,6-sialylated Fab region rather than α2,6-sialylated Fc region[197; 198; 199]. Moreover, both SNA-enriched and depleted IVIg fractions could equally protect herpes simplex virus (HSV)-induced encephalitis and ITP in mice[195; 199]. Furthermore, several groups report the sialic acid-independent IVIg effect in the fatal HSV-induced encephalitis and ITP mouse models[195; 200]. Some of these apparently contradictory results may be explained by the fact that different mouse strains respond differentially to IVIg treatment, as is the case for the ITP model[170; 200; 201; 202].

1.7.7. DC-SIGN as The Receptor for α2,6-sialylated Fc

The cellular receptor for the α2,6-sialylated Fc has recently been identified to be the murine SIGN-R1 of which the human orthologue is DC-SIGN[39]. The direct interaction between sFc and the DC-SIGN was initially inferred from the ability of DC-SIGN-transfected CHO cells to deplete sFc from cell culture supernatant[39], and more recently confirmed by the ability of sFc to directly bind DC-SIGN-transfected CHO cells compared with non-sialylated Fc[135]. Consistent with the requirement of α2,6-linkage for IVIg activity *in vivo*, α2,3-sialylated Fc was not depleted from cell supernatant[39]. A number of *in vivo* experiments support this central role of DC-SIGN. For example, antibodies which down-regulate or block the carbohydrate recognition domain (CRD) of SIGN-R1 abolish the effect of IVIg in ITP and serum-induced RA models[39; 170]. Removal of SIGN-R1 removes the effect of IVIg in serum-induced RA model whereas subsequent knock-in with DC-SIGN restores efficacy[39; 40]. In a transgenic mouse model of IVIg wherein SIGN-R1 was replaced by DC-SIGN, the introduction of sFc induces the expression of immunoregulatory cytokines, interleukin (IL)-4 and IL-33, and exogenous addition of either of these cytokines can offer protection similar to that seen for IVIg[40]; moreover, macrophages or DCs from human DC-SIGN transgenic mice pulsed with either sFc or IVIg can reverse RA. Notably, the efficacy of these introduced cells required that the recipient mouse was competent for FcγRIIB, IL-4, and IL-4 receptor[40]. This sFc-dependent and DC-SIGN-mediated anti-inflammatory effect is suggestive of a novel immunosuppressive pathway[40] (Fig. 1.13). In addition to sFc, a number of antigens have been shown to activate immunosuppressive pathways through direct interaction with DC-SIGN, including the salivary gland protein salp15 from the insect Ixodes ticks[203] and the HIV1 surface envelope glycoprotein gp120[204; 205].

Although significant immunological data support a central role for DC-SIGN/SIGN-R1 in many of the anti-inflammatory effects of IVIg[39; 40; 170], current biophysical data of DC-SIGN,

from glycan array studies, X-ray crystal structures (Fig. 1.14), and from solution-phase binding assays, do not suggest an obvious binding mechanism between sFc and DC-SIGN[206; 207; 208]. The well resolved CRD of DC-SIGN readily explains the selective, calcium-dependent binding to D-mannose, L-fucose and *N*-acetyl-D-glucosamine residues but does not reveal a likely binding site for sialic acid[206]. Similarly, glycan-array binding data indicate that sialylated biantennary *N*-linked glycan structures found on IgG Fc are not ligands for DC-SIGN or SIGN-R1[209; 210]. The interaction between DC-SIGN and sialylated IgG lies at the nexus of the current model of the IVIg pathway(s), and represents a key target for therapeutic exploitation. To date, however, no direct, controlled, binding measurements of this interaction have been reported. In this thesis, the direct interaction between the full soluble domain of tetrameric DC-SIGN and sFc, and its glycoform-dependence were extensively re-evaluated by direct biophysical measurements using recombinant glycoproteins.

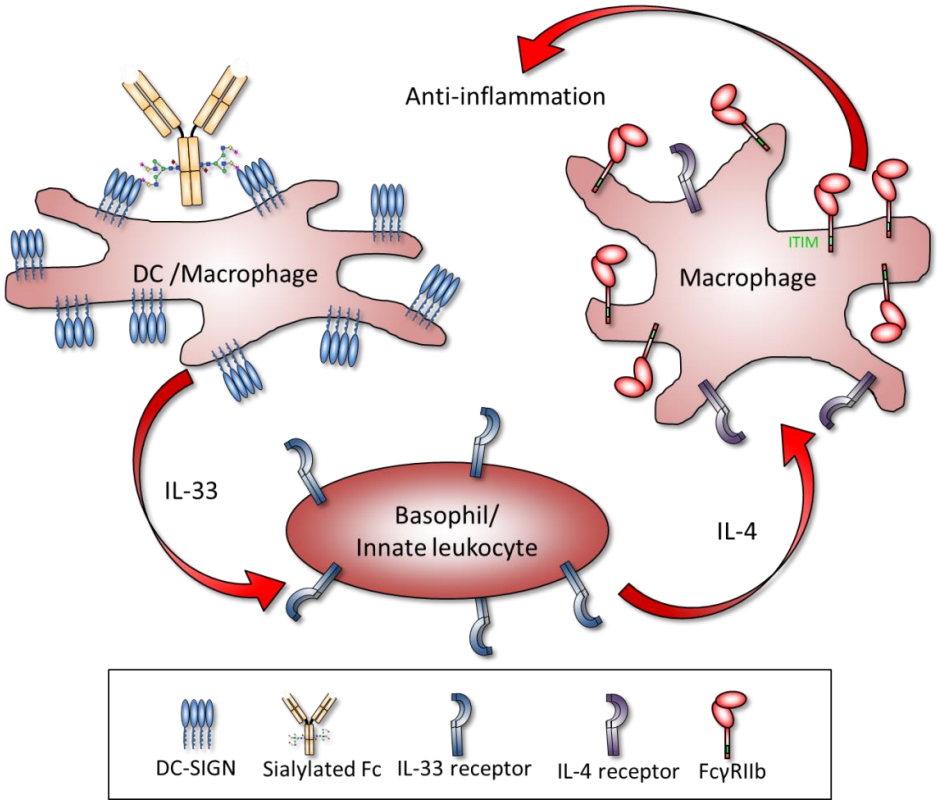

Figure 1.13. Current molecular model of anti-inflammatory IVIg mediated through sFc. The sFc initiates IVIg-mediated anti-inflammation via a T-helper type 2 (TH_2) response. The binding of sFc to the C-type lectin DC-SIGN on DCs or macrophages induces cellular secretion of IL-33, which in turn prompts basophils to produce IL-4, a cytokine that upregulates the inhibitory FcγRIIB level on macrophages. Upregulation of FcγRIIB, signalling via the inhibitory ITIM motif (green box), promotes anti-inflammation. Figure drawn based on results reported by Anthony *et al*, 2011[40] and 2012[211].

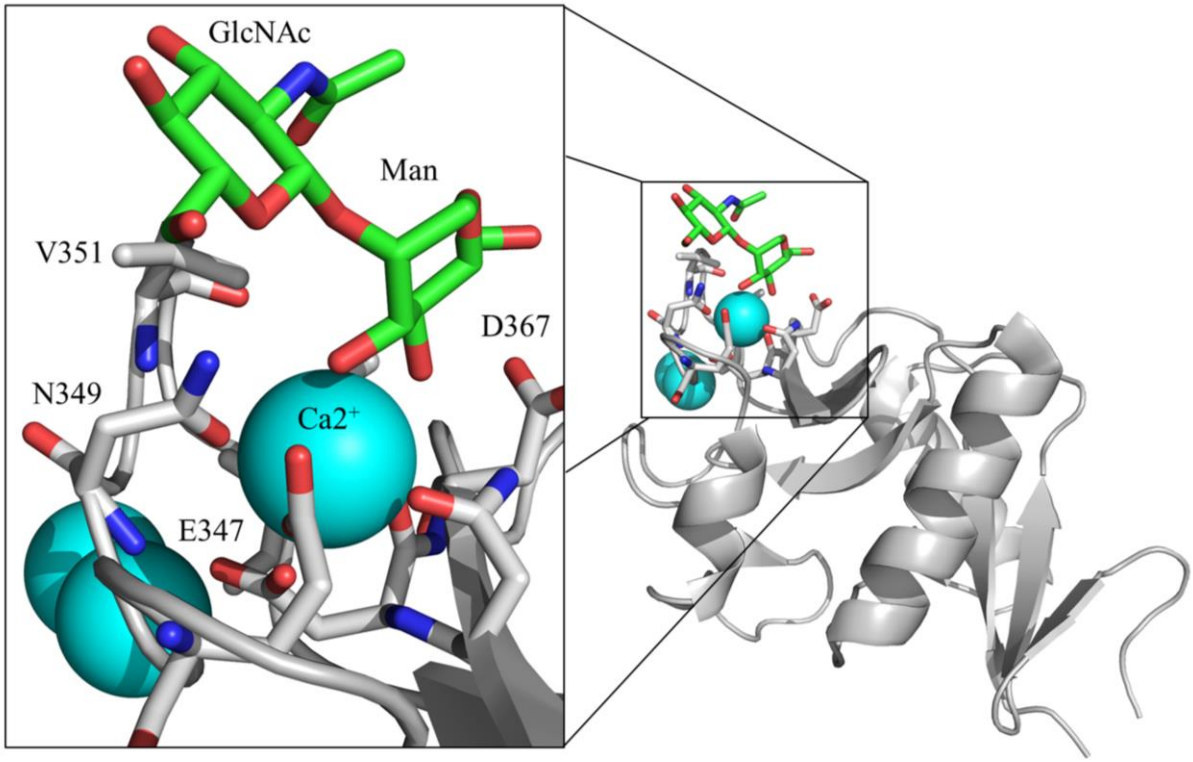

Figure 1.14. Structure of monomeric extracellular domain of DC-SIGN in complex with the oligosaccharide $GlcNAc_1Man_1$ (PDB ID 1K9I). DC-SIGN is shown in grey ribbon representation, the DC-SIGN ligand $GlcNAc_1Man_1$ is shown in stick, and the calcium cations are shown in cyan sphere. The detailed DC-SIGN CRD domain in complex with $GlcNAc_1Man_1$ is shown on the left panel. Selective residues on DC-SIGN CRD important for carbohydrate binding are labelled. The image is generated using Pymol Molecular Graphics System, DeLano Scientific LLC.

1.8. Effect of IVIg on Different Immune Cell Populations *in vitro*

1.8.1. Overview

IVIg has been shown to affect the cytokine profile and activation states of different immune cell populations[212; 213]. Cells of both innate and adaptive immune arms are affected by IVIg. Given that immune responses are regulated by the antigen presenting cells such as DCs and macrophages, it is possible that the observed IVIg-effect on the adaptive immune system is indirectly mediated by the innate immune cells, particularly the antigen presenting cells.

1.8.2. Effect of IVIg on Innate Immune Cells

DCs act as the sentinels of the immune system by ingesting and presenting antigens to the effector arms of the immune system[214]. DCs primed with IVIg *in vitro* has been shown to improve inflammation in recipient mice inflicted with ITP[215; 216] and RA[40]. IVIg has been shown to prime DCs for an immunosuppressive state. For example, treating immature DCs (imDCs) with IVIg at a dose similar to the physiological level not only dramatically decreased activatory surface markers, including CD1a, CD40, CD80 and CD86, but also became refractory to lipopolysaccharide (LPS) mediated maturation[180; 217]. Furthermore, IVIg decreases the DC cell surface expression of FcγRIIA while the FcγRIIB level remains unaffected[64]. In addition, pre-treatment of DCs with IVIg was found to decrease LPS-mediated secretion of inflammatory IL-12p70 and TNF-α and increase LPS-mediated secretion of the immunosuppressive IL-10[180]. Similarly, using the *ex vivo* whole blood assay, IVIg was found to decrease the LPS and Phytohemagglutinin (PHA)-mediated upregulation of CD54, a cellular adhesion molecule upregulated upon inflammation, on monocytes; and also decrease monocyte chemotactic protein-1 (MCP-1), an inflammatory chemokine detected in supernatant[198]. This IVIg-mediated anti-inflammatory effect was sialic acid-dependent and could be recapitulated with SNA-enriched sialylated Fab fragments, but not sialylated Fc fragments[198]. Functionally, pre-treatment of DCs with IVIg inhibited interferon (IFN)-α-induced DC differentiation and DC-mediated autologous and allogeneic mixed leukocyte reactions[180; 217; 218]. IVIg was also found to regulate the expression of CD1 molecules, which is a family of lipid antigen presenting molecules, through the FcγRIIA[219]. In contrast to the high dose IVIg therapy that induces immunosuppressive DCs, IVIg corresponding to normal serum IgG concentration has been shown to maintain DCs in a differentiated state[220].

Similar to DCs, monocytes and macrophages treated with IVIg adopt an immunosuppressive state, shown partially by decreased levels of the activatory FcγRIA and FcγRIIIA[221]. As discussed in section 1.7.5, dramatic increase in the inhibitory FcγRIIB expression on macrophages after IVIg treatment *in vivo* was also observed, a phenomenon required for the IVIg-mediated protection in a number of mouse models[10; 40; 133; 184]. The Fc domain of IVIg was also found to inhibit the TNF-α and IL-1 production by rabbit macrophages of the peritoneal exudate cells[222]. Moreover, the LPS-induced IL-6 production, but not TNF-α, by monocytes was significantly inhibited by IVIg treatment[223]. Human neutrophils and eosinophils have been shown to undergo cell death after IVIg treatment under inflammatory conditions, an effect shown to be mediated by the anti-Siglec8 and anti-Siglec9 antibodies contained in the IVIg preparation[176; 224]. Furthermore, IVIg has been shown to inhibit neutrophil adhesion to endothelium to reduce neutrophil recruitment to inflamed areas in a mouse sickle cell disease model[225]. On the other hand, dimeric IgG and anti-neutrophil cytoplasmic antibodies contained in IVIg preparations have been shown to enhance neutrophil activation, which could antagonize the anti-inflammatory IVIg therapy[226; 227]. In addition, basophils were found to increase secretion of IL-4 in response to sFc via a novel immunosuppressive pathway essential for sFc-mediated protection in a mouse RA model[40] (Fig. 1.13), but not required for IVIg protection in mouse ITP model[170].

1.8.3. Effect on Adaptive Immune Cells

Although both B cells and T cells have been shown to be dispensable for IVIg-mediated protection in ITP and RA mouse models[39; 184; 196], their function and viability have been shown to be profoundly modulated by IVIg treatment[212]. These adaptive immune cells mediate important effector functions in the immune system, and their malfunction are underlying causes for a range of autoimmune and inflammatory diseases[228; 229]. B cells have been shown to selectively bind the sialic acid enriched fraction of IVIg, via the α2,6-sialic

acid binding siglec CD22 shown by fluorescent microscopy[230]. However, conflicting data show that the interaction between IVIg and B cell is independent of CD22 and the sialic acid on IVIg[196]. The contradicting results might be explained by the different detection methods used. The CD22-IVIg interaction has been shown to dramatically increase CD22 phosphorylation and induced B cell apoptosis[230]. The apoptotic effect of IVIg on B cells has also been reported by other groups[231; 232]. Moreover, IVIg has been shown to inhibit mitogen activated B cell activation and proliferation[233]. On the other hand, cytokine-induced B cell and hybridoma proliferation is not affected by IVIg[234]. Similar to that seen for B cells, IVIg primes T cells towards an immunosuppressive state[212]. IVIg has been shown to directly bind T cells[196; 235] and inhibits mitogen-induced T cell activation and proliferation[235; 236], while concomitantly induce the proliferation of forkhead box $P3^+$ T regulatory cells[237; 238]. Nevertheless, the inhibitory property of IVIg on mitogen-induced T cell activation was shown to be due to the polyreactivity of IVIg towards the mitogen[234; 239]; and mitogen- or T cell receptor-crosslinking-induced T cell proliferation could be suppressed by autologous IgG from a single donor[240]. The production of the stimulatory IL-2 by T cells was also dramatically reduced[236; 241], accompanied by increased apoptosis by IVIg[231; 242]. On the other hand, the production of immunosuppressive cytokines IL-10 and transforming growth factor-β by T cells were not modulated by IVIg[238].

1.9. Objectives

In this thesis, the influence of the Fc protein-glycan interface on Fc glycosylation and Fc-FcγRs interaction was evaluated, built on previously published Fc mutagenesis studies. Increasing the understanding of the role of Fc protein-glycan interaction on Fc-mediated biological functions could provide novel routes to generate antibodies with bespoke functions, such as antigen-specific immunosuppression and general anti-inflammation. Moreover, the

molecular mechanism of the anti-inflammatory IVIg was examined, with an emphasis on the Fc glycoform-dependence of this effect. Specifically, the proposed novel interaction between sFc and DC-SIGN was re-evaluated, and the effect of IVIg glycosylation on human DCs were investigated. Understanding the molecular basis of anti-inflammatory IVIg could lead to novel anti-inflammatory therapeutics.

Chapter 2

Materials and Methods

2. Materials and Methods

2.1. Molecular Cloning and Site-directed Mutagenesis

2.1.1. Source of Plasmids

Recombinant proteins cloned in this thesis include: human IgG1 Fc (Accession number: J00228); human FcγRIA (Accession number: BC152383), FcγRIIA (Accession number: BC020823; His131 variant), FcγRIIB (Accession number: NM_001190828), FcγRIIIA (Accession number: BC033678; V158 variant), and FcγRIIIB (Accession number: BC128562), rat α2,6-sialyltransferase (ST6GAL1) (Accession number: NP_001106815), mouse β1,4-galactosyltransferase (B4GALT1) (Accession number: BC053006), CD22 (Accession number: P20273), and CD33 (Accession number: BC028152). All recombinant proteins were cloned into the mammalian expression vector pHLSec that encodes a hexahistidine tag at the C-terminus, and has an AgeI and KpnI restriction site at the N-terminus and C-terminus respectively. The pFUSE vector encoding the constant region of human IgG1 heavy chain was purchased from InvivoGen, UK; vectors encoding the full length human FcγRs and mouse B4GALT1 were from Open Biosystems, UK; vector encoding the full length rat ST6GAL1 was a gift from Karen J Colley at University of Illinois, USA. The pHLSec vector containing the full length soluble ectodomain of the HIV1 $gp120_{Bal}$ (residues 1-507, numbering based on alignment with the HxB2 reference strain) was cloned as described before[243]. The plasmids encoding the heavy and light chains of IgG1 b12 antibody were gifts from Professor Ian A. Wilson at The Scripps Research Institute, USA. Unless otherwise stated, all accession numbers cited are cited according to the National Center for Biotechnology Information database.

2.1.2. Molecular Cloning

The sequence of forward and reverse primers used to clone the soluble region of each protein is listed in Table 2.1; all primers were purchased from Thermo Scientific, Germany. Each forward primer contains a restriction site for AgeI and each cloning reverse primer contains a restriction site for KpnI (or BsiWI), for insertion into the mammalian expression vector pHLSec with a hexahistidine tag. After polymerase chain reaction (PCR) amplification of the soluble region of each protein, the PCR products were separated using agarose gel electrophoresis, and then purified from the agarose gel using NucleoSpin Gel and PCR Clean-up kit (Macherey-Nagel, UK). The purified PCR product was then double digested with restriction enzymes AgeI and KpnI (or BsiWI) (New England Biolabs, UK) for 2 hours at 37^{o}C, followed by a clean-up using the NucleoSpin Gel and PCR Clean-up kit, and ligation with pHLSec vector (pre-digested with AgeI and KpnI and phosphatase-treated) using T4 DNA ligase (New England Biolabs, UK) for one hour at room temperature. After ligating the soluble region of each protein into the pHLSec vector, the plasmid was transformed into the XL-Blue Competent *E. coli* cells (Agilent Technology, UK) and selected for carbenicillin resistance. After overnight incubation at 37^{o}C, bacterial colonies were picked and grown overnight before plasmid extraction using NucleoSpin Plasmid kit (Macherey-Nagel, UK). The extracted pHLSec plasmids were verified by DNA sequencing (Source BioScience, UK). The forward sequencing primer of pHLSec vector is: 5′-GCTGGTTGTTGTGCTGTCTCATC-3′; and the reverse sequencing primer of pHLSec is: 5′-CACCAGCCACCACCTTCTGATAG-3′. The soluble region of CD22 was cloned by Dr Camille Bonomelli (University of Oxford). The soluble region of FcγRIIB was cloned by Snezana Vasiljevic (University of Oxford). The amino acid sequence of all recombinant proteins cloned could be found in Appendix D.

Table 2.1. Nucleic acid sequence of cloning primers.

Name	Cloned soluble region	Cloning primer sequence (5′-3′)
IgG1 Fc	225-447	Forward: ATACACCGGTCACACATGCCCACCGTGC Reverse: CGATGGTACCACCCGGAGACAGGGAGAGG
FcγRIA	16-288	Forward: ATACACCGGTCAAGTGGACACCACAAAGGC Reverse: CGATGGTACCAGGAGTTGGTAACTGGAGGCC
FcγRIIA	34-217	Forward: ATACACCGGTCAAGCTGCTCCCCCAAAG Reverse: CGATGGTACCCATGCTGGGCACTTGGAC
FcγRIIB	38-225	Forward: TGAAACCGGTGGGACA CCTGCA GCT Reverse: CATGGTACCAATGATCCCCATCGGTG
FcγRIIIA	16-288	Forward: ATACACCGGTGGCATGCGGACTGAAGATC Reverse: GCTGGTACCTTGGTAGCCAGGTGGAAA
FcγRIIIB	17-200	Forward: ATACACCGGTATGCGGACTGAAGATCTC Reverse: CGATGGTACCTGAGATGGTTGACACTGC
CD33	18-258	Forward: GCCACCGGTGATCCAAATTTCTGGCTGCAA Reverse: ATCGGTACCAACCACTCCTGCTCTGGTCTC
CD22	20-687	Forward: CCGCACCGGTGACTCAAGTAAATGGGTTTTTG Reverse: ATAACGTACGTCGCCTGCCGATGGTCTC
ST6GAL1	89-403	Forward: TACACCGGTTCCTTCCAGGTGTGGGAC Reverse: GCTGGTACCACAACGAATGTTCCGGAA
B4GALT1	127-399	Forward: TATACCGGTTCGCTGCCAGCTTGCCCTGAG Reverse: ATTGGTACCTCTCGGTGTCCCGATGTCCAC

The AgeI restriction site is highlighted in red; KpnI restriction site is highlighted in green; and BsiWI restriction site is highlighted in blue. Nucleic acid sequence upstream of the restriction site is flanking junk DNA.

2.1.3. Site-directed Mutagenesis

Site-directed mutagenesis of the IgG1 b12 was carried out using the Quikchange Lightening Kit (Agilent Technology, UK) according to manufacturer's protocol. The recombinant Fc mutagenesis was performed first in pFUSE vector, and then cloned into the pHLSec vector using the IgG1 Fc cloning primers listed in Table 2.1. The residue Cys339 of B4GALT1 was mutated to Thr, as previously described[244], using two-step PCR mutagenesis approach, to eliminate the uneven number of cysteine residues. The sequence of the forward primer containing the Cys339Thr mutation (highlighted in red) is: 5′-GCTGTAGTAGGGAGGACACGAATG-3′; and the sequence of the reverse primer

containing the Cys339Thr mutation (highlighted in red) is 5′-CATTCGTGTCCTCCCTACTACAGC-3′. Mutagenesis of each protein was confirmed by sequencing.

2.2. Large Scale DNA Preparation

Endotoxin-free maxiprep or megaprep (Qiagen, UK) was used to prepare cell culture grade DNA for mammalian cell transfection. Briefly, bacterium containing the plasmid DNA of interest was cultured overnight in 100 mL (for maxiprep) or 500 mL (for megaprep) of Luria Broth medium. After approximately 16 hours of shaking incubation, bacteria were pelleted, lysed and extracted for the plasmid DNA of interest according to manufacturer's protocol. The yield and purity of extracted DNA were assessed using a Nanodrop (Eppendorf, UK); and a ratio of absorbance at 260 nm and 280 nm above 1.8 was considered pure.

2.3. Protein Expression and Purification

2.3.1. Protein Expression

Recombinant proteins were expressed using the HEK 293T cells (ATCC number CRL-1573) or the HEK 293S cells, which is a GnTI-deficient derivative of HEK 293T cells[245]. HEK 293T and HEK 293S cells were cultured in Dulbecco's Modified Eagle's Medium (DMEM) supplemented with 10% fetal calf serum (FCS) and 1X penicillin-streptomycin (for HEK 293S cells, 1X non-essential amino acid was supplemented) (all reagents from Invitrogen, UK). Cells were grown to 90% confluence and transiently transfected with polyethyleneimine (PEI) (a gift from Dr Thomas A. Bowden, University of Oxford, UK), using a transfection mix with a DNA: PEI molecular mass ratio of 1:1.5. For IgG1 b12 transfection, the molecular mass ratio of light chain to heavy chain was 4:1. The transfection mix was incubated on a roller mixer for 30 minutes before being added to cell culture. Following transfection, cells

were grown in serum-free DMEM supplemented with 1X penicillin-streptomycin (for HEK 293S cells, 1X non-essential amino acid was further supplemented) at 37^{o}C, 5% CO_2 for 5 days before the cell culture supernatant was harvested by centrifugation, sterile-filtered and then diluted with one volume of phosphate-buffered saline (PBS). Proteins of homogenous $Man_5GlcNAc_2$ glycoform were derived by expression in HEK 293S cells[245]; and proteins of homogenous $Man_9GlcNAc_2$ glycoform were derived by expression in HEK 293T cells in the presence of 20 μM α-mannosidase inhibitor kifunensine (Cayman Europe, Estonia)[246]. Biotinylation of $gp120_{BaL}$ was carried out using the Sulfo-NHS-Biotin and Biotinylation Kits (Thermo Scientific, UK) according to manufacturer's protocol.

2.3.2. Protein Purification

Recombinant proteins encoded in the pHLSec vector were purified by immobilized metal affinity chromatography using Chelating Sepharose Fast Flow Ni^{2+}-agarose beads (GE Healthcare, UK). Cell culture supernatant was incubated on a roller mixer (Eppendorf, UK) with Ni^{2+} beads in the presence of 10 mM imidazole for 2 hours, and then pour through the Econo-Column Chromatography Column (Bio-rad UK) to retain the Ni^{2+} beads. The beads were then washed with at least 50 bead-volume of PBS 20 mM imidazole pH 8, and the Ni^{2+} bound proteins were eluted using 20 bead-volume of PBS 500 mM imidazole pH 8. Protein samples were further purified by size exclusion chromatography using a Superdex S-200 column (GE Healthcare, UK) equilibrated in PBS.

The IgG1 b12 antibody was purified by affinity chromatography using Protein A Sepharose (GE Healthcare, UK). Cell culture supernatant was incubated with Protein A Sepharose beads for 2 hours at room temperature, the beads were washed with at least 50 bead-volume of PBS before elution using 20 bead-volume of 0.1 M citric acid pH 3.4. The elution was immediately neutralized by adding 2M Tris and buffer exchanged into PBS. Protein purity

was assessed by Coomassie Blue-stained sodium dodecyl sulfate polyacrylamide gel electrophoresis (SDS-PAGE) analysis using 4-12% Bis-Tis gels (Invitrogen, UK). For protein reduction, protein samples were treated with dithiothreitol (DTT) and boiled for 5 minutes at 95^{o}C.

2.4. *In vitro* Modulation of IgG and Fc Glycosylation

Pooled human serum IgG and Privigen (clinical grade therapeutic IVIg) were purchased from Sigma, UK and CSL Behring Ltd, UK respectively. Protein deglycosylation and desialylation were achieved by incubation with PNGase F or linkage non-specific neuraminidase from *Clostridium perfringens* (both from New England Biolabs, UK) for 48 hours at 37˚C respectively. Hyper-α2,6-sialylated proteins were generated by first incubating with B4GALT1 in the presence of 80 μM Uridine 5'-diphosphogalactose (UDP-galactose) (Sigma, UK) in 50 mM (4-(2-Hydroxyethyl) Piperazine-1-Ethanesulfonic Acid) HEPES, 150 mM NaCl, 10 mM $MnCl_2$, pH7.5 for 48 hours at 37˚C. Afterwards, the hyper-β1,4-galactosylated IgG was treated with ST6GAL1 in the presence of 70 μM cytidine-5′-monophospho-*N*-acetylneuraminic acid (CMP-sialic acid) (Sigma, UK) in 50 mM HEPES, 150 mM NaCl, 10 mM $MnCl_2$, pH 6.5 for 48 hours at 37˚C. The antibody glycoform after each enzymatic treatment was verified by HPLC analysis. IgG deglycosylation was confirmed by a heavy chain band shift in SDS-PAGE.

2.5. *N*-glycosylation Analysis

2.5.1. Enzymatic Release of *N*-linked Glycans

Oligosaccharides were released from Coomassie Blue-stained SDS-PAGE gel bands as previously reported[247]. Gel bands were excised, washed 5 times with alternating acetonitrile and water, and air-dried. Each gel band was rehydrated with 30 μL of 30 mM $NaHCO_3$ pH

7.0 containing 500 units/mL PNGase F and incubated for 12 hours at 37°C[247]. The enzymatically released *N*-linked glycans were eluted with 150 μL of water after the gel band was vortexed vigorously.

2.5.2. Matrix-assisted Laser Desorption/Ionization Time-of-flight Mass Spectrometry (MALDI-TOF-MS) Analysis of *N*-linked Glycans

Aqueous solutions of the glycans (1 μL) were cleaned with a Nafion 117 membrane (Sigma, UK) for at least 3 hours[248]. Positive ion MALDI-TOF mass spectra were recorded with a Shimadzu-Kratos (Kratos Analytical, UK) AXIMA TOF2 instrument (nitrogen laser), using Reflection-DHB mode as described before[248]. The source voltage was 20 kV and the delayed extraction was optimized at m/z 1700. Samples were prepared by mixing 1 μL Nafion 117 membrane-cleaned sample solution with 0.5 μL of 2,5-dihydroxybenzoic acid (DHB) solution (7 mg/mL, DBH dissolved in acetonitrile and water 7/3, v/v) and 0.3 μL of aqueous NaCl solution (1 mg/mL) on the stainless steel target plate, and allowed to dry at room temperature. The dried sample/matrix mixture was then recrystallized by adding 0.2 μL ethanol, before insertion of the target plate into the machine. A list of mass and composition of commonly detected *N*-glycans (in their Na^+ conjugates) are shown in Appendix B.

2.5.3. High Performance Liquid Chromatography (HPLC) Analysis of *N*-linked Glycans

Glycans were labeled with 2-aminoanthranilic acid (2-AA) as described before[249] and separated using TSKgel Amide-80 column (Sigma, UK). Briefly, *N*-glycans dissolved in water were mixed with 2-AA labeling buffer (4% sodium acetate trihydrate, 2% boric acid, 3% 2-AA, and 4.5% sodium cyanoborohydride, dissolved in methanol) (3/8, v/v), and incubated for 1 hour at 80°C; excess 2-AA dye was removed using a Spe-ed Amide-2 column (Systematic Systems, UK) and 2-AA labeled glycan was eluted with water. HPLC was carried out in a linear gradient of solvents at room temperature. Solvent A was acetonitrile,

solvent B was MilliQ water, and solvent C was 800 mM ammonium hydroxide adjusted to pH 3.85 using acetic acid. Solvent C was in a constant gradient of 2.5% throughout the run. The gradient was a constant 71.6% A for 6 mins at a flow rate of 0.8 mL/min, followed by a linear gradient of 71.6-35% A over 80 mins at 0.8 mL/min. Afterwards, the gradient was a linear 35-71.6% A for 1 min at a flow rate of 0.8 mL/min; then at the same gradient, the flow rate increases from 0.8 mL/min to 1.2 mL/min over 1 minute and followed by the same gradient and flow rate for 13 minutes. The run finishes by returning the flow rate to 0.8 mL/min over 1 min, giving a total run time of 105 minutes. Fluorescence was detected at 425 nm and the excitation wavelength was 360 nm. All the chromatography instruments were controlled and collected data were processed by the Empower software (all instruments and software from Interlink Scientific Services Limited, UK). Assignments of glycan structures were confirmed by MALDI-TOF-MS, electrospray mass spectrometry (ES-MS) and exoglycosidase digestions. All ES-MS experiments and data analysis were carried out by Prof. David Harvey (University of Oxford).

This HPLC running protocol was used until Feb 2012, when the column was switch to LudgerSep N2amide HPLC column (Ludger, UK) to yield better resolution and shorten the running time. HPLC was carried out in a linear gradient of solvents at 30^{o}C. Solvent A was 50 mM ammonium formate buffer pH 4.4, solvent B was acetonitrile. The gradient was a linear gradient of 35-46% A over 22 minutes at 1 mL/min. Followed by a linear gradient of 46-100% A over 30 seconds at 1 mL/min. Afterwards, the gradient was a linear 100% A for 2 minute at a flow rate of 1 mL/min; then at a linear gradient of 100-35% A over 1 minute 30 seconds, followed by the same gradient for 4 minutes. The run finishes by a linear 100% A gradient for 16 minute, giving a total runtime of 46 minutes. Fluorescence and excitation wavelengths were 420 nm and 330 nm respectively. All the chromatography instruments were controlled and collected data were processed by the Empower software.

2.6. In-Gel Tryptic Digestion of IgG

Deglycosylated IgG were prepared using PNGase F. The in-gel digestion of native and hydrophobic IgG1 b12 mutants was carried out using the In-Gel Tryptic Digestion Kit (Thermo Scientific, UK) according to manufacturer's protocol. Gel bands containing IgG were excised and destained extensively, followed by reduction and alkylation. The gel slices were then digested with trypsin for 6 hours at 37˚C, and the peptides were extracted with 1% trifluoracetic acid (Sigma-Aldrich, UK). The trypsin-digested peptides were analyzed on a MALDI-TOF-MS instrument (Kratos Analytical, Manchester, U.K.), and α-Cyano-4-hydroxycinnamic acid (CHCA) (Sigma, UK) was used as the matrix, no recrystallization of the dried peptide was required. The tryptic peptide mass of the native and deglycosylated IgG were calculated online using the PeptideMass program at the ExPASy SIB Bioinformatics Resource Portal. A detailed MALDI tryptic peptide mass fingerprint of IgG1 b12 could be found in Appendix C.

2.7. Analysis of Protein-Protein Interaction

2.7.1. ELISA Analysis of Fc- FcγR Interaction

For the analysis of IgG/Fc-FcγR using ELISA, each receptor was coated at 5 μg/mL onto a high-binding mircotitre plate (Corning, UK) overnight at 4˚C. The next day, coated plates were washed with PBS containing 0.05% Tween 20 (Sigma, UK) and blocked for 2 hours at room temperature with 5% BSA in PBS. IgG/Fc was added onto designated plate and incubated for 1.5 hours. Binding of IgG and Fc to FcγRs was detected by horseradish peroxidase (HRP)-conjugated rabbit anti-human IgG Fab (1/2500) and HRP-conjugated rabbit anti-human Fc (1/25,000) (both from Thermo Scientific, UK) respectively. For comparing the binding affinity of IgG and Fc to the FcγRIIIA, binding of both IgG and Fc was detected by HRP-conjugated rabbit anti-human Fc (1/25,000). The quantity of each

IgG/Fc variant added during the 1.5-hour incubation step was controlled by additional experiments, in which IgG1 b12 and Fc were tested for their binding to gp120 and monoclonal anti-human Fc antibody respectively. The final affinity of IgG/Fc for FcγRs was adjusted for amount of each IgG/Fc variant added accordingly.

2.7.2. ELISA Analysis of Fc- DC-SIGN Interaction

The soluble tetrameric DC-SIGN, representing the full extracellular region of DC-SIGN, was a gift from Dr Daniel Mitchell at Warwick University, UK, and was coated at 5 μg/mL onto a high-binding mircotitre plate overnight at 4˚C. Coated plates were washed with DC-SIGN binding buffer (25 mM HEPES, 150mM NaCl, 3 mM $CaCl_2$, pH7.4) containing 0.05% Tween 20 (all from Sigma, UK) and blocked for 2 hours at room temperature with 5% BSA in DC-SIGN binding buffer. For direct binding assay, differentially glycosylated IgG, Fc and biotinylated $gp120_{Bal}$ were added and allowed to bind for 1.5 hours at room temperature. To compete with biotinylated $gp120_{BaL}$ binding to DC-SIGN, various monosaccharides (all from Sigma, UK), and serum IgG were added to wells containing 0.1 ng/mL biotinylated $gp120_{Bal}$ and allowed to bind for 1.5 hours at room temperature. Plates were washed five times with DC-SIGN binding buffer containing 0.05% Tween. IgG and Fc binding was detected using HRP-conjugated rabbit anti-human Fc (1/25,000) and biotinylated $gp120_{BaL}$ was detected using a HRP-conjugated streptavidin (1/8000) (Thermo Scientific, UK).

To compare the binding affinity of serum IgG for DC-SIGN and various nonspecific antigens including HIV1 $gp120_{Bal}$, fetuin, and BSA (Sigma, UK), each antigen was coated at 5 μg/mL onto a high-binding mircotitre plate overnight at 4˚C. Coated plates were washed with DC-SIGN binding buffer containing 0.05% Tween 20 and blocked for 2 hours at room temperature with 5% BSA in DC-SIGN binding buffer. Serum IgG was added and allowed to bind for 1.5 hours at room temperature. Plates were washed five times with DC-SIGN

binding buffer containing 0.05% Tween. IgG binding was detected using HRP-conjugated rabbit anti-human Fab (1/2500). For all ELISA experiments, the 3,3',5,5'-Tetramethylbenzidine (TMB) substrate (Thermo Scientific, UK) was used for colour development according to manufacturer's directions. Colour development was stopped by the addition of 2M H_2SO_4 (Sigma, UK) and absorbance was measured at 450 nm on a Spectramax M5 (Molecular Devices, California, U.S.A.) multiwell plate reader.

2.7.3. Surface Plasmon Resonance (SPR) Analysis of Fc-FcγR Interaction

SPR experiments were carried out on the BIAcore T100 instrument (GE Healthcare, UK). The recombinant soluble FcγRIIIA (Val158 variant) was immobilized onto the surface of CM5 sensor chip (GE Healthcare, UK) to approximately 1000 RU during each independent experiment. All experiments were carried out in the HBS-EP running buffer (10 mM HEPES, 150 mM NaCl, 3mM EDTA and 0.005% Surfactant P20), at a flow rate of 30 µl/min. The monoclonal IgG1 b12 protein and its glyco-variants were injected at 5 different concentrations, allowed 2 minutes for association, and 3 minutes for dissociation. After each run, the sensor chip was regenerated using 10 mM glycine-HCl, pH1.7. The sensorgrams were fitted to a global 1:1 interaction, and the k_{on}, k_{off}, and equilibrium dissociation constant K_D were calculated, all using BIAevaluation software 2.0.3 (GE Healthcare, UK).

2.8. *In vitro* Derivation of Human DCs

Peripheral human blood was drawn from healthy donors intravenously, following the ethical rules set by the Department of Biochemistry, Oxford University. Peripheral blood mononuclear cells (PBMCs) were isolated by Ficoll density gradient centrifugation techniques as described previously[250] using Lymphoprep solution (Axis Shield, UK). The ACCUSPIN Tubes (Sigma, UK) were loaded with 15 ml of Lymphoprep prior to the addition of 25 ml of peripheral blood, and centrifuged at 800G for 30 minutes (brake off) at room

temperature, followed by the careful removal of the buffy coat layer using pastettes. The $CD14^+$ monocytes were positively selected using anti-CD14 monoclonal antibodies coupled with magnetic beads according to the manufacture's protocol (Miltenyi Biotec, UK), and then cultured in six-well plates at $1x10^6$ cells/mL for 5 days in Roswell Park Memorial Institute (RPMI)-1640 medium supplemented with 10% FCS, 50 μg/mL gentamycin, 1X glutamine (Invitrogen, UK), 500 IU/mL rhIL-4 and 1000 IU/mL human recombinant granulocyte-macrophage colony-stimulating factor (rhGM-CSF) (both from R&D systems, UK). Medium was replaced by fresh medium with all the supplements every two days, and imDCs were derived after 5 days.

2.9. Effect of IVIg on Human Monocyte-derived DCs

2.9.1. Preparation of Endotoxin-free Protein Samples

Protein samples used in DC assays underwent endotoxin removal steps. The native IVIg, neuraminidase-treated IVIg, PNGase F-treated IVIg, and human serum albumin (HSA), were first purified through the Superdex S-200 gel-filtration column equilibrated in PBS. Care was taken to keep the environment as sterile as possible. After gel filtration, each protein sample was filtered through a 0.22 μm filter and then resuspended in approximately 20 mL PBS and treated with Triton X-114 (Thermo Scientific, UK) to remove endotoxin as described before[251]. Briefly, pre-diluted 10% Triton X-114 was mixed with protein samples in PBS at a ratio of 1:10 (v/v), so that the final concentration of Triton X-114 was 1%. The protein solution was mixed until the solution became clear, and then incubated on ice for 30 minutes, followed by incubation in a 37˚C water bath for 10 minutes until the solution became opaque. The solution was then spun at 4000 rpm for 10 minutes. The upper phase of the solution that contains the protein samples was carefully taken off, while the bottom phase Triton X-114 containing endotoxin was discarded. The cleaning step was repeated to further eliminate

endotoxin. The endotoxin level of every protein sample was checked using the Limulus amebocyte lysate (LAL) chromogenic endotoxin quantitation kit (Fisher Scientific, UK) according to the manufacturer's protocol.

2.9.2. Effect of IVIg Pre-treatment on LPS-mediated Maturation of DCs

The $CD14^+$ monocyte-derived imDCs were plated at $4x10^5$ cells/well on a 48-well plate. After pre-treating these imDCs with 0.15 mM IVIg, 0.15 mM neuraminidase-treated IVIg, 0.15 mM deglycosylated IVIg, or 0.15 mM HSA for 12 hours, cell culture supernatant was harvested and cells were washed once with media. All the harvesting and washing steps were carried out with great care, and the cell number in each well was checked by microscopy. The cells were then stimulated with 1 μg/mL LPS for an additional 24 hours. Cytokine analysis was carried out for cell culture supernatant harvested using Luminex Bio-Plex assays kit (Bio-Rad Laboratories, UK) and the Luminex 200 instrument (Bio-Rad Laboratories, UK).

2.9.3. Fluorescence Activated Cell Sorting (FACS) Analysis of DC Cell Surface Molecules

For cell surface molecule analysis, DCs were stained with anti-CD11c-FITC, anti-CD40-FITC, anti-CD80-FITC, anti-CD86-PE, anti-HLA-DR-PE and anti-CD14-PE (all are mouse antibodies, from BD Biosciences, UK), anti-CD33-PE, anti-CD22-PE, anti-Siglec 5-PE, anti-Siglec 7-PE, anti-Siglec 9-PE (all are mouse antibodies, from Biolegend, UK), according to manufacturers' recommended protocols. After being harvested from culture wells, cells were washed with staining buffer (PBS 0.5% FCS) twice, incubated with respective monoclonal antibodies for 30 minutes, and then washed 3 times before being resuspended in staining buffer for FACS analysis. FACS analysis was carried out using FACScalibur (BD Bioscience), and data analysis was carried out using BD CellQuest Version 5.2.1 software (BD Bioscience).

Chapter 3

Fc protein-glycan interaction and Fc *N*-glycosylation

3. Fc Protein-Glycan Interaction and Fc *N*-glycosylation

3.1. Summary

IgG1 Fc *N*-glycan forms abundant hydrophobic and electrostatic interactions with the Fc protein backbone at the Cγ2 domain[4; 81]. This protein-glycan interaction has been shown to be critical in restricting Fc glycan processing[4]. Lund and colleagues[87] first demonstrated that abolishing the hydrophobic or electrostatic interactions on the human-mouse chimeric IgG3 antibody, by site-directed mutagenesis, dramatically increased the Fc glycan terminal processing, most notably galactosylation and sialylation. A concomitant decrease in binding to the FcγRIA and the complement molecule C1q was observed. Several reports following that study[95; 96; 97] have since confirmed the role of Fc protein-glycan interaction in restricting Fc terminal glycan processing.

In this chapter, the impact of Fc protein-glycan interaction on Fc glycan processing was further explored by characterizing the full spectrum of Fc glycoforms resulting from the hydrophobic mutations. Moreover, the synergistic effect of multiple hydrophobic mutations on Fc glycan processing was examined. To this end, the human IgG1 b12, a HIV1-specific monoclonal antibody[252], and the recombinant human IgG1 Fc were used as a model for mutagenesis. The hydrophobic Fc mutants generated also provided a basis for the investigation of the role of Fc protein-glycan interface in Fc-FcγR interaction, which is discussed in Chapter 4.

3.2. Effect of Hydrophobic Mutations on Fc Glycoforms

3.2.1. Cloning, Expression and Glycan Analysis of IgG1 Fc

The recombinant Fc construct that encompasses the lower hinge region, Cγ2, and Cγ3 domains was cloned as described before[81] (protein sequence shown in Appendix D). The

plasmids encoding full-length human anti-HIV1 glycoprotein gp120 antibody, IgG1 b12, were a gift from Prof. Ian A. Wilson (Scripps Research Institute, USA). Four hydrophobic residues, F241, F243, V262 and V264, located on the Fc protein-glycan interface and in close proximity, were mutated to non-hydrophobic alanine or glutamate by site-directed mutagenesis, as previously described[87]. The b12 and recombinant Fc mutants were expressed in HEK 293T cells, and were affinity purified by protein-A and Ni^{2+} Sepharose beads respectively. The purity of the recombinant proteins was checked by Coomassie-Blue stained SDS-PAGE (Fig. 3.1). The *N*-glycans released from b12 and Fc mutants were analysed by a combination of MALDI-TOF-MS, ES-MS, and normal-phase HPLC. The experimental procedures and data analysis pertaining to ES-MS were all carried out by Prof. David Harvey.

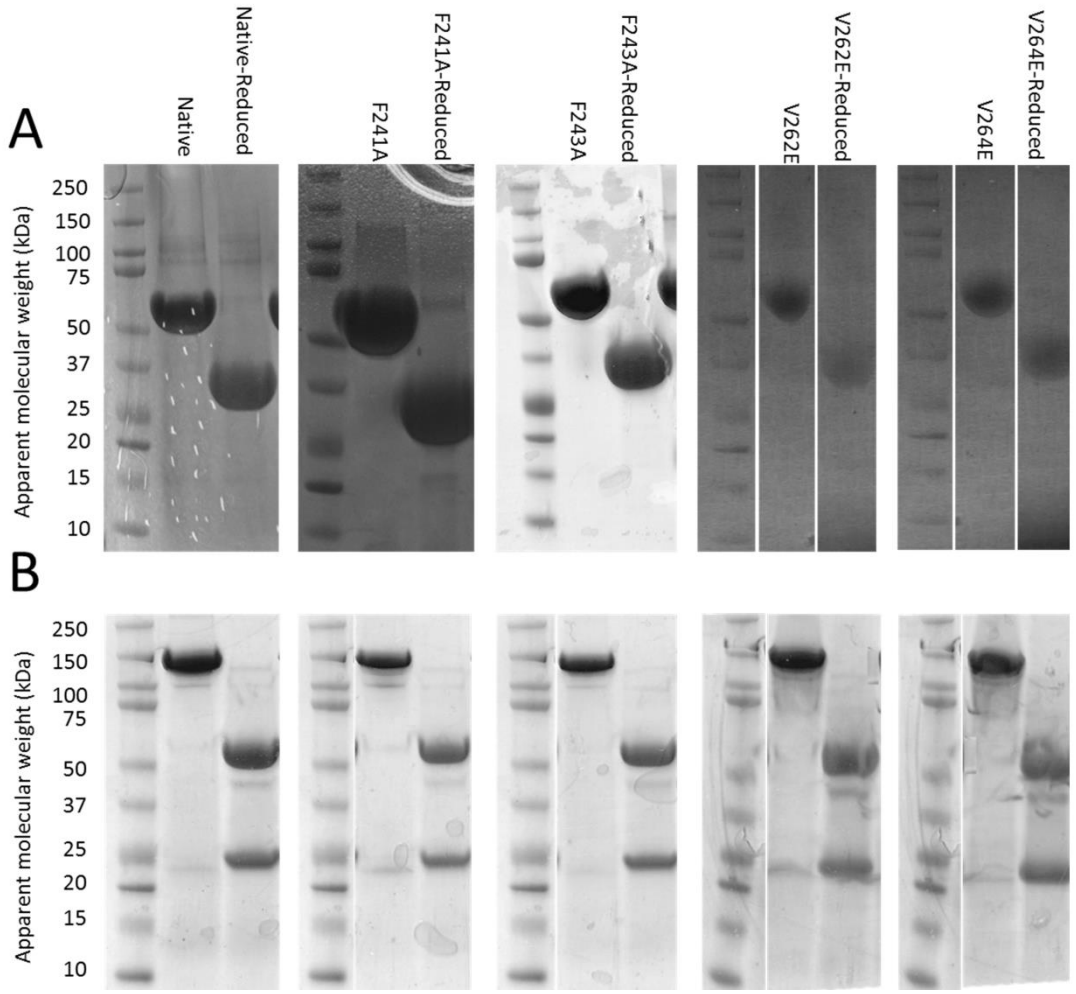

Figure 3.1. SDS-PAGE analysis of recombinant human IgG1 Fc and full length IgG1 b12 antibody. Proteins were expressed in HEK 293T cells, and affinity-purified by Ni^{2+} (for Fc) or protein A Sepharose beads (for b12). For protein denaturation, the samples were boiled for 5 minutes in the presence of DTT. Protein samples were run on 4-12% gradient Bis-Tris gel and then stained by Coomassie Blue. SDS-PAGE analysis of: (A) Recombinant Fc and its hydrophobic mutants. (B) Recombinant full length b12 and its hydrophobic mutants.

3.2.2. Glycoform of Single Hydrophobic Mutants

Consistent with previous reports on human-murine chimeric IgG3[87], abolition of Fc hydrophobic protein-glycan interactions at F241A or F243A dramatically increased Fc terminal galactosylation, sialylation and branching compared with the native Fc (Fig. 3.2A, B, C and D). Moreover, an unusual tri-galactosylated, tetra-sialylated glycoform was detected using ES-MS, and confirmed by negative ion collision-induced fragmentation carried out by Prof. David Harvey (Fig. 3.3). Similar unusually siaylated structures have been observed in

mouse serum glycoproteins[253; 254], but not in IgG. Detailed high-resolution analysis of *N*-glycans from full length IgG1 b12 mutants was enabled later in the project, by a more robust HPLC system purchased by the laboratory. The increased glycan processing in recombinant Fc mutants was broadly recapitulated in the IgG1 b12 antibody (Fig. 3.4). For example, the level of sialylation increased from being virtually non-detectable in wild type to approximately 40% in F241A, and 57% in V264E, the galactosylation and sialylation levels of b12 mutants are summarized on Table 3.1. Sialidase digestion confirmed the extensive sialylation, predominantly in α2,3-linkage (Fig. 3.5), consistent with the dominance of α2,3-sialyltransferase activity observed in HEK 293T cells[255]. Similar to the tri-galactosylated, tetra-sialylated glycoform observed in Fc (Fig. 3.3D), a rare population of di-galactosylated, tri-sialylated glycan was detected in b12 mutants (Fig. 3.4D-E). To further confirm the assignment of the individual sialylated species, each sialylated peak during the HPLC analysis of V264E was collected, treated with sialidase and then re-analysed by HPLC. As shown in Figure 3.6, certain single peaks on HPLC spectrum contain multiple glycoforms. Thus, higher resolution analysis is needed to further uncouple these peaks. In addition to HPLC, MALDI-TOF-MS (Fig. 3.7) and ES-MS (Fig. 3.8 and Fig. 3.9) analysis both confirmed the extensive processing of b12 *N*-glycan and support the assignment of HPLC spectrum (Fig. 3.4).

Besides sialylation, the level of galactosylation increased from approximately 61% to 96% across the mutants (Fig. 3.4 and Table 3.1). For example, the G2 level increased from 17% in wild type to 69% in F241A, with concomitant decrease in levels of G1 and G0. The increase in galactosylation was accompanied by increased branching. For example, the presence of tri-antennary glycans (G3), not detected in normal human serum IgG, was clearly observed in V262E (12%), and V264E (18%) (Fig. 3.4 D and E, Fig. 3.7D and E). In addition, a small amount of tetra-antennary glycans (G4) was detected for V262E (0.6%) and V264E (1.6%)

(Fig. 3.4 D and E, Fig. 3.7D and E). No significant changes in fucosylation level was observed (Fig. 3.4). A comparison of glycan profile of the 4 single mutants reveals that mutating the valines of the hydrophobic ladder resulted in greater Fc glycan terminal processing than mutating the phenoalanines, which suggests that residues structurally closer to the N297 (Fig. 1.8A), which anchors the glycan to the protein backbone, are more crucial in maintaining the stability of the protein-glycan interface.

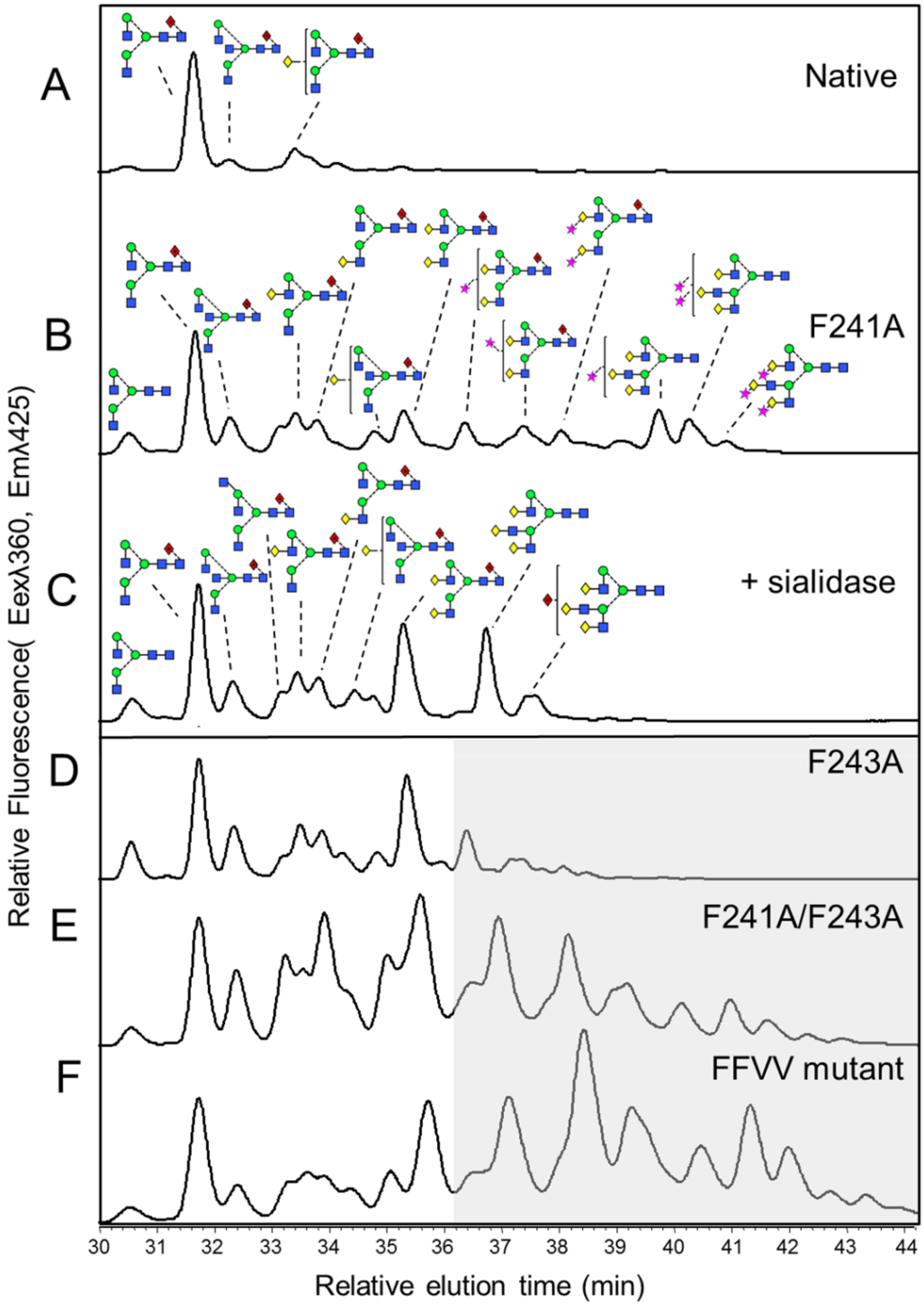

Figure 3.2. HPLC analysis of 2AA-labelled *N*-linked glycans from recombinant IgG1 Fc mutants expressed in HEK 293T cells. Normal-phase HPLC analysis of 2-AA-labelled *N*-linked glycans, released from target protein by in-gel protein PNGase F digestion. Glycan profile of IgG1 Fc expressed in HEK 293T for the following variants: (A) Native. (B) F241A. (C) Desialylated F241A. (D) F243A. (E) F241A/F243A. (F) F241A/F243A/V262E/V264E. Shaded regions of (D), (E), and (F) indicate mainly sialylated glycoforms.

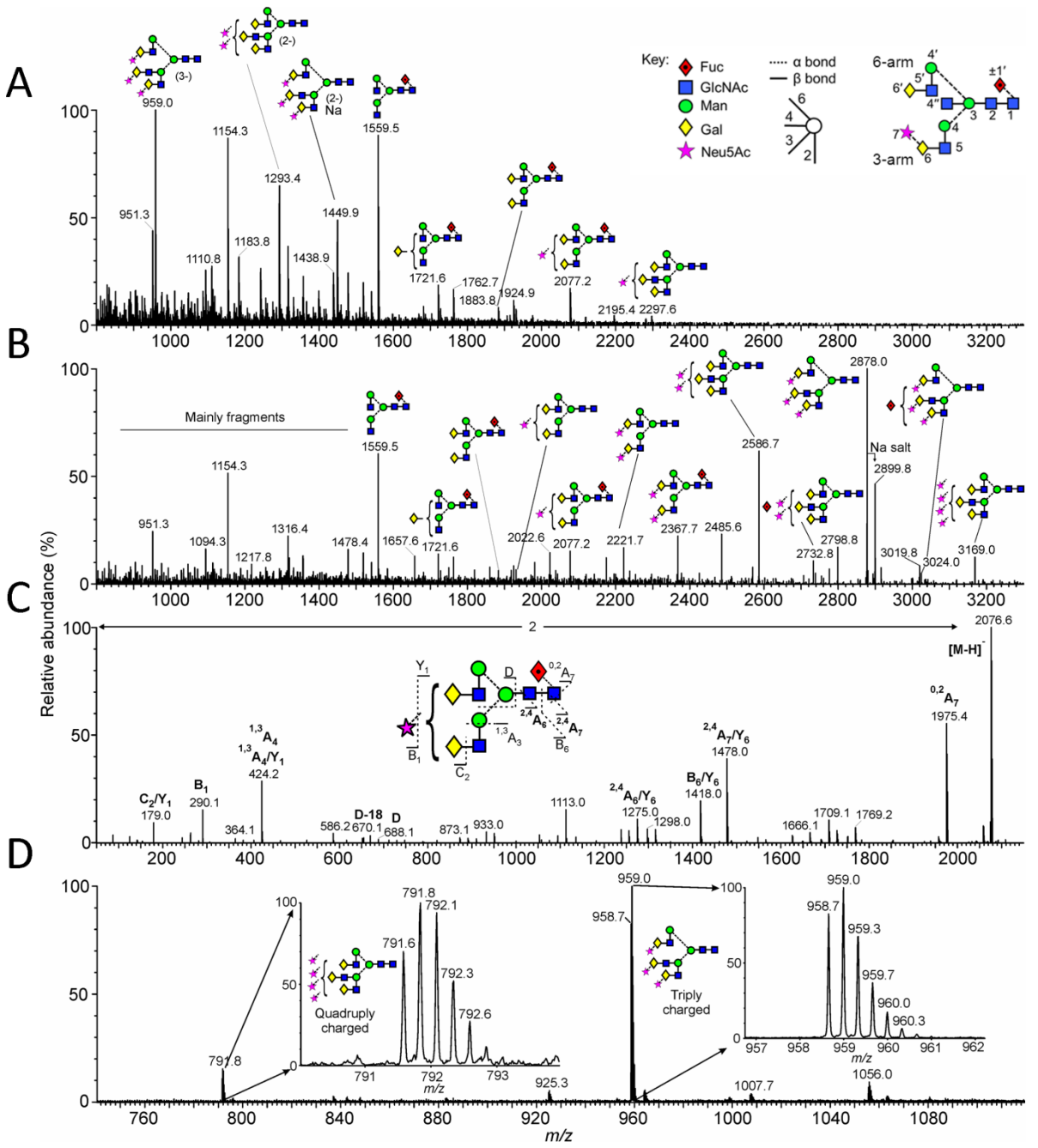

Figure 3.3. Mass spectrometric analysis of *N*-glycans released from IgG1 Fc-F241A. (A) Negative ion ESI spectrum. (B) The data from panel A processed with the Maximum Entropy 3 function of MassLynx to convert multiply charged ions to singly charged ions. The position of the fucose residue in the triantennary glycans was not determined. The ion at *m/z* 3169 gave a composition corresponding to the tetra-sialylated triantennary glycan but this was not confirmed by fragmentation. (C) An example of negative ion collision-induced dissociation spectrum of the monosialylated, fucosylated biantennary glycan. Fragment ions are labeled according to the scheme devised by Domon and Costello[256]. (D) Spectra showing tri-galactosylated structures with three (triply charged) and four (quadruply charged) sialic acids attached, respectively. The ES-MS experiment and subsequent data analysis were carried out by Prof. David Harvey.

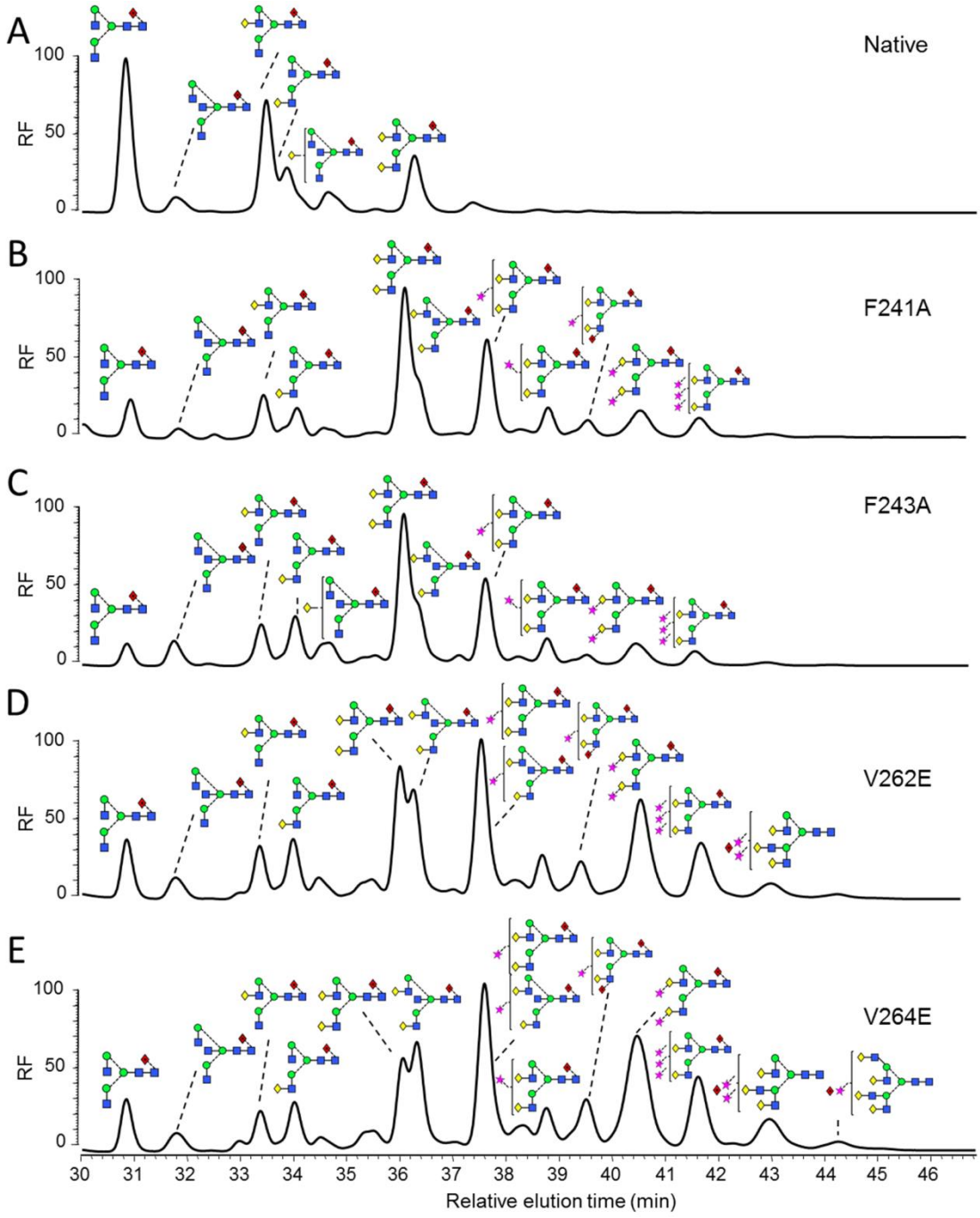

Figure 3.4. HPLC analysis of 2AA-labelled *N*-linked glycans from monoclonal IgG1 b12 mutants expressed in HEK 293T cells. Normal-phase HPLC analysis of 2-AA-labelled *N*-linked glycans, released from target antibody glycoforms by in-gel protein PNGase F digestion. Glycan profile of IgG1 b12 expressed in HEK 293T cells for the following variants: (A) Wild type. (B) F241A. (C) F243A. (D) V262E. (E) V264E. The y-axis displays relative fluorescence (RF).

Table 3.1. Summary of galacosylation and sialylation levels for IgG1 b12 mutants.

Mutant	Galactosylation (%)						Total SA (%)
	G0	G1	G2	G3	G4	Total Gal	
Native	39.4±3.3	43.6±2.0	17±1.3	N.D	N.D	60.6±3.3	N.D
F241A	8.25±0	18.4±2.4	69.2±2.1	4.1±0.3	N.D	91.7±0	39.7±1.5
F243A	9.4±0.8	25.8±0.7	60.8±1.5	3.9±0.1	N.D	90.6±0.8	32.3±1.4
V262E	8.0±1.4	15.6±0.8	64.3±0.1	11.6±1.1	0.6±0	92.0±0.4	52.2±1.5
V264E	6.8±1.4	13.7±1.2	60.3±3.7	17.6±1.0	1.6±0.1	93.2±1.4	56.9±7.4
F241A/F243A	5.2±0.1	14.5±0.1	71.6±0.7	8.2±0.8	0.5±0	94.8±0.1	56.0±0.5
V262E/V264E	4.9±0.7	14.4±0.9	66.0±5.9	13.6±5.3	1.1±0.5	95.1±0.8	62.7±5.1
F241A/F243A/V264E	4.3±1.1	14.0±2.2	69.7±2.9	11.0±4.3	1.0±0.2	95.7±1.1	57.5±3.8

Percentage of each glycoform was calculated based on HPLC spectra of 2AA-labelled *N*-glycans, using Water's Empower software. Values are reported as Mean ± SD, calculated from 2 independent experiments. N.D. Non-detectable.

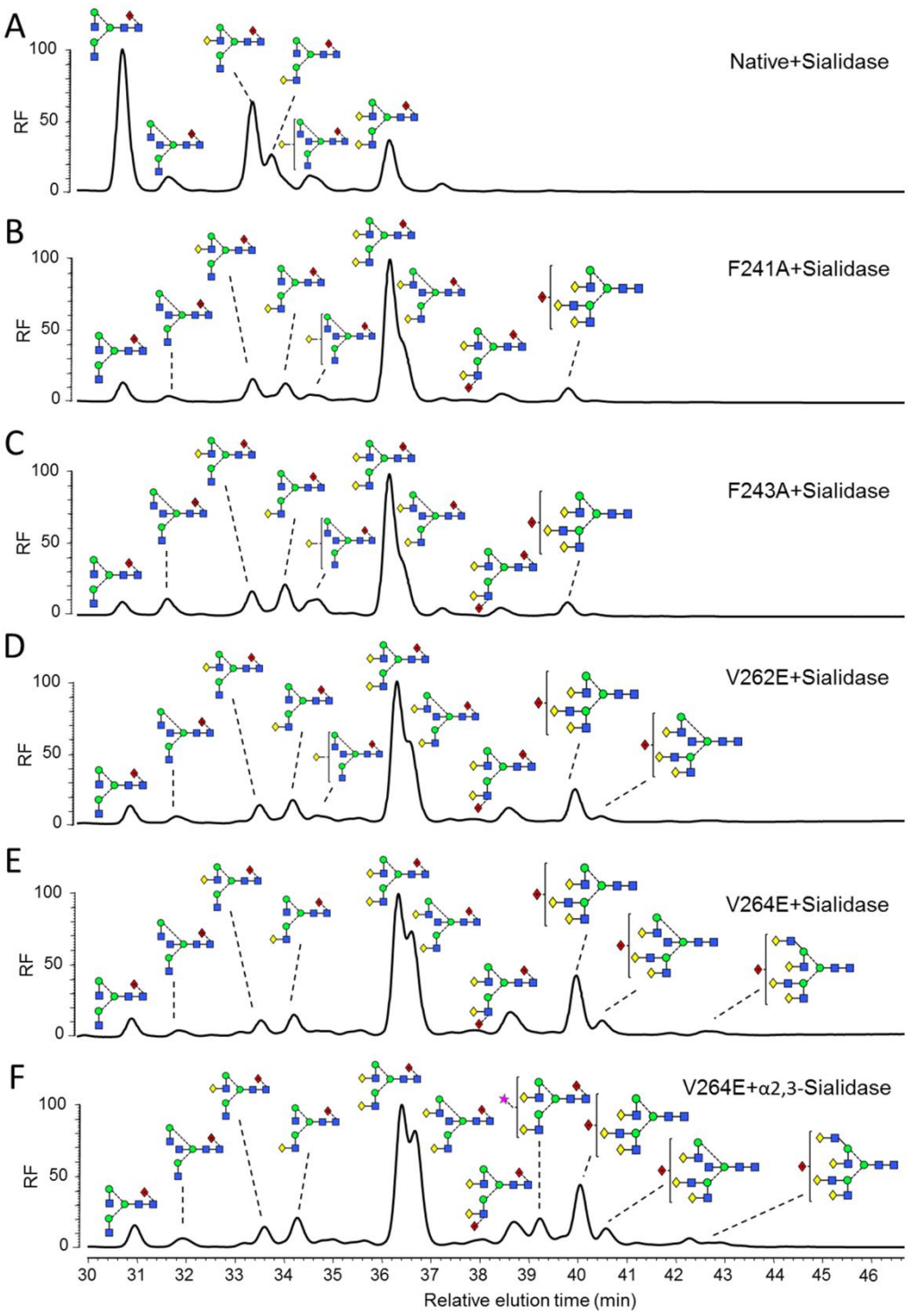

Figure 3.5. HPLC analysis of 2AA-labelled, desialylated *N*-linked glycans from monoclonal IgG1 b12 mutants expressed in HEK 293T cells. Normal-phase HPLC analysis of 2-AA-labelled, desialylated *N*-linked glycans, released from target antibody glycoforms by in-gel protein PNGase F digestion. Desialylated glycan profile of IgG1 b12 expressed in HEK 293T for the following variants: (A) Wild type. (B) F241A. (C) F243A. (D) V262E. (E) V264E. (F) α2,3-sialiase-treated V264E. The y-axis displays relative fluorescence (RF).

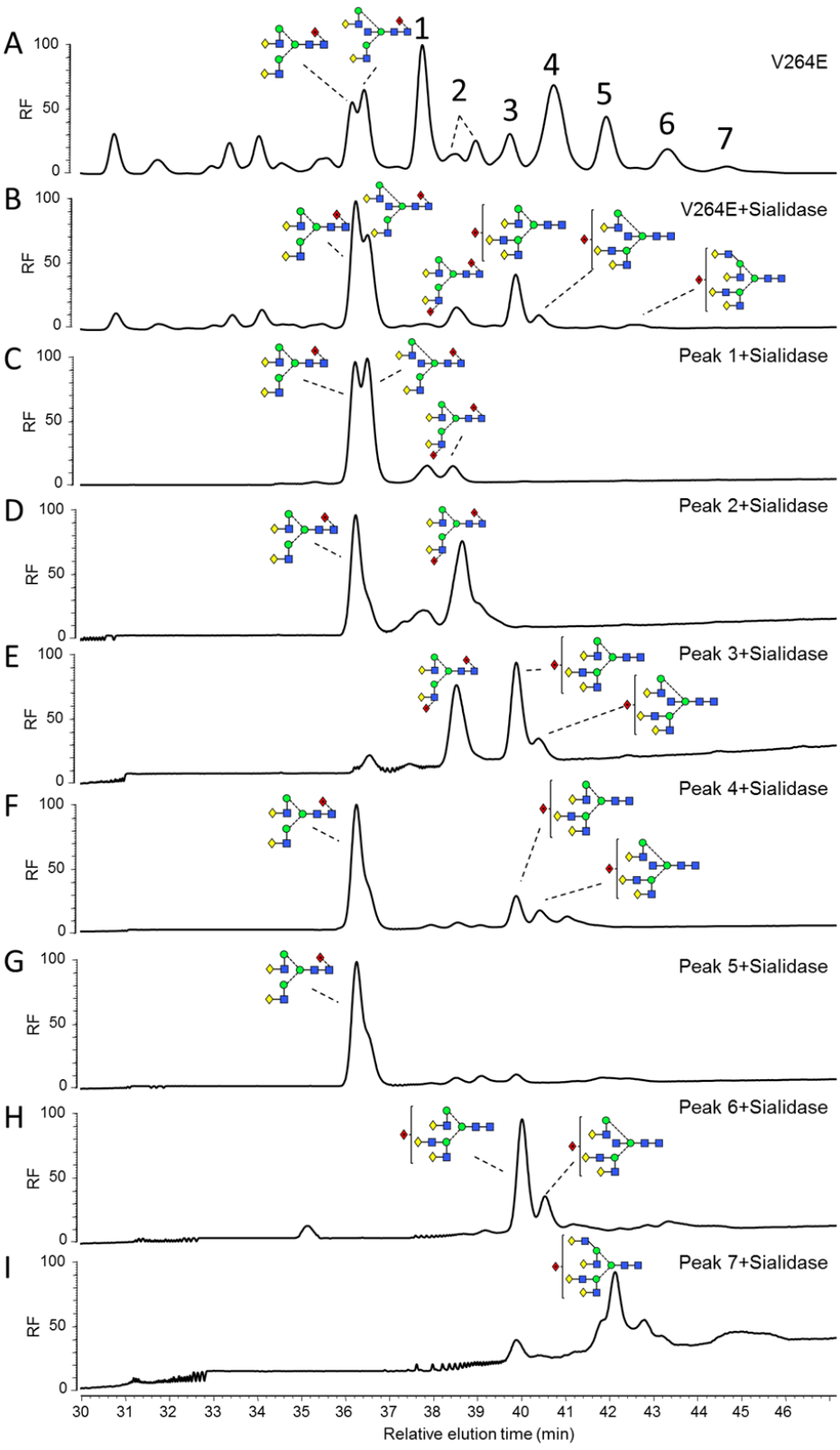

Figure 3.6. HPLC analysis of sialylated glycans of mutant V264E. Individual HPLC sialylated peaks were collected, neuraminidase-treated, and re-analyzed by HPLC. (A) Complete HPLC profile of V264E expressed in HEK 293T cells. (B) HPLC profile of neuraminidase-digested V264E. (C) HPLC spectrum of desialylated peak 1. (D) HPLC spectrum of desialylated peak 2. (E) HPLC spectrum of desialylated peak 3. (F) HPLC spectrum of desialylated peak 4. (G) HPLC spectrum of desialylated peak 5. (H) HPLC spectrum of desialylated peak 6. (I) HPLC spectrum of desialylated peak 7. The y-axis displays relative fluorescence (RF).

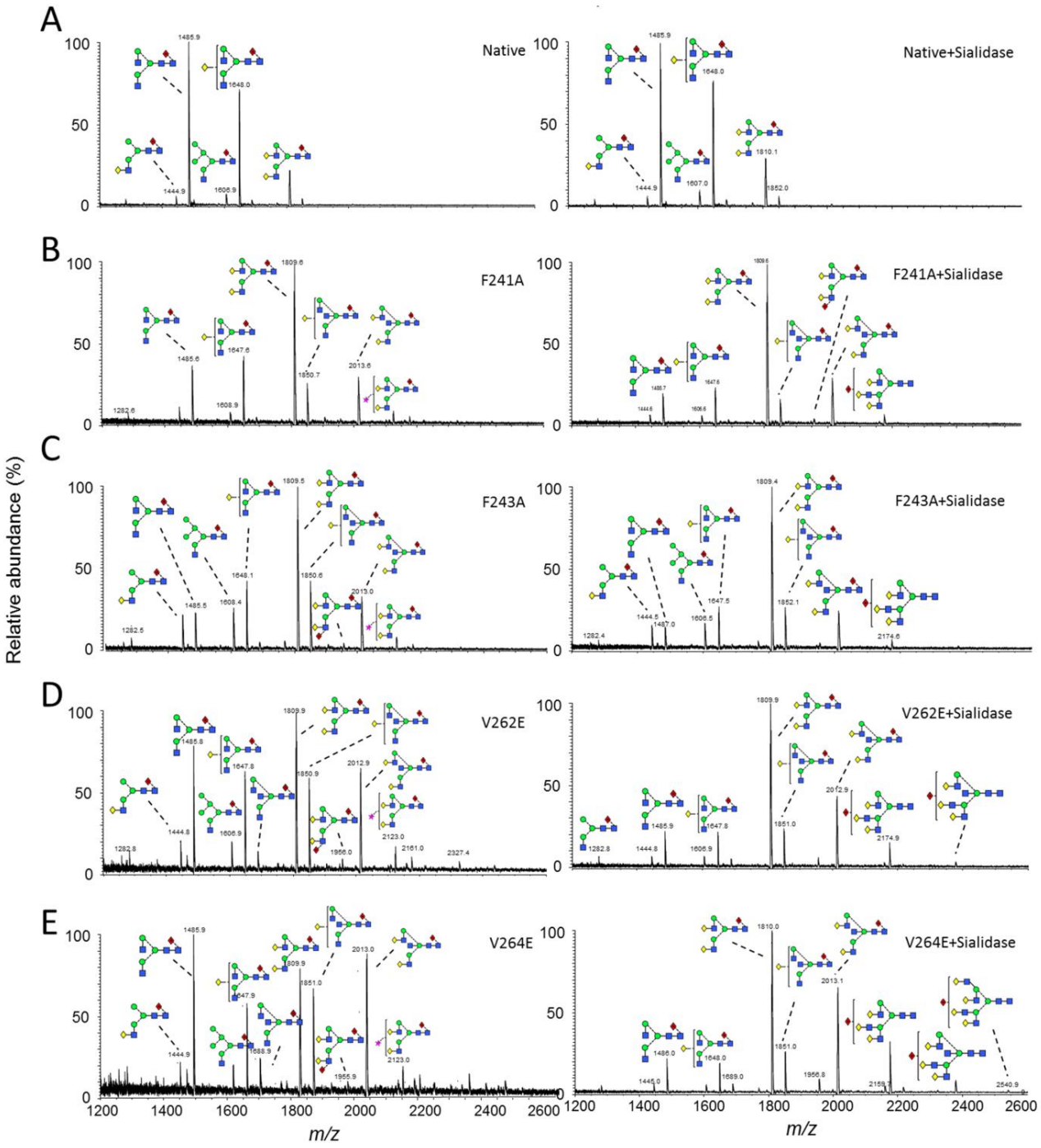

Figure 3.7. MALDI-TOF-MS analysis of *N*-linked glycans released from IgG b12 variants and their desialylated counterparts. The *N*-linked glycans were released from IgG by PNGase F digestion. For desialylation, released sugars were treated with neuraminidase. *N*-linked glycans were analyzed by MALDI-TOF-MS, in Reflection-DHB mode, with DHB as the matrix. (A) Wild type. (B) F241A. (C) F243A. (D) V262E. (E) V264E.

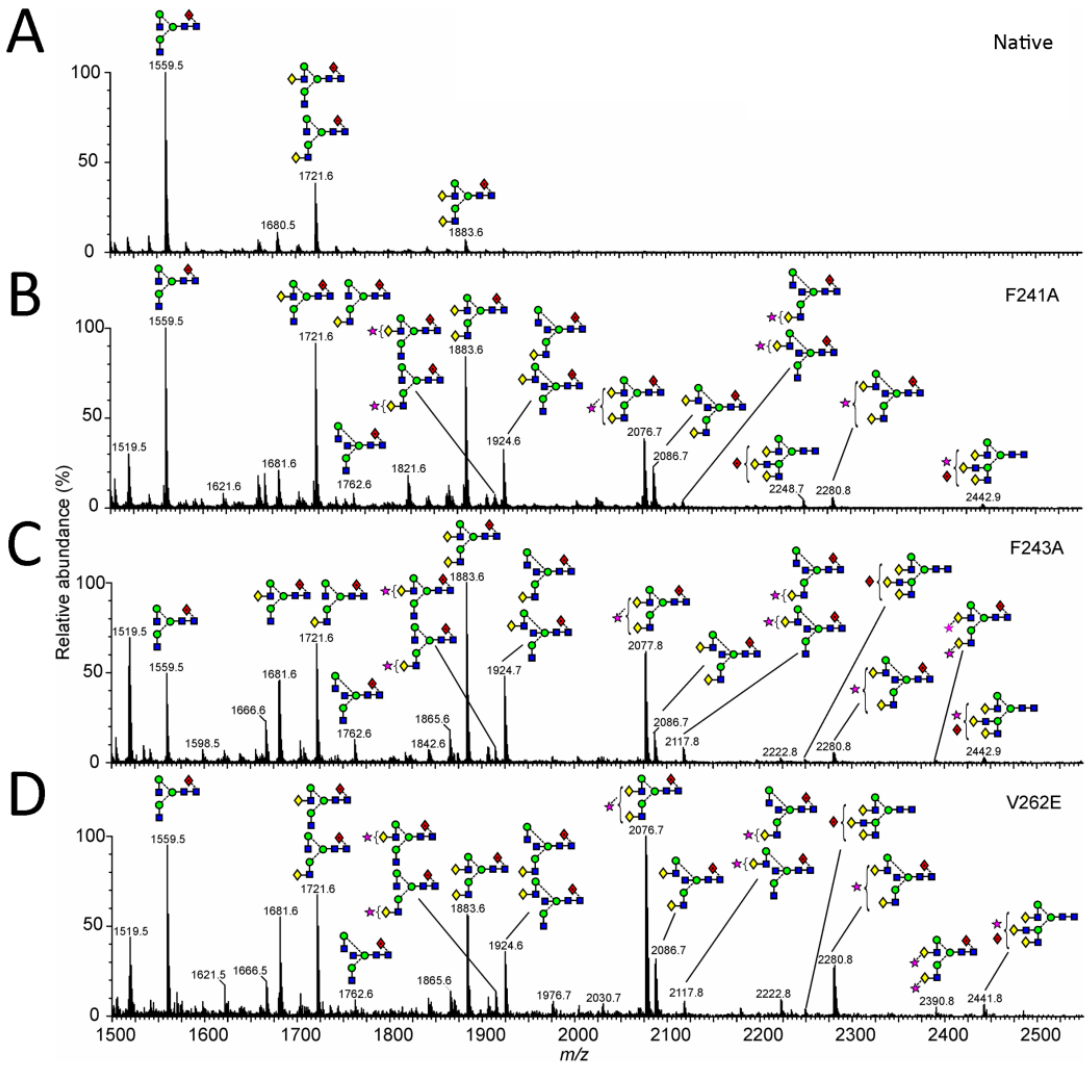

Figure 3.8. ES-MS analysis of *N*-glycans released from IgG1 b12 mutants. Spectra shown represent singly charged ions and were extracted using ion mobility from their respective negative ion ESI spectra. Spectra showing singly charged ions from (A) Native, (B) F241A, (C) F243A, (D) V262E. Masses, compositions and structures of the *N*-glycans are shown in Appendix B. The ES-MS experiments and data analysis were carried out by Prof. David Harvey.

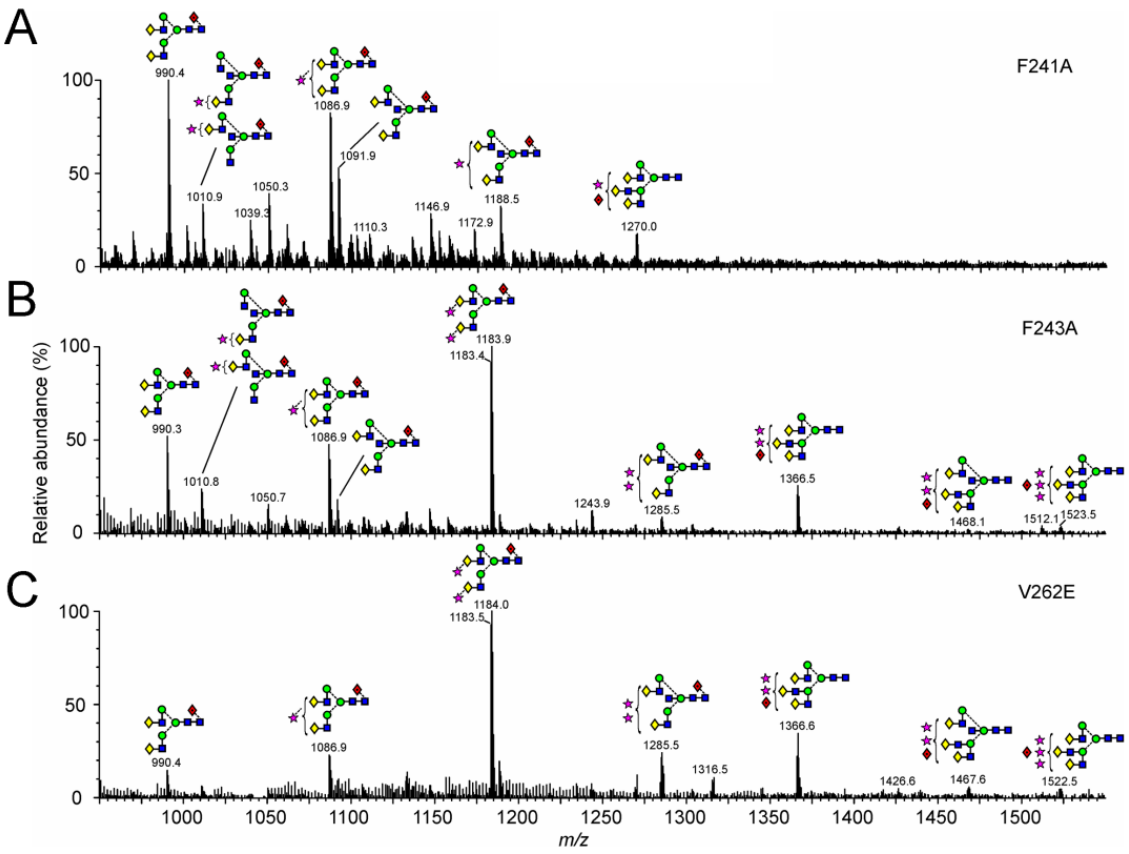

Figure 3.9. ES-MS analysis of *N*-glycans released from IgG1 b12 mutants. Spectra shown represent doubly charged ions and were extracted using ion mobility from their respective negative ion ESI spectra. Spectra showing doubly charged ions from (A) F241A, (B) F243A, (C) V262E. Masses, compositions and structures of the *N*-glycans are shown in Appendix B. This ES-MS experiment and data analysis were carried out by Prof. David Harvey.

3.2.3. Fc Glycoforms of Multi-hydrophobic Mutants

Having confirmed that single hydrophobic mutations resulted in dramatic increase in Fc terminal glycan processing, double mutants (F241A/F243A; V262E/V264E) and triple mutant (F241A/F243A/V264E) were generated to investigate the synergistic effect of multiple hydrophobic mutations on Fc glycan processing. Similar to the single mutants, these double and triple mutants exhibit significantly enhanced terminal galactosylation and sialylation (Fig. 3.10, Fig. 3.11). For example, F241A/F243A exhibits a sialylation level of 56%, similar to a previously reported double mutant human IgG1 F241S/F243S[95], higher than single mutants F241A (40%) and F243A (32%) (Table 3.1). Moreover, V262E/V264E has a sialylation level of approximately 63%, higher than the triple mutant F241A/F243A/V264E (58%) (Table 3.1). The higher sialylation level observed in V262E/V264E supports data from single hydrophobic mutants in showing that mutating valines in the hydrophobic ladder is more effectively in promoting Fc glycan processing. In addition to sialylation, the increase in G2, G3 and G4 glycoforms was similar to those observed for the single mutants (Table 3.1). Thus, data presented here show that multiple mutations at the Fc glycan-protein interface synergistically enhance Fc glycan processing; consistent with the hypothesis that Fc glycan-protein interaction restricts Fc glycan processing.

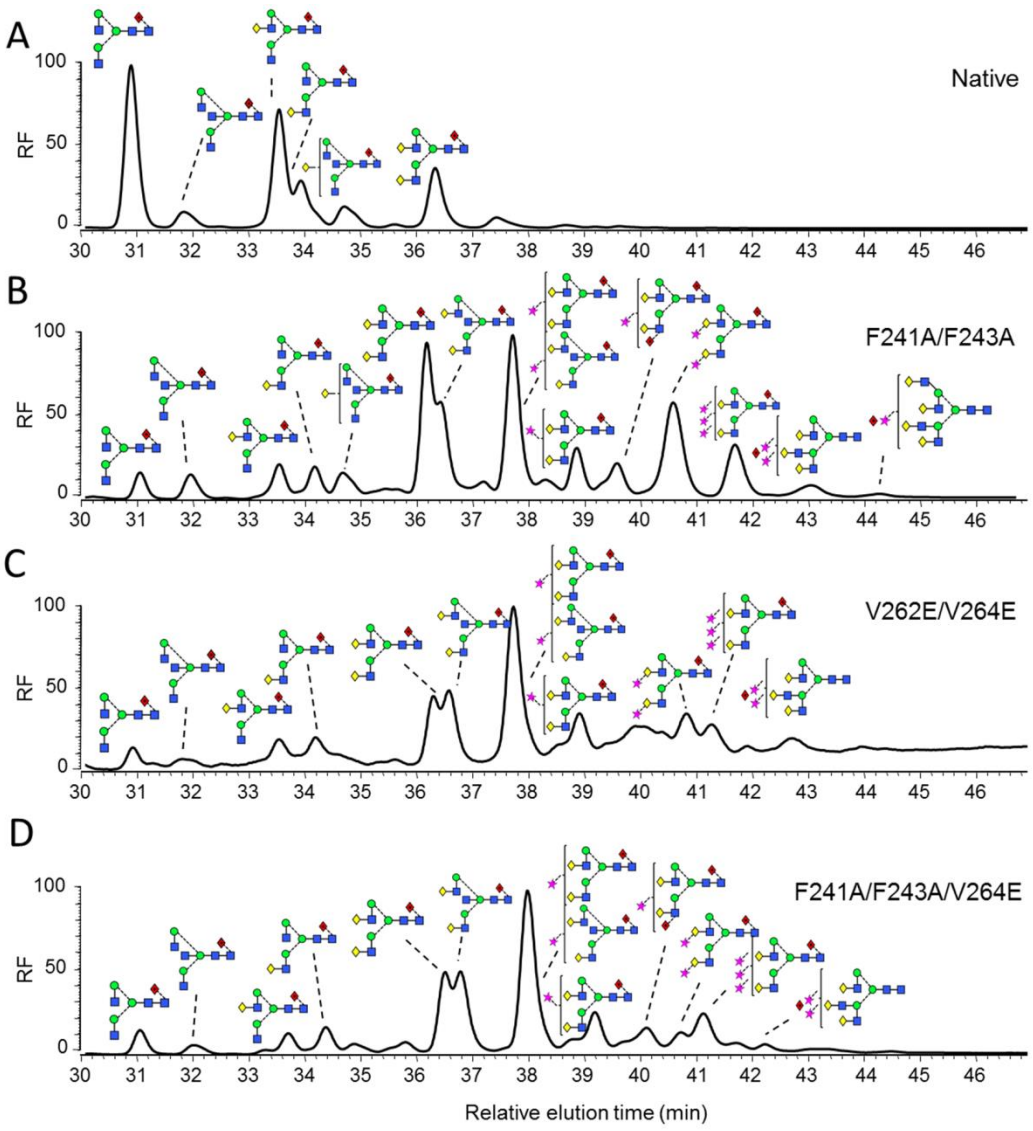

Figure 3.10. HPLC analysis of 2AA-labelled *N*-linked glycans from monoclonal IgG1 b12 mutants expressed in HEK 293T. Normal-phase HPLC analysis of 2-AA-labelled *N*-linked glycans, released from target antibody glycoforms by in-gel protein PNGase F digestion. Glycan profile of IgG1 b12 expressed in HEK 293T cells for the following variants: (A) Native. (B) F241A/F243A. (C) V262E/V264E. (D) F241A/F243A/V264E. The y-axis displays relative fluorescence (RF).

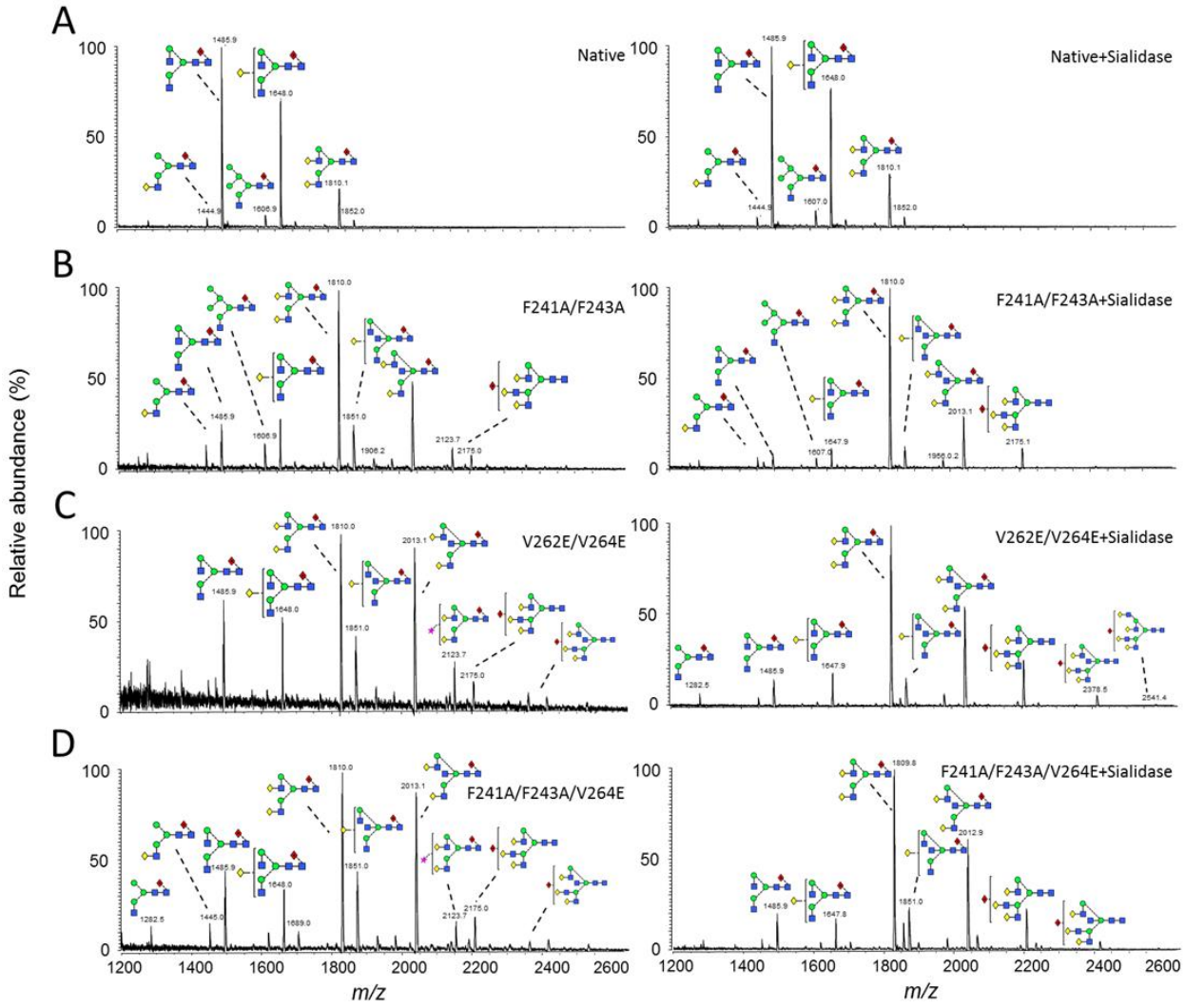

Figure 3.11. MALDI-TOF-MS analysis of *N*-linked glycans released from IgG b12 variants and their desialylated counterparts. The *N*-linked glycans were released from IgG by PNGase F digestion. For desialylation, released sugars were treated with neuraminidase. *N*-linked glycans were analyzed by MALDI-TOF-MS, in Reflection-DHB mode, with DHB as the matrix. (A) Wild type. (B) F241A/F243A. (C) V262E/V264E. (D) F241A/F243A/V264E.

3.3. Effect of Hydrophobic Mutations on Fc *N*-glycosylation Site Occupancy

Lund and colleagues previous showed that, in addition to increasing Fc glycan processing, the hydrophobic mutations decreased the *N*-glycan site occupancy at the conserved Fc N297[87]. This decreased site occupancy was inferred from the decreased amount of monosaccharide detected in mutants, based on the colorimetric orcinol-H_2SO_4 assay[87]. As Fc N297 is one of the most conserved *N*-glycosylation sites among glycoproteins, the effect of hydrophobic

mutations on Fc *N*-glycan site occupancy was re-evaluated, using the more sensitive MALDI-TOF-MS, in combination with trypsin and PNGase F digestion.

Tryptic digestion of the IgG1 b12 generated a series of characteristic peptides, whose sequences correspond to both heavy and light chains of the b12 antibody (Fig. 3.12A). The *N*-glycosylated peptide containing the Fc N297 was undetectable on MALDI-TOF-MS (Fig. 3.12A), consistent with the incompatibility of the instrument with glycopeptide analysis. Deglycosylation of b12 before trypsin digestion generated a nonglycosylated peptide containing the D297 derived from Fc N297 by PNGase F-catalysed deamination, and this peptide was detected by MALDI-TOF-MS as highlighted in red (Fig. 3.12B). Same mass spectrometric analysis was carried out for deglycosylated hydrophobic mutants. The mass spectra show full site occupancy at Fc N297, as nonglycosylated peptide containing N297 was not detected in the hydrophobic mutants (Fig. 3.13C-F). The full glycan site occupancy shows the robust en bloc transfer of glycan to Fc N297.

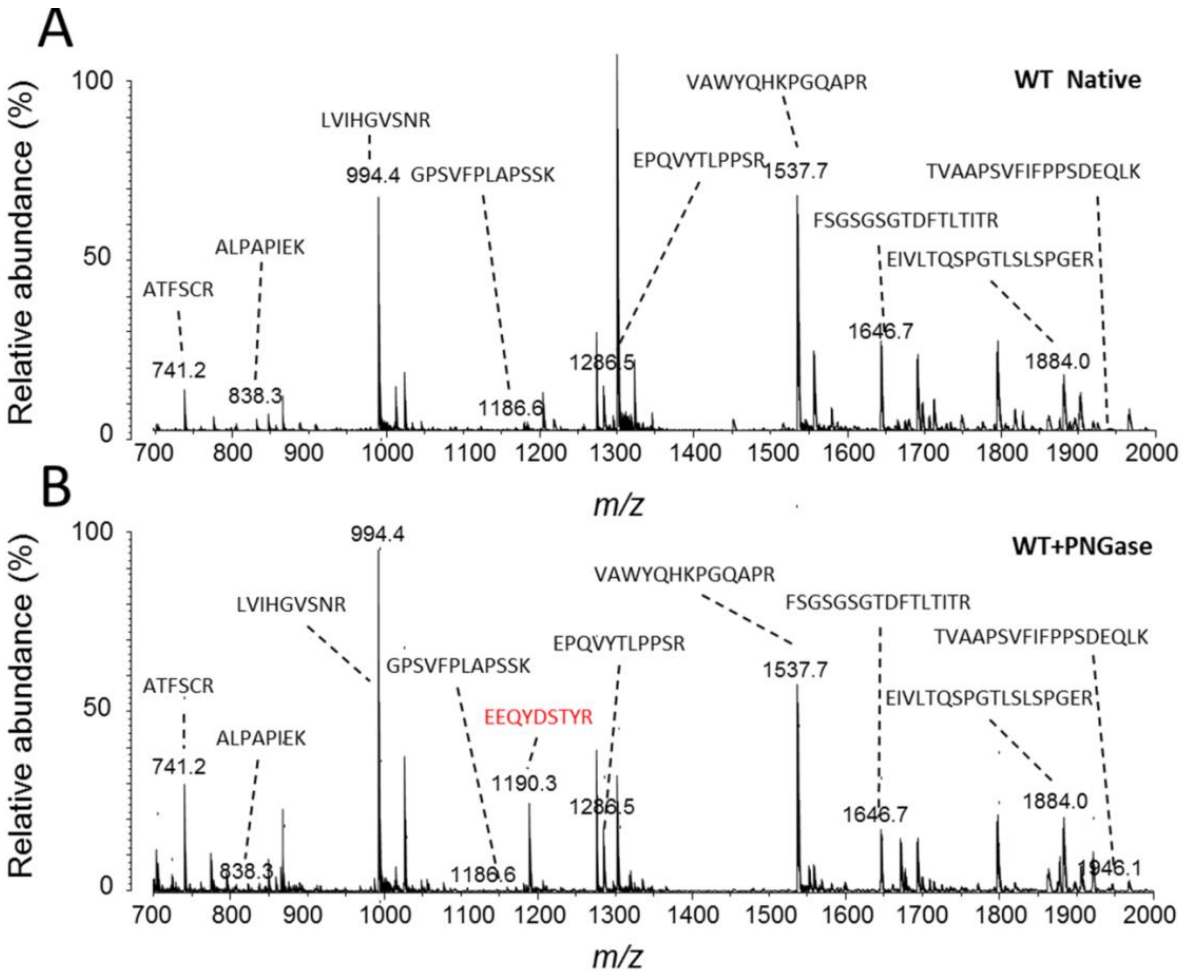

Figure 3.12. Mass spectra of trypsin-digested native and deglycosylated IgG1 b12. IgG variants were first PNGase F-treated, then reduced, alkylated and digested with trypsin for 6 hours at 37^{o}C, before analysis by MALDI-TOF-MS. The tryptic peptide mass of the native and deglycosylated IgG were calculated online using the PeptideMass program at the ExPASy SIB Bioinformatics Resource Portal. (A) Mass spectrum of trypsin-digested native IgG. (B) Mass spectrum of trypsin-digested, deglycosylated IgG. The deglycosylated peptide containing the conserved *N*-glycosylation site, Asn297, is highlighted in red.

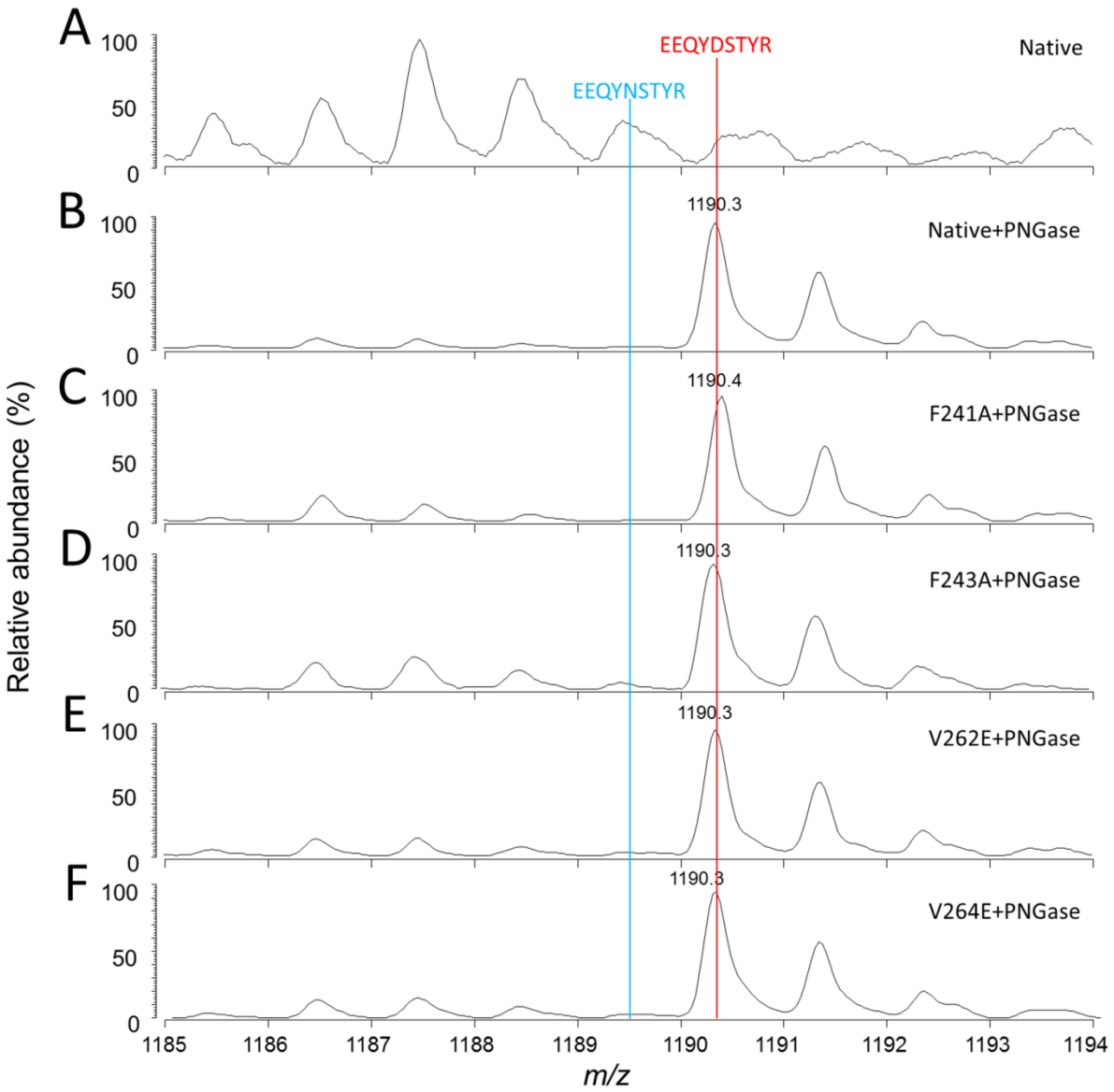

Figure 3.13. Stacked plot of mass spectra of trypsin digested, deglycosylated native IgG1 b12 and deglycosylated hydrophobic mutants. IgG deglycosylation was achieved by PNGase F-digestion overnight. For trypsin digestion, IgG variants were reduced, alkylated and digested with trypsin for 6 hours before analysis by MALDI-TOF-MS. The tryptic peptide mass of the native and deglycosylated IgG were calculated online using the PeptideMass program at the ExPASy SIB Bioinformatics Resource Portal. (A) Native glycosylated IgG. (B) Deglycosylated IgG. (C) Deglycosylated F241A IgG variant. (D) Deglycosylated F243A IgG variant. (E) Deglycosylated V262E IgG variant. (F) Deglycosylated V264E IgG variant. The position of peptide peaks corresponding to the native deglycosylated peptide containing the conserved *N*-glycosylation site, N297, is indicated by a red vertical line. The position of the peptide peaks corresponding to non-glycosylated peptide containing the conserved *N*-glycosylation site, N297, is indicated by a blue vertical line.

3.4. Structural Analysis of Fc F241A

The crystal structure of Fc F241A was determined to a resolution of 1.9 Å by Dr Kavitha Baruah (University of Oxford) and Dr Thomas Bowden. In contrast to the dramatic increase in glycan processing (Fig. 3.2B, Fig. 3.3), the crystal structure of Fc F241A shows that the glycan lies in the established position along the Cγ2 domain, with defined electron density corresponding to the 6-arm (Fig. 3.14). However, the 3-arm exhibits only diffuse density, this weak density indicates that the 3-arm is either conformationally disordered or glycoforms differing in 3-arm composition are adopting different conformations where the X-ray scattering does not sum to yield consensus electron density. Previous reports suggested that the intrinsic flexibility of the 3-arm causes the lack of electron density of the galactose in native galactosylated Fc[35; 149]. Consistent with a loss of electron density of the 3-arm, detailed negative-ion ES-MS with fragmentation analysis revealed extensive branching on the 3-arm but not the 6-arm (Fig. 3.3). The localized induction of disorder at the 3-arm does not fully account for the apparent increase in accessibility of the glycans to Golgi-resident glycosyltransferases (e.g. increase in 6-arm galactosylation).

The mutation may influence the dynamics of the glycan–protein interface, not sufficiently captured by low-temperature X-ray crystallographic methods[100]. For example, the hydrophobic interface mutations may affect the position of equilibrium between the protein 'bound' and 'free' conformations proposed by NMR studies to yield more accessible glycans and potentially more widely spaced Cγ2 domains[100]. Interestingly, NMR studies have indicated that α2,6-sialylation has minimal impact on glycan dynamics in the Fc domain[257]. This finding is entirely consistent with the conserved conformation of the 6-arm observed by X-ray crystallography (Fig. 3.14C and F). The relatively mild structural changes also support

the site occupancy data presented in section 3.3, in that the co- and post-translational *en bloc* transfer of *N*-glycan to Fc N297 is resistant to the disruption of Fc protein-glycan interface.

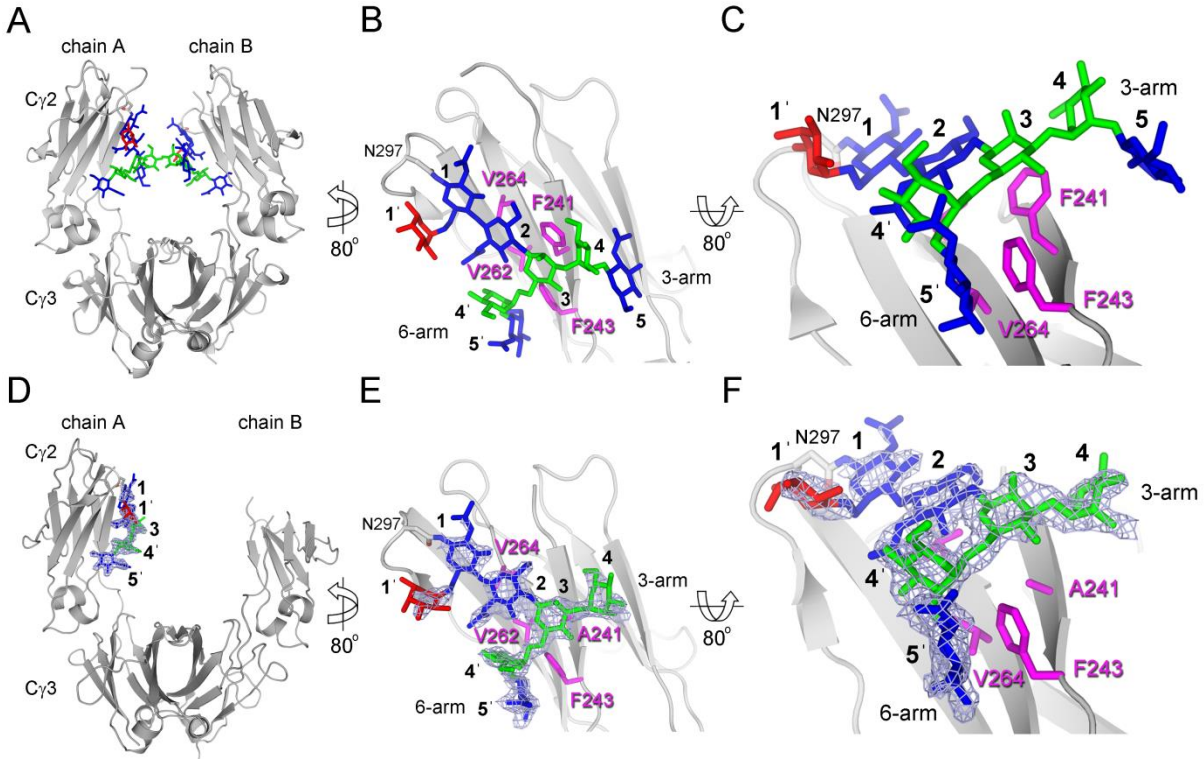

Figure 3.14. Packing of *N*-link glycans in native (A–C) and F241A mutant (D–F) IgG1 Fc. Glycans are displayed as blue (GlcNAc), red (Fuc), and green (Man) sticks. Protein is displayed as a grey cartoon with four hydrophobic residues at the protein–glycan interface highlighted in pink (sticks). Overall structure of (A) native (PDB ID 3AVE) and (D) F241A mutant IgG1 Fc. The Cγ2 domain is shown (B and E), together with a close-up of the hydrophobic interface (C and F). Four hydrophobic residues located on the protein–glycan interface are highlighted in pink (sticks). Electron density corresponding to carbohydrate is depicted as a blue mesh around the carbohydrate moiety of the mutant Fc reported herein. The Fc F241A was crystallized and data were collected by Dr Kavitha Baruah, structural refinement was carried out by Dr Thomas Bowden.

3.5. Conclusions

Native Fc glycosylation exhibits protein-directed, restricted, biantennary complex type glycoforms. This restricted glycan processing is rationalized by the hydrophobic Fc protein-glycan interface maintained by abundant Fc glycan-protein interactions[87; 95]. The full spectrum of glycoforms resulting from the hydrophobic mutations on the Fc protein backbone was characterized here, using a combination of *N*-glycan analytical methods including MALDI-TOF-MS, normal-phase HPLC, and ES-MS. The results revealed several Fc glycoforms, not usually observed in human IgG1 Fc, such as tri- and tetra-galactosylated species. In addition, abolishing multiple hydrophobic interactions on the Fc protein-glycan interface synergistically increases Fc glycan processing. In contrast to previous report, the *N*-glycan site occupancy at the conserved N297 was found to be unaffected by hydrophobic mutations. The hydrophobic mutation-mediated variations in Fc glycan processing provide another tool to generate glycoform-specific Fc, and the Fc variants with intrinsically high galactosylation and sialylation present as potential anti-inflammatory therapeutics, given the newly revealed immunosuppressive effect of sFc that is discussed in Chapter 5.

Chapter 4

Engineering Hydrophobic Protein–Glycan Interactions to Fine-tune Monoclonal Antibodies

4. Engineering Hydrophobic Protein–Glycan Interactions to Fine-tune Monoclonal Antibodies

4.1. Summary

Data analysis shown in Chapter 3 demonstrates that hydrophobic mutations along the Fc protein-glycan interface increases glycan processing, characterized by increased terminal sialylation and galactosylation. These hydrophobic mutations have also been found to reduce Fc affinity for the FcγRIA and the complement molecule C1q, leading to decreased Fc-dependent, complement-mediated cytotoxicity and Fc-mediated superoxide production by monocytes[87]. It is unknown, however, whether the decreased Fc-mediated effector functions are due to altered glycan processing, or the disruption of protein-glycan interaction. To delineate the mechanism of hydrophobic mutation-mediated reduction in Fc-mediated effector functions, the panel of hydrophobic mutants were glycan-engineered to be uniformly glycosylated. Moreover, the effect of Fc protein-glycan interface on Fc-FcγR interaction was exploited to fine-tune the antibody Fc effector functions.

4.2. Effect of Disrupting Fc Protein-Glycan Interface on Fc-FcγR Interaction

4.2.1. Clonings and Expressions of FcγRs

The soluble region of human FcγRIA, FcγRIIA, FcγRIIB, FcγRIIIA, and FcγRIIIB was cloned into the mammalian expression vector pHLSec and expressed in HEK 293T cells. The soluble region of FcγRIIB was cloned by Snezana Vasiljevic. Proteins were purified by Ni^{2+} Sepharose Beads, followed by gel filtration to obtain >90% purity as assessed Coomassie Blue-stained SDS-PAGE (Fig. 4.1). The *N*-glycan profile of these FcγRs was determined by MALDI-TOF-MS, which exhibits extensive, mostly non-protein directed, glycan processing (Fig. 4.2). Interestingly, FcγRIA has a large amount of $Man_5GlcNAc_2$ glycoform (Fig. 4.2A),

which is an early glycoform during *N*-glycan biosynthesis, while FcγRIIIB exhibits significantly more high-mannose glycoforms than other receptors (Fig. 4.2E). The extensive FcγR glycan processing is broadly consistent with previous reports that FcγRIIIA glycosylation is largely non-protein directed, dominated by complex type glycans[85; 109; 114].

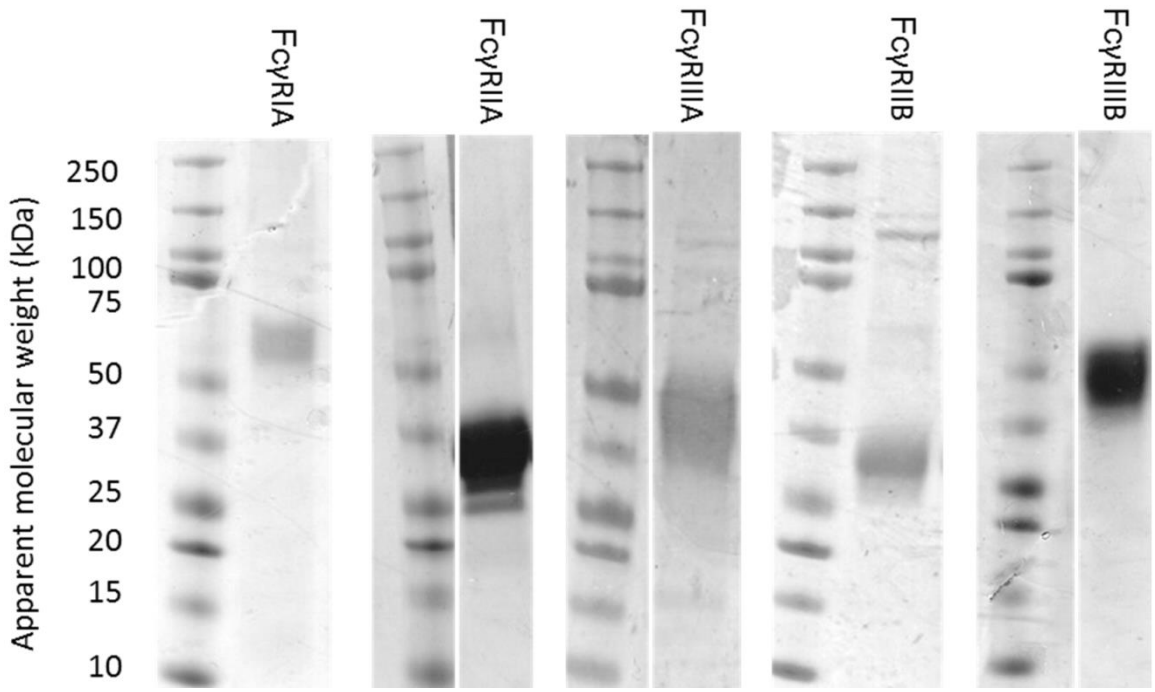

Figure 4.1. SDS-PAGE analysis of recombinant human FcγRIA, FcγRIIA, FcγRIIB, FcγRIIIA, and FcγRIIIB. Soluble region of each FcγR was cloned into a hexahistidine-tagged mammalian expression vector and expressed in HEK 293T cells. Proteins were affinity-purified by Ni^{2+} Sepharose beads, followed by gel filtration. Protein samples were run on 4-12% gradient Bis-Tris gel and then stained by Coomassie Blue. The dominant band of each lane corresponds to the individual FcγRs.

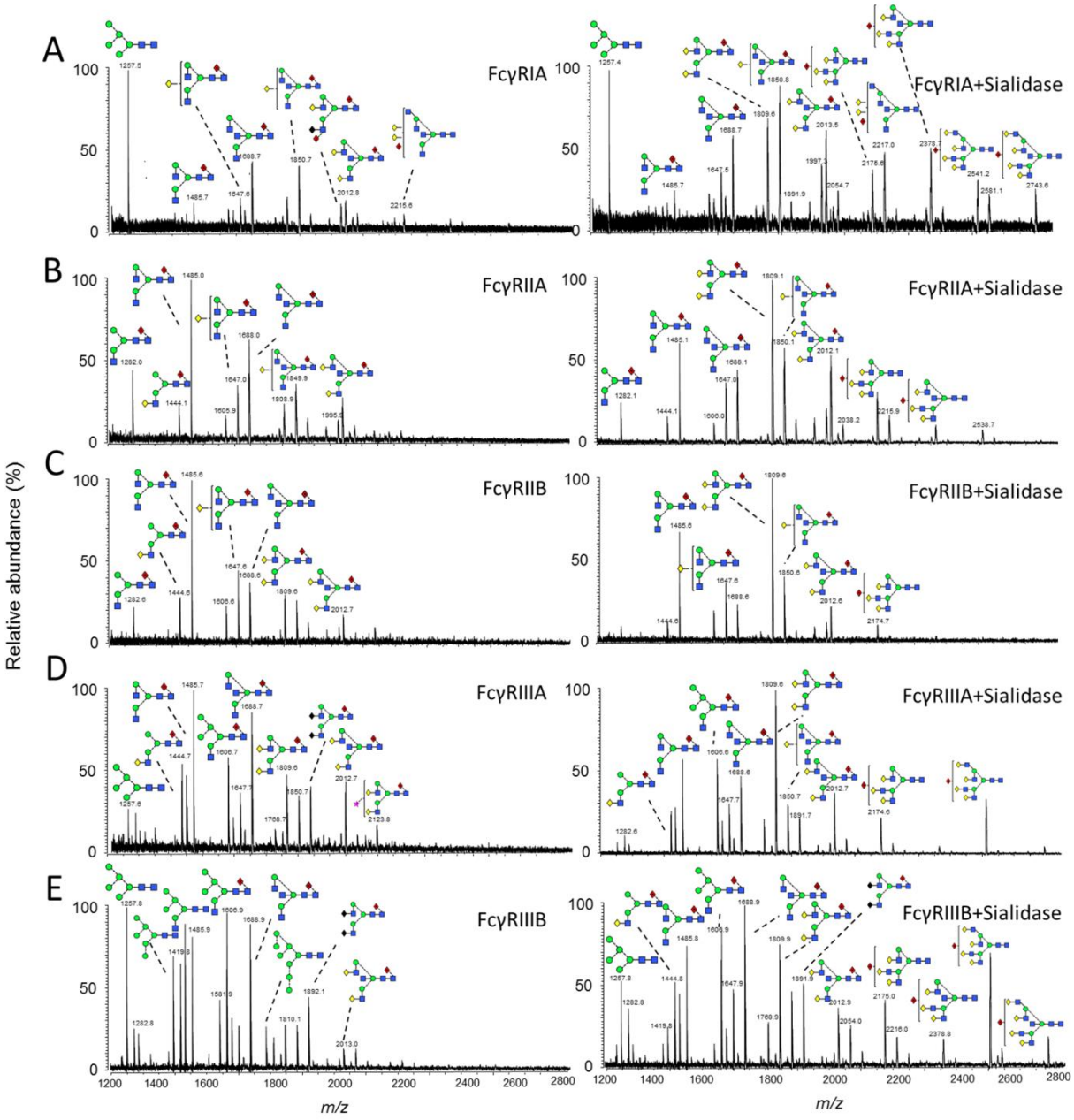

Figure 4.2. MALDI-TOF-MS analysis of *N*-linked glycans released from FcγRs and their desialylated counterparts. The *N*-linked glycans were released from FcγRs by PNGase F digestion. For desialylation, released sugars were treated with neuraminidase. *N*-linked glycans were analyzed by MALDI-TOF-MS, in Reflection-DHB mode, with DHB as the matrix. (A) FcγRIA. (B) FcγRIIA. (C) FcγRIIB. (D) FcγRIIIA. (E) FcγRIIIB.

4.2.2. Affinity of Native, Differentially Glycosylated Hydrophobic Mutants for FcγRs

The wild type IgG1 binds to FcγRIA, FcγRIIA, FcγRIIB, FcγRIIIA, and FcγRIIIB with differential affinities, similar to the previously reported values[258] (Fig. 4.3). Hydrophobic mutants expressed in HEK 293T cells, hence differentially glycosylated with complex type glycans (Fig. 4.4; black specta), were tested for their affinity for the FcγRs. As shown in Figure 4.3, the hydrophobic mutants have broadly decreased affinity, albeit to different extents, for all FcγRs, including FcγRIA, FcγRIIA, FcγRIIB, FcγRIIIA, and FcγRIIIB. The high affinity activatory FcγRIA and low-affinity, inhibitory FcγRIIB were least prone to such modulation. Interestingly, the V264E mutant, which exhibits the most disruption in Fc-FcγR interaction (Fig. 4.3), contains the highest level of sialylated structures among mutants tested (Fig. 4.4E). Consistent with previous reports[140; 141], wild type IgG1 Fc with $Man_5GlcNAc_2$ glycosylation exhibits increased affinity for FcγRIIIA (Fig. 4.3D), and decreased affinity for the FcγRIIB (Fig. 4.3C), when compared with Fc with native biantennary complex glycans. Moreover, the $Man_5GlcNAc_2$ glycoform exhibits decreased Fc affinity for FcγRIIA which is highly homologous to FcγRIIB (Fig. 4.3B).

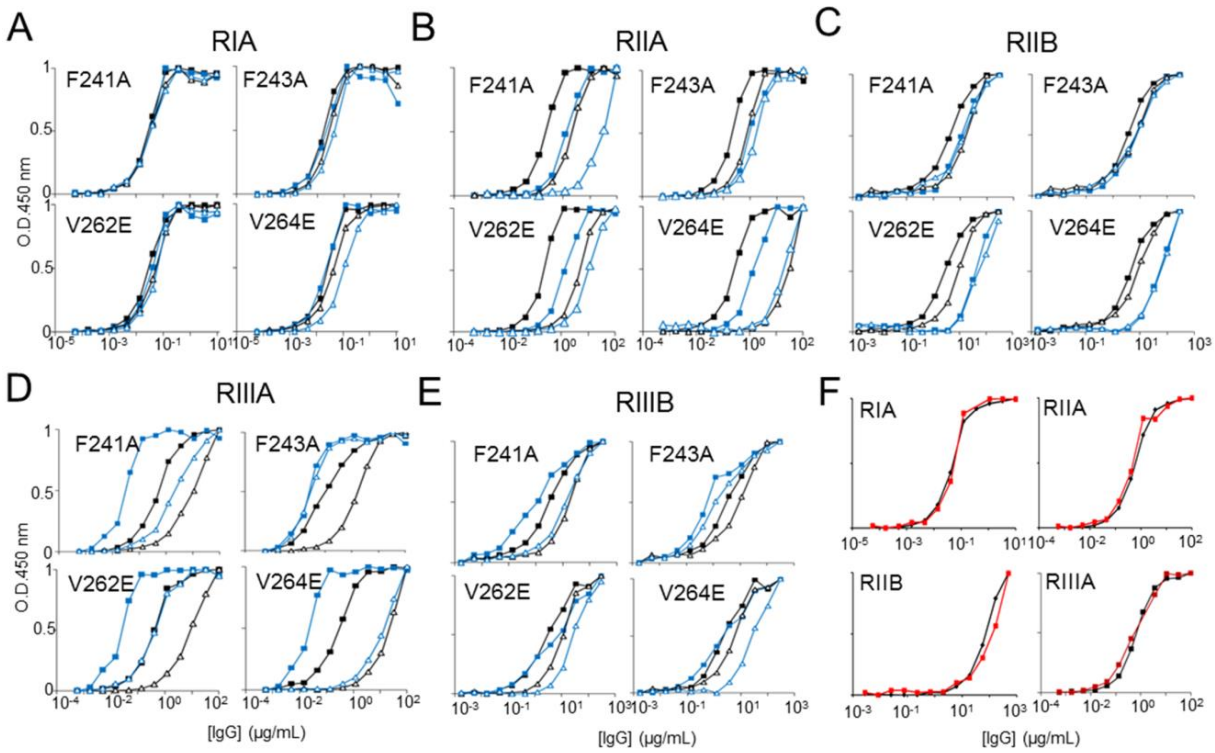

Figure 4.3. ELISA of monoclonal IgG1 b12 variants binding human FcγRIA, FcγRIIA, FcγRIIB, FcγRIIIA and FcγRIIIB. The FcγRs were plated at 5 µg/mL overnight at 4°C, IgG variants F241A, F243A, V262E and V264E were incubated for 1.5 hours and binding was detected by HRP-conjugated goat anti-human Fab antibody. Symbolic representation of IgG mutation and glycovariants: ■ = wild type native, ■ = wild type $Man_5GlcNAc_2$, △ = mutant native, △ = mutant $Man_5GlcNAc_2$, ■ = wild type hypergalactosylated and hypersialylated, ELISA binding curves of the four IgG hydrophobic mutants for (A) FcγRIA, IgG variant starting concentration at 10 µg/mL. (B) FcγRIIA, IgG variant starting concentration at 100 µg/mL. (C) FcγRIIB, IgG variant starting concentration at 300 µg/mL. (D) FcγRIIIA, IgG variant starting concentration at 100 µg/mL. (E) FcγRIIIB, IgG variant starting concentration at 300 µg/mL. (F) FcγRIA, FcγRIIA, FcγRIIB, and FcγRIIIA, IgG variant starting concentration at 10 µg/mL, 100 µg/mL, 500 µg/mL, and 100 µg/mL respectively . All data points represent the calculated mean of two independent measurements from a total of at least two experiments.

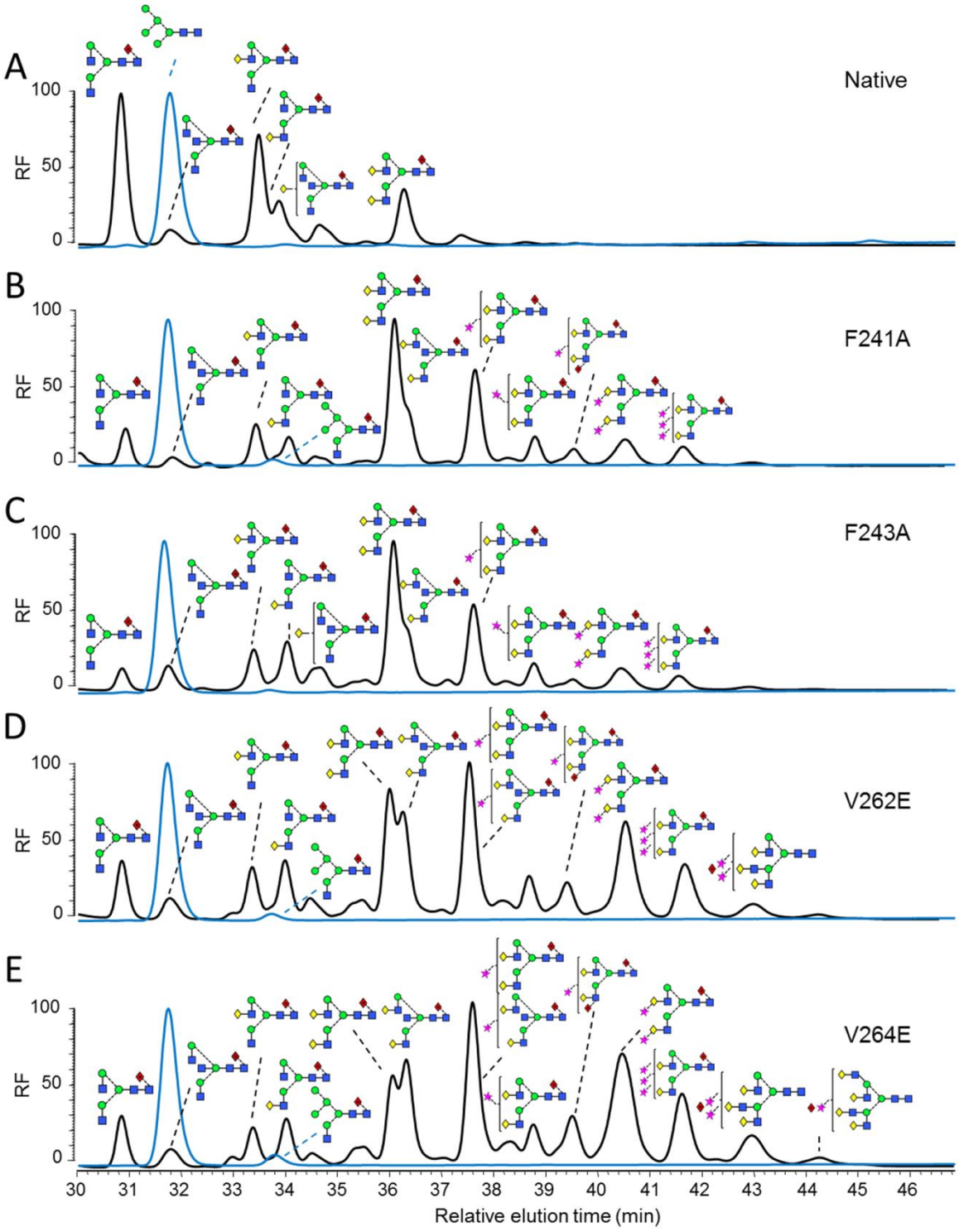

Figure 4.4. HPLC analysis of 2AA-labelled *N*-linked glycans from monoclonal IgG1 b12 mutants expressed in HEK 293T and HEK 293S cells. Normal-phase HPLC analysis of 2-AA-labelled *N*-linked glycans, released from target antibody glycoforms by in-gel protein PNGase F digestion. Glycan profile of IgG1 b12 expressed in HEK 293T (black) and HEK 293S (blue) for the following variants: (A) Wild type. (B) F241A. (C) F243A. (D) V262E. (E) V264E. The y-axis displays relative fluorescence (RF).

4.2.3. Affinity of Uniformly Glycosylated Hydrophobic Mutants for FcγRs

To separate the contribution of disrupted Fc protein-glycan interaction and increased Fc glycan processing in decreasing Fc affinity for the FcγRs, the hydrophobic mutants were expressed in the GnT I-deficient HEK 293S cells to derive mutants uniformly glycosylated with $Man_5GlcNAc_2$ (Fig. 4.4; blue specta). A small population of $Man_5GlcNAc_2Fuc$ was detected, consistent with the GnTI-independent fucosylation pathway described previously[259]. A comparison of the wild-type and mutants expressed in GnTI-deficient HEK 293S cells demonstrates that mutations that disrupt the hydrophobic protein-glycan interface significantly decrease the Fc affinity for FcγRIIA, FcγRIIIA and FcγRIIIB, largely independently of the glycoform (Fig. 4.3B, D and E); whilst interestingly, no significant changes were observed for FcγRIIB binding (Fig. 4.3C). For the high affinity FcγRIA, only V264E caused a significant decrease in binding (Fig. 4.3A). These results suggest that abolishing the hydrophobic Fc protein-glycan interactions disrupts Fc binding to the activatory FcγRs independently of the Fc glycoform, indicating that the productive engagement between Fc and FcγR requires the native protein-glycan interaction at the Fc Cγ2 domain.

Unlike F241A, V262E, and V264E, the F243A mutant expressed as the $Man_5GlcNAc_2$ glycoform has a minimal effect on FcγRs binding (Fig. 4.3A-E). This minimal effect can be explained by the different protein–glycan interfaces of oligomannose-, hybrid- and complex-type antibody glycoforms as revealed by X-ray crystallography[81]. In contrast to the other residues, F243 exhibits minimal van der Waals contacts with the 6-arm mannose residues in the predicted structure of the $Man_5GlcNAc_2$ glycoform[81] (Fig. 1.9). Therefore, in contrast to the significant effect of F243A mutation on the mobility of complex-type glycans, F243A would be predicted to have a minimal impact on the mobility of $Man_5GlcNAc_2$ structures.

The inability of F243A to affect Fc-FcγR interaction has, acting as a positive control, confirmed the important role of Fc protein-glycan interface on Fc-FcγR interaction. The relative affinity of the single mutants for FcγRs is summarized on Table 4.1.

Table 4.1. Summary of single IgG1 b12 mutants' affinity for FcγRs

FcγR	Glycoform	WT	F241A	F243A	V262E	V264E
RIA	Man5	1	1.00	0.40	0.40	0.17
	Native	1	1.00	0.67	0.40	0.40
RIIA	Man5	1	0.02	0.75	0.15	0.02
	Native	1	0.10	0.25	0.05	n.b
RIIB	Man5	1	0.83	1.00	1.00	0.95
	Native	1	0.25	0.37	0.31	0.46
RIIIA	Man5	1	0.01	1.17	0.09	n.b
	Native	1	0.02	0.26	0.05	0.01
RIIIB	Man5	1	0.09	0.37	0.23	0.07
	Native	1	0.19	0.31	0.25	0.41

Single IgG1 b12 mutants' affinity for FcγRs relative to the native (black) or $Man_5GlcNAc_2$ (blue) wild type glycoforms. Each value represents the apparent affinity of a particular mutant glycoform over the same wild type glycoform (i.e. value < 1 indicates weaker binding than the same wild type glycoform and vice versa). All data points represent the calculated mean of two independent measurements from a total of at least two experiments. n.b. no binding.

4.2.4. Generation of Novel FcγRIIB-enhancing Fc Mutants

Data presented in section 4.2.3 shows that the interaction between FcγRIIB and IgG1 Fc is relatively unperturbed by the disruption of Fc protein–glycan interactions (Fig. 4.3C). It is therefore hypothesized that further enhancements to the FcγRIIB selectivity could be achieved by combining the glycan–protein interface mutations, presented here, with previously reported hinge-proximal Cγ2 mutations (S267E/L328F) that exhibit selective FcγRIIB-binding[30; 55]. Two novel IgG1 Fc mutants were generated: V262E/S267E/L328F and

V264E/S267E/L328F which exhibited enhanced affinity for the FcγRIIB (Fig. 4.5C) and, by comparison to the double mutant alone[9; 10], significantly decreased affinity for FcγRIA, FcγRIIA and FcγRIIIB (Fig. 4.5A, B, and E). The double mutant S267E/L328F shows significantly increased affinity for the inhibitory FcγRIIB and decreased affinity for the activatory FcγRIIIA, while the binding for the other FcγRs remain similar to the wild type (Fig. 4.5), consistent with published data[55]. The increased levels of glycan terminal processing and bisection of these triple mutants are comparable to those of the single V262E and V264E mutants (Fig. 4.4D and E, Fig.4.6B and C). The relative affinity of the FcγRIIB-enhancing mutants for FcγRs is summarized on Table 4.2. As discussed in section 1.2.2, generation of Fc variants with enhanced FcγRIIB affinity presents as an attractive strategy to generate immunosuppressive antibodies by engaging and activating the inhibitory signalling associated with FcγRIIB. Although the novel FcγRIIB-enhancing triple mutants reported here have lower affinity for FcγRIIB than the previous reported double mutant (S267E/L328F), they exhibit finer selectivity for FcγRIIB given their reduced affinity for all the activatory FcγRs (Fig. 4.5).

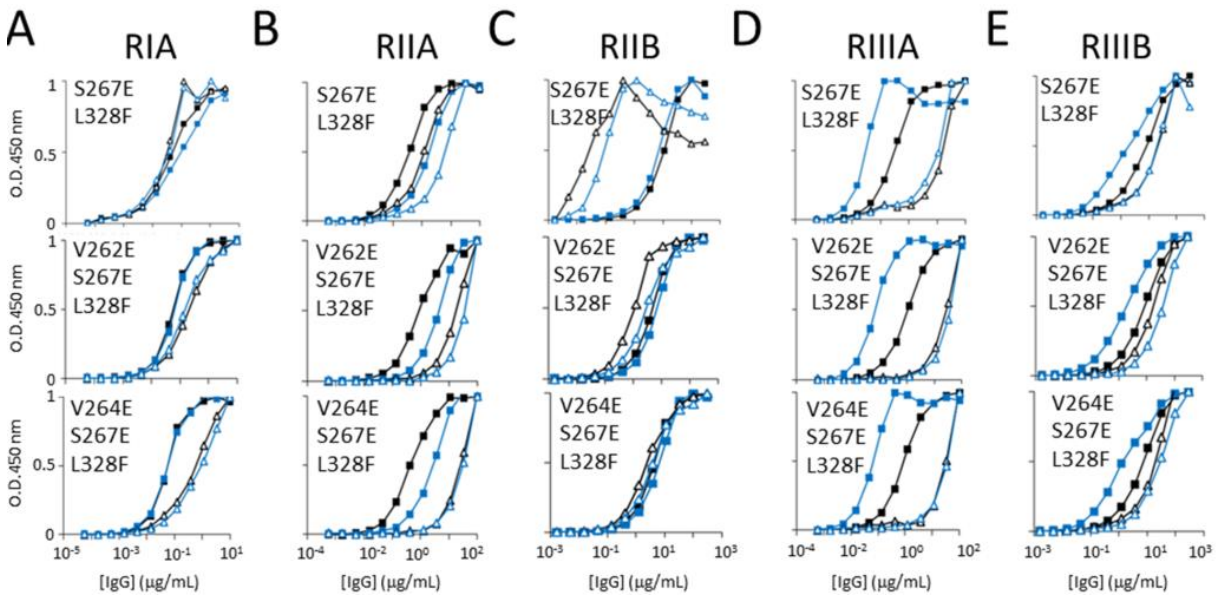

Figure 4.5. ELISA of monoclonal IgG1 b12 variants binding human FcγRIA, FcγRIIA, FcγRIIB, FcγRIIIA and FcγRIIIB. The FcγRs were plated at 5 µg/mL overnight at 4°C, IgG variants S267E/L328F, V262E/S267E/L328F and V264E/S267E/L328F were incubated for 1.5 hours and binding was detected by HRP-conjugated goat anti-human Fab antibody. Symbolic representation of IgG mutation and glycovariants: ■ = wild type native, ■ = wild type $Man_5GlcNAc_2$, △ = mutant native, △ = mutant $Man_5GlcNAc_2$, ELISA binding curves of the four IgG hydrophobic mutants for (A) FcγRIA, IgG variant starting concentration at 10 µg/mL. (B) FcγRIIA, IgG variant starting concentration at 100 µg/mL. (C) FcγRIIB, IgG variant starting concentration at 300 µg/mL. (D) FcγRIIIA, IgG variant starting concentration at 100 µg/mL. (E) FcγRIIIB, IgG variant starting concentration at 300 µg/mL. All data points represent the calculated mean of two independent measurements from a total of at least two experiments.

Table 4.2. Summary of double and triple IgG1 b12 mutants' affinity for FcγRs

FcγR	Glycoform	WT	S267E L328F	V262E S267E L328F	V264E S267E L328F
RIA	Man5	1	3.33	0.23	0.01
	Native	1	2	0.15	0.04
RIIA	Man5	1	0.3	n.b	n.b
	Native	1	0.03	0.02	n.b
RIIB	Man5	1	77.8	2.57	2.57
	Native	1	357.1	4.29	2.5
RIIIA	Man5	1	0.003	n.b	n.b
	Native	1	0.02	n.b	n.b
RIIIB	Man5	1	0.2	n.b	0.04
	Native	1	0.57	0.38	0.11

Summary of double and triple IgG1 b12 mutants' affinity for FcγRs relative to the native (black) or $Man_5GlcNAc_2$ (blue) wild type glycoforms. Each value represents the apparent affinity of a particular mutant glycoform over the same wild type glycoform (i.e. value < 1 indicates weaker binding than the same wild type glycoform and vice versa). All data points represent the calculated mean of two independent measurements from a total of at least two experiments.

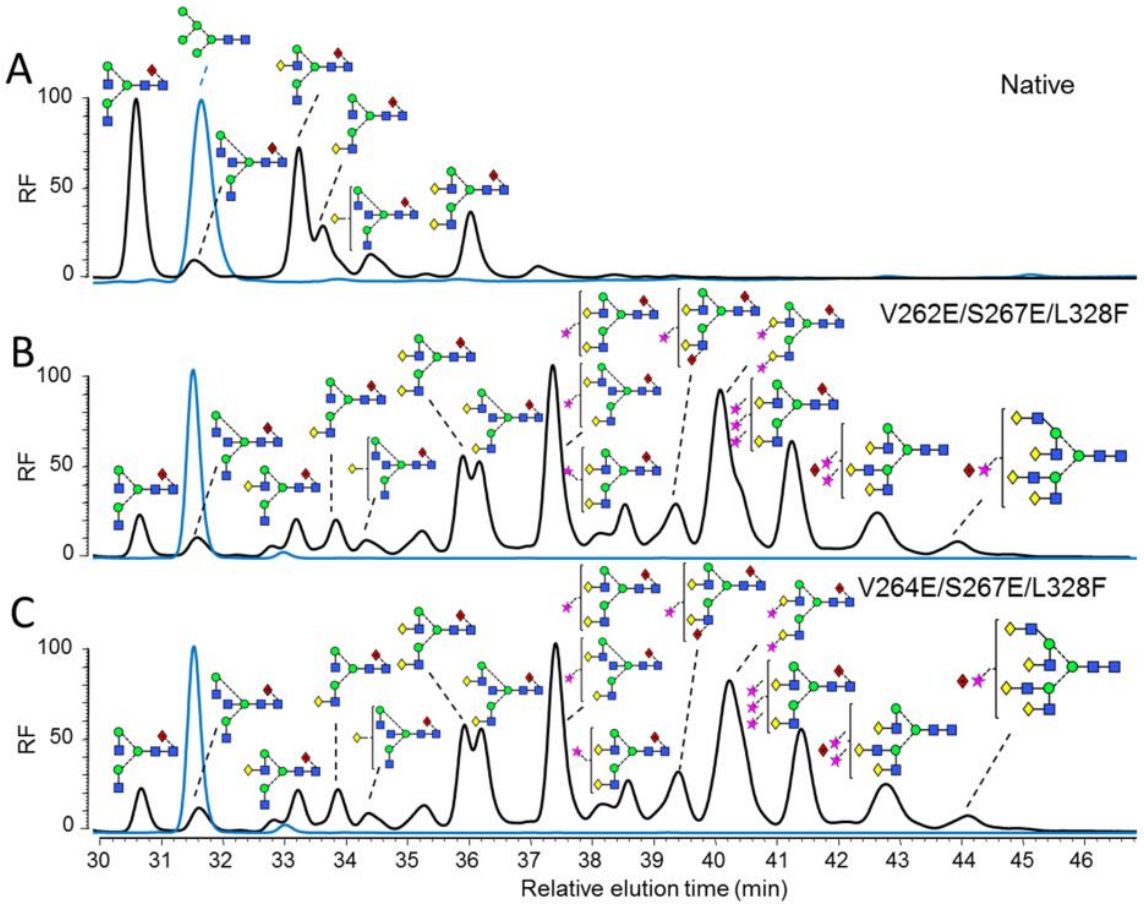

Figure 4.6. HPLC analysis of 2AA-labelled *N*-linked glycans from IgG b12 mutants expressed in HEK 293T and HEK 293S cells. Normal-phase HPLC analysis of 2-AA-labelled *N*-linked glycans, released from target antibody glycoforms by in-gel PNGase F digestion. Glycan profile of IgG expressed in HEK 293T (black) and HEK 293S (blue) for the following variants: (A) Wild type. (B) V262E/S267E/L328F. (C) V264E/S267E/L328F.

4.3. Effect of Fc Terminal Sialylation on FcγR Binding

4.3.1. Generation of Hypergalactosylated and Hypersialylated Human IgG1 b12

Data presented in this chapter so far indicate that destabilization of Fc protein-glycan interactions modify Fc structure relevant for FcγR binding; however, it has previously been shown that hypersialylation of IgG1 Fc, regardless of the linkage type, decreases Fc binding to the FcγRIA, FcγRIIB and FcγRIIIA, which also reduces antibody-mediated cytotoxicity both *in vivo* and *in vitro*[67; 132; 133]. Therefore, to confirm the effect of sialylation on Fc-FcγR

interaction, hypergalactosylated and hypersialylated human IgG1 Fc was generated and their affinity for FcγRIIIA, a critical determinant of natural killer cell-mediated ADCC, was examined. In order to generate hypergalactosylated and hypersialylated glycoproteins, the soluble domains of B4GALT1 and ST6GAL1, which contain the active catalytic domains, were cloned into the mammalian expression vector encoding a hexahistidine tag. The B4GALT1, which contains no *N*-glycosylation site, was expressed in HEK 293T cells, and ST6GAL1, which contains 3 *N*-glycosylation sites, were expressed in HEK 293S cells. After affinity purification using Ni^{2+} Sepharose Beads, ST6GAL1 was deglycosylated by Endoglycosidase H (EndoH) treatment. Both enzymes were further purified by gel filtration, and their purities were assessed by Coomassie Blue-stained SDS-PAGE (Fig. 4.7). Hypergalactosylated and hypersialylated IgG1 b12 was generated by first incubating with B4GALT1 in the presence of $MnCl_2$ and UDP-galactose to achieve hypergalactosylation (Fig. 4.8C), followed by incubating with ST6GAL1 in the presence of $MnCl_2$ and CMP-sialic acid to achieve hypersialylation (Fig. 4.8D).

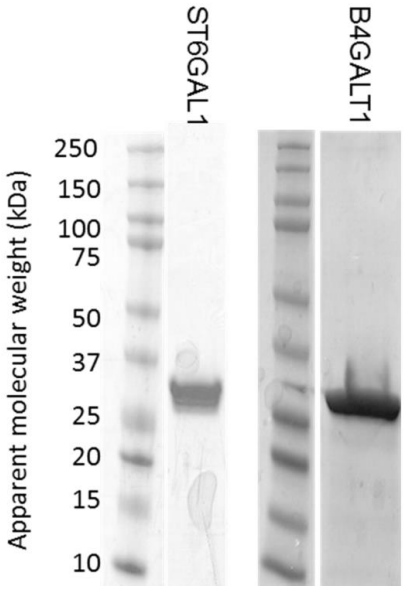

Figure 4.7. SDS-PAGE analysis of recombinant human B4GALT1 and ST6GAL1. Soluble region of each enzyme was cloned into a hexahistidine-tagged mammalian expression vector and expressed in HEK 293T cells. Proteins were affinity-purified by Ni^{2+} Sepharose beads, followed by gel filtration. Protein samples were run on 4-12% gradient Bis-Tris gel and then stained by Coomassie Blue.

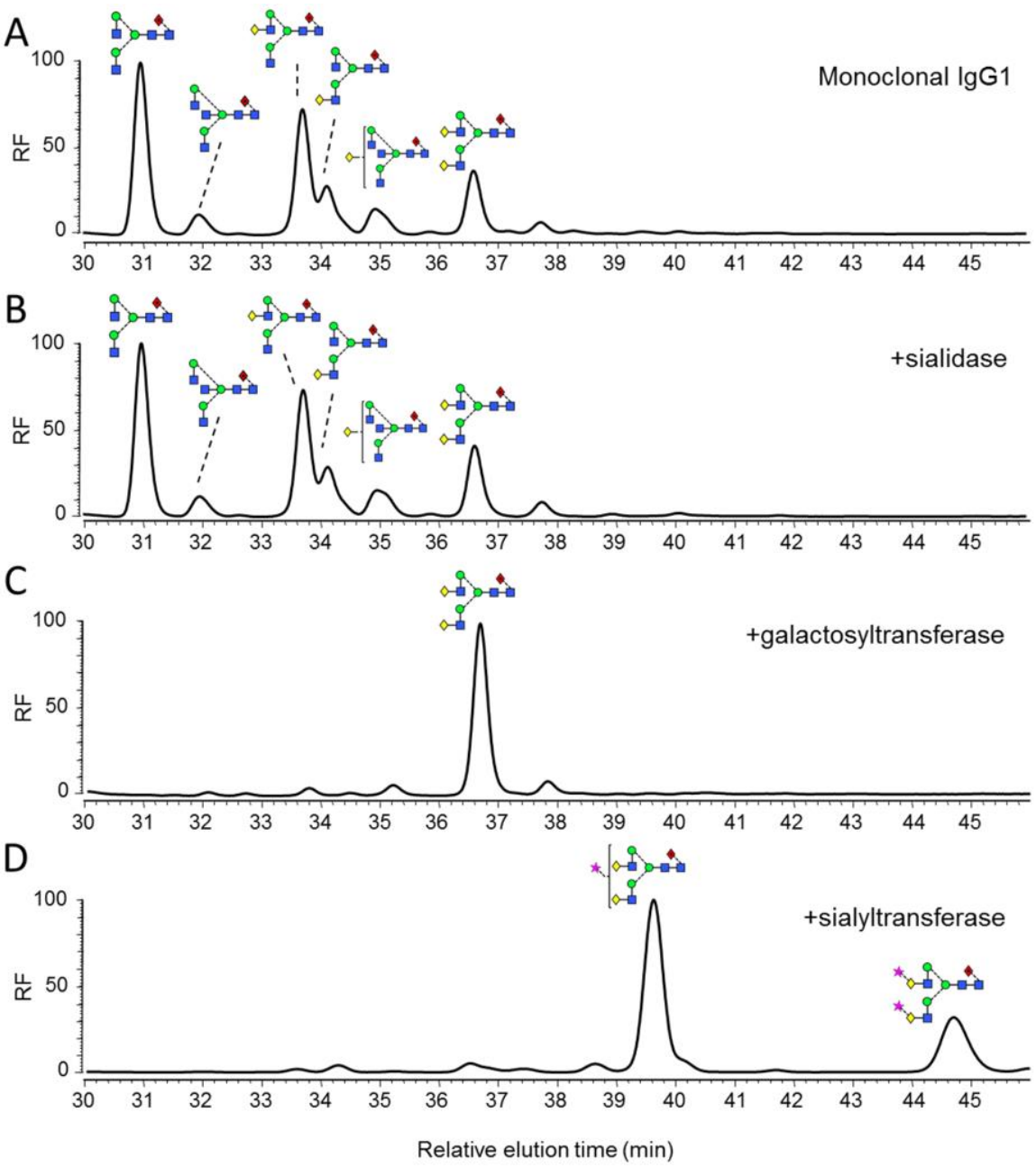

Figure 4.8. Generation of hypergalactosylated and hypersialylated IgG1 b12. Normal-phase HPLC analysis of 2-AA-labelled *N*-linked glycans, released from target antibody glycoforms by in-gel PNGase F digestion. (A) Glycan profile of monoclonal IgG1 b12. (B) Glycan profile of IgG1 b12 incubated with 50 U/mL *Clostridium perfringens* neuraminidase for 48 hours at 37˚C. (C) Glycan profile of IgG1 b12 incubated with 25 µg/mL B4GALT1 and 80 µM UDP-galactose in 50 mM HEPES, 10 mM $MnCl_2$, pH 7.5 for 48 hours at 37˚C. (D) Glycan profile of IgG1 b12 sequentially treated with B4GALT1 and ST6GAL1.

4.3.2. Effect of Fc Sialylation on FcγR Binding

Usually, the Fc–FcγR affinity strongly correlates with effector functions measured by cellular assays[30; 55; 112; 115; 134; 153; 260]. However, data reported here indicate that the hypersialylated Fc binds to the FcγRIIIA with very similar affinity to the wild type, supported by both ELISA (Fig. 4.3F) and SPR data (Fig. 4.9). This minimal effect of Fc sialylation on FcγRIIIA binding is also observed for the FcγRIA and FcγRIIA (Fig. 4.3F), while a decreased for the FcγRIIB was detected (Fig. 4.3F). The generally unaltered Fc-FcγR interaction upon sialylation is also supported by the crystallographic analysis of sFc, which is presented in Chapter 5. The insignificant effect of Fc sialylation on Fc affinity for FcγRIIIA points to factors other than sialylation which mediate the sialylation-induced reduction in ADCC. One possible explanation for the reduced cytotoxicity is that terminal sialic acid might interact with inhibitory siglecs present on the surface of immune cells including macrophages and natural killer cells[261].

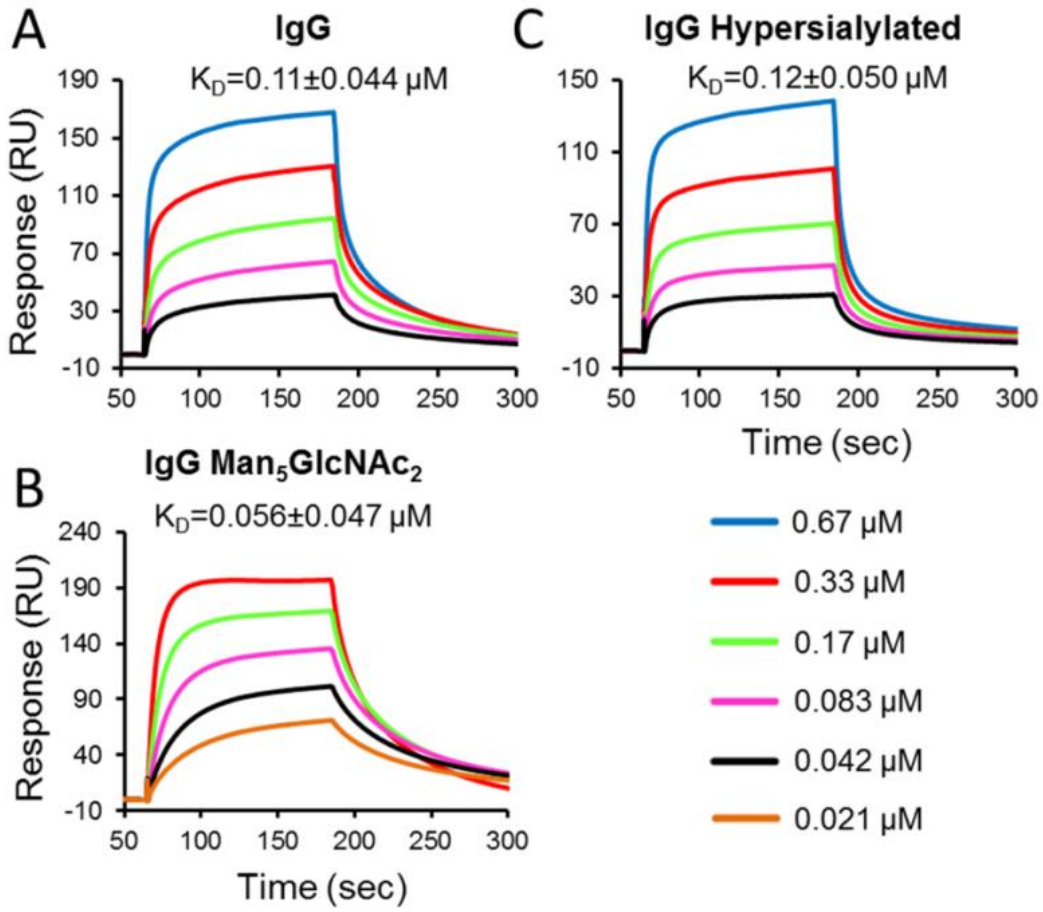

Figure 4.9. SPR analysis of monoclonal IgG1 b12 variants binding to human FcγRIIIA. The recombinant human FcγRIIIA was immobilized on the CM5 sensorchip by amine coupling. The IgG variants were injected at 5 different concentrations at a flow rate of 30 µL/min: IgG and Hypersialylated IgG (0.67, 0.33, 0.17, 0.083, and 0.042 µM); IgG $Man_5GlcNAc_2$ (0.33, 0.17, 0.083, 0.042 and 0.021 µM). The association time was 2 minutes and dissociation time was 3 minutes. The chip was regenerated with 10 mM glycine-HCl, pH 1.7. Sensorgrams were fitted with a global 1:1 interaction, and the k_{on}, k_{off}, and K_D were calculated, all using BIAevaluation software 2.0.3. K_D values are reported as Mean ± SD, and sensorgrams are representative a total of 3 independent experiments.

4.4. Conclusions

The hydrophobic mutations on the Fc protein-glycan interface have been shown to decrease antibody Fc-mediated effector functions, via reduced binding to FcγR[87]. However, it is unknown whether this decreased Fc- FcγR interaction was due to increased glycan processing, or the disrupted protein-glycan interface. Here, both wild type Fc and its hydrophobic mutants were engineered to express the uniform $Man_5GlcNAc_2$ glycoform, and their affinities for the FcγRs were compared. This comparison reveals that disruption of the Fc protein-glycan interface broadly reduces Fc affinity for FcγRs, though to different extents, independent of Fc glycoform. The differential effect of hydrophobic mutations on Fc-FcγRs interaction was then explored to generate novel Fc mutants with enhanced selectivity for the inhibitory FcγRIIB. Thus, the integrity of Fc protein-glycan interface, demonstrated here to be crucial for FcγR binding, presents a novel parameter to allow the fine-tuning of Fc effector functions.

Chapter 5

The Interaction between DC-SIGN and IVIg

5. The Interaction between DC-SIGN and IVIg

5.1. Summary

IVIg is used to treat a wide range of autoimmune and inflammatory diseases, including ITP, RA, multiple sclerosis and Kawasaki syndrome[23; 157; 158; 159; 160]. It consists of mainly IgG pooled from at least thousands of healthy donors[139; 202]. The cellular receptor for IVIg has been elusive until recently, the C-type lectin DC-SIGN has been identified as the cellular receptor for IVIg, in a model describing that the binding of sFc to DC-SIGN initiates a TH_2-dependent anti-inflammatory pathway. However, this direct sFc-DC-SIGN interaction was inferred from the ability of DC-SIGN-transfected cells to deplete α2,6-sFc (but not α2,3-sFc) from cell culture supernatant; and this depletion could be inhibited by known ligands of the DC-SIGN CRD[39]. Indeed, it has been shown, more recently, that the α2,6-sFc directly bind to DC-SIGN-transfected CHO cells, in a sialic acid-dependent manner, and this binding could be inhibited by DC-SIGN in a dose-dependent manner[135]. However, this novel sFc-DC-SIGN interaction is not supported by existing biophysical data of DC-SIGN[29; 30;26; 27; 28]. Here, the direct interaction between sFc and the tetrameric extracellular region of DC-SIGN was re-evaluated extensively using direct biophysical methods.

5.2. Generation of an Array of Differentially Glycosylated Proteins

Differentially glycosylated IVIg (desialylated, deglycosylated, and hypergalactosylated and hypersialylated) and recombinant Fc ($Man_5GlcNAc_2$, and hypergalactosylated and hypersialylated) were generated to probe their interactions with DC-SIGN. Recombinant tetrameric DC-SIGN used in this experiment was provided by Dr Daniel Mitchell at Warwick University, UK. The hypersialylated proteins were generated by sequential treatment with B4GALT1 and ST6GAL1 as described in section 4.3.1. The level of galactosylation and sialylation for both IgG (Fig. 5.1C and D) and Fc (Fig. 5.2B and C) was monitored after each

enzymatic treatment. The 3-arm was more efficiently sialylated than the 6-arm for both IgG and Fc (Fig. 5.1D, Fig. 5.2C), consistent with previous branch-preference of ST6GAL1 sialylation, a property retained in the absence of Fc protein backbone[257]. Interestingly, full length IgG, regardless of antigen specificity, was generally less efficiently sialylated on the 6-arm than recombinant Fc (Fig. 4.8D, Fig. 5.1D, Fig. 5.2C). Desialylated and deglycosylated IgG were generated by treatment with neuraminidase and PNGase F respectively. IgG desialylation was confirmed by HPLC analysis (Fig. 5.1B), and deglycosylation was confirmed by the shift of the IgG heavy chain in Coomassie-Blue stained SDS-PAGE (Fig. 5.3A).

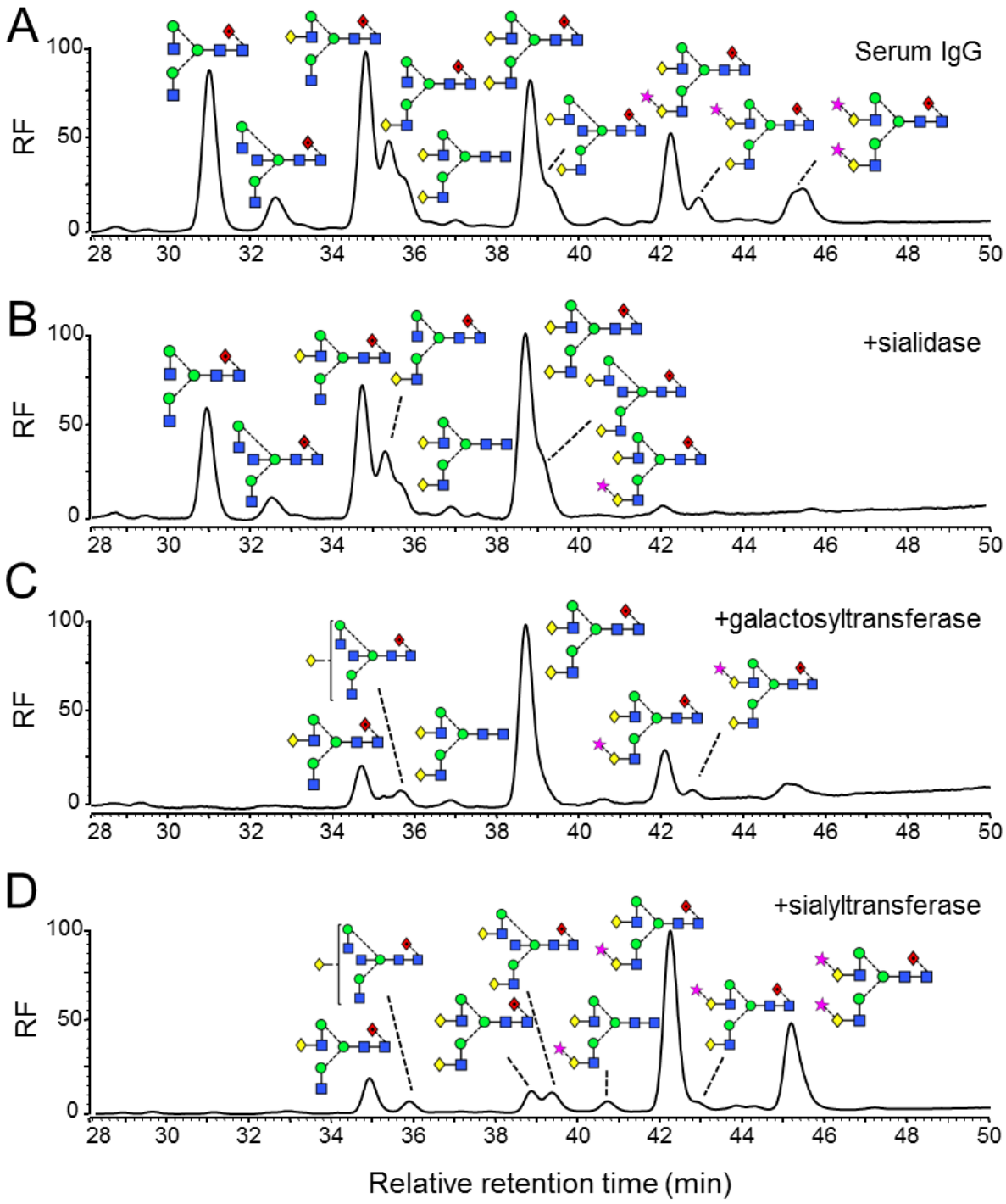

Figure 5.1. Generation of differentially glycosylated human serum IgG. Normal-phase HPLC analysis of 2-AA-labelled *N*-linked glycans, released from target antibody glycoforms by in-gel PNGase F digestion. (A) Glycan profile of polyclonal serum IgG. (B) Glycan profile of serum IgG incubated with 50 U/mL *Clostridium perfringens* neuraminidase for 48 hours at 37˚C. (C) Glycan profile of serum IgG incubated with 25 µg/mL B4GALTI and 80 µM UDP-galactose in 50 mM HEPES, 10 mM $MnCl_2$, pH 7.5 for 48 hours at 37˚C. (D) Glycan profile of serum IgG sequentially treated with B4GALT1 and ST6GAL1.

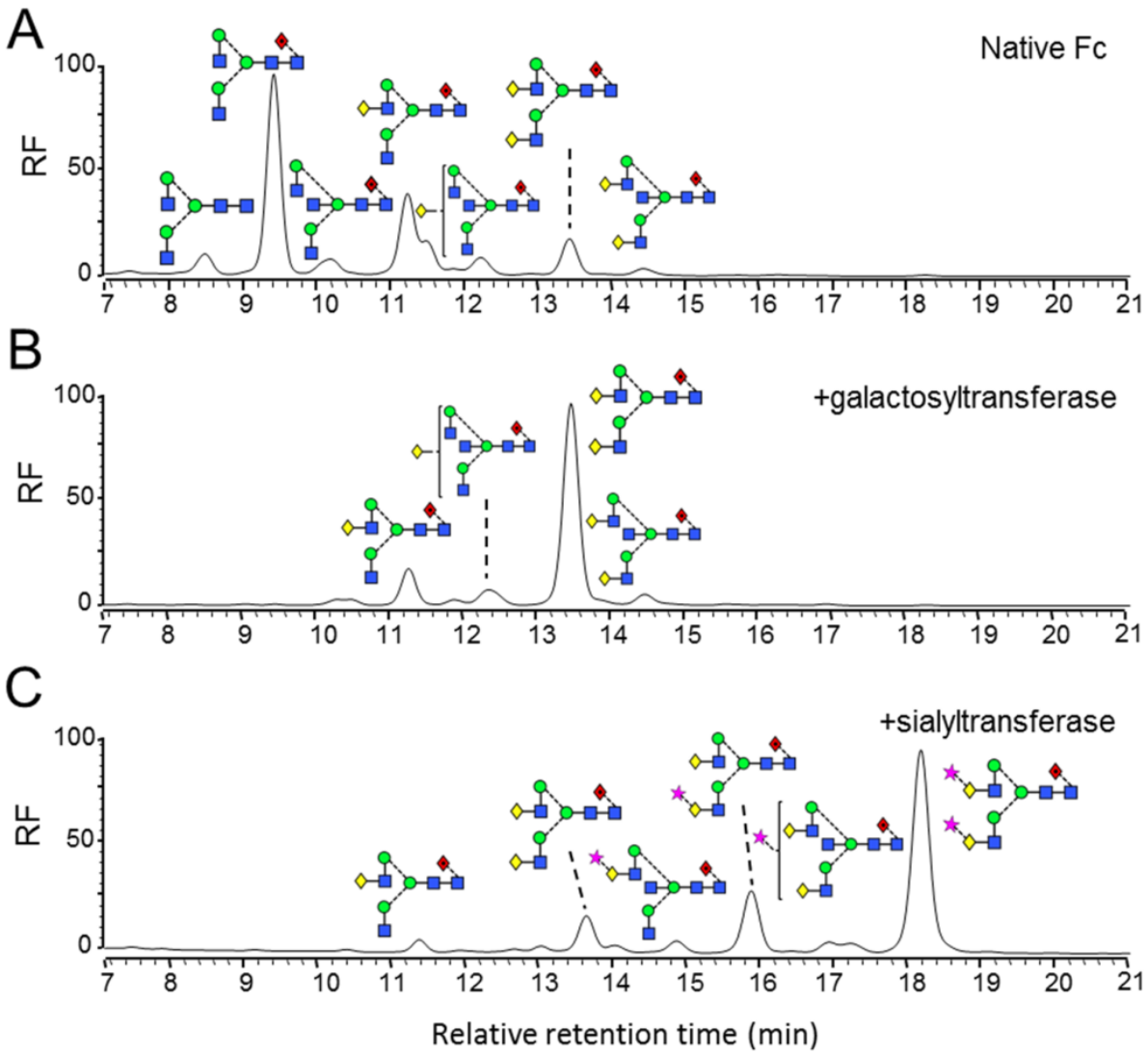

Figure 5.2. Generation of differentially glycosylated recombinant human IgG1 Fc. Normal-phase HPLC analysis of 2-AA-labelled *N*-linked glycans, released from target antibody glycoforms by in-gel PNGase F digestion. (A) Glycan profile of recombinant IgG1 Fc. (B) Glycan profile of recombinant IgG1 Fc incubated with 25 μg/mL B4GALT1 and 80 μM UDP-Gal in 50 mM HEPES, 10 mM $MnCl_2$, pH 7.5 for 48 hours at 37˚C. (C) Glycan profile of recombinant IgG1 Fc sequentially treated with B4GALT1 and ST6GAL1.

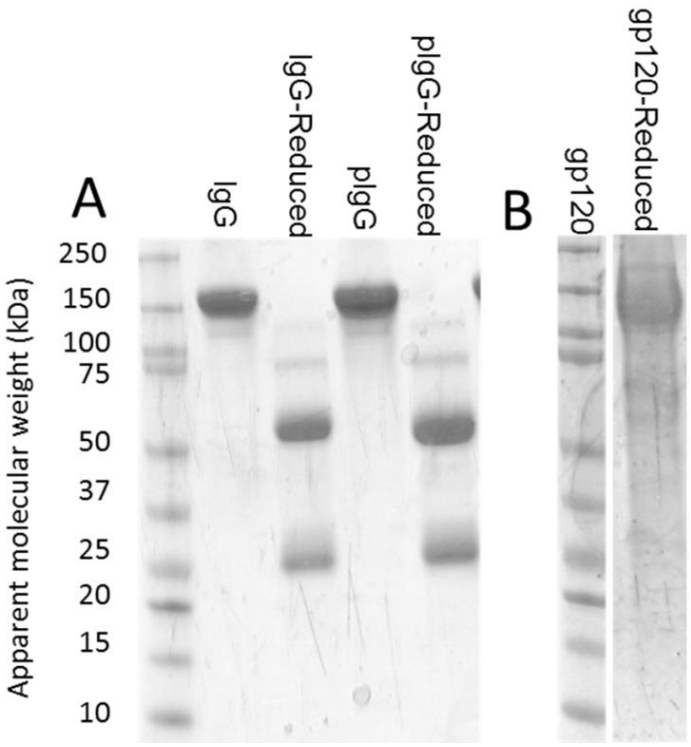

Figure 5.3. SDS-PAGE analysis of deglycosylated serum IgG and recombinant gp120. Deglycosylated serum IgG was generated by incubation with PNGase F for 48 hours at 37˚C. For protein denaturation, the samples were boiled for 5 minutes in the presence of DTT. Protein samples were run on 4-12% gradient Bis-Tris gel and then stained by Coomassie Blue. SDS-PAGE analysis of (A) Native serum IgG and deglycosylated serum IgG (pIgG). (B) Recombinant gp120

The ectodomain of the HIV1 glycoprotein gp120 was cloned into a mammalian expression vector and expressed in HEK 293T cells from the laboratory[262]. Monomeric gp120 was purified by gel filtration, and its purity was assessed by Coomassie-Blue stained SDS-PAGE (Fig. 5.3B). Glycan analysis shows that this recombinant gp120 is dominated by oligomannose glycoforms (Fig. 5.4), consistent with previous reports[262; 263]. The gp120 was biotinylated, according to manufacturer's recommended protocol, to allow subsequent detection by HRP-conjugated Streptavidin. The gp120 with $Man_9GlcNAc_2$ glycoform was obtained by expression in HEK 293T cells supplemented with 20 μM Kifunensine, a potent inhibitor of α-mannosidase in the endoplasmic reticulumn[264]. The expression and purification of gp120 with $Man_9GlcNAc_2$ glycoform was carried out by Snezana Vasiljevic. The recombinant human IgG1 Fc with complex type and $Man_5GlcNAc_2$ glycoforms was cloned

and expressed as described in section 3.2.1, and their glycan profiles were verified by HPLC (Fig. 5.5).

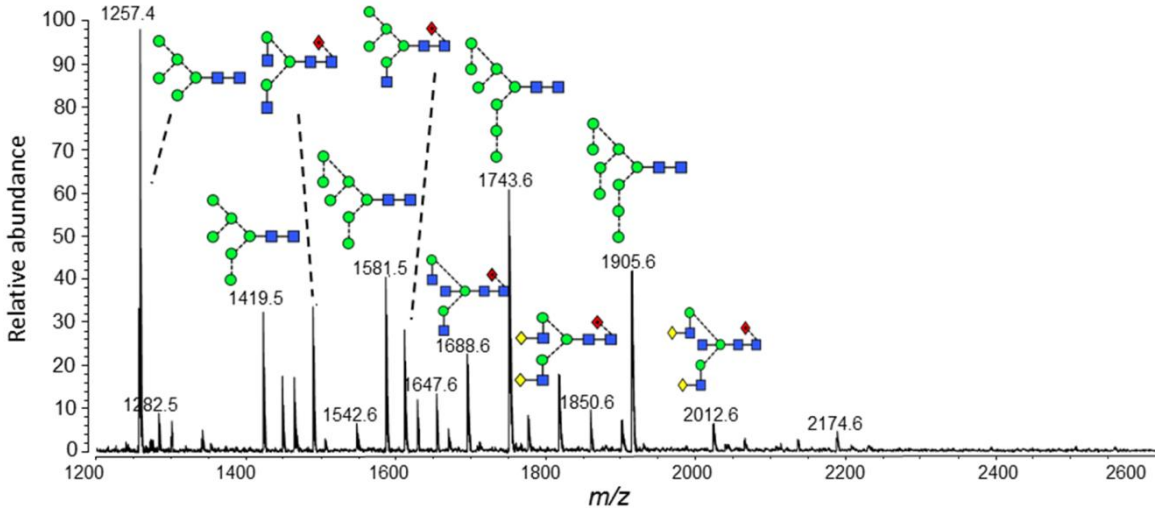

Figure 5.4. MALDI-TOF-MS analysis of *N*-linked glycans released from recombinant gp120. The *N*-linked glycans were released from IgG by PNGase F digestion and then analysed by MALDI-TOF-MS in Reflection-DHB mode, with DHB as the matrix.

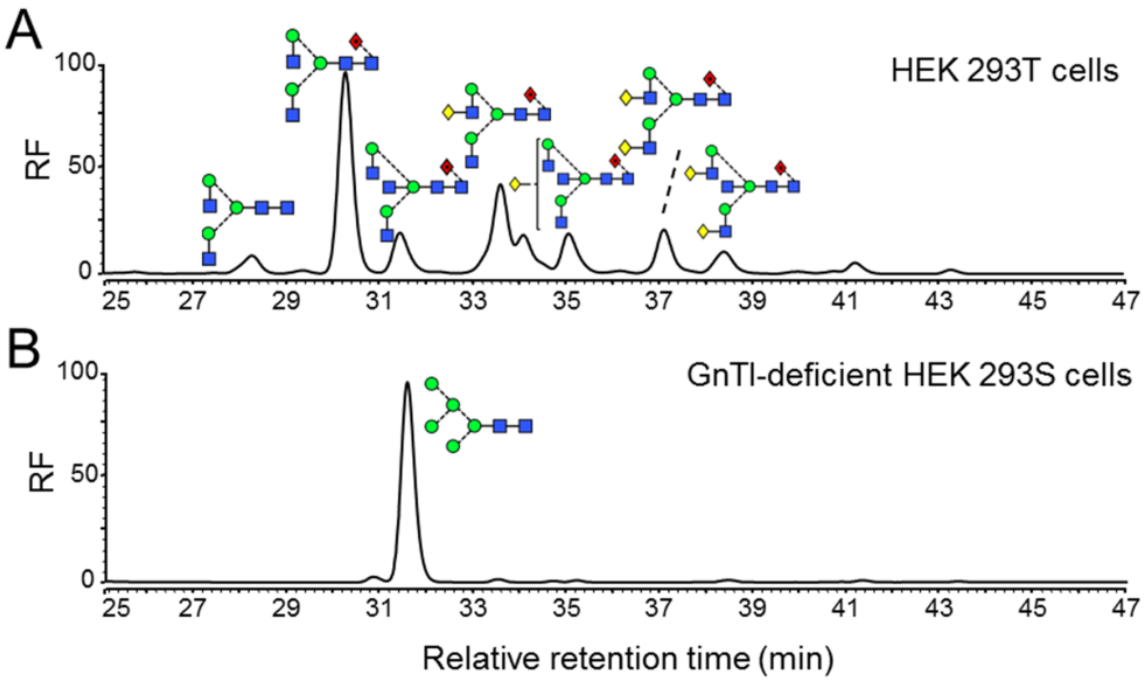

Figure 5.5. HPLC analysis of 2AA-labelled *N*-linked glycans from recombinant human IgG1 Fc expressed in HEK 293T and HEK 293S cells. Normal-phase HPLC analysis of 2-AA-labelled *N*-linked glycans, released from target Fc glycoforms by in-gel PNGase F digestion. Glycan profile of recombinant Fc expressed in (A) HEK 293T cells and (B) HEK 293S cells.

5.3. Direct Interaction between IVIg, Fc and DC-SIGN

The integrity of the tetrametric DC-SIGN was validated by its high affinity (about 1 nM) for the HIV1 glycoprotein gp120 (Fig. 5.6A), consistent with previous report[205]. The serum IgG showed a 1000-fold less apparent affinity (about 1μM) for DC-SIGN than that of gp120, consistent with the affinity inferred from the cellular depletion assay reported previously[39]. Notably, both hypersialylated and desialylated serum IgG bound to DC-SIGN with very similar affinities to that of naturally glycosylated material (Fig. 5.6A). Furthermore, even fully deglycosylated serum IgG exhibited an unchanged affinity for DC-SIGN (Fig. 5.6A). In addition, both recombinant Fc and its hypersialylated counterpart did not exhibit any measurable binding to DC-SIGN (Fig. 5.6A); even Fc with uniform $Man_5GlcNAc_2$ glycoform, a known high affinity glycan for DC-SIGN, did not show any significant binding to DC-SIGN (Fig. 5.6B). As expected, however, both IgG and Fc bind to the established FcγRIIIA with similar affinities (Fig. 5.7). The insensitivity of DC-SIGN/IVIg interaction to modulation of IgG Fc glycosylation, combined with a lack of Fc affinity for DC-SIGN, points to a Fab-dependent polyclonal IgG affinity for DC-SIGN. Indeed, serum IgG binds irrelevant antigens such as fetuin, gp120 and BSA with very similar affinity to DC-SIGN (Fig. 5.8A), whereas the Fc domain does not exhibit nonspecific binding (Fig. 5.8B).

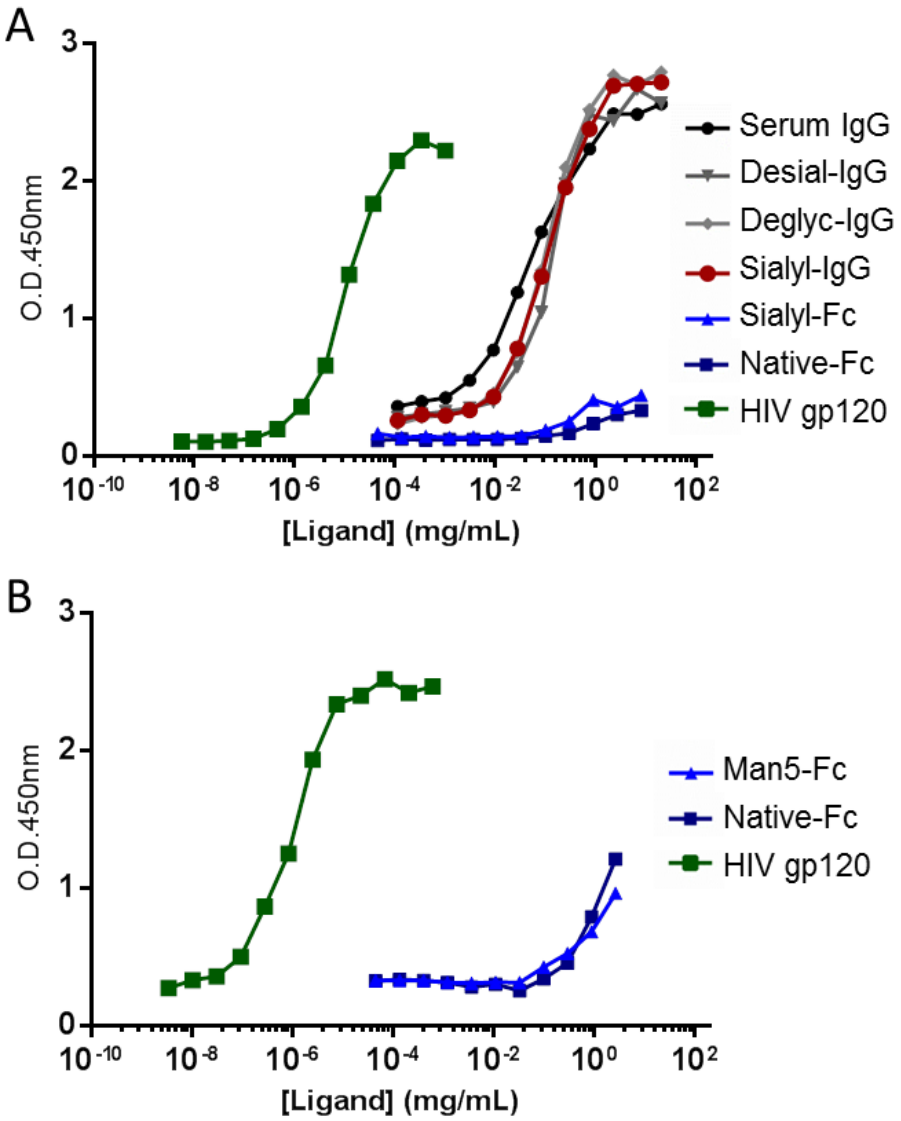

Figure 5.6. Interaction of DC-SIGN with different glycoforms of serum IgG. (A) ELISA probing the binding between immobilized DC-SIGN and the following target glycoproteins: serum IgG; desialylated serum IgG (Desial-IgG); deglycosylated serum IgG (Deglyc-IgG); hyper-α2,6-sialylated serum IgG (Sialyl-IgG); hyper-α2,6-sialylated glycoform of recombinant IgG1 Fc (Sialyl-Fc); native glycoform of recombinant IgG1 Fc (Native-Fc); HIV gp120. IgG and Fc binding was detected by HRP-conjugated anti-human Fc antibody and biotinylated gp120 binding was detected by HRP-conjugated streptavidin. (B) ELISA probing the binding between immobilized DC-SIGN and the following target glycoproteins: Native-Fc; $Man_5GlcNAc_2$ glycoform of Fc (Man5-Fc); and HIV gp120. Fc binding was detected by HRP-conjugated anti-human Fc antibody and biotinylated gp120 binding was detected by HRP-conjugated streptavidin. All data points represent the calculated mean of two independent measurements from a total of at least two experiments.

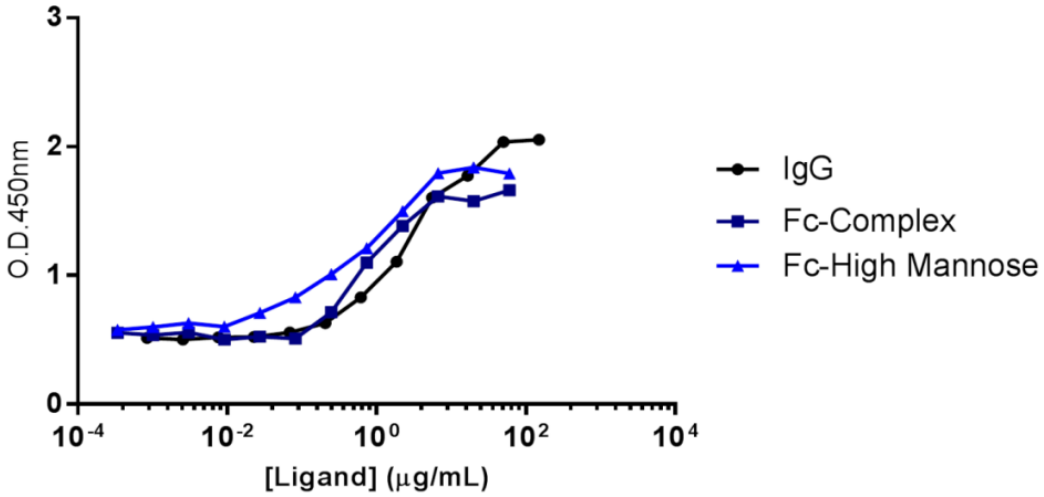

Figure 5.7. Binding of FcγRIIIA to serum IgG and recombinant glycoforms of Fc. ELISA plate was coated with FcγRIIIA at 5 μg/mL overnight. Both Fc and IgG binding were detected by HRP-conjugated anti-human Fc antibody.

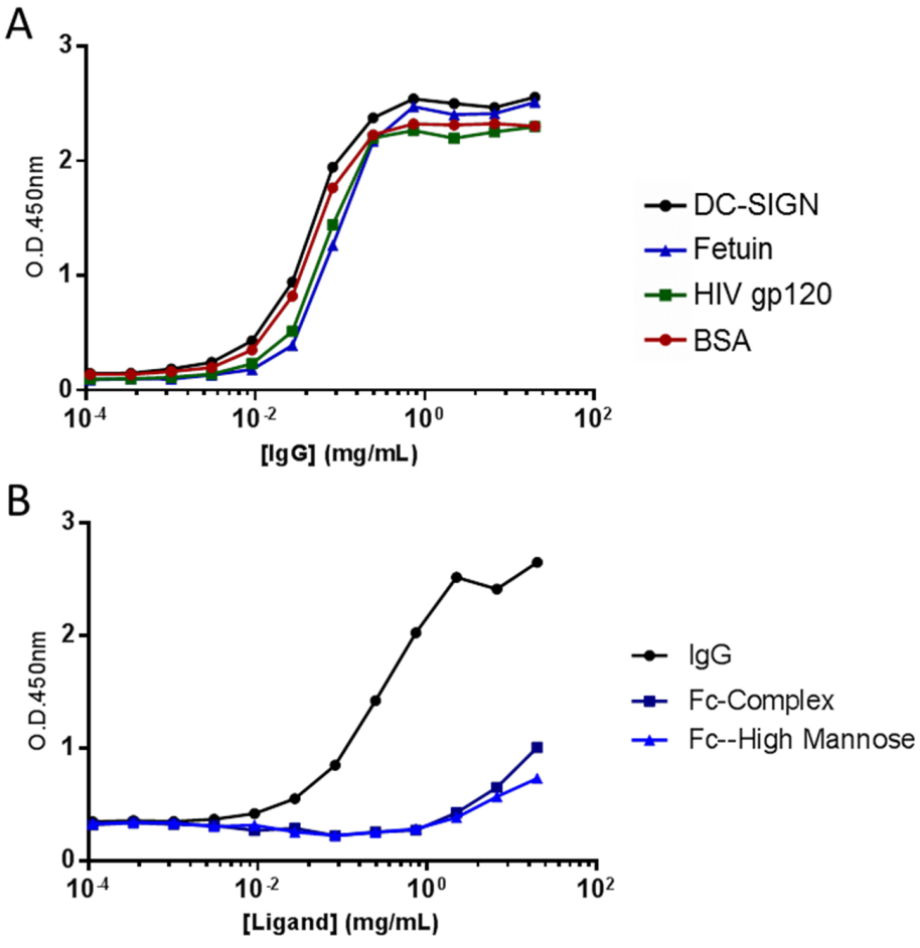

Figure 5.8. Interaction of serum IgG with irrelevant antigens. (A) ELISA probing the binding between polyclonal serum IgG and a panel of immobilised antigens: DC-SIGN; fetuin; HIV gp120 and BSA. Binding was detected by HRP-conjugated anti-human Fab antibody. (B) ELISA probing the binding of IgG and Fc to DC-SIGN. Both IgG and Fc binding were detected by HRP-conjugated anti-human Fc antibody. All data points represent the calculated mean of two independent measurements from a total of at least two experiments.

5.4. Inhibition of Interaction between DC-SIGN and Serum IgG

The lack any detectable, specific affinity for DC-SIGN (Fig. 5.6A) in human serum would appear to contradict reports that DC-SIGN binds selectively to α2,6-sialylated IgG and that this interaction can be blocked by known ligands of the DC-SIGN CRD[39], and the soluble extracellular domain of DC-SIGN[135]. Therefore, the inhibition, by serum IgG, of the interaction between DC-SIGN and a known CRD ligand (gp120) was tested. Consistent with previous analyses[207], monosaccharides with vicinal, equatorial 3- and 4- hydroxyls inhibited gp120 binding to the DC-SIGN CRD (K_I for D-mannose and D-glucose = 16 and 27 mM, respectively). Other monosaccharide only weakly inhibited this interaction (K_I for D-galactose and Neu5Ac = 132 mM and 265 mM, respectively) (Fig. 5.9). Unlabelled (i.e. non-biotinylated) gp120 showed a high-affinity interaction (K_I = 0.03 μM) with DC-SIGN. Moreover, gp120 engineered to contain a purely oligomannose glycoform (> 95% $Man_9GlcNAc_2$) exhibited improved inhibition compared the wild-type gp120 (containing < 50% oligomannose glycans[243]) (Fig. 5.9). In contrast to these known low- and high-affinity CRD ligands, serum IgG did not show any detectably inhibitory activity, even at IgG concentrations significantly in excess of physiological values for human sera.

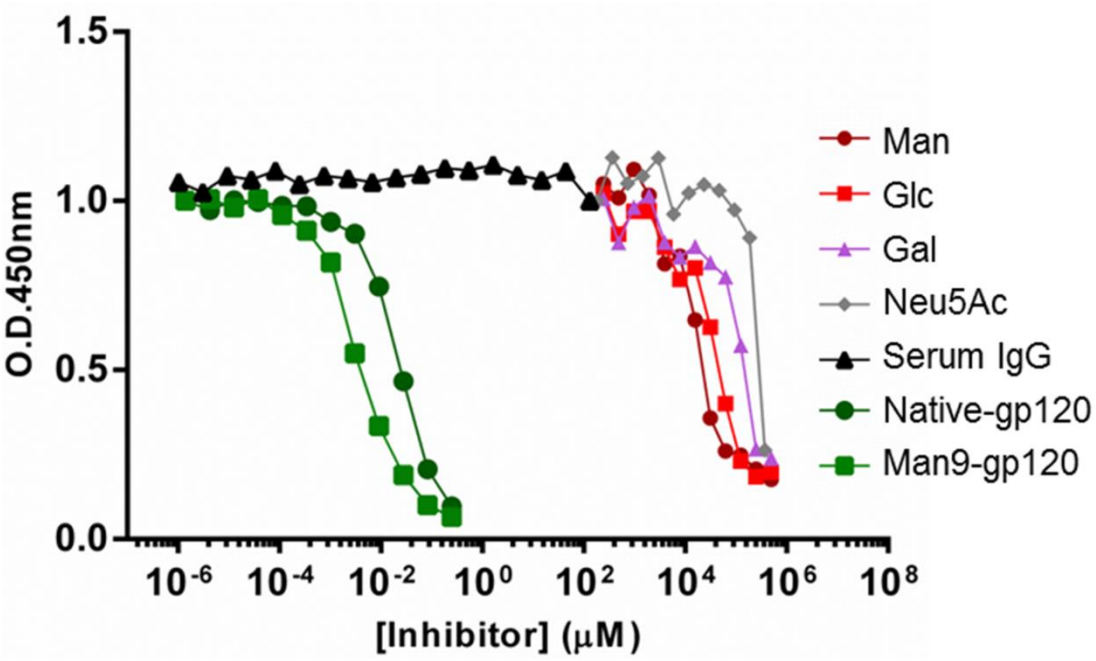

Figure 5.9. Competition ELISA between biotinylated gp120 and immobilised DC-SIGN in the presence of known and candidate inhibitors. Biotinylated gp120 binding was detected by HRP-conjugated streptavidin. The concentration of biotinylated gp120 (2.5 ng/mL) was binding mid-point to DC-SIGN (Fig. 5.6A). Solution-phase inhibitors were titrated across a range of concentrations and included monosaccharides, serum IgG, and the native and $Man_9GlcNAc_2$-glycoforms of HIV gp120 (native-gp120 and Man9-gp120, respectively). All data points represent the calculated mean of two independent measurements from a total of at least two experiments.

Recently, one group demonstrated the direct binding of sIgG to DC-SIGN-transfected CHO cells, in a sialic acid-dependent manner[135], and proposed that Fc sialylation induces conformational changes in the Fc protein backbone, including the induction of a "closed" Fc conformation, which allows a previously unidentified interaction between sFc and DC-SIGN, in a manner similar to the newly illustrated IgE-CD23 interaction[135; 265]. Moreover, this proposed model precludes the interaction between sIgG and soluble tetrameric DC-SIGN in solution phase[135]; nevertheless, the direct interaction between sIgG and cell surface tetrameric DC-SIGN could be inhibited by soluble tetrameric DC-SIGN[135], from which the direct interaction between sIgG and soluble tetrameric DC-SIGN could be inferred. To validate this novel model of protein-protein interaction, extensive mutagenesis of DC-SIGN and/or Fc is needed to identify the key regions required for this interaction.

5.5. Crystal Structure of sFc

In addition to the extensive ELISA studies presented here, the crystal structure of sFc was determined, in collaboration with Dr Thomas Bowden, to a resolution of 2.3 Å, which also contradicts the proposed sIgG-DC-SIGN model. As mentioned in section 5.4, upon the recent observation that DC-SIGN-transfected CHO cells bind sIgG in a sialic acid-dependent manner, a molecular model for sIgG-DC-SIGN interaction was built based on homology with the co-crystal structure of the IgE receptor CD23 and IgE Fc[135]. It was proposed, in this model, that Fc sialylation induces a "closed" Fc conformation, similar to the CD23-bound IgE Fc[265], which allows a previously unidentified Fc interaction with DC-SIGN[135]. The model is supported by the finding that sIgG is able to bind CD23-transfected CHO cells in a sialic acid-dependent manner[135].

To validate this model, the sFc crystal structure was determined to examine the structural modifications associated with Fc sialylation (Fig. 5.10). The level of di-sialylated Fc population in the sFc preparation was determined to be approximately 80% by HPLC (Fig. 5.10A), before sFc was crystallized. The electron density corresponding to the α2,6-sialic acid residue on the 6-arm was clearly visible, to a degree that the sialic acid residue was able to be built onto the structure (Fig. 5.10C). Structural analysis of sFc shows an overall similar conformation to the classical asialylated Fc with well-defined Cγ2 and Cγ3 domains (Fig. 5.10B). Moreover, an overlay of the sFc structure with the asialylated Fc structure demonstrates that sFc maintains the classical "open" conformation (Fig. 5.10D). Thus, a re-evaluation of the proposed sIgG-DC-SIGN interaction model is warranted. The conventional sFc structure presented here also supports the conclusion, presented in section 4.3.2, that Fc hypersialylation does not generally affect Fc-FcγRs interaction.

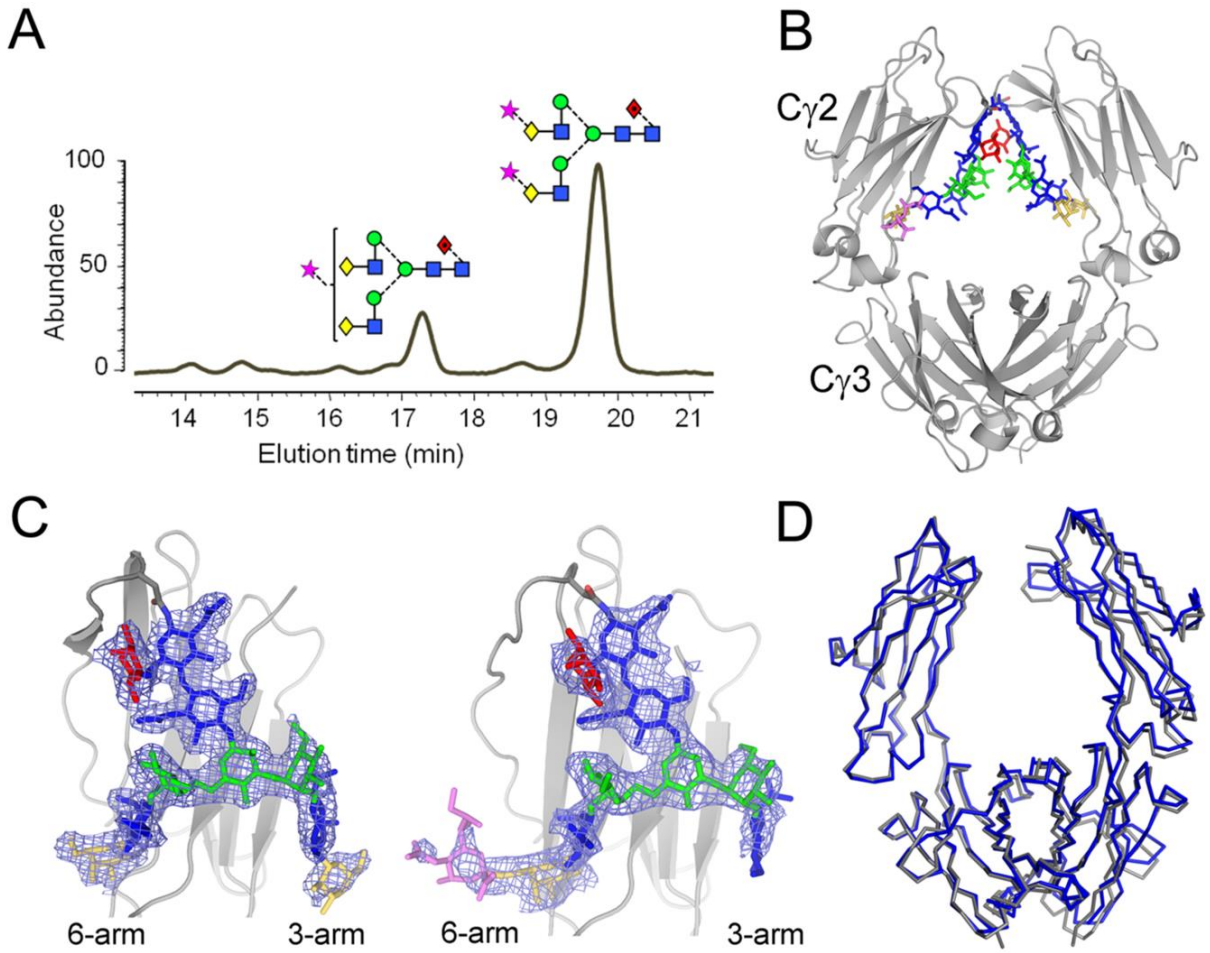

Figure 5.10. Crystal structure of hypersialylated IgG1 Fc. (A) HPLC analysis of fluorescently-labelled *N*-linked glycans released from recombinant, hypergalactosylated and hypersialylated IgG1 Fc. Hypersialylation was achieved by sequential enzymatic treatment with B4GALT1 and ST6GAL1. (B) Structure of sFc with monosaccharide residues in stick representation and coloured according to Panel A. Protein backbone is in ribbon representation. (C) Comparison of conformation of the glycans on sFc and asialylated Fc (PDB ID 1H3Y), with electron density for monosaccharides shown in blue mesh. (D) Overlay of sFc structure with the asialylated Fc (PDB ID 1H3Y). The sFc crystal was prepared and X-ray diffraction data were collected by Dr Thomas Bowden. Structural refinement was carried out by Dr Thomas Bowden and Dr Max Crispin. For crystallographic analysis, sFc (6.5 mg/mL) was crystallized at 25 ^{o}C in 4.0 M NaCl, 0.1 M citrate pH 4.0 using the sitting-drop vapour diffusion method using 100 nL protein plus 100 nL precipitant equilibrated against 95 µL reservoirs. Crystals were flash frozen by immersion in a cryoprotectant containing the mother liquor diluted in 5 M NaCl and then rapidly transferred to a gaseous nitrogen stream. X-ray diffraction data were recorded at Beamline I04 at Diamond Light Source, Oxfordshire, UK. This figure was produced by Dr Thomas Bowden and Dr Max Crispin (University of Oxford).

5.6. Interaction between IgG and Siglecs

In the light that no glycan-dependent interaction was observed between IVIg and DC-SIGN, it is noted that the cross-linking of the sialic-acid binding siglecs and Fc receptors induces

inhibitory signalling[266; 267], as well as the sialic acid-dependent, IVIg-mediated suppression of B cell activation by engaging the siglec CD22[230]. The widespread presence of ITIM motifs on cytosolic domains of many α2,6-linked sialic acid-specific siglecs prompt the investigation of their interaction with IVIg. To this end, the extracellular domains of two siglecs with preferential specificity for α2,6-linked sialic acid, CD22 and CD33, were cloned and tested for their affinity for sIgG. Both siglecs contain *N*-glycosylation sites; therefore, they were expressed in the HEK 293S to attain homogenous $Man_5GlcNAc_2$ glycoform, to prevent any potential *cis*-interactions[268]. The purity of recombinant CD22 and CD33 was checked by SDS-PAGE (Fig. 5.11A and B), and their glycform was confirmed by MALDI-TOF-MS (Fig. 5.11C).

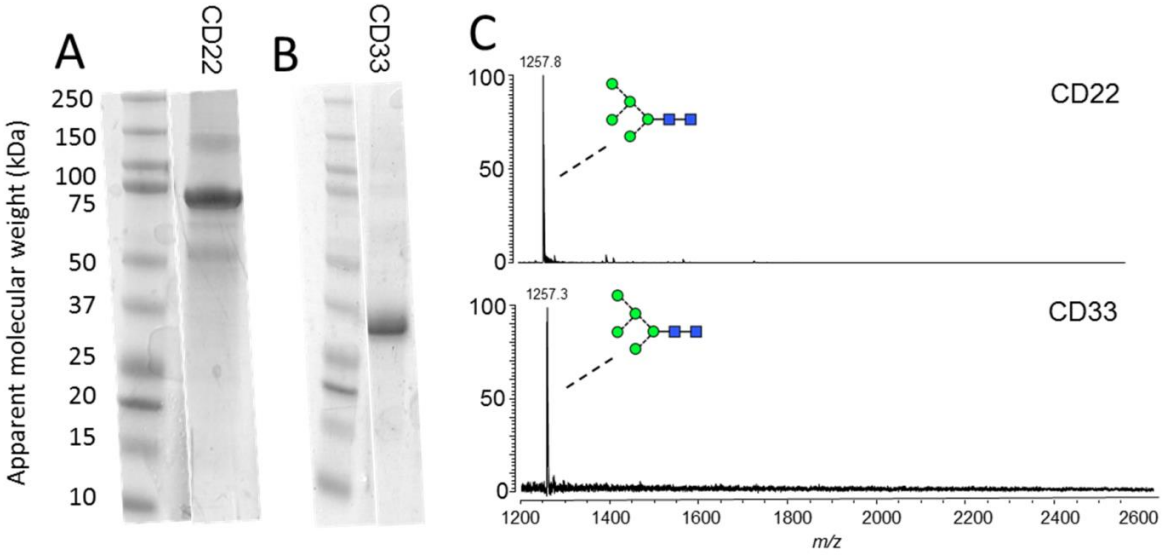

Figure 5.11. Expression of extracellular domains of human CD22 and CD33. Recombinant CD22 and CD33 were expressed in HEK 293S cells and subsequently purified by Ni^{2+} Sepharose beads, followed by gel filtration. SDS-PAGE analysis of (A) Recombinant CD22. (B) Recombinant CD33. (C) Glycan profile of recombinant CD22 and CD33 analysed by MALDI-TOF-MS.

Both polyclonal serum IgG and monoclonal IgG1 b12 were investigated for their interaction with CD22 and CD33. Interestingly, sialylation decreased the affinity of both serum and monoclonal IgG for CD22 (Fig. 5.12A) and CD33 (Fig. 5.12B), which appears to be counter-

intuitive since both siglecs are known to bind sialylated glycans. The direct, sialic acid-dependent interaction between serum IgG and CD22 on B cells has been demonstrated by confocal microscopy[230], though the sialic acid-containing domain (Fab and Fc) that mediates the binding was not determined. Direct biophysical assays probing the interaction between recombinant CD22 or CD33 and a glycoprotein were rarely reported, as most of the knowledge about siglecs ligand specificity was derived from glycan array studies. One possibility for a lack of such data is the low-affinity interaction between siglecs and glycoproteins. In the context of IgG Fc, the putatively shielded *N*-glycan might present an extra obstacle for siglecs access, as manifested by the inaccessibility of Fc oligomannose glycans to DC-SIGN, discussed in section 5.3. On the other hand, one group reported positive SPR data for the interaction between siglecs and gp120[269], a glycoprotein with multiple *N*-glycosylation sites that provide potential multi-valency. However, the affinity constants reported varied dramatically between different experimental setups, especially for CD33[269]. The interaction between siglecs and glycoproteins is under-studied compared with other protein-protein interactions; and new methodologies might be needed to accurately capture the exquisite siglec-glycoprotein interactions.

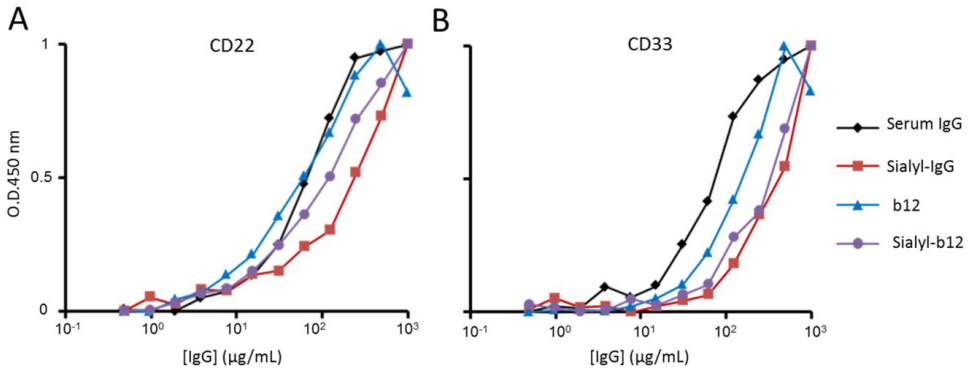

Figure 5.12. Interaction of recombinant human CD22 and CD33 with serum and monoclonal IgG. (A) ELISA probing the binding between immobilized CD22 and the following target glycoproteins: serum IgG; hyper-α2,6-sialylated serum IgG (Sialyl-IgG); monoclonal IgG1 b12; hyper-α2,6-sialylated monoclonal IgG b12 (Sialyl-b12). (B) ELISA probing the binding between immobilized CD33 and the following target glycoproteins: serum IgG; hyper-α2,6-sialylated serum IgG (Sialyl-IgG); monoclonal IgG b12; hyper-α2,6-sialylated glycoform of monoclonal IgG b12 (Sialyl-b12). All data points represent the calculated mean of two independent measurements. A total of one experiment was carried out.

5.7. Conclusions

The *in vivo* studies have demonstrated the critical role of α2,6-linked sialic acid on IgG Fc for the anti-inflammatory effect of IVIg; however, the molecular basis for this mechanism remains elusive. Recently, the C-type lectin DC-SIGN has been proposed to bind the α2,6-linked sialic acid on sFc to initiate a TH_2-dependent, anti-inflammatory signalling pathway that also involves the up-regulation of the inhibitory receptor, FcγRIIB, on macrophages[40]. Consistently, the immunosuppressive effect of Fc sialylation also manifests in its ability to decrease ADCC[22;23]. Data presented here indicate that human serum IgG bound DC-SIGN in a carbohydrate-independent manner, suggesting that the proposed molecular interaction between terminal sFc and DC-SIGN is not the primary recognition event responsible for triggering the IVIg effect. These data therefore suggest that alternative receptor(s) for the Fc and glycan components of IVIg are responsible for the therapeutic effect of sFc. The widespread presence of ITIM motifs on cytosolic domains of many α2,6-linked sialic acid-specific siglecs has prompted the investigation of the their interaction with sFc; to this end, no conclusive data have been generated due to a lack of positive controls for siglecs. Novel assays might be needed to accurately study the week interaction between siglecs and glycoproteins.

Chapter 6

Immunomodulatory Property of IVIg on DCs

6. Immunomodulatory Property of IVIg on DCs

6.1. Summary

Experiments have demonstrated the anti-inflammatory role of sFc *in vivo*[40; 138]; however, as discussed in Chapter 5, the molecular receptor for such immunosuppressive sFc has not been conclusively determined. In an attempt to identify potential DC cell surface receptors for the anti-inflammatory IVIg, a cellular assay using human DCs was developed. Human DCs are professional antigen presenting cells critical in initiating and modulating the immune response. Importantly, DCs that have been primed with IVIg *in vitro* could ameliorate inflammation when adoptively transferred to recipient mouse models of ITP[215; 216] and RA[40]. Previously, IVIg has been shown to suppress LPS-mediated activation of human imDC[180] *in vitro*; however, contrasting data show that IVIg-treated human monocytes differentiated into a mature DC phenotype[270]. To date, however, the effect of IVIg glycosylation on human DCs has not been examined.

Given the immunomodulatory role of DCs in the immune system, and the therapeutic properties of IVIg-primed DCs[40; 215; 216], the effect of differential IVIg glycoforms on DCs could provide a cellular basis for the glycosylation-dependent effect of anti-inflammatory IVIg. Thus, in this chapter, differentially glycosylated IVIg were generated, and their effect on human DCs were investigated. To characterize the direct effect of IVIg on DCs, the levels of various pro- and anti-inflammatory cytokines secreted, as well as changes in the levels of immunomodulatory cell surface receptors and siglecs, in response to IVIg treatment, were determined. In addition, the effect of IVIg-priming on subsequent DC activation in response to the TLR-4 agonist LPS was investigated, in an attempt to characterize the indirect effect of IVIg on DC activation.

6.2. Establish an *in vitro* DC Activation Model

6.2.1. Derivation of Human DCs

Human DCs were derived from $CD14^+$ monocytes isolated from peripheral blood of healthy donors. Blood was drawn from donors via venepuncture by trained phlebotomist Dr Amanda Unsworth (University of Oxford); all procedures follow the ethical rules set by the Department of Biochemistry, University of Oxford. Peripheral blood was subject to Ficoll density gradient centrifugation and the buffy coat containing the PBMCs was harvested[250]. The $CD14^+$ monocytes were positively selected from PBMCs using magnetic anti-CD14 antibody according to manufacturer's protocol, and cultured at $1x10^6$ cells/mL in RPMI-1640 supplemented with GM-CSF and IL-4 for 5 days to derive imDCs.

6.2.2. LPS-mediated Modulation of DC Cell Surface Receptor Expression

LPS potently activates DCs via the TLR-4 pathway[271]. It is well-known that LPS induces DCs to non-specifically secrete a large amount of cytokines, both pro- and anti-inflammatory, and modifies DC cell surface molecule expression[272; 273; 274]. The $CD14^+$ monocytes-derived human imDCs were thus first tested for their ability to respond to LPS. Cell surface analysis of imDCs shows moderate levels of the integrin molecule CD11c, costimulatory molecule CD40 and the siglec molecule CD33, and low levels of costimulatory molecules CD80, CD86, and the major histocompatibility complex class II molecule human leukocyte antigen-DR (HLA-DR) (Fig. 6.1). Moreover, CD14 were detected at a very low level, while CD22 were undetectable (Fig. 6.1B and C), consistent with previous report[268]. After 24-hour stimulation with 1 μg/mL LPS, the level of HLA-DR, CD40, CD80, and CD86 was dramatically upregulated (Fig. 6.1D, E, F and G), while the level of CD11c remains constant, as previously reported[275] (Fig. 6.1A). In addition to the traditionally examined cell surface molecules, the changes in level of siglecs were also checked in response to LPS stimulation.

The CD33 and Siglec7 showed decreases of 40% and 14% respectively after LPS treatment (Fig. 6.2A and C), while Siglec5 and Siglec9 levels were less prone to modulation (Fig. 6.2B and D), consistent with previous reports[276; 277; 278]. The level of CD22 remained undetectable after LPS stimulation (Fig. 6.1C).

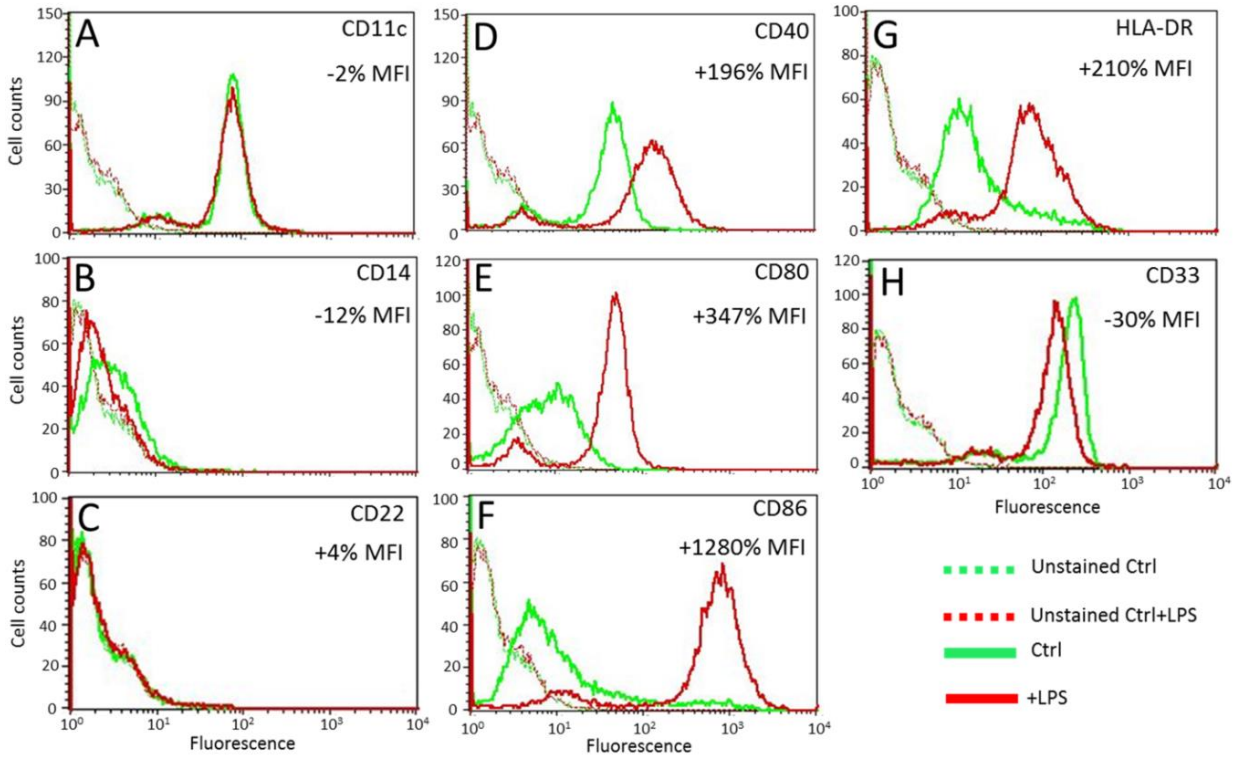

Figure 6.1. FACS analysis of DC cell surface molecules before and after LPS stimulation. Human $CD14^+$ monocytes derived from a single donor were cultured *in vitro* at $1x10^6$ cells/mL, supplemented with IL-4 (500 IU/mL) and GM-CSF (1000 IU/mL) for 5 days, to derived imDCs. The imDCs were then treated with 1 μg/mL LPS or medium alone for 24 hours, before cells were harvested and analysed for their surface receptor expressions. All staining antibodies were mouse antibodies: anti-CD11c-FITC, anti-CD40-FITC, anti-CD80-FITC, anti-CD86-PE, anti-HLA-DR-PE, anti-CD14-PE, anti-CD33-PE and anti-CD22-PE. FACS histograms for the following cell surface molecules: (A) CD11c. (B) CD14. (C) CD22. (D) CD40. (E) CD80. (F) CD86. (G) HLA-DR. (H) CD33. A total of 10,000 events were recorded for each analysis. Data representative of at least two independent experiments.

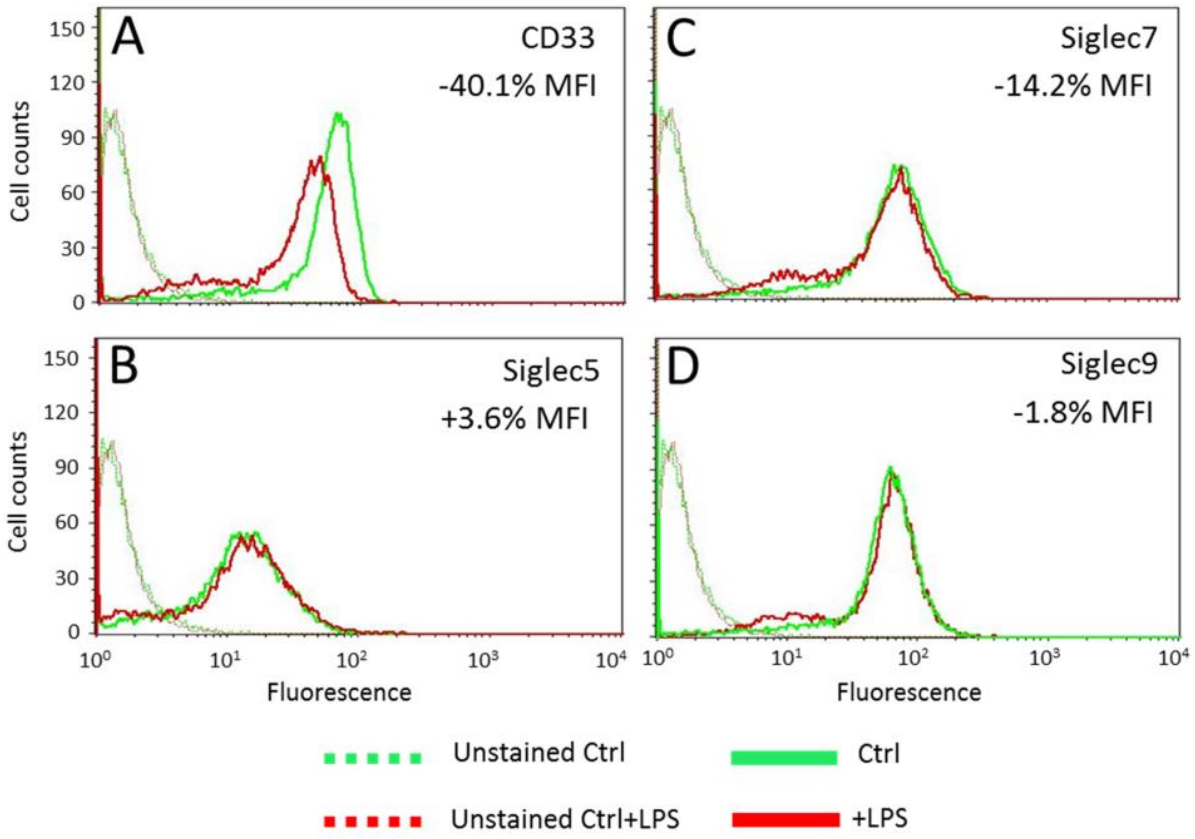

Figure 6.2. FACS analysis of DC cell surface siglecs before and after LPS stimulation. Human $CD14^+$ monocytes derived from a single donor were cultured *in vitro* at $1x10^6$ cells/mL, supplemented with IL-4 (500 IU/mL) and GM-CSF (1000 IU/mL) for 5 days, to derived imDCs. The imDCs were then treated with 1 μg/mL LPS or medium alone for 24 hours, before cells were harvested and analysed for their surface receptor expressions. All staining antibodies were mouse antibodies: anti-CD33-PE, anti-Siglec5-PE, anti-Siglec7-PE, and anti-Siglec9-PE. FACS histograms for the following cell surface siglecs: (A) CD33. (B) Siglec5. (C) Siglec7. (D) Siglec9. A total of 10,000 events were recorded for each analysis. Data representative of two independent experiments.

6.2.3. LPS-mediated DC Cytokine Production

DC cell culture supernatant was harvested after LPS treatment and analysed for the levels of IL-10, IL-12p70, IFN-γ-induced protein 10 (IP-10), TNF-α and IFN-γ. Consistent with previous reports[271], LPS dose-dependently increases the level of all cytokines analysed (Fig. 6.3). The production of IP-10 was particularly responsive to LPS, as 1 ng/mL LPS triggered the IP-10 production beyond the detection limit (Fig. 6.3C). After validating the *in vitro* DC cellular assay, the effects of various IVIg glyco-variants on DCs were investigated.

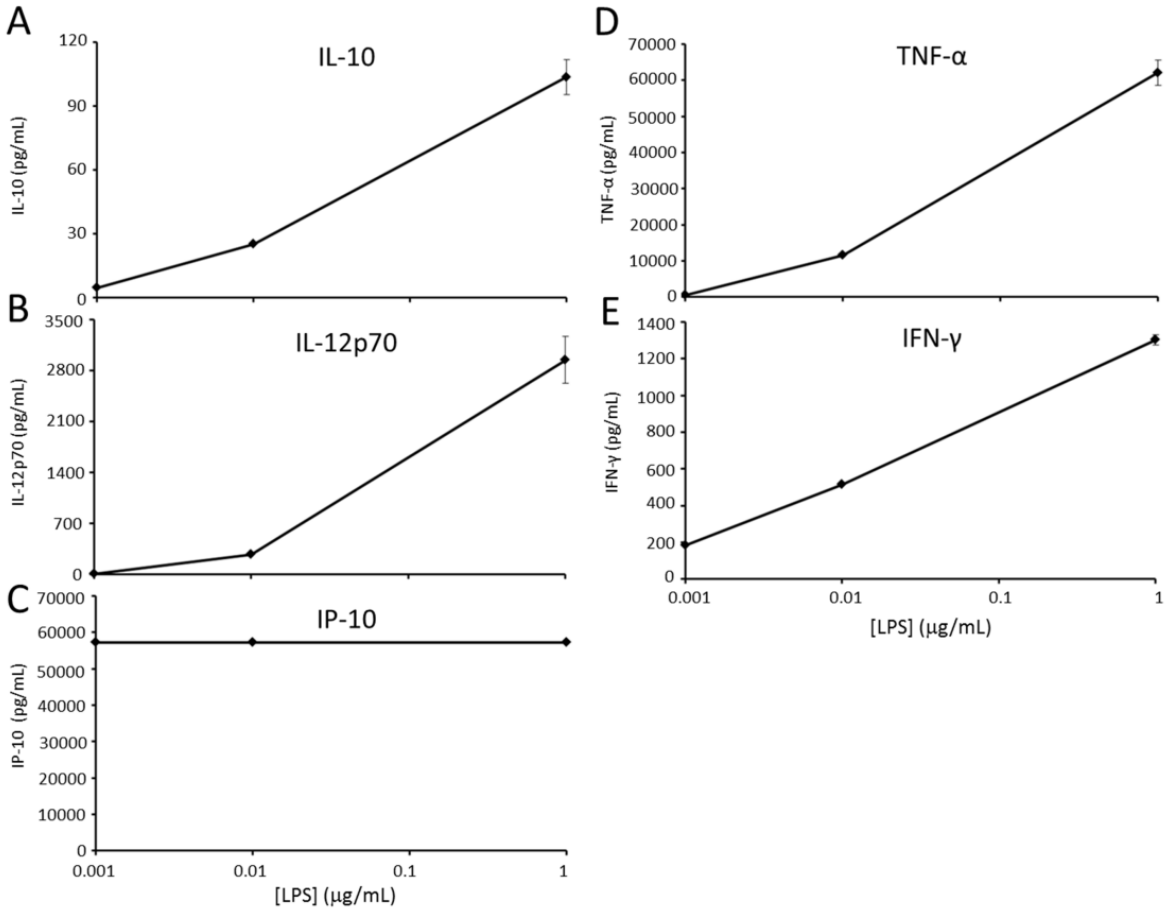

Figure 6.3. Cytokine analysis of cell culture supernatant of LPS-stimulated DCs. Human imDCs derived from a single donor were stimulated with 0.001, 0.01 or 1 μg/mL LPS for 24 hours, before cell culture supernatant was harvested and analysed for the level of IL-10, IL-12p70, IP-10, TNF-α and IFN-γ. Cytokine analysis was carried out using Luminex Bio-Plex assay kits and Luminex 200 Instrument. Concentration of the following cytokines in cell culture supernatant (A) IL-10. (B) IL-12p70. (C) IP-10. (D) TNF-α. (E) IFN-γ. All data points are reported as Mean ± SD, calculated from two independent measurements. A total of one experiment was carried out for this LPS titration experiments.

6.3. Glycosylation Dependent Effect of IVIg on DCs

6.3.1. Preparation of Differentially Glycosylated IVIg and HSA

Desialylated and deglycosylated IVIg were generated as described in section 5.2, using neuraminidase and PNGase F respectively. All protein samples prepared for the cellular assays were purified by gel filtration equilibrated in sterile PBS. As enzymatic treatment and gel filtration procedures involve the exposure of proteins to non-sterile environment, endotoxin removal was carried out after protein purification using Triton X-114 as described

before[251]. After gel filtration, Triton X-114 was added to protein solution resuspended in PBS, to a final concentration of 1%, and incubated on ice for 30 minutes, followed by incubation at 37°C to allow phase separation of Triton X-114 and the protein solution. The endotoxin, along with Triton X-114 was then separated from protein solution by centrifugation. This endotoxin removal step was performed at least 3 times, and the final endotoxin level was quantified by the LAL chromogenic assay. The majority of endotoxin was removed by this method (Fig. 6.4), and the purity of protein samples after endotoxin removal was checked by Coomassie Blue-stained SDS-PAGE (Fig. 6.5).

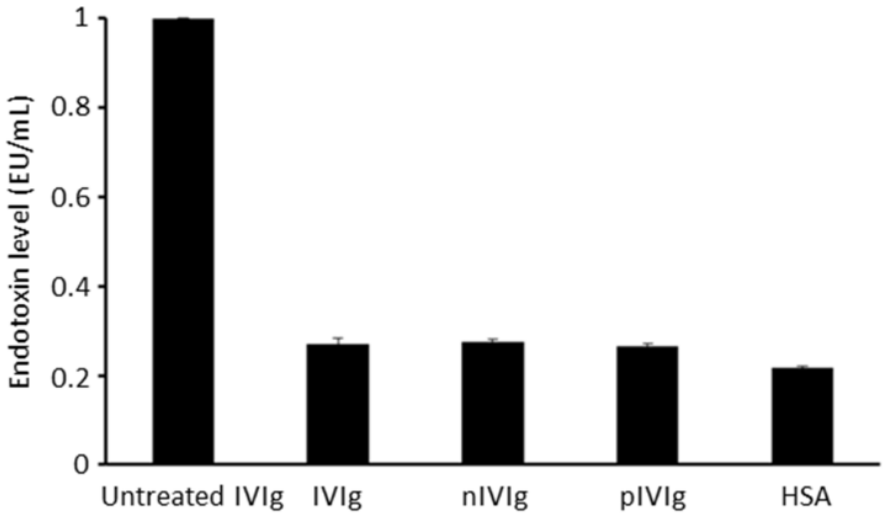

Figure 6.4. Endotoxin detection of protein samples before and after endotoxin removal with Triton X-114. Protein samples: IVIg, neuraminidase-treated IVIg (nIVIg), PNGase F-treated IVIg (pIVIg) and HSA were incubated with 1% Triton X-114 for 30 minutes, followed by 10-minute incubation at 37°C to allow phase separation. Endotoxin, along with Triton X-114, was removed from protein samples following centrifugation. Endotoxin-removed protein samples were concentrated to 0.15 mM and then incubated with LAL solution for 10 minutes. Endotoxin was detected by colorimetric changes after addition of chromogenic substrate to the solution. Absorbance at 405 nm was measured, and the level of endotoxin was calculated from a standard curve with a sensitivity range of 0.1-1 EU/mL (1 EU/mL = 0.1 ng/mL). All data points are reported as Mean ± SD, calculated from two independent measurements.

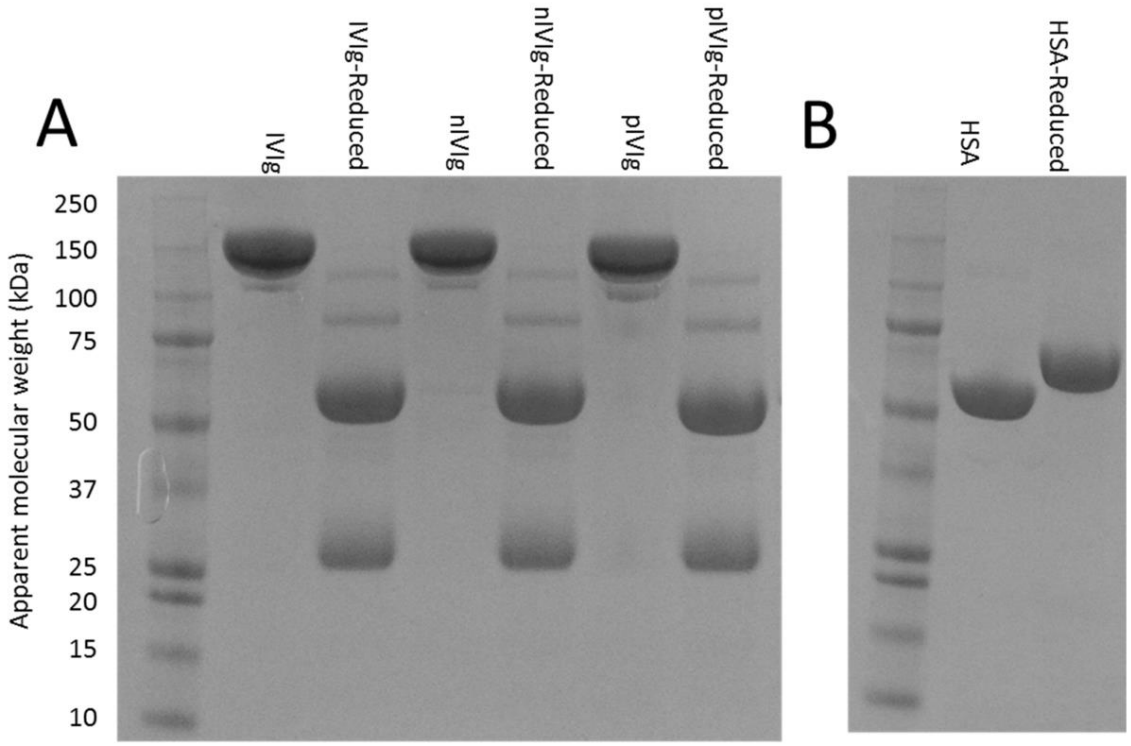

Figure 6.5. SDS-PAGE analysis of native, desialylated, deglycosylated IVIg, and HSA after endotoxin removal using Triton X-114. Desialylated and deglycosylated IVIg were generated by incubation with neuraminidase and PNGase F for 48 hours at 37˚C. For protein denaturation, the samples were boiled for 5 minutes in the presence of DTT. Protein samples were run on 4-12% gradient Bis-Tris gel and then stained by Coomassie Blue. SDS-PAGE analysis of (A) Native, desialylated (nIVIg) and deglycosylated (pIVIg) IVIg. (B) HSA.

6.3.2. Effect of Direct IVIg Treatment on DCs

The imDCs were pre-treated with IVIg or its glyco-variants for 12 hours, before cells were washed once with media and LPS was added to activate DCs. For each experiment, an independent low-level endotoxin control (Low ET) was added, as low-level endotoxin-sensitization is known to have inhibitory effects on DC activation[279; 280]. Cytokine analysis of the 12-hour cell culture supernatant shows that IVIg alone induced minimal production of IL-10 and IL-12 (Fig. 6.6A and B), consistent with previous report[180], while the level of IFN-γ was below detection threshold for all treatments. In contrast, the levels of pro-inflammatory MCP1 and TNF-α, both of which are production early during inflammation[281], were notably higher than the control (Fig. 6.6C and D). The IVIg-induced cytokine production shown here

agrees with the cytokine-inducing property of IVIg in humans[281; 282; 283]. Interestingly, this IVIg-induced cytokine production was significantly inhibited by deglycosylation, but not desialylation (Fig. 6.6). A summary of cytokine profile from 4 independent experiments is shown in Figure 6.7. Longer incubation times are needed to confirm these findings. Data shown there are consistent with the crystallographic observation that sialylation does not significantly influence Fc structure (Fig. 5.10), whereas deglycosylation does.

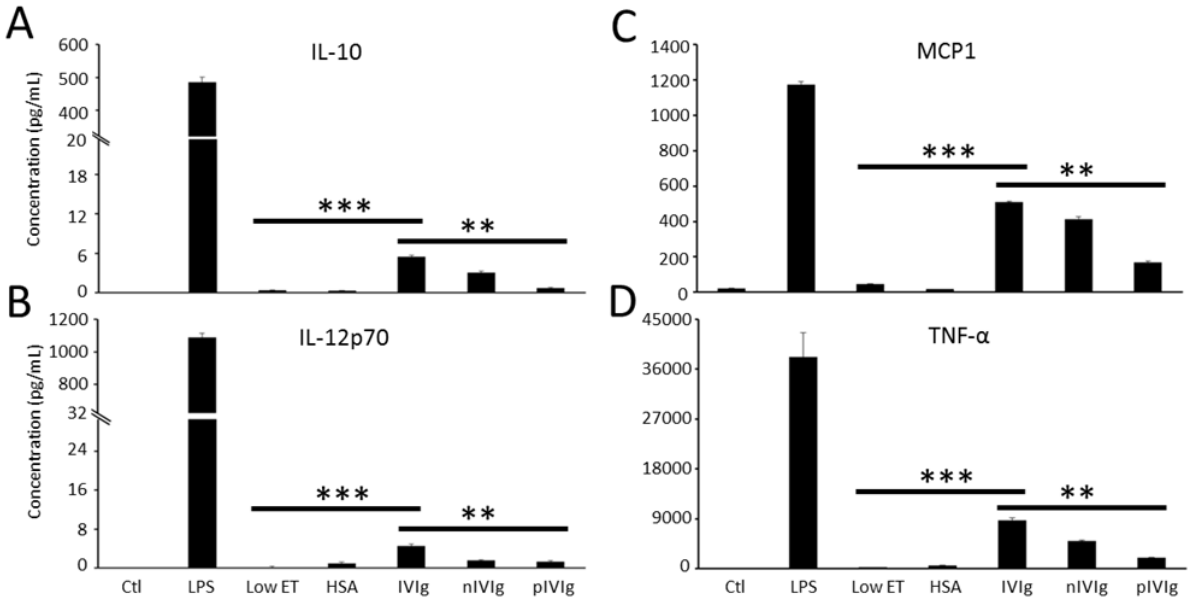

Figure 6.6. Cytokine analysis of cell culture supernatant of DCs treated with IVIg for 12 hours. Human monocyte-derived imDCs derived from a single donor were plated at $4x10^5$ cells per well and pre-treated with 0.15 mM IVIg, neuraminidase-treated IVIg (nIVIg), PNGase F-treated IVIg (pIVIg), HSA, or a Low ET for 12 hours, before cell culture supernatant was harvested. Cytokine analysis was carried out using Luminex Bio-Plex assay kits and Luminex 200 Instrument. Concentration of the following cytokines in cell culture supernatant of IVIg-treated DCs: (A) IL-10. (B) IL-12. (C) MCP1. (D) TNF-α. All data points are reported as Mean ± SD, calculated from three independent measurements. Data representative of at least three independent experiments. $^{**}p < 0.01$; $^{***}p < 0.001$.

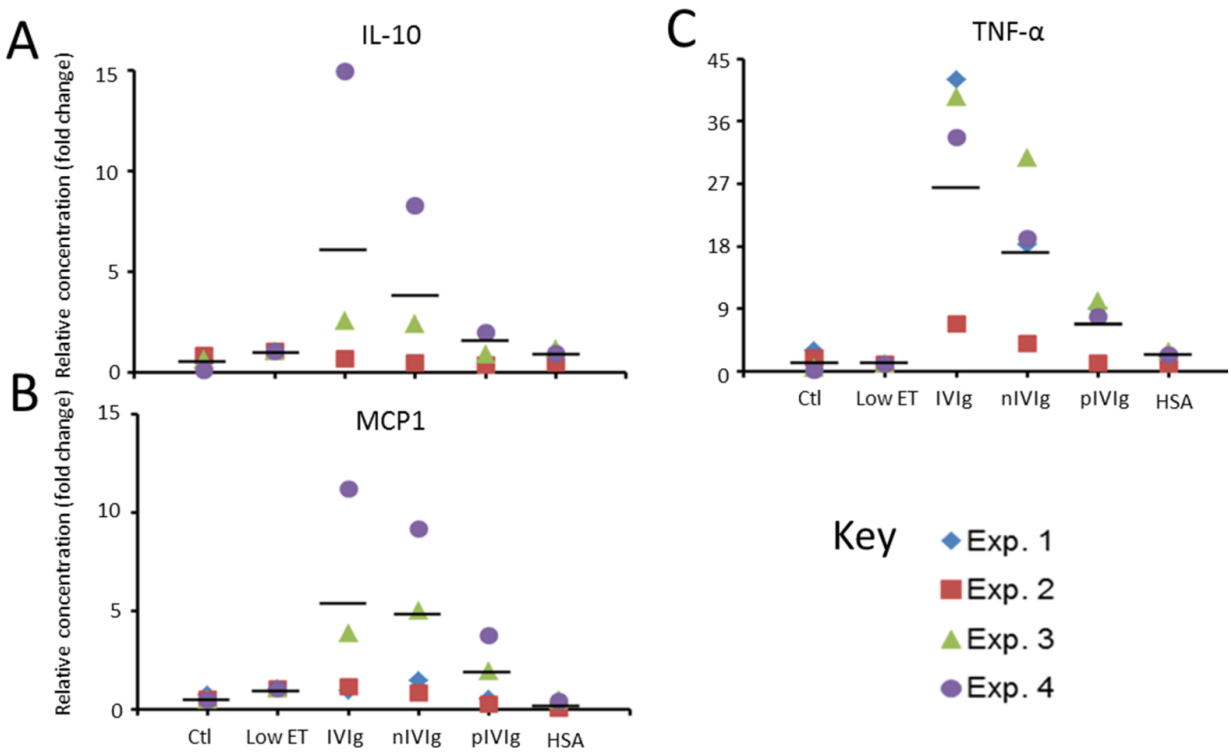

Figure 6.7. Summary of Cytokine analysis of cell culture supernatant of DCs treated with IVIg for 12 hours from a total of 4 independent experiments. Human monocyte-derived imDCs derived from a single donor were plated at $4x10^5$ cells per well and pre-treated with 0.15 mM IVIg, neuraminidase-treated IVIg (nIVIg), PNGase F-treated IVIg (pIVIg), HSA, or a Low ET for 12 hours, before cell culture supernatant was harvested. Cytokine analysis was carried out using Luminex Bio-Plex assay kits and Luminex 200 Instrument. Concentration of the following cytokines in cell culture supernatant (A) IL-10. (B) IL-12. (C) MCP1. For each independent experiment, the average value of each treatment was normalized against the Low ET. The average of all independent experiments is shown by a horizontal bar (black). The absence of cytokine data means that the values were below detection level.

6.3.3. Effect of IVIg Pre-treatment on LPS-mediated DC Activation

This IVIg-induced, glycan-dependent, cytokine production persists when DCs were subsequently stimulated with LPS in the absence of IVIg or its glycovariants (Fig. 6.8). The imDCs that had been pre-treated with IVIg exhibited a generally enhanced cytokine production, including the putative immunosuppressive IL-10 (Fig. 6.8A), compared with the control. This enhanced cytokine production contradicts previous reports that IVIg reduces DC and PBMC activation[180; 284], which might be explained by the different experimental procedures used. Here, IVIg or its glycovariant was removed from imDCs after pre-treatment, and then the cells were washed to prevent the polyclonal IVIg-LPS interaction[180; 198] during

LPS stimulation that might lead to partial LPS neutralization. This differs from the commonly used experimental setup, which involves the simultaneous presence of IVIg and LPS (or other stimulants) in the cell culture[49; 63; 198]. Indeed, IVIg decreased LPS-induced DC production of IL-10, IL-12p70, IP-10, TNF-α and IFN-γ when it was added to the imDC cell culture simultaneously with LPS (Fig. 6.9). Here, the pro-inflammatory cytokine profile induced by IVIg-pre-treatment was significantly inhibited upon IVIg deglycosylation, but not desialylation (Fig. 6.8). Apart from IL-12p70, the production of IL-10, MCP1, TNF-α and IFN-γ all decreased upon IVIg deglycosylation (Fig. 6.8A, C, D and E). The decrease was particularly notable for IL-10 (Fig. 6.8A) and IFN-γ (Fig. 6.8E), when their levels were reduced close to the control. A summary of cytokine profile from 4 independent experiments is shown in Figure 6.10.

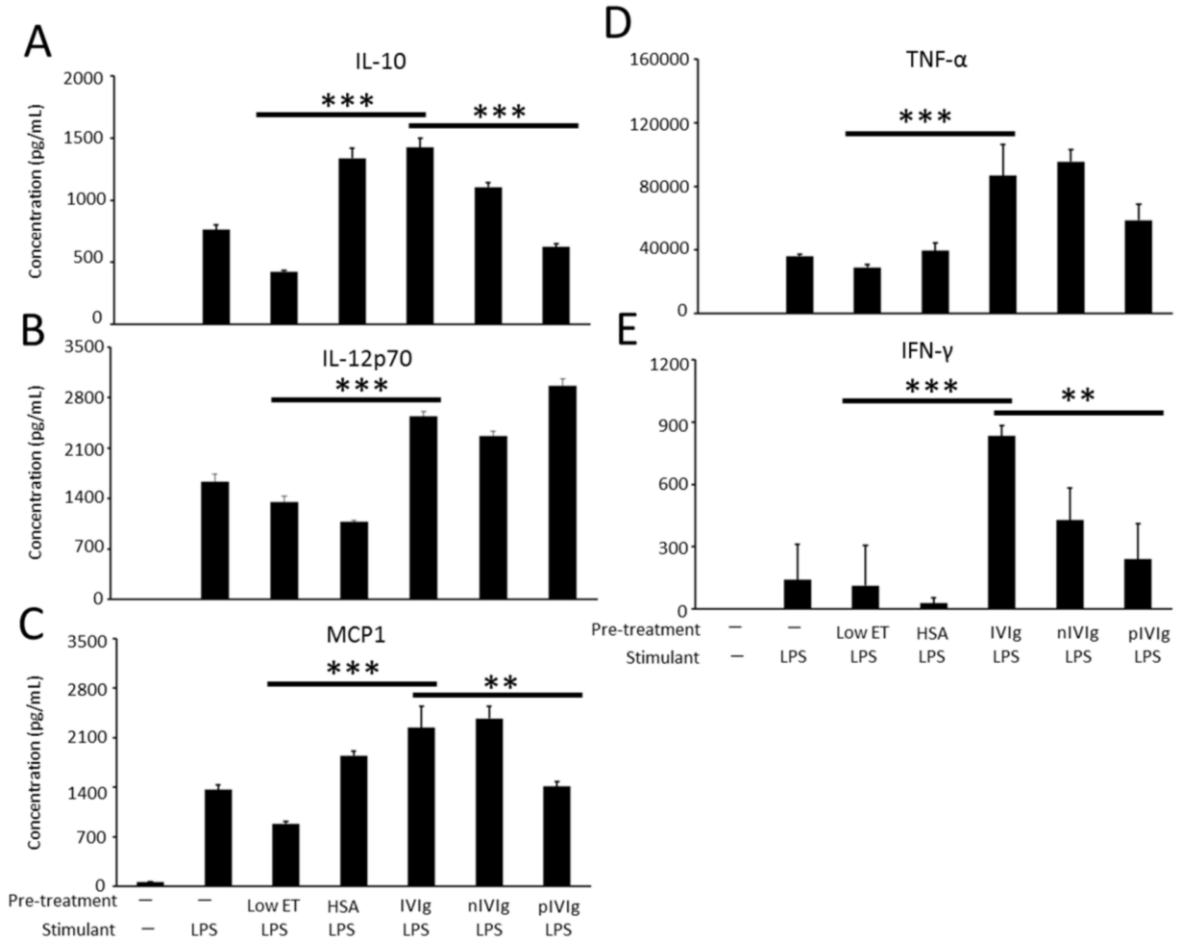

Figure 6.8. Cytokine analysis of cell culture supernatant of IVIg-pretreated, LPS-stimulated DCs. Human monocyte-derived imDCs derived from a single donor were plated at $4x10^5$ cells per well and pre-treated with 0.15 mM IVIg, neuraminidase-treated IVIg (nIVIg), PNGase F-treated IVIg (pIVIg), HSA, or a Low ET for 12 hours, before cell culture supernatant was harvested and cells were washed once with media to clean residual pre-treatment reagents. Afterwards, cells were stimulated with 1 μg/mL LPS for 24 hours, before supernatant was harvested. Cytokine analysis was carried out using Luminex Bio-Plex assay kits and Luminex 200 Instrument. Concentration of the following cytokines in cell culture supernatant of DCs after LPS stimulation (A) IL-10. (B) IL-12. (C) MCP1. (D) TNF-α. (E) IFN-γ. All data points are reported as Meanm ± SD, calculated from three independent measurements. Data representative of at least three independent experiments. $^{**}p < 0.01$; $^{***}p < 0.001$.

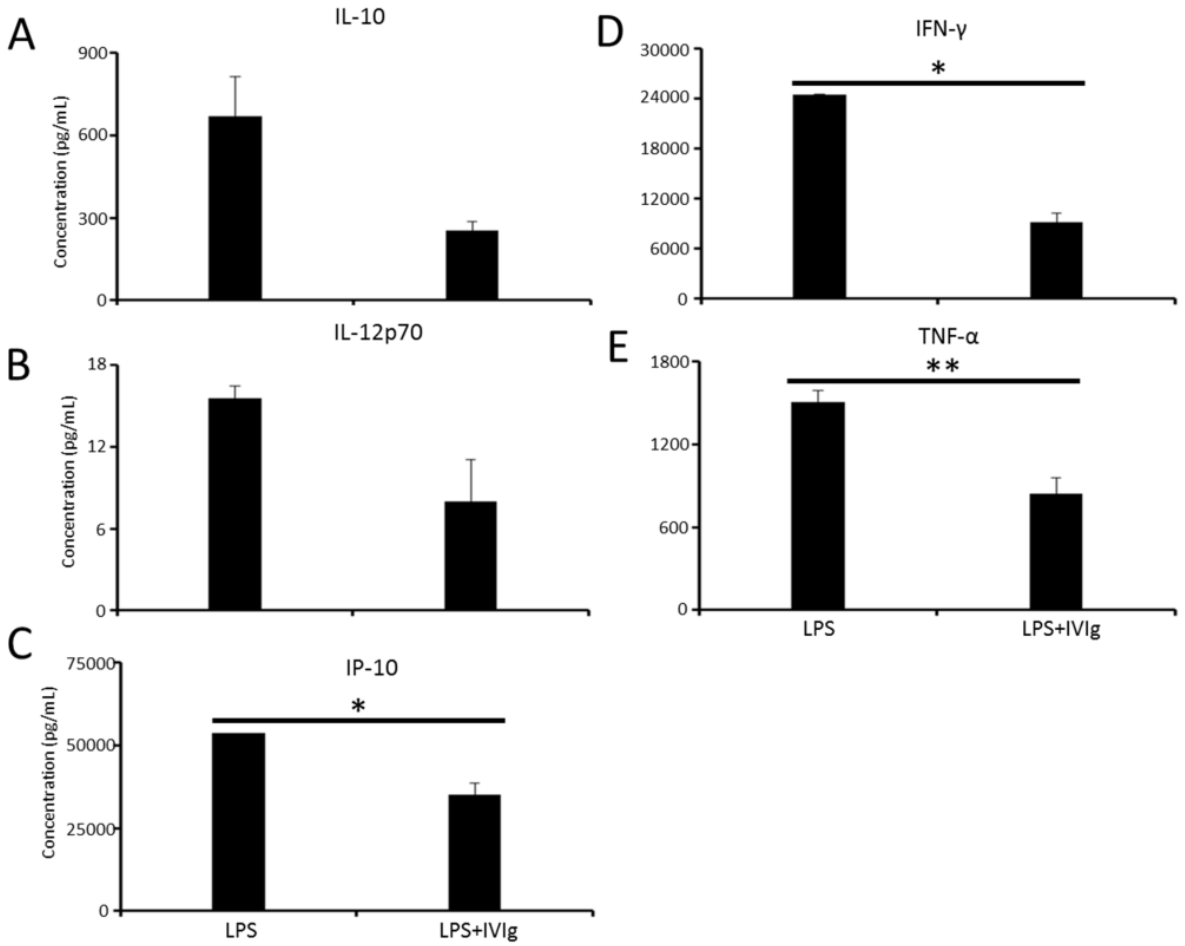

Figure 6.9. Cytokine analysis of cell culture supernatant of LPS-stimulated DCs cultured with or without IVIg. Human monocyte-derived imDCs derived from a single donor were plated at $2.5x10^5$ cells per well and stimulated with 1 μg/mL LPS, either with or without IVIg. After 24 hours stimulation, cell culture supernatant was harvested, and cytokine analysis was carried out using Luminex Bio-Plex assay kits and Luminex 200 Instrument. Concentration of the following cytokines in cell culture supernatant of DCs after LPS stimulation (A) IL-10. (B) IL-12p70. (C) IP-10. (D) IFN-γ. (E) TNF-α. All data points are reported as Mean ± SD, calculated from two independent measurements. A total of one experiment was carried out. $^{**}p < 0.01$; $^{*}p < 0.05$.

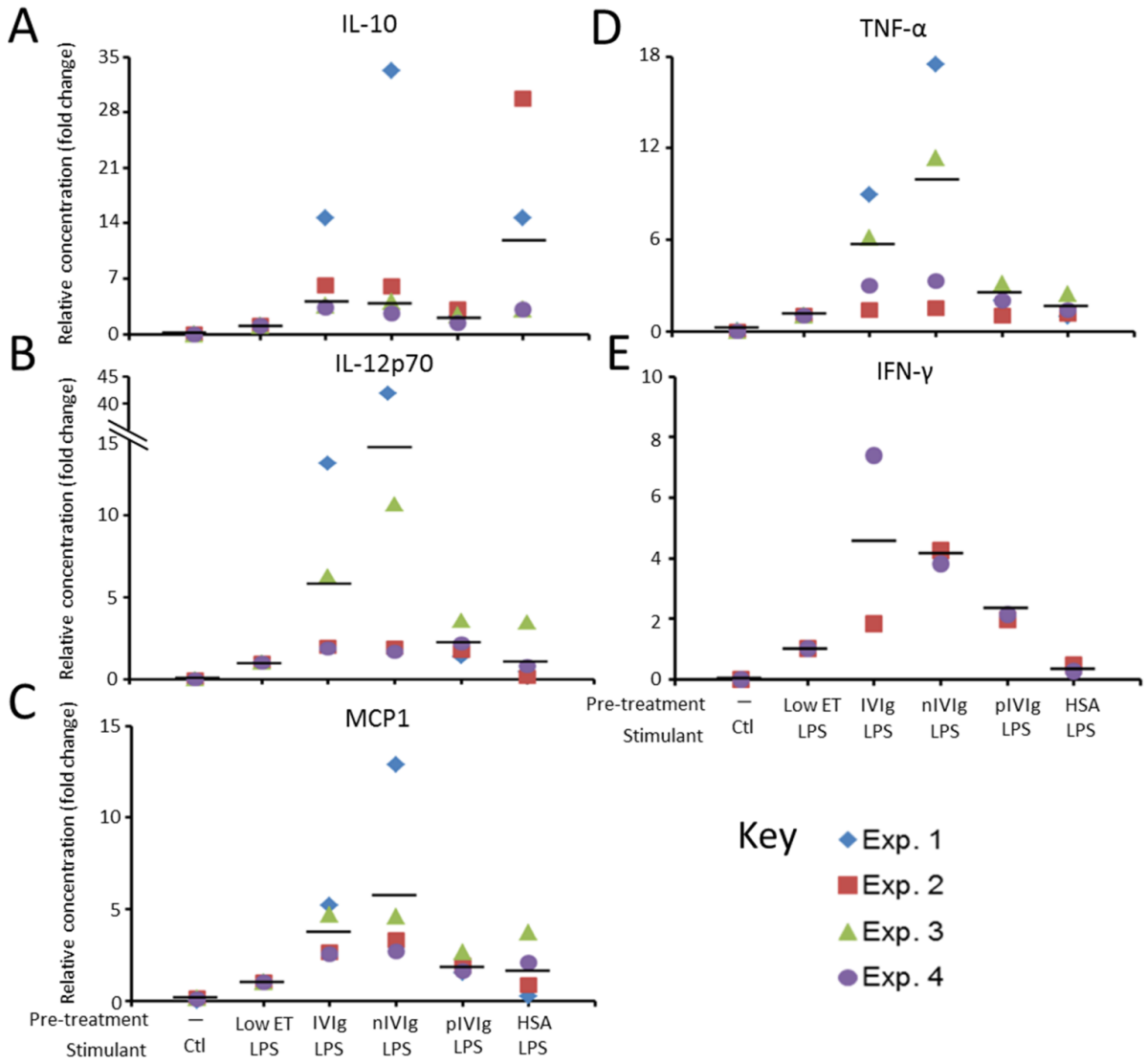

Figure 6.10. Summary of cytokine analysis of cell culture supernatant of IVIg-treated, LPS-stimulated DCs from a total of 4 experiments. Human monocyte-derived imDCs derived from a single donor were plated at $4x10^5$ cells per well and pre-treated with 0.15 mM IVIg, neuraminidase-treated IVIg (nIVIg), PNGase F-treated IVIg (pIVIg), HSA, or a Low ET for 12 hours, before cell culture supernatant was harvested and cells were washed once with media to clean residual pre-treatment reagents. Afterwards, cells were stimulated with 1 µg/mL LPS for 24 hours, before supernatant was harvested. Cytokine analysis was carried out using Luminex Bio-Plex assay kits and Luminex 200 Instrument. Concentration of the following cytokines in cell culture supernatant (A) IL-10. (B) IL-12p70. (C) MCP1. (D) TNF-α. (E) IFN-γ. For each independent experiment, the average value of each treatment was normalized against the Low ET. The average of all independent experiments is shown by a horizontal bar (black). The absence of cytokine data means that the values were below detection level.

In addition to cytokine analysis, FACS analysis was carried out to examine the modulation of selective cell surface markers (CD86, HLA-DR, CD33 and Siglec7). In contrast to the cytokine profile, IVIg and its glyco-variants do not significantly modulate the level of co-stimulatory receptors and the siglecs upon LPS stimulation (Fig. 6.11), except a small decrease in HLA-DR in a non-glycoform-dependent manner (6.11B). This inhibitory effect of IVIg deglycosylation on DCs described here is consistent with the newly emerged, dominant, immunosuppressive effect of EndoS-treated IgG in a mouse model of RA[108]. In that study, Nandakumar and colleagues demonstrated that the addition of exogenous EndoS-treated IgG, regardless of antigen specificity, could ameliorate RA, via disruption of the endogenous inflammatory immune complexes by the EndoS-treated Fc domain[108]. Although the mode of action of immune complex disruption was not determined, disruption of the inflammatory immune complex in the presence of EndoS-treated IgG was clearly demontrated[108]. EndoS-treatment of IgG has previously been shown to either disrupt or enhance IgG binding to different FcgRs, depending on the IgG subclass[285]; therefore, characterizing the *in vivo* effect of EndoS-mediated deglycosylation using different IgG subclasses might help explain the immunosuppression observed by Nandakumar and colleagues[108]. Interestingly, previous studies show that deglycosylated IVIg failed to protect mice from HSV-mediated encephalitis[195] and serum-induced arthritis[133]. Thus, different animal models and differential methods of Fc "deglycosylation" used might have significant impact on the therapeutic effect of anti-inflammatory IVIg.

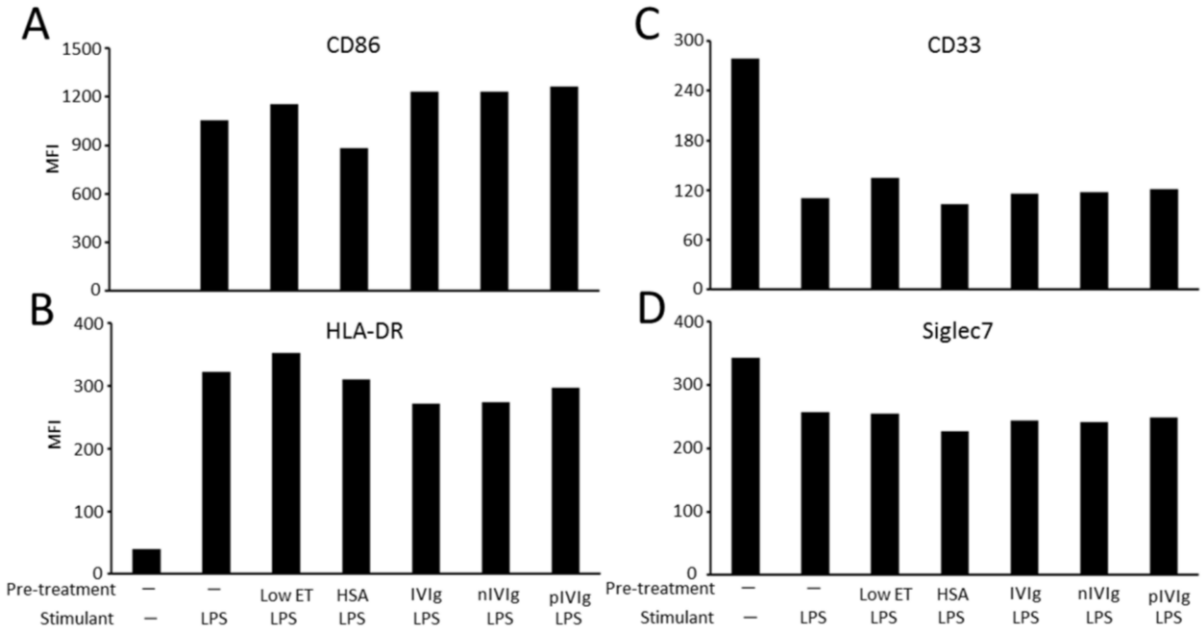

Figure 6.11. FACS analysis of cell surface receptors of IVIg-pre-treated, LPS-stimulated DCs. Human monocyte-derived imDCs derived from a single donor were plated at $4x10^5$ cells per well and pre-treated with 0.15 mM IVIg, neuraminidase-treated IVIg (nIVIg), PNGase F-treated IVIg (pIVIg), HSA, or a Low ET for 12 hours, before cell culture supernatant was harvested and cells were washed once with media to clean residual pre-treatment reagents. Afterwards, cells were stimulated with 1 μg/mL LPS for 24 hours, before cells were harvested and stained for the expression of (A) CD86. (B) HLA-DR. (C) CD33. (D) Siglec7. A total of 10,000 events were recorded for each analysis. Data representative of two independent experiments.

6.3.4. Effect of HSA on LPS-mediated DC Activation

In contrast to IVIg, HSA-pre-treated DCs exhibited a broadly immunosuppressive cytokine profile in response to LPS stimulation (Fig. 6.8), characterized by significantly increased IL-10 (Fig. 6.8A). Moreover, DCs-pre-treated with HSA displayed reduced levels of CD86 and HLA-DR (Fig. 6.11A and B); however, further experimental replications are needed to confirm the results. Although co-incubation of LPS and HSA has not been reported to affect LPS-mediated DC activation[180], our results are consistent with recent findings that HSA is an immunosuppressive molecule both *in vitro* and *in vivo*[286; 287; 288].

The immunosuppressive effect of HSA was further investigated for its direct effect on LPS-stimulated DC activation. After imDCs were stimulated with LPS for 3 hours, cell culture supernatant was removed and HSA was added for additional 24 hours. In the presence of

HSA, the level of IL-10 and MCP1 was dramatically reduced, while the level of TNF-α increased (Fig. 6.12A, C and D). Interestingly, IL-12 production was not significantly affected (Fig. 6.12B). Cell surface analysis showed that the level of both co-stimulatory molecule CD86 and HLA-DR was dramatically reduced (Fig. 6.13). However, more experimental repeats, which analyse more cell surface molecules, are needed to confirm these findings. Previously, the small molecule (< 3 kDa) aspartyl-alanyl diketopiperazine (DA-DKP), a by-product generated from the first 2 residues of the N-terminus of HSA during industrial preparation of HSA, has been shown to be responsible for the immunsuppressive effect of HSA *in vitro*[44; 45; 46]. For experiments described here, the HSA were purified by size exclusion column and its purity was confirmed by SDS-PAGE before use; thus, it is unclear whether the anti-inflammatory effect of HSA observed here results from DA-DKP.

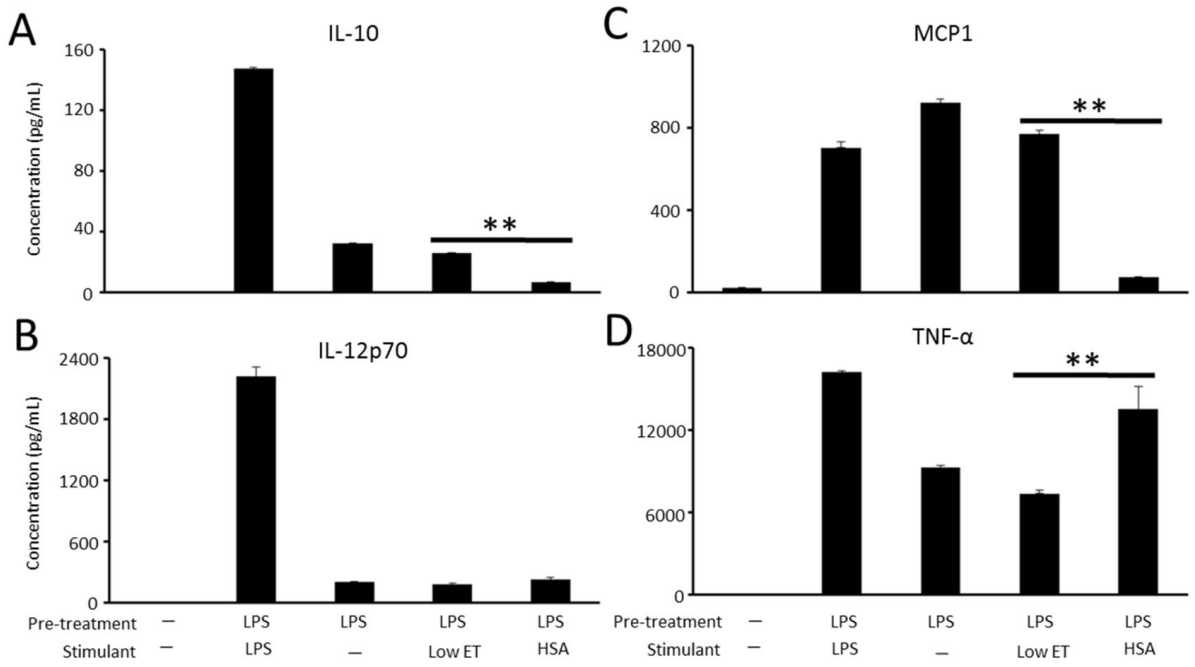

Figure 6.12. Cytokine analysis of cell culture supernatant of LPS-pre-stimulated, HSA-treated DCs. The imDCs derived from a single donor were pre-stimulated with 1 μg/mL LPS for 3 hours, then cell culture supernatant was harvested and cells were washed once with media to clean residual LPS. Afterwards, cells were treated with 0.15 mM HSA for 24 hours, before supernatant was harvested. Cytokine analysis was carried out using Luminex Bio-Plex assay kits and Luminex 200 Instrument. Concentration of the following cytokines in cell culture supernatant (A) IL-10. (B) IL-12. (C) MCP1. (D) TNF-α. All data points are reported as Mean ± SD, calculated from two independent measurements. A total of one experiment was carried out. $^{**}p < 0.01$.

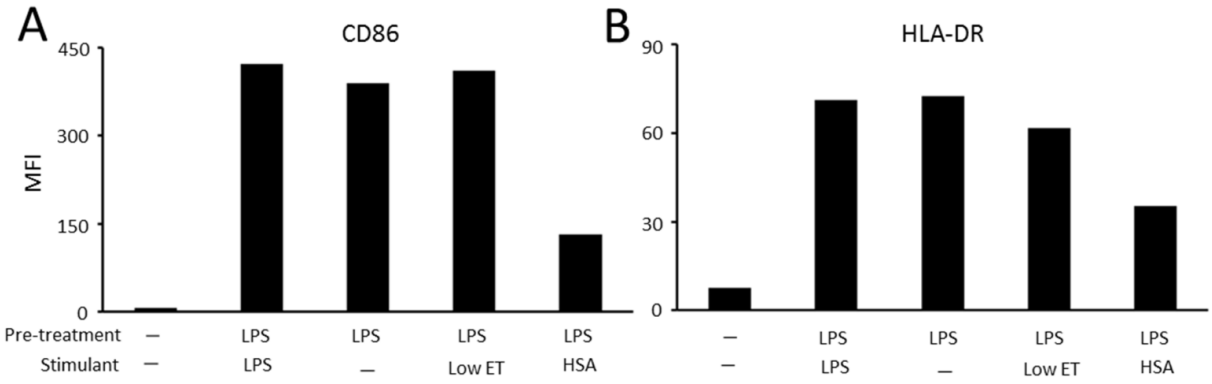

Figure 6.13. FACS analysis of cell surface receptors for LPS-pre-stimulated, HSA-treated DCs. The imDCs derived from a single donor were pre-stimulated with 1 μg/mL LPS for 3 hours, before cell culture supernatant was harvested and cells were washed once with media to clean residual LPS. Afterwards, cells were treated with 0.15 mM HSA for 24 hours, before cells were harvested and stained for the expression of (A) CD86. (B) HLA-DR. A total of 10,000 events were recorded for each analysis. A total of one experiment was carried out.

6.4. Conclusions

DCs are professional antigen-presenting cells critical in initiating and modulating immune responses. The importance of DCs in IVIg-mediated anti-inflammation is reflected in the efficacy of exogenously IVIg-primed DCs in ameliorating autoimmune mouse models[40; 215; 216]. Given the importance of Fc sialic acid in the anti-inflammatory effect of IVIg in various mouse models[133; 138; 170], the *in vitro* effect of IVIg and its glycovariants on DCs were investigated as a pilot to search for the DC cell surface receptor(s) for IVIg. The induction of DC cytokine secretion, both pro- and anti-inflammatory, by high concentrations of IVIg, could be, in part, due to the intrinsic sensitivity of DCs to their environ. Indeed, the *in vitro* culturing of DCs does not systematically capture the complexity of the *in vivo* environment. A multitude of physiological conditions are known to significantly modulate DCs' immunomodulatory properties, such as the physiological serum antibody concentration and the interplay between various cytokines[214; 272]. Therefore, the *in vitro* data presented should be interpreted with caution and perspectives.

The glycan-dependent activatory effect of IVIg on DC cytokine production observed here demonstrates the relevance of glycosylation in the anti-inflammatory effect of IVIg *in vitro*. In the light of the newly reported efficacy of deglycosylated Fc in treating mouse RA via immune complex disruption[108], data report here could provide a cellular basis for the anti-inflammatory deglycosylated Fc. Further dissection of the glycan-dependent, IVIg-mediated, activatory effect on DCs would require the selective glycan modification at the Fab and Fc domains of IVIg.

Chapter 7

Perspectives

7. Perspectives

The *N*-glycan attached to the Fc domain of IgG is known to maintain the Fc structural integrity required for a number of Fc-mediated effector functions, and the Fc protein-glycan interface, dominated by hydrophobic interactions, is known to modulate the Fc glycan processing[87]. A combination of glycan engineering, structural and biological examinations has yielded important knowledge about the role of Fc glycosylation in antibody-mediated effector functions, and also spawned Fc engineering as a significant approach during antibody design.

The integrity of the Fc protein-glycan interface, previously shown to modulate Fc glycosylation and FcγR binding, is demonstrated here to be crucial for the general productive engagement of Fc with FcγRs, independent of Fc glycoform. Moreover, the ineffectiveness of F243A $Man_5GlcNAc_2$ glycoform (F243 does not form interactions with Fc glycan in $Man_5GlcNAc_2$ glycoform) in disrupting Fc-FcγRs interactions confirms that the protein-glycan interaction represents a novel, independent, parameter in regulating Fc-FcγRs interactions. Disruption of this interface, via protein backbone mutagenesis, is likely to exert most influence on the Fc glycan flexibility, rather than on Fc conformation; and indeed, the crystal structure of F241A mutant indicates increased glycan flexibility. The structure of other more disruptive mutants, such as V264E, could provide further insights.

The Fc glycan undergoes significant changes in its flexibility during its natural biosynthesis, when the 6-arm GlcNAc**5′** and Gal**6′** are sequentially transferred to the glycan terminus, which allows stable protein-glycan interactions. Moreover, no flexibility variations were associated upon Fc terminal sialylation, as shown by data presented here, or core fucosylation[110]. Naturally, the only way to modulate the Fc protein-glycan interface is via

enzymatic modifications of the glycan, as natural Fc hydrophobic mutations have not been observed to date.

Despite unaltered Fc glycan flexibility upon sialylation, the *in vivo* anti-inflammatory effect of sFc is evident in several mouse models[40; 138], and desialylation-mediated abolition of the anti-inflammatory effect of IVIg *in vivo* has been verified by two independent research groups[133; 170]. However, the molecular receptor for IVIg is not completely clear. Genetic knockout studies have led to the identification of DC-SIGN as the receptor for the anti-inflammatory sFc[39]. Data presented here, primarily biophysical, do not support the existence of such a glycan-specific interaction between DC-SIGN and sFc, although, there are clear difficulties in proving a negative. However, we can conclude that the recombinant glycoproteins generated in this study exhibited other known interactions that could be effectively probed using standard biophysical techniques. Following this work, there should be sufficient evidence to both bring into question the role of DC-SIGN as the direct receptor for IVIg and to prompt the search for an alternative receptor(s) for sFc, stemming from known properties about Fc and sialic acid. In this context, the cell surface siglecs, which are known to mediate immunosuppressive effects, present as attractive candidates. Besides the anti-inflammatory sFc, which would require a receptor, numerous studies have attributed the anti-inflammatory effect of IVIg to the antigen-specific Fab domain[202], in which case no single cell surface receptor would be responsible the anti-inflammatory IVIg. Indeed, there could well be multiple modes of action of IVIg therapy. The Fc and Fab-mediated anti-inflammation have not been shown to be mutually exclusive; importantly, dissecting the molecular mechanism of anti-inflammatory IVIg Fc could provide a basis for a more effective and economical substitute for IVIg.

Although data presented here does not support the role of sialylation in influencing Fc interaction with FcγRs or DC-SIGN, the cellular data shown here, which unexpectedly point

deglycosylated IVIg to an inhibitory role, suggest that there might still be a component of Fc-glycosylation in the anti-inflammatory IVIg. This is especially encouraging, as deglycosylated Fc has recently been shown to improve RA in mice, via an unclarified, deglycosylated Fc-mediated disruption of endogenous IC. More animal models are needed to confirm such a novel effect, as different disease models, and indeed different mouse strains, could react very differently. For the cellular assay described here, the inhibitory effect of deglycosylated IVIg need to be tested in more activatory DC models, and the effects of Fab and Fc domains need to be uncoupled. A combination of such *in vitro* cellular assay and *in vivo* animal models could lead to a more comprehensive understanding and provide a resolution towards the molecular mechanism of IVIg and the development of a recombinant therapeutic.

Appendix A: Abbreviations

2-AA	2-Aminoanthranilic Acid
µg	Microgram
µL	Microlitre
µM	Micromolar
Å	Angstorm
ADCC	Antibody Dependent Cell-mediated Cytotoxicity
B4GALT1	β1,4-Galactosyltransferase
CDC	Complement-Dependent Cytotoxicity
CHCA	α-Cyano-4-Hydroxycinnamic Acid
CHO	Chinese Hamster Ovary
CMP-sialic acid	Cytidine-5'-Monophospho-*N*-Acetylneuraminic Acid
CRD	Carbohydrate Recognition Domain
DA-DKP	Aspartyl-Alanyl Diketopiperazine
DC	Dendritic Cell
DC-SIGN	Dendritic Cell-Specific Intercellular Adhesion Molecule-3-Grabbing Non-Integrin
DHB	2,5-Dihydroxybenzoic Acid
DMEM	Dulbecco's Modified Eagle's Medium
DNA	Deoxyribonucleic Acid
DTT	Dithiothreitol
EndoH	Endoglycosidase H
EndoS	Endoglycosidase S
ES-MS	Electrospray Mass Spectrometry
Fab	Fragment Antigen Binding
Fc	Fragment Crystallisable
FcR	Fc Receptor

FcRn	Neonatal Fc Receptor
Fuc	Fucose
G0	Agalactosylated Biantennary Complex Type Glycan
G1	Mono-Galactosylated Biantennary Complex Type Glycan
G2	Di-Galactosylated Biantennary Complex Type Glycan
G3	Tri-Galactosylated Biantennary Complex Type Glycan
G4	Tetra-Galactosylated Biantennary Complex Type Glycan
GlcNAc	*N*-Acetylglucosamine
GnTI	GlcNAc Transferase I
GPI	Glycophosphatidylinositol
HEK	Human Embryonic Kidney
HEPES	4-(2-Hydroxyethyl)Piperazine-1-Ethanesulfonic Acid
HIV	Human Immunodeficiency Virus
HLA-DR	Human Leukocyte Antigen-DR
HPLC	High-Performance Liquid Chromatography
HRP	Horseradish Peroxidase
HSA	Human Serum Albumin
HSV	Herpes Simplex Virus
IFN	Interferon
Ig	Immunoglobulins
IL	Interleukin
imDCs	Immature Dendritic Cells
IP-10	IFN-γ Induced Protein 10
ITAM	Immunoreceptor Tyrosine-Based Activation Motif
ITIM	Immunoreceptor Tyrosine-Based Inhibition Motif
ITP	Immune Thrombocytopenia
IVIg	Intravenous Immunoglobulin Therapy

LAL	Limulus Amebocyte Lysate
LPS	Lipopolysaccharide
MALDI-TOF-MS	Matrix-Assisted Laser Desorption/Ionization Time-Of-Flight Mass Spectrometry
Man	Mannose
MBL	Mannose Binding Lectin
MCP1	Monocyte Chemotactic Protein-1
mg	Milligram
nM	Nonomolar
NMR	Nuclear Magnetic Resonance
PBMC	Peripheral Blood Mononuclear Cells
PBS	Phosphate-Buffered Saline
PCR	Polymerase Chain Reaction
PDB	Protein Data Bank
PEI	Polyethyleneimine
PHA	Phytohemagglutinin
PNGase F	Peptide-*N*-Glycosidase F
RA	Rheumatoid Arthritis
RPMI	Roswell Park Memorial Institute
SDS-PAGE	Sodium Dodecyl Sulfate Polyacrylamide Gel Electrophoresis
sFc	α2,6-Sialylated Fc
SIGN-R1	Specific Intracellular Adhesion Molecule-Grabbing Non-Integrin R1
SNA	*Sambucus Nigra* Lectin
SPR	Surface Plasmon Resonance
ST6GAL1	α2,6-Sialyltransferase
TH_2	T-Helper Type 2
TLR	Toll-Like Receptor

TMB	3,3',5,5'-Tetramethylbenzidine
TNF-α	Tumor Necrosis Factor-α
UDP-galactose	Uridine 5’-Diphosphogalactose

Appendix B: Glycan Mass Tables

Table A1. Mass and composition of commonly observed *N*-glycans in MALDI-TOF-MS

MALDI m/z ([M+Na]+)	Composition			Proposed structure
	Hex	HexNAc	dHex	
1095.4	4	2	0	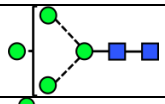
1257.4	5	2	0	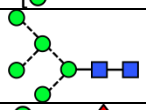
1282.5	3	3	1	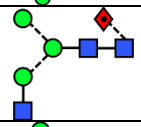
1298.5	4	3	0	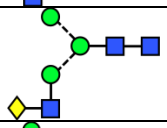
1339.5	3	4	0	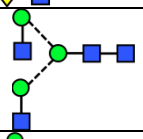
1419.5	6	2	0	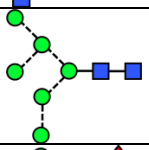
1444.5	4	3	1	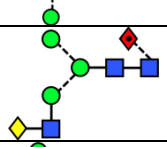
1460.5	5	3	0	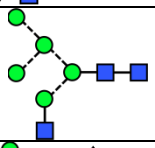
1485.5	3	4	1	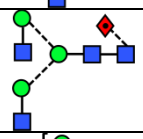
1501.5	4	4	0	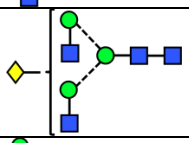
1542.6	3	5	0	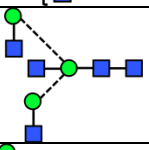
1581.5	7	2	0	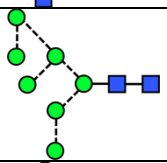
1606.6	5	3	1	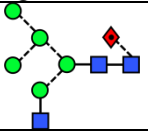

1622.6	6	3	0	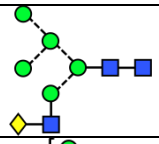
1647.6	4	4	1	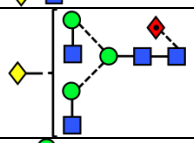
1663.6	5	4	0	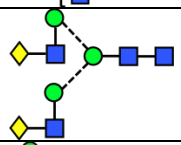
1688.6	3	5	1	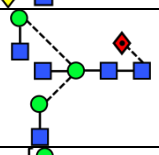
1704.6	4	5	0	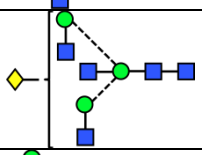
1743.6	8	2	0	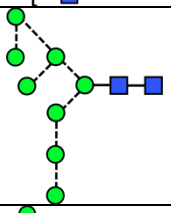
1768.6	6	3	1	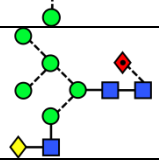
1793.7	4	4	2	
1809.7	5	4	1	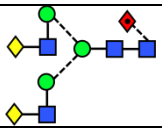
1825.6	6	4	0	
1850.7	4	5	1	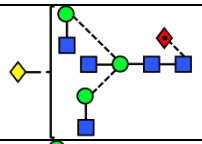
1866.7	5	5	0	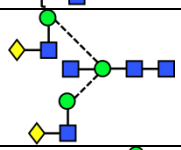
1891.7	3	6	1	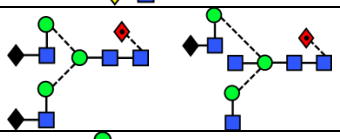
1905.6	9	2	0	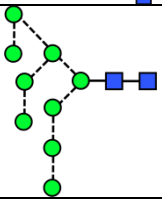

1955.7	5	4	2	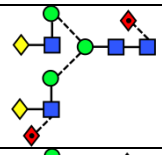
1996.7	4	5	2	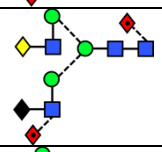
2012.7	5	5	1	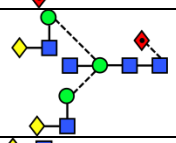
2028.7	6	5	0	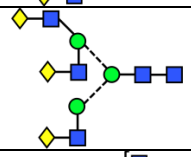
2053.7	4	6	1	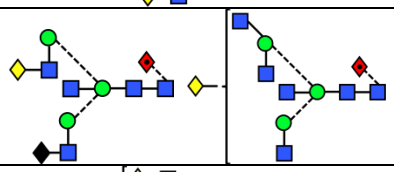
2174.8	6	5	1	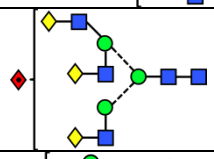
2122.7	5	4	1	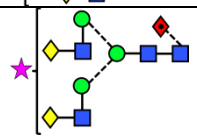
2215.8	5	6	1	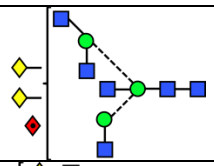
2377.9	6	6	1	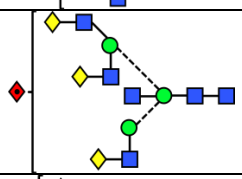
2540.5	7	6	1	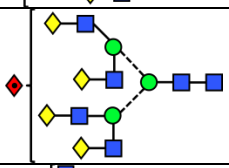
2580.9	6	7	1	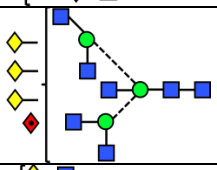
2743.8	7	7	1	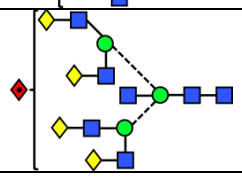

Table A2. Mass and composition of commonly observed *N*-glycans in ESI-MS

m/z	Ion	Composition				Structure
		Hex	GlcNAc	Fuc	Neu5Ac	
1559.5	$[M + H_2PO_4]^-$	3	4	1	0	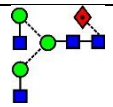
1721.6	$[M + H_2PO_4]^-$	4	4	1	0	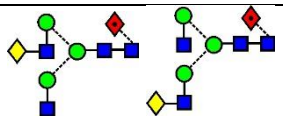
1762.6	$[M + H_2PO_4]^-$	3	5	1	0	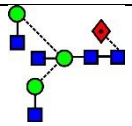
1883.6	$[M + H_2PO_4]^-$	5	4	1	0	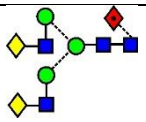
990.3	$[M+(H_2PO_4)_2]^{2-}$					
1914.7	$[M-H]^-$	4	4	1	1	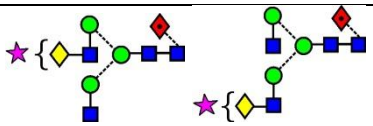
1924.6	$[M + H_2PO_4]^-$	4	5	1	0	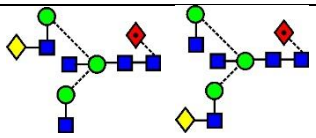
1010.8	$[M+(H_2PO_4)_2]^{2-}$					
2076.7	$[M-H]^-$	5	4	1	1	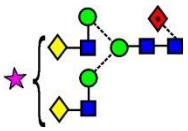
1086.6	$[M-H+H_2PO_4]^{2-}$					
2086.7	$[M + H_2PO_4]^-$	5	5	1	0	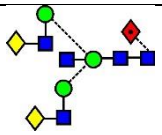
1091.8	$[M+(H_2PO_4)_2]^{2-}$					
2117.8	$[M-H]^-$	4	5	1	1	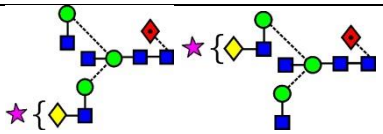
2248.8	$[M + H_2PO_4]^-$	6	5	1	0	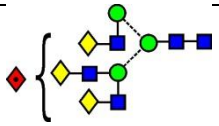
2279.9	$[M-H]^-$	5	5	1	1	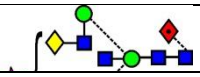

1188.4	$[M-H+H_2PO_4]^{2-}$					
1183.4	$[M-H_2]^{2-}$	5	4	1	2	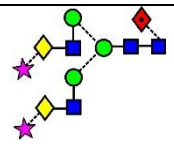
2389.8	$[M-H_2+Na]^{-}$				2	
2441.9	$[M-H]^{-}$	6	5	1	1	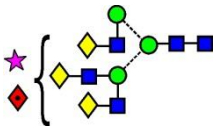
1269.4	$[M-H+H_2PO_4]^{2-}$					
1285.0	$[M-H_2]^{2-}$	5	5	1	2	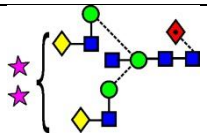
1366.0	$[M-H_2]^{2-}$	6	5	1	2	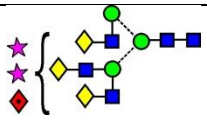
1467.5	$[M-H_2]^{2-}$	6	6	1	2	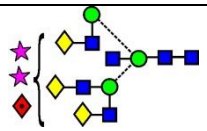
1511.5	$[M-H_2]^{2-}$	6	5	1	3	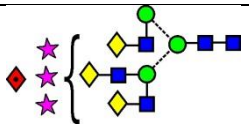
1522.5	$[M-H_3+Na]^{2-}$	6	5	1	3	

Appendix C: Tryptic Peptide Fingerprint

MALDI-TOF tryptic peptide mass fingerprinting of IgG1 b12 (FASTA sequence ID 1HZH)

The tryptic peptide mass of the native and deglycosylated IgG were calculated online using the PeptideMass program at the ExPASy SIB Bioinformatics Resource Portal. Before trypsin digestion, IgG was subject to reduction, alkylation (with iodoacetamide) and methionine oxidation.

Table A3-Tryptic peptide mass fingerprint of b12 heavy chain

Mass	Position	Peptide sequence
6656.3	158-220	DYFPEPVTVSWNSGALTSGV HTFPAVLQSSGLYSLSSVVT VPSSSLGTQTYICNVNHKPS NTK
2744.2	427-449	WQQGNVFSCSVMHEALHNHY TQK
2730.4	233-258	THTCPPCPAPELLGGPSVFL FPPKPK
2544.1	381-402	GFYPSDIAVEWESNGQPENN YK
2522.1	99-119	VGPYSWDDSPQDNYYMDVWG K
2082.0	266-284	TPEVTCVVVDVSHEDPEVK
1890.9	68-84	VTFTADTSANTAYMELR
1873.9	403-419	TTPPVLDSDGSFFLYSK
1808.0	312-327	VVSVLTVLHQDWLNGK
1755.8	45-58	FEWMGWINPYNGNK
1677.8	285-298	FNWYVDGVEVHNAK
1304.7	29-38	FSNFVIHWVR
1286.7	355-365	EPQVYTLPPSR
1285.7	1-12	QVQLVQSGAEVK
1264.7	144-157	STSGGTAALGCLVK
1219.5	88-98	SADTAVYYCAR
1189.5	303-311	EEQYNSTYR
1186.6	132-143	GPSVFPLAPSSK
1150.6	120-131	GTTVIVSSASTK
1104.6	371-380	NQVSLTCLVK
970.4	20-28	VSCQASGYR
838.5	337-344	ALPAPIEK
835.4	259-265	DTLMISR
788.5	450-457	SLSLSPGK
686.4	13-19	KPGASVK
656.3	39-44	QAPGQR
605.3	366-370	DELTK
581.3	59-63	EFSAK
575.3	420-424	LTVDK
565.3	64-67	FQDR
501.3	299-302	TKPR

Table A4-Tryptic peptide mass fingerprint of b12 light chain

Mass	Position	Peptide sequence
2923.3	79-104	VEPEDFALYYCQVYGASSYT FGQGTK
2136.0	151-170	VDNALQSGNSQESVTEQDSK
1946.0	110-127	TVAAPSVFIFPPSDEQLK
1884.0	Jan-18	EIVLTQSPGTLSLSPGER
1818.9	192-208	VYACEVTHQGLSSPVTK
1740.9	128-143	SGTASVVCLLNNFYPR
1646.8	63-78	FSGSGSGTDFTLTITR
1537.8	34-46	VAWYQHKPGQAPR
1502.8	171-184	DSTYSLSSTLTLSK
994.6	47-55	LVIHGVSNR
705.4	56-62	ASGISDR
686.4	25-30	SSHSIR
684.3	19-24	ATFSCR
625.3	185-189	ADYEK
560.3	147-150	VQWK
523.3	209-212	SFNR

Appendix D: Amino Acid Sequence of Recombinant Proteins

Amino acid sequences of soluble hexahistidine-tagged recombinant protein- Sequence corresponding to AgeI restriction site is highlighted in red; sequence corresponding to KpnI restriction site is highlighted in green; and sequence corresponding to BsiWI restriction site is highlighted in blue.

IgG1 Fc (Molecular Weight: 26.4 kDa; Number of *N*-glycosylation site: 1)

ETGHTCPPCPAPELLGGPSVALFPPKPKDTLMISRTPEVTCVVVDVSHEDPEVKFNW
YVDGVEVHNAKTKPREEQYNSTYRVVSVLTVLHQDWLNGKEYKCKVSNKALPAPI
EKTISKAKGQPREPQVYTLPPSREEMTKNQVSLTCLVKGFYPSDIAVEWESNGQPEN
NYKTTPPVLDSDGSFFLYSKLTVDKSRWQQGNVFSCSVMHEALHNHYTQKSLSLSP
GGTKHHHHHH

FcγRIA (Molecular Weight: 32.0 kDa; Number of *N*-glycosylation site: 7)

ETGQVDTTKAVITLQPPWVSVFQEETVTLHCEVLHLPGSSSTQWFLNGTATQTSTPS
YRITSASVNDSGEYRCQRGLSGRSDPIQLEIHRGWLLLQVSSRVFTEGEPLALRCHAW
KDKLVYNVLYYRNGKAFKFFHWNSNLTILKTNISHNGTYHCSGMGKHRYTSAGISV
TVKELFPAPVLNASVTSPLLEGNLVTLSCETKLLLQRPGLQLYFSFYMGSKTLRGRNT
SSEYQILTARREDSGLYWCEAATEDGNVLKRSPELELQVLGLQLPTPGTKHHHHHH

FcγRIIA (Molecular Weight: 21.1 kDa; Number of *N*-glycosylation site: 2)

ETGQAAPPKAVLKLEPPWINVLQEDSVTLTCQGARSPESDSIQWFHNGNLIPTHTQPS
YRFKANNNDSGEYTCQTGQTSLSDPVHLTVLSEWLVLQTPHLEFQEGETIMLRCHS
WKDKPLVKVTFFQNGKSQKFSHLDPTFSIPQANHSHSGDYHCTGNIGYTLFSSKPVTI
TVQVPSMGTKHHHHHH

FcγRIIB (Molecular Weight: 21.5 kDa; Number of *N*-glycosylation site: 3)

ETGGTPAAPPKAVLKLEPQWINVLQEDSVTLTCRGTHSPESDSIQWFHNGNLIPTHTQ
PSYRFKANNNDSGEYTCQTGQTSLSDPVHLTVLSEWLVLQTPHLEFQEGETIVLRCH
SWKDKPLVKVTFFQNGKSKKFSRSDPNFSIPQANHSHSGDYHCTGNIGYTLYSSKPV
TITVQAPSSSPMGIIGTKHHHHHH

FcγRIIIA (Molecular Weight: 23.2 kDa; Number of *N*-glycosylation site: 5)

ETGGMRTEDLPKAVVFLEPQWYRVLEKDSVTLKCQGAYSPEDNSTQWFHNESLISS
QASSYFIDAATVDDSGEYRCQTNLSTLSDPVQLEVHIGWLLLQAPRWVFKEEDPIHL
RCHSWKNTALHKVTYLQNGKGRKYFHHNSDFYIPKATLKDSGSYFCRGLVGSKNVS
SETVNITITQGLSVSTISSFFPPGYQGTKHHHHHH

FcγRIIIB (Molecular Weight: 22.2 kDa; Number of *N*-glycosylation site: 6)

ETGMRTEDLPKAVVFLEPQWYSVLEKDSVTLKCQGAYSPEDNSTQWFHNESLISSQ
ASSYFIDAATVNDSGEYRCQTNLSTLSDPVQLEVHIGWLLLQAPRWVFKEEDPIHLR
CHSWKNTALHKVTYLQNGKDRKYFHHNSDFHIPKATLKDSGSYFCRGLVGSKNVSS
ETVNITITQGLAVSTISGTKHHHHHH

CD22 (Molecular Weight: 76.6 kDa; Number of *N*-glycosylation site: 12)

ETGDSSKWVFEHPETLYAWEGACVWIPCTYRALDGDLESFILFHNPEYNKNTSKFDG
TRLYESTKDGKVPSEQKRVQFLGDKNKNCTLSIHPVHLNDSGQLGLRMESKTEKWM
ERIHLNVSERPFPPHIQLPPEIQESQEVTLTCLLNFSCYGYPIQLQWLLEGVPMRQAAV
TSTSLTIKSVFTRSELKFSPQWSHHGKIVTCQLQDADGKFLSNDTVQLNVKHTPKLEI
KVTPSDAIVREGDSVTMTCEVSSSNPEYTTVSWLKDGTSLKKQNTFTLNLREVTKDQ
SGKYCCQVSNDVGPGRSEEVFLQVQYAPEPSTVQILHSPAVEGSQVEFLCMSLANPL
PTNYTWYHNGKEMQGRTEEKVHIPKILPWHAGTYSCVAENILGTGQRGPGAELDVQ
YPPKKVTTVIQNPMPIREGDTVTLSCNYNSSNPSVTRYEWKPHGAWEEPSLGVLKIQ
NVGWDNTTIACAACNSWCSWASPVALNVQYAPRDVRVRKIKPLSEIHSGNSVSLQC
DFSSSHPKEVQFFWEKNGRLLGKESQLNFDSISPEDAGSYSCWVNNSIGQTASKAWT
LEVLYAPRRLRVSMSPGDQVMEGKSATLTCESDANPPVSHYTWFDWNNQSLPYHS
QKLRLEPVKVQHSGAYWCQGTNSVGKGRSPLSTLTVYYSPETIGRRRTGHHHHHH

CD33 (Molecular Weight: 28.0 kDa; Number of *N*-glycosylation site: 5)

ETGDPNFWLQVQESVTVQEGLCVLVPCTFFHPIPYYDKNSPVHGYWFREGAIISGDSP
VATNKLDQEVQEETQGRFRLLGDPSRNNCSLSIVDARRRDNGSYFFRMERGSTKYSY
KSPQLSVHVTDLTHRPKILIPGTLEPGHSKNLTCSVSWACEQGTPPIFSWLSAAPTSLG
PRTTHSSVLIITPRPQDHGTNLTCQVKFAGAGVTTERTIQLNVTYVPQNPTTGIFPGDG
SGKQETRAGVVGTKHHHHHH

ST6GAL1 (Molecular Weight: 38.1 kDa; Number of *N*-glycosylation site: 3)

ETGSFQVWDKDSTYSKLNPRLLKIWRNYLNMNKYKVSYKGPGPGVKFSVEALRCH
LRDHVNVSMIEATDFPFNTTEWEGYLPKENFRTKVGPWQRCAVVSSAGSLKNSQLG
REIDNHDAVLRFNGAPTDNFQQDVGSKTTIRLMNSQLVTTEKRFLKDSLYTEGILIV

WDPSVYHADIPKWYQKPDYNFFETYKSYRRLNPSQPFYILKPQMPWELWDIIQEISA
DLIQPNPPSSGMLGIIIMMTLCDQVDIYEFLPSKRKTDVCYYHQKFFDSACTMGAYHP
LLFEKNMVKHLNEGTDEDIYLFGKATLSGFRNIRCGTKHHHHHH

B4GALT1 (Molecular Weight: 33.0 kDa; Number of *N*-glycosylation site: 0)

ETGSLPACPEESPLLVGPMLIDFNIAVDLELLAKKNPEIKTGGRYSPKDCVSPHKVAIII
PFRNRQEHLKYWLYYLHPILQRQQLDYGIYVINQAGDTMFNRAKLLNIGFQEALKD
YDYNCFVFSDVDLIPMDDRNAYRCFSQPRHISVAMDKFGFSLPYVQYFGGVSALSK
QQFLAINGFPNNYWGWGGEDDDIFNRLVHKGMSISRPNAVVGRTRMIRHSRDKKNE
PNPQRFDRIAHTKETMRFDGLNSLTYKVLDVQRYPLYTQITVDIGTPRGTKHHHHHH

Gp120$_{Bal}$ (Molecular Weight: 54.5 kDa; Number of *N*-glycosylation site: 23)

VSPSTEKLWVTVYYGVPVWKEATTTLFCASDAKAYDTEVHNVWATHACVPTDPNP
QEVELENVTENFNMWKNNMVEQMHEDIISLWDQSLKPCVKLTPLCVTLNCTDLRN
ATNGNDTNTTSSSREMMGGGEMKNCSFKITTNIRGKVQKEYALFYELDIVPIDNNSN
NRYRLISCNTSVITQACPKISFEPIPIHYCAPAGFAILKCKDKKFNGKGPCSNVSTVQC
THGIRPVVSTQLLLNGSLAEEEVVIRSENFADNAKTIIVQLNESVEINCTRPNNNTRKS
IHIGPGRALYTTGEIIGDIRQAHCNLSRAKWNDTLNKIVIKLREQFGNKTIVFKHSSGG
DPEIVTHSFNCGGEFFYCNSTQLFNSTWNVTEESNNTVENNTITLPCRIKQIINMWQK
VGRAMYAPPIRGQIRCSSNITGLLLTRDGGPEDNKTEVFRPGGGDMRDNWRSELYK
YKVVKIEPLGVAPTKAISSVVKHHHHHH

References

1. Wesolowski, J., Alzogaray, V., Reyelt, J., Unger, M., Juarez, K., Urrutia, M., Cauerhff, A., Danquah, W., Rissiek, B., Scheuplein, F., Schwarz, N., Adriouch, S., Boyer, O., Seman, M., Licea, A., Serreze, D. V., Goldbaum, F. A., Haag, F. & Koch-Nolte, F. (2009). Single domain antibodies: promising experimental and therapeutic tools in infection and immunity. *Med Microbiol Immunol* **198**, 157-74.

2. Amzel, L. M. & Poljak, R. J. (1979). Three-dimensional structure of immunoglobulins. *Annu Rev Biochem* **48**, 961-97.

3. Davies, D. R. & Metzger, H. (1983). Structural basis of antibody function. *Annu Rev Immunol* **1**, 87-117.

4. Arnold, J. N., Wormald, M. R., Sim, R. B., Rudd, P. M. & Dwek, R. A. (2007). The impact of glycosylation on the biological function and structure of human immunoglobulins. *Annu Rev Immunol* **25**, 21-50.

5. Padlan, E. A. (1994). Anatomy of the antibody molecule. *Mol Immunol* **31**, 169-217.

6. Edelman, G. M., Cunningham, B. A., Gall, W. E., Gottlieb, P. D., Rutishauser, U. & Waxdal, M. J. (1969). The covalent structure of an entire gammaG immunoglobulin molecule. *Proc Natl Acad Sci U S A* **63**, 78-85.

7. Litman, G. W., Anderson, M. K. & Rast, J. P. (1999). Evolution of antigen binding receptors. *Annu Rev Immunol* **17**, 109-47.

8. Saphire, E. O., Stanfield, R. L., Crispin, M. D., Parren, P. W., Rudd, P. M., Dwek, R. A., Burton, D. R. & Wilson, I. A. (2002). Contrasting IgG structures reveal extreme asymmetry and flexibility. *J Mol Biol* **319**, 9-18.

9. Ravetch, J. V. & Bolland, S. (2001). IgG Fc receptors. *Annu Rev Immunol* **19**, 275-90.

10. Samuelsson, A., Towers, T. L. & Ravetch, J. V. (2001). Anti-inflammatory activity of IVIG mediated through the inhibitory Fc receptor. *Science* **291**, 484-6.

11. Saphire, E. O., Parren, P. W., Pantophlet, R., Zwick, M. B., Morris, G. M., Rudd, P. M., Dwek, R. A., Stanfield, R. L., Burton, D. R. & Wilson, I. A. (2001). Crystal structure of a neutralizing human IGG against HIV-1: a template for vaccine design. *Science* **293**, 1155-9.

12. Stavnezer, J., Guikema, J. E. & Schrader, C. E. (2008). Mechanism and regulation of class switch recombination. *Annu Rev Immunol* **26**, 261-92.

13. Gould, H. J., Sutton, B. J., Beavil, A. J., Beavil, R. L., McCloskey, N., Coker, H. A., Fear, D. & Smurthwaite, L. (2003). The biology of IGE and the basis of allergic disease. *Annu Rev Immunol* **21**, 579-628.

14. Gonzalez-Quintela, A., Alende, R., Gude, F., Campos, J., Rey, J., Meijide, L. M., Fernandez-Merino, C. & Vidal, C. (2008). Serum levels of immunoglobulins (IgG, IgA, IgM) in a general adult population and their relationship with alcohol

consumption, smoking and common metabolic abnormalities. *Clin Exp Immunol* **151**, 42-50.

15. Monteiro, R. C. & Van De Winkel, J. G. (2003). IgA Fc receptors. *Annu Rev Immunol* **21**, 177-204.

16. Chen, K. & Cerutti, A. (2010). New insights into the enigma of immunoglobulin D. *Immunol Rev* **237**, 160-79.

17. Nitschke, L., Kosco, M. H., Kohler, G. & Lamers, M. C. (1993). Immunoglobulin D-deficient mice can mount normal immune responses to thymus-independent and -dependent antigens. *Proc Natl Acad Sci U S A* **90**, 1887-91.

18. Roes, J. & Rajewsky, K. (1993). Immunoglobulin D (IgD)-deficient mice reveal an auxiliary receptor function for IgD in antigen-mediated recruitment of B cells. *J Exp Med* **177**, 45-55.

19. Oortwijn, B. D., Roos, A., Royle, L., van Gijlswijk-Janssen, D. J., Faber-Krol, M. C., Eijgenraam, J. W., Dwek, R. A., Daha, M. R., Rudd, P. M. & van Kooten, C. (2006). Differential glycosylation of polymeric and monomeric IgA: a possible role in glomerular inflammation in IgA nephropathy. *J Am Soc Nephrol* **17**, 3529-39.

20. Arnold, J. N., Radcliffe, C. M., Wormald, M. R., Royle, L., Harvey, D. J., Crispin, M., Dwek, R. A., Sim, R. B. & Rudd, P. M. (2004). The glycosylation of human serum IgD and IgE and the accessibility of identified oligomannose structures for interaction with mannan-binding lectin. *J Immunol* **173**, 6831-40.

21. Arnold, J. N., Wormald, M. R., Suter, D. M., Radcliffe, C. M., Harvey, D. J., Dwek, R. A., Rudd, P. M. & Sim, R. B. (2005). Human serum IgM glycosylation: identification of glycoforms that can bind to mannan-binding lectin. *J Biol Chem* **280**, 29080-7.

22. Ding, Y., Xu, G., Yang, M., Yao, M., Gao, G. F., Wang, L., Zhang, W. & Rao, Z. (2003). Crystal structure of the ectodomain of human FcalphaRI. *J Biol Chem* **278**, 27966-70.

23. Nimmerjahn, F. & Ravetch, J. V. (2008). Anti-inflammatory actions of intravenous immunoglobulin. *Annu Rev Immunol* **26**, 513-33.

24. Jefferis, R. (2007). Antibody therapeutics: isotype and glycoform selection. *Expert Opin Biol Ther* **7**, 1401-13.

25. Torres, M. & Casadevall, A. (2008). The immunoglobulin constant region contributes to affinity and specificity. *Trends Immunol* **29**, 91-7.

26. Aalberse, R. C. & Schuurman, J. (2002). IgG4 breaking the rules. *Immunology* **105**, 9-19.

27. Burton, D. R., Gregory, L. & Jefferis, R. (1986). Aspects of the molecular structure of IgG subclasses. *Monogr Allergy* **19**, 7-35.

28. Harada, S., Takagi, S., Kosada, Y. & Kondo, E. (1992). Hinge region of human IgG2 protein: conformational studies with monoclonal antibodies. *Mol Immunol* **29**, 145-9.

29. Roux, K. H., Strelets, L. & Michaelsen, T. E. (1997). Flexibility of human IgG subclasses. *J Immunol* **159**, 3372-82.

30. Shields, R. L., Namenuk, A. K., Hong, K., Meng, Y. G., Rae, J., Briggs, J., Xie, D., Lai, J., Stadlen, A., Li, B., Fox, J. A. & Presta, L. G. (2001). High resolution mapping of the binding site on human IgG1 for Fc gamma RI, Fc gamma RII, Fc gamma RIII, and FcRn and design of IgG1 variants with improved binding to the Fc gamma R. *J Biol Chem* **276**, 6591-604.

31. Duncan, A. R. & Winter, G. (1988). The binding site for C1q on IgG. *Nature* **332**, 738-40.

32. DeLano, W. L., Ultsch, M. H., de Vos, A. M. & Wells, J. A. (2000). Convergent solutions to binding at a protein-protein interface. *Science* **287**, 1279-83.

33. Kim, J. K., Firan, M., Radu, C. G., Kim, C. H., Ghetie, V. & Ward, E. S. (1999). Mapping the site on human IgG for binding of the MHC class I-related receptor, FcRn. *Eur J Immunol* **29**, 2819-25.

34. Scanlan, C. N., Burton, D. R. & Dwek, R. A. (2008). Making autoantibodies safe. *Proc Natl Acad Sci U S A* **105**, 4081-2.

35. Krapp, S., Mimura, Y., Jefferis, R., Huber, R. & Sondermann, P. (2003). Structural analysis of human IgG-Fc glycoforms reveals a correlation between glycosylation and structural integrity. *J Mol Biol* **325**, 979-89.

36. Borrok, M. J., Jung, S. T., Kang, T. H., Monzingo, A. F. & Georgiou, G. (2012). Revisiting the role of glycosylation in the structure of human IgG Fc. *ACS Chem Biol* **7**, 1596-602.

37. Heyman, B. (2000). Regulation of antibody responses via antibodies, complement, and Fc receptors. *Annu Rev Immunol* **18**, 709-37.

38. Roopenian, D. C. & Akilesh, S. (2007). FcRn: the neonatal Fc receptor comes of age. *Nat Rev Immunol* **7**, 715-25.

39. Anthony, R. M., Wermeling, F., Karlsson, M. C. & Ravetch, J. V. (2008). Identification of a receptor required for the anti-inflammatory activity of IVIG. *Proc Natl Acad Sci U S A* **105**, 19571-8.

40. Anthony, R. M., Kobayashi, T., Wermeling, F. & Ravetch, J. V. (2011). Intravenous gammaglobulin suppresses inflammation through a novel T(H)2 pathway. *Nature*.

41. Gardiner, E. E., Karunakaran, D., Arthur, J. F., Mu, F. T., Powell, M. S., Baker, R. I., Hogarth, P. M., Kahn, M. L., Andrews, R. K. & Berndt, M. C. (2008). Dual ITAM-mediated proteolytic pathways for irreversible inactivation of platelet receptors: de-ITAM-izing FcgammaRIIa. *Blood* **111**, 165-74.

42. Maxwell, K. F., Powell, M. S., Hulett, M. D., Barton, P. A., McKenzie, I. F., Garrett, T. P. & Hogarth, P. M. (1999). Crystal structure of the human leukocyte Fc receptor, Fc gammaRIIa. *Nat Struct Biol* **6**, 437-42.

43. Powell, M. S., Barnes, N. C., Bradford, T. M., Musgrave, I. F., Wines, B. D., Cambier, J. C. & Hogarth, P. M. (2006). Alteration of the Fc gamma RIIa dimer interface affects receptor signaling but not ligand binding. *J Immunol* **176**, 7489-94.

44. Nimmerjahn, F. & Ravetch, J. V. (2008). Fcgamma receptors as regulators of immune responses. *Nat Rev Immunol* **8**, 34-47.

45. Ravetch, J. V. & Perussia, B. (1989). Alternative membrane forms of Fc gamma RIII(CD16) on human natural killer cells and neutrophils. Cell type-specific expression of two genes that differ in single nucleotide substitutions. *J Exp Med* **170**, 481-97.

46. Graf, S. W., Lester, S., Nossent, J. C., Hill, C. L., Proudman, S. M., Lee, A. & Rischmueller, M. (2012). Low copy number of the FCGR3B gene and rheumatoid arthritis: a case-control study and meta-analysis. *Arthritis Res Ther* **14**, R28.

47. Fossati, G., Moots, R. J., Bucknall, R. C. & Edwards, S. W. (2002). Differential role of neutrophil Fcgamma receptor IIIB (CD16) in phagocytosis, bacterial killing, and responses to immune complexes. *Arthritis Rheum* **46**, 1351-61.

48. Smith, K. G. & Clatworthy, M. R. (2010). FcgammaRIIB in autoimmunity and infection: evolutionary and therapeutic implications. *Nat Rev Immunol* **10**, 328-43.

49. Takai, T., Ono, M., Hikida, M., Ohmori, H. & Ravetch, J. V. (1996). Augmented humoral and anaphylactic responses in Fc gamma RII-deficient mice. *Nature* **379**, 346-9.

50. Nakamura, A., Yuasa, T., Ujike, A., Ono, M., Nukiwa, T., Ravetch, J. V. & Takai, T. (2000). Fcgamma receptor IIB-deficient mice develop Goodpasture's syndrome upon immunization with type IV collagen: a novel murine model for autoimmune glomerular basement membrane disease. *J Exp Med* **191**, 899-906.

51. Yuasa, T., Kubo, S., Yoshino, T., Ujike, A., Matsumura, K., Ono, M., Ravetch, J. V. & Takai, T. (1999). Deletion of fcgamma receptor IIB renders H-2(b) mice susceptible to collagen-induced arthritis. *J Exp Med* **189**, 187-94.

52. McGaha, T. L., Sorrentino, B. & Ravetch, J. V. (2005). Restoration of tolerance in lupus by targeted inhibitory receptor expression. *Science* **307**, 590-3.

53. Brownlie, R. J., Lawlor, K. E., Niederer, H. A., Cutler, A. J., Xiang, Z., Clatworthy, M. R., Floto, R. A., Greaves, D. R., Lyons, P. A. & Smith, K. G. (2008). Distinct cell-specific control of autoimmunity and infection by FcgammaRIIb. *J Exp Med* **205**, 883-95.

54. Hogarth, P. M. & Pietersz, G. A. (2012). Fc receptor-targeted therapies for the treatment of inflammation, cancer and beyond. *Nat Rev Drug Discov* **11**, 311-31.

55. Chu, S. Y., Vostiar, I., Karki, S., Moore, G. L., Lazar, G. A., Pong, E., Joyce, P. F., Szymkowski, D. E. & Desjarlais, J. R. (2008). Inhibition of B cell receptor-mediated activation of primary human B cells by coengagement of CD19 and FcgammaRIIb with Fc-engineered antibodies. *Mol Immunol* **45**, 3926-33.

56. Horton, H. M., Chu, S. Y., Ortiz, E. C., Pong, E., Cemerski, S., Leung, I. W., Jacob, N., Zalevsky, J., Desjarlais, J. R., Stohl, W. & Szymkowski, D. E. (2011). Antibody-mediated coengagement of FcgammaRIIb and B cell receptor complex suppresses humoral immunity in systemic lupus erythematosus. *J Immunol* **186**, 4223-33.

57. Li, F. & Ravetch, J. V. (2011). Inhibitory Fcgamma receptor engagement drives adjuvant and anti-tumor activities of agonistic CD40 antibodies. *Science* **333**, 1030-4.

58. White, A. L., Chan, H. T., French, R. R., Beers, S. A., Cragg, M. S., Johnson, P. W. & Glennie, M. J. (2013). FcgammaRIotaIotaB controls the potency of agonistic anti-TNFR mAbs. *Cancer Immunol Immunother* **62**, 941-8.

59. Magnusson, S. E., Andren, M., Nilsson, K. E., Sondermann, P., Jacob, U. & Kleinau, S. (2008). Amelioration of collagen-induced arthritis by human recombinant soluble FcgammaRIIb. *Clin Immunol* **127**, 225-33.

60. Ellsworth, J. L., Hamacher, N., Harder, B., Bannink, K., Bukowski, T. R., Byrnes-Blake, K., Underwood, S., Oliver, C., Waggie, K. S., Noriega, C., Hebb, L., Rixon, M. W. & Lewis, K. E. (2009). Recombinant soluble human FcgammaR1A (CD64A) reduces inflammation in murine collagen-induced arthritis. *J Immunol* **182**, 7272-9.

61. Shashidharamurthy, R., Hennigar, R. A., Fuchs, S., Palaniswami, P., Sherman, M. & Selvaraj, P. (2008). Extravasations and emigration of neutrophils to the inflammatory site depend on the interaction of immune-complex with Fcgamma receptors and can be effectively blocked by decoy Fcgamma receptors. *Blood* **111**, 894-904.

62. Wines, B. D., Gavin, A., Powell, M. S., Steinitz, M., Buchanan, R. R. & Mark Hogarth, P. (2003). Soluble FcgammaRIIa inhibits rheumatoid factor binding to immune complexes. *Immunology* **109**, 246-54.

63. Ellsworth, J. L., Maurer, M., Harder, B., Hamacher, N., Lantry, M., Lewis, K. B., Rene, S., Byrnes-Blake, K., Underwood, S., Waggie, K. S., Visich, J. & Lewis, K. E. (2008). Targeting immune complex-mediated hypersensitivity with recombinant soluble human FcgammaRIA (CD64A). *J Immunol* **180**, 580-9.

64. Boruchov, A. M., Heller, G., Veri, M. C., Bonvini, E., Ravetch, J. V. & Young, J. W. (2005). Activating and inhibitory IgG Fc receptors on human DCs mediate opposing functions. *J Clin Invest* **115**, 2914-23.

65. Radstake, T. R., van Lieshout, A. W., van Riel, P. L., van den Berg, W. B. & Adema, G. J. (2005). Dendritic cells, Fc{gamma} receptors, and Toll-like receptors: potential allies in the battle against rheumatoid arthritis. *Ann Rheum Dis* **64**, 1532-8.

66. Dhodapkar, K. M., Kaufman, J. L., Ehlers, M., Banerjee, D. K., Bonvini, E., Koenig, S., Steinman, R. M., Ravetch, J. V. & Dhodapkar, M. V. (2005). Selective blockade of inhibitory Fcgamma receptor enables human dendritic cell maturation with IL-

12p70 production and immunity to antibody-coated tumor cells. *Proc Natl Acad Sci U S A* **102**, 2910-5.

67. Lu, J., Ellsworth, J. L., Hamacher, N., Oak, S. W. & Sun, P. D. (2011). Crystal structure of Fcgamma receptor I and its implication in high affinity gamma-immunoglobulin binding. *J Biol Chem* **286**, 40608-13.

68. Sondermann, P., Huber, R. & Jacob, U. (1999). Crystal structure of the soluble form of the human fcgamma-receptor IIb: a new member of the immunoglobulin superfamily at 1.7 A resolution. *EMBO J* **18**, 1095-103.

69. Sondermann, P., Huber, R., Oosthuizen, V. & Jacob, U. (2000). The 3.2-A crystal structure of the human IgG1 Fc fragment-Fc gammaRIII complex. *Nature* **406**, 267-73.

70. Radaev, S., Motyka, S., Fridman, W. H., Sautes-Fridman, C. & Sun, P. D. (2001). The structure of a human type III Fcgamma receptor in complex with Fc. *J Biol Chem* **276**, 16469-77.

71. Woof, J. M. & Burton, D. R. (2004). Human antibody-Fc receptor interactions illuminated by crystal structures. *Nat Rev Immunol* **4**, 89-99.

72. Ferrara, C., Grau, S., Jäger, C., Sondermann, P., Brünker, P., Waldhauer, I., Hennig, M., Ruf, A., Rufer, A. C., Stihle, M., Umaña, P. & Benz, J. (2011). Unique carbohydrate–carbohydrate interactions are required for high affinity binding between FcγRIII and antibodies lacking core fucose. *Proceedings of the National Academy of Sciences* **108**, 12669-12674.

73. Mimoto, F., Katada, H., Kadono, S., Igawa, T., Kuramochi, T., Muraoka, M., Wada, Y., Haraya, K., Miyazaki, T. & Hattori, K. (2013). Engineered antibody Fc variant with selectively enhanced FcgammaRIIb binding over both FcgammaRIIaR131 and FcgammaRIIaH131. *Protein Eng Des Sel*.

74. Bruhns, P. (2012). Properties of mouse and human IgG receptors and their contribution to disease models. *Blood* **119**, 5640-9.

75. Kono, H., Kyogoku, C., Suzuki, T., Tsuchiya, N., Honda, H., Yamamoto, K., Tokunaga, K. & Honda, Z. (2005). FcgammaRIIB Ile232Thr transmembrane polymorphism associated with human systemic lupus erythematosus decreases affinity to lipid rafts and attenuates inhibitory effects on B cell receptor signaling. *Hum Mol Genet* **14**, 2881-92.

76. Rudd, P. M. & Dwek, R. A. (1997). Glycosylation: heterogeneity and the 3D structure of proteins. *Crit Rev Biochem Mol Biol* **32**, 1-100.

77. Jefferis, R. (2005). Glycosylation of recombinant antibody therapeutics. *Biotechnol Prog* **21**, 11-6.

78. Radcliffe, C. M., Arnold, J. N., Suter, D. M., Wormald, M. R., Harvey, D. J., Royle, L., Mimura, Y., Kimura, Y., Sim, R. B., Inoges, S., Rodriguez-Calvillo, M., Zabalegui, N., de Cerio, A. L., Potter, K. N., Mockridge, C. I., Dwek, R. A., Bendandi, M., Rudd, P. M. & Stevenson, F. K. (2007). Human follicular lymphoma cells contain

oligomannose glycans in the antigen-binding site of the B-cell receptor. *J Biol Chem* **282**, 7405-15.

79. Weerapana, E. & Imperiali, B. (2006). Asparagine-linked protein glycosylation: from eukaryotic to prokaryotic systems. *Glycobiology* **16**, 91R-101R.

80. Harvey, D. J., Merry, A. H., Royle, L., Campbell, M. P., Dwek, R. A. & Rudd, P. M. (2009). Proposal for a standard system for drawing structural diagrams of N- and O-linked carbohydrates and related compounds. *Proteomics* **9**, 3796-801.

81. Bowden, T. A., Baruah, K., Coles, C. H., Harvey, D. J., Yu, X., Song, B. D., Stuart, D. I., Aricescu, A. R., Scanlan, C. N., Jones, E. Y. & Crispin, M. (2012). Chemical and Structural Analysis of an Antibody Folding Intermediate Trapped during Glycan Biosynthesis. *J Am Chem Soc* **134**, 17554-63.

82. Vliegenthart, J. F. G., Dorland, L. & van Halbeek, H. (1983). High-resolution 1H nuclear magnetic resonance spectroscopy as a tool in the structural analysis of carbohydrates related to glycoproteins. *Adv. Carbohydr. Chem. & Biochem.* **41**, 209-374.

83. Holland, M., Yagi, H., Takahashi, N., Kato, K., Savage, C. O., Goodall, D. M. & Jefferis, R. (2006). Differential glycosylation of polyclonal IgG, IgG-Fc and IgG-Fab isolated from the sera of patients with ANCA-associated systemic vasculitis. *Biochim Biophys Acta* **1760**, 669-77.

84. Guile, G. R., Rudd, P. M., Wing, D. R., Prime, S. B. & Dwek, R. A. (1996). A rapid high-resolution high-performance liquid chromatographic method for separating glycan mixtures and analyzing oligosaccharide profiles. *Anal Biochem* **240**, 210-26.

85. Shibata-Koyama, M., Iida, S., Okazaki, A., Mori, K., Kitajima-Miyama, K., Saitou, S., Kakita, S., Kanda, Y., Shitara, K., Kato, K. & Satoh, M. (2009). The N-linked oligosaccharide at Fc gamma RIIIa Asn-45: an inhibitory element for high Fc gamma RIIIa binding affinity to IgG glycoforms lacking core fucosylation. *Glycobiology* **19**, 126-34.

86. Takasaki, S. & Kobata, A. (1986). Asparagine-linked sugar chains of fetuin: occurrence of tetrasialyl triantennary sugar chains containing the Gal beta 1----3GlcNAc sequence. *Biochemistry* **25**, 5709-15.

87. Lund, J., Takahashi, N., Pound, J. D., Goodall, M. & Jefferis, R. (1996). Multiple interactions of IgG with its core oligosaccharide can modulate recognition by complement and human Fc gamma receptor I and influence the synthesis of its oligosaccharide chains. *J Immunol* **157**, 4963-9.

88. Matsumiya, S., Yamaguchi, Y., Saito, J., Nagano, M., Sasakawa, H., Otaki, S., Satoh, M., Shitara, K. & Kato, K. (2007). Structural comparison of fucosylated and nonfucosylated Fc fragments of human immunoglobulin G1. *J Mol Biol* **368**, 767-79.

89. Mimura, Y., Church, S., Ghirlando, R., Ashton, P. R., Dong, S., Goodall, M., Lund, J. & Jefferis, R. (2000). The influence of glycosylation on the thermal stability and effector function expression of human IgG1-Fc: properties of a series of truncated glycoforms. *Mol Immunol* **37**, 697-706.

90. Mimura, Y., Ghirlando, R., Sondermann, P., Lund, J. & Jefferis, R. (2001). The molecular specificity of IgG-Fc interactions with Fc gamma receptors. *Adv Exp Med Biol* **495**, 49-53.

91. Oganesyan, V., Damschroder, M. M., Leach, W., Wu, H. & Dall'Acqua, W. F. (2008). Structural characterization of a mutated, ADCC-enhanced human Fc fragment. *Mol Immunol* **45**, 1872-82.

92. Crispin, M., Bowden, T. A., Coles, C. H., Harlos, K., Aricescu, A. R., Harvey, D. J., Stuart, D. I. & Jones, E. Y. (2009). Carbohydrate and domain architecture of an immature antibody glycoform exhibiting enhanced effector functions. *J Mol Biol* **387**, 1061-6.

93. Crispin, M., Yu, X. & Bowden, T. A. (2013). Crystal structure of sialylated IgG Fc: Implications for the mechanism of intravenous immunoglobulin therapy. *Proc Natl Acad Sci U S A*.

94. Butler, M., Quelhas, D., Critchley, A. J., Carchon, H., Hebestreit, H. F., Hibbert, R. G., Vilarinho, L., Teles, E., Matthijs, G., Schollen, E., Argibay, P., Harvey, D. J., Dwek, R. A., Jaeken, J. & Rudd, P. M. (2003). Detailed glycan analysis of serum glycoproteins of patients with congenital disorders of glycosylation indicates the specific defective glycan processing step and provides an insight into pathogenesis. *Glycobiology* **13**, 601-22.

95. Voynov, V., Chennamsetty, N., Kayser, V., Helk, B., Forrer, K., Zhang, H., Fritsch, C., Heine, H. & Trout, B. L. (2009). Dynamic fluctuations of protein-carbohydrate interactions promote protein aggregation. *PLoS One* **4**, e8425.

96. Stewart, R., Thom, G., Levens, M., Guler-Gane, G., Holgate, R., Rudd, P. M., Webster, C., Jermutus, L. & Lund, J. (2011). A variant human IgG1-Fc mediates improved ADCC. *Protein Eng Des Sel* **24**, 671-8.

97. Jassal, R., Jenkins, N., Charlwood, J., Camilleri, P., Jefferis, R. & Lund, J. (2001). Sialylation of human IgG-Fc carbohydrate by transfected rat alpha2,6-sialyltransferase. *Biochem Biophys Res Commun* **286**, 243-9.

98. Sazinsky, S. L., Ott, R. G., Silver, N. W., Tidor, B., Ravetch, J. V. & Wittrup, K. D. (2008). Aglycosylated immunoglobulin G1 variants productively engage activating Fc receptors. *Proc Natl Acad Sci U S A* **105**, 20167-72.

99. Wormald, M. R., Rudd, P. M., Harvey, D. J., Chang, S. C., Scragg, I. G. & Dwek, R. A. (1997). Variations in oligosaccharide-protein interactions in immunoglobulin G determine the site-specific glycosylation profiles and modulate the dynamic motion of the Fc oligosaccharides. *Biochemistry* **36**, 1370-80.

100. Barb, A. W. & Prestegard, J. H. (2011). NMR analysis demonstrates immunoglobulin G N-glycans are accessible and dynamic. *Nat Chem Biol* **7**, 147-53.

101. Yamaguchi, Y., Kato, K., Shindo, M., Aoki, S., Furusho, K., Koga, K., Takahashi, N., Arata, Y. & Shimada, I. (1998). Dynamics of the carbohydrate chains attached to the Fc portion of immunoglobulin G as studied by NMR spectroscopy assisted by selective 13C labeling of the glycans. *J Biomol NMR* **12**, 385-94.

102. Prabakaran, P., Vu, B. K., Gan, J., Feng, Y., Dimitrov, D. S. & Ji, X. (2008). Structure of an isolated unglycosylated antibody C(H)2 domain. *Acta Crystallogr D Biol Crystallogr* **64**, 1062-7.

103. Nose, M. & Wigzell, H. (1983). Biological significance of carbohydrate chains on monoclonal antibodies. *Proc Natl Acad Sci U S A* **80**, 6632-6.

104. Baruah, K., Bowden, T. A., Krishna, B. A., Dwek, R. A., Crispin, M. & Scanlan, C. N. (2012). Selective Deactivation of Serum IgG: A General Strategy for the Enhancement of Monoclonal Antibody Receptor Interactions. *J Mol Biol* **420**, 1-7.

105. Collin, M. & Olsen, A. (2001). EndoS, a novel secreted protein from Streptococcus pyogenes with endoglycosidase activity on human IgG. *EMBO J* **20**, 3046-55.

106. Lux, A., Yu, X., Scanlan, C. N. & Nimmerjahn, F. (2013). Impact of Immune Complex Size and Glycosylation on IgG Binding to Human FcgammaRs. *J Immunol* **190**, 4315-23.

107. Jung, S. T., Kelton, W., Kang, T. H., Ng, D. T., Andersen, J. T., Sandlie, I., Sarkar, C. A. & Georgiou, G. (2013). Effective phagocytosis of low Her2 tumor cell lines with engineered, aglycosylated IgG displaying high FcgammaRIIa affinity and selectivity. *ACS Chem Biol* **8**, 368-75.

108. Nandakumar, K. S., Collin, M., Happonen, K. E., Croxford, A. M., Lundstrom, S. L., Zubarev, R. A., Rowley, M. J., Blom, A. M. & Holmdahl, R. (2013). Dominant suppression of inflammation by glycan-hydrolyzed IgG. *Proc Natl Acad Sci U S A*.

109. Ferrara, C., Stuart, F., Sondermann, P., Brunker, P. & Umana, P. (2006). The carbohydrate at FcgammaRIIIa Asn-162. An element required for high affinity binding to non-fucosylated IgG glycoforms. *J Biol Chem* **281**, 5032-6.

110. Ferrara, C., Grau, S., Jager, C., Sondermann, P., Brunker, P., Waldhauer, I., Hennig, M., Ruf, A., Rufer, A. C., Stihle, M., Umana, P. & Benz, J. (2011). Unique carbohydrate-carbohydrate interactions are required for high affinity binding between Fc{gamma}RIII and antibodies lacking core fucose. *Proc Natl Acad Sci U S A* **108**, 12669-74.

111. Okazaki, A., Shoji-Hosaka, E., Nakamura, K., Wakitani, M., Uchida, K., Kakita, S., Tsumoto, K., Kumagai, I. & Shitara, K. (2004). Fucose depletion from human IgG1 oligosaccharide enhances binding enthalpy and association rate between IgG1 and FcgammaRIIIa. *J Mol Biol* **336**, 1239-49.

112. Shields, R. L., Lai, J., Keck, R., O'Connell, L. Y., Hong, K., Meng, Y. G., Weikert, S. H. & Presta, L. G. (2002). Lack of fucose on human IgG1 N-linked oligosaccharide improves binding to human Fcgamma RIII and antibody-dependent cellular toxicity. *J Biol Chem* **277**, 26733-40.

113. Shinkawa, T., Nakamura, K., Yamane, N., Shoji-Hosaka, E., Kanda, Y., Sakurada, M., Uchida, K., Anazawa, H., Satoh, M., Yamasaki, M., Hanai, N. & Shitara, K. (2003). The absence of fucose but not the presence of galactose or bisecting N-acetylglucosamine of human IgG1 complex-type oligosaccharides shows the critical role of enhancing antibody-dependent cellular cytotoxicity. *J Biol Chem* **278**, 3466-73.

114. Zeck, A., Pohlentz, G., Schlothauer, T., Peter-Katalinic, J. & Regula, J. T. (2011). Cell type-specific and site directed N-glycosylation pattern of FcgammaRIIIa. *J Proteome Res* **10**, 3031-9.

115. Forthal, D. N., Gach, J. S., Landucci, G., Jez, J., Strasser, R., Kunert, R. & Steinkellner, H. (2010). Fc-glycosylation influences Fcgamma receptor binding and cell-mediated anti-HIV activity of monoclonal antibody 2G12. *J Immunol* **185**, 6876-82.

116. Satoh, M., Iida, S. & Shitara, K. (2006). Non-fucosylated therapeutic antibodies as next-generation therapeutic antibodies. *Expert Opin Biol Ther* **6**, 1161-73.

117. Mori, K., Iida, S., Yamane-Ohnuki, N., Kanda, Y., Kuni-Kamochi, R., Nakano, R., Imai-Nishiya, H., Okazaki, A., Shinkawa, T., Natsume, A., Niwa, R., Shitara, K. & Satoh, M. (2007). Non-fucosylated therapeutic antibodies: the next generation of therapeutic antibodies. *Cytotechnology* **55**, 109-14.

118. Jefferis, R. (2009). Glycosylation as a strategy to improve antibody-based therapeutics. *Nat Rev Drug Discov* **8**, 226-34.

119. Wuhrer, M., Porcelijn, L., Kapur, R., Koeleman, C. A., Deelder, A., de Haas, M. & Vidarsson, G. (2009). Regulated glycosylation patterns of IgG during alloimmune responses against human platelet antigens. *J Proteome Res* **8**, 450-6.

120. Houde, D., Peng, Y., Berkowitz, S. A. & Engen, J. R. (2010). Post-translational modifications differentially affect IgG1 conformation and receptor binding. *Mol Cell Proteomics* **9**, 1716-28.

121. Rademacher, T. W., Williams, P. & Dwek, R. A. (1994). Agalactosyl glycoforms of IgG autoantibodies are pathogenic. *Proc Natl Acad Sci U S A* **91**, 6123-7.

122. Parekh, R., Roitt, I., Isenberg, D., Dwek, R. & Rademacher, T. (1988). Age-related galactosylation of the N-linked oligosaccharides of human serum IgG. *J Exp Med* **167**, 1731-6.

123. Parekh, R. B., Dwek, R. A., Sutton, B. J., Fernandes, D. L., Leung, A., Stanworth, D., Rademacher, T. W., Mizuochi, T., Taniguchi, T., Matsuta, K. & et al. (1985). Association of rheumatoid arthritis and primary osteoarthritis with changes in the glycosylation pattern of total serum IgG. *Nature* **316**, 452-7.

124. Parekh, R., Isenberg, D., Rook, G., Roitt, I., Dwek, R. & Rademacher, T. (1989). A comparative analysis of disease-associated changes in the galactosylation of serum IgG. *J Autoimmun* **2**, 101-14.

125. Rook, G. A., Steele, J., Brealey, R., Whyte, A., Isenberg, D., Sumar, N., Nelson, J. L., Bodman, K. B., Young, A., Roitt, I. M. & et al. (1991). Changes in IgG glycoform levels are associated with remission of arthritis during pregnancy. *J Autoimmun* **4**, 779-94.

126. Axford, J. S., Mackenzie, L., Lydyard, P. M., Hay, F. C., Isenberg, D. A. & Roitt, I. M. (1987). Reduced B-cell galactosyltransferase activity in rheumatoid arthritis. *Lancet* **2**, 1486-8.

127. Alavi, A. & Axford, J. (1995). Beta 1,4-galactosyltransferase variations in rheumatoid arthritis. *Adv Exp Med Biol* **376**, 185-92.

128. Garred, P., Madsen, H. O., Marquart, H., Hansen, T. M., Sorensen, S. F., Petersen, J., Volck, B., Svejgaard, A., Graudal, N. A., Rudd, P. M., Dwek, R. A., Sim, R. B. & Andersen, V. (2000). Two edged role of mannose binding lectin in rheumatoid arthritis: a cross sectional study. *J Rheumatol* **27**, 26-34.

129. Nimmerjahn, F., Anthony, R. M. & Ravetch, J. V. (2007). Agalactosylated IgG antibodies depend on cellular Fc receptors for in vivo activity. *Proc Natl Acad Sci U S A* **104**, 8433-7.

130. Karsten, C. M., Pandey, M. K., Figge, J., Kilchenstein, R., Taylor, P. R., Rosas, M., McDonald, J. U., Orr, S. J., Berger, M., Petzold, D., Blanchard, V., Winkler, A., Hess, C., Reid, D. M., Majoul, I. V., Strait, R. T., Harris, N. L., Kohl, G., Wex, E., Ludwig, R., Zillikens, D., Nimmerjahn, F., Finkelman, F. D., Brown, G. D., Ehlers, M. & Kohl, J. (2012). Anti-inflammatory activity of IgG1 mediated by Fc galactosylation and association of FcgammaRIIB and dectin-1. *Nat Med* **18**, 1401-6.

131. Dalziel, M., McFarlane, I. & Axford, J. S. (1999). Lectin analysis of human immunoglobulin G N-glycan sialylation. *Glycoconj J* **16**, 801-7.

132. Scallon, B. J., Tam, S. H., McCarthy, S. G., Cai, A. N. & Raju, T. S. (2007). Higher levels of sialylated Fc glycans in immunoglobulin G molecules can adversely impact functionality. *Mol Immunol* **44**, 1524-34.

133. Kaneko, Y., Nimmerjahn, F. & Ravetch, J. V. (2006). Anti-inflammatory activity of immunoglobulin G resulting from Fc sialylation. *Science* **313**, 670-3.

134. Dall'Acqua, W. F., Cook, K. E., Damschroder, M. M., Woods, R. M. & Wu, H. (2006). Modulation of the effector functions of a human IgG1 through engineering of its hinge region. *J Immunol* **177**, 1129-38.

135. Sondermann, P., Pincetic, A., Maamary, J., Lammens, K. & Ravetch, J. V. (2013). General mechanism for modulating immunoglobulin effector function. *Proc Natl Acad Sci U S A*.

136. Oefner, C. M., Winkler, A., Hess, C., Lorenz, A. K., Holecska, V., Huxdorf, M., Schommartz, T., Petzold, D., Bitterling, J., Schoen, A. L., Stoehr, A. D., Vu Van, D., Darcan-Nikolaisen, Y., Blanchard, V., Schmudde, I., Laumonnier, Y., Strover, H. A., Hegazy, A. N., Eiglmeier, S., Schoen, C. T., Mertes, M. M., Loddenkemper, C., Lohning, M., Konig, P., Petersen, A., Luger, E. O., Collin, M., Kohl, J., Hutloff, A., Hamelmann, E., Berger, M., Wardemann, H. & Ehlers, M. (2012). Tolerance induction with T cell-dependent protein antigens induces regulatory sialylated IgGs. *J Allergy Clin Immunol* **129**, 1647-55 e13.

137. Selman, M. H., de Jong, S. E., Soonawala, D., Kroon, F. P., Adegnika, A. A., Deelder, A. M., Hokke, C. H., Yazdanbakhsh, M. & Wuhrer, M. (2012). Changes in antigen-specific IgG1 Fc N-glycosylation upon influenza and tetanus vaccination. *Mol Cell Proteomics* **11**, M111 014563.

138. Anthony, R. M., Nimmerjahn, F., Ashline, D. J., Reinhold, V. N., Paulson, J. C. & Ravetch, J. V. (2008). Recapitulation of IVIG anti-inflammatory activity with a recombinant IgG Fc. *Science* **320**, 373-6.

139. Gelfand, E. W. (2012). Intravenous immune globulin in autoimmune and inflammatory diseases. *N Engl J Med* **367**, 2015-25.

140. Kanda, Y., Yamada, T., Mori, K., Okazaki, A., Inoue, M., Kitajima-Miyama, K., Kuni-Kamochi, R., Nakano, R., Yano, K., Kakita, S., Shitara, K. & Satoh, M. (2007). Comparison of biological activity among nonfucosylated therapeutic IgG1 antibodies with three different N-linked Fc oligosaccharides: the high-mannose, hybrid, and complex types. *Glycobiology* **17**, 104-18.

141. Zou, G., Ochiai, H., Huang, W., Yang, Q., Li, C. & Wang, L. X. (2011). Chemoenzymatic synthesis and Fcgamma receptor binding of homogeneous glycoforms of antibody Fc domain. Presence of a bisecting sugar moiety enhances the affinity of Fc to FcgammaIIIa receptor. *J Am Chem Soc* **133**, 18975-91.

142. Goetze, A. M., Liu, Y. D., Zhang, Z., Shah, B., Lee, E., Bondarenko, P. V. & Flynn, G. C. (2011). High-mannose glycans on the Fc region of therapeutic IgG antibodies increase serum clearance in humans. *Glycobiology* **21**, 949-59.

143. Millward, T. A., Heitzmann, M., Bill, K., Langle, U., Schumacher, P. & Forrer, K. (2008). Effect of constant and variable domain glycosylation on pharmacokinetics of therapeutic antibodies in mice. *Biologicals* **36**, 41-7.

144. Chen, X., Liu, Y. D. & Flynn, G. C. (2009). The effect of Fc glycan forms on human IgG2 antibody clearance in humans. *Glycobiology* **19**, 240-9.

145. Wright, A., Sato, Y., Okada, T., Chang, K., Endo, T. & Morrison, S. (2000). In vivo trafficking and catabolism of IgG1 antibodies with Fc associated carbohydrates of differing structure. *Glycobiology* **10**, 1347-55.

146. Hodoniczky, J., Zheng, Y. Z. & James, D. C. (2005). Control of recombinant monoclonal antibody effector functions by Fc N-glycan remodeling in vitro. *Biotechnol Prog* **21**, 1644-52.

147. Baudino, L., Shinohara, Y., Nimmerjahn, F., Furukawa, J., Nakata, M., Martinez-Soria, E., Petry, F., Ravetch, J. V., Nishimura, S. & Izui, S. (2008). Crucial role of aspartic acid at position 265 in the CH2 domain for murine IgG2a and IgG2b Fc-associated effector functions. *J Immunol* **181**, 6664-9.

148. Malhotra, R., Wormald, M. R., Rudd, P. M., Fischer, P. B., Dwek, R. A. & Sim, R. B. (1995). Glycosylation changes of IgG associated with rheumatoid arthritis can activate complement via the mannose-binding protein. *Nat Med* **1**, 237-43.

149. Raju, T. S. (2008). Terminal sugars of Fc glycans influence antibody effector functions of IgGs. *Curr Opin Immunol* **20**, 471-8.

150. Beck, A., Cochet, O. & Wurch, T. (2010). GlycoFi's technology to control the glycosylation of recombinant therapeutic proteins. *Expert Opin Drug Discov* **5**, 95-111.

151. Kanda, Y., Yamane-Ohnuki, N., Sakai, N., Yamano, K., Nakano, R., Inoue, M., Misaka, H., Iida, S., Wakitani, M., Konno, Y., Yano, K., Shitara, K., Hosoi, S. & Satoh, M. (2006). Comparison of cell lines for stable production of fucose-negative antibodies with enhanced ADCC. *Biotechnol Bioeng* **94**, 680-8.

152. Yamane-Ohnuki, N., Kinoshita, S., Inoue-Urakubo, M., Kusunoki, M., Iida, S., Nakano, R., Wakitani, M., Niwa, R., Sakurada, M., Uchida, K., Shitara, K. & Satoh, M. (2004). Establishment of FUT8 knockout Chinese hamster ovary cells: an ideal host cell line for producing completely defucosylated antibodies with enhanced antibody-dependent cellular cytotoxicity. *Biotechnol Bioeng* **87**, 614-22.

153. Iida, S., Misaka, H., Inoue, M., Shibata, M., Nakano, R., Yamane-Ohnuki, N., Wakitani, M., Yano, K., Shitara, K. & Satoh, M. (2006). Nonfucosylated therapeutic IgG1 antibody can evade the inhibitory effect of serum immunoglobulin G on antibody-dependent cellular cytotoxicity through its high binding to FcgammaRIIIa. *Clin Cancer Res* **12**, 2879-87.

154. Umana, P., Jean-Mairet, J., Moudry, R., Amstutz, H. & Bailey, J. E. (1999). Engineered glycoforms of an antineuroblastoma IgG1 with optimized antibody-dependent cellular cytotoxic activity. *Nat Biotechnol* **17**, 176-80.

155. Bakchoul, T., Greinacher, A., Sachs, U. J., Krautwurst, A., Renz, H., Harb, H., Bein, G., Newman, P. J. & Santoso, S. (2013). Inhibition of HPA-1a alloantibody-mediated platelet destruction by a deglycosylated anti-HPA-1a monoclonal antibody: towards targeted treatment of fetal-alloimmune thrombocytopenia. *Blood*.

156. Karlnoski, R. A., Rosenthal, A., Alamed, J., Ronan, V., Gordon, M. N., Gottschall, P. E., Grimm, J., Pons, J. & Morgan, D. (2008). Deglycosylated anti-Abeta antibody dose-response effects on pathology and memory in APP transgenic mice. *J Neuroimmune Pharmacol* **3**, 187-97.

157. Muscat, C., Bertotto, A., Ercolani, R., Bistoni, O., Agea, E., Cesarotti, M., Fiorucci, G., Spinozzi, F. & Gerli, R. (1995). Long term treatment of rheumatoid arthritis with high doses of intravenous immunoglobulins: effects on disease activity and serum cytokines. *Ann Rheum Dis* **54**, 382-5.

158. van Doorn, P. A. (1994). Intravenous immunoglobulin treatment in patients with chronic inflammatory demyelinating polyneuropathy. *J Neurol Neurosurg Psychiatry* **57 Suppl**, 38-42.

159. Sorensen, P. S. (1994). Treatment of multiple sclerosis with IVIg: potential effects and methodology of clinical trials. *J Neurol Neurosurg Psychiatry* **57 Suppl**, 62-4.

160. Fehr, J., Hofmann, V. & Kappeler, U. (1982). Transient reversal of thrombocytopenia in idiopathic thrombocytopenic purpura by high-dose intravenous gamma globulin. *N Engl J Med* **306**, 1254-8.

161. Imbach, P., Barandun, S., d'Apuzzo, V., Baumgartner, C., Hirt, A., Morell, A., Rossi, E., Schoni, M., Vest, M. & Wagner, H. P. (1981). High-dose intravenous gammaglobulin for idiopathic thrombocytopenic purpura in childhood. *Lancet* **1**, 1228-31.

162. Basta, M. & Dalakas, M. C. (1994). High-dose intravenous immunoglobulin exerts its beneficial effect in patients with dermatomyositis by blocking endomysial deposition of activated complement fragments. *J Clin Invest* **94**, 1729-35.

163. Basta, M., Fries, L. F. & Frank, M. M. (1991). High doses of intravenous Ig inhibit in vitro uptake of C4 fragments onto sensitized erythrocytes. *Blood* **77**, 376-80.

164. Teeling, J. L., Jansen-Hendriks, T., Kuijpers, T. W., de Haas, M., van de Winkel, J. G., Hack, C. E. & Bleeker, W. K. (2001). Therapeutic efficacy of intravenous immunoglobulin preparations depends on the immunoglobulin G dimers: studies in experimental immune thrombocytopenia. *Blood* **98**, 1095-9.

165. Siragam, V., Brinc, D., Crow, A. R., Song, S., Freedman, J. & Lazarus, A. H. (2005). Can antibodies with specificity for soluble antigens mimic the therapeutic effects of intravenous IgG in the treatment of autoimmune disease? *J Clin Invest* **115**, 155-60.

166. Hansen, R. J. & Balthasar, J. P. (2002). Effects of intravenous immunoglobulin on platelet count and antiplatelet antibody disposition in a rat model of immune thrombocytopenia. *Blood* **100**, 2087-93.

167. Hansen, R. J. & Balthasar, J. P. (2002). Intravenous immunoglobulin mediates an increase in anti-platelet antibody clearance via the FcRn receptor. *Thromb Haemost* **88**, 898-9.

168. Li, N., Zhao, M., Hilario-Vargas, J., Prisayanh, P., Warren, S., Diaz, L. A., Roopenian, D. C. & Liu, Z. (2005). Complete FcRn dependence for intravenous Ig therapy in autoimmune skin blistering diseases. *J Clin Invest* **115**, 3440-50.

169. Akilesh, S., Petkova, S., Sproule, T. J., Shaffer, D. J., Christianson, G. J. & Roopenian, D. (2004). The MHC class I-like Fc receptor promotes humorally mediated autoimmune disease. *J Clin Invest* **113**, 1328-33.

170. Schwab, I., Biburger, M., Kronke, G., Schett, G. & Nimmerjahn, F. (2012). IVIg-mediated amelioration of ITP in mice is dependent on sialic acid and SIGNR1. *Eur J Immunol* **42**, 826-30.

171. Crow, A. R., Suppa, S. J., Chen, X., Mott, P. J. & Lazarus, A. H. (2011). The neonatal Fc receptor (FcRn) is not required for IVIg or anti-CD44 monoclonal antibody-mediated amelioration of murine immune thrombocytopenia. *Blood* **118**, 6403-6.

172. Vassilev, T. L., Kazatchkine, M. D., Duong Van Huyen, J. P., Mekrache, M., Bonnin, E., Mani, J. C., Lecroubier, C., Korinth, D., Baruch, D., Schriever, F. & Kaveri, S. V. (1999). Inhibition of cell adhesion by antibodies to Arg-Gly-Asp (RGD) in normal immunoglobulin for therapeutic use (intravenous immunoglobulin, IVIg). *Blood* **93**, 3624-31.

173. Krause, I., Blank, M. & Shoenfeld, Y. (1998). Anti-DNA and antiphospholipid antibodies in IVIG preparations: in vivo study in naive mice. *J Clin Immunol* **18**, 52-60.

174. Shoenfeld, Y., Rauova, L., Gilburd, B., Kvapil, F., Goldberg, I., Kopolovic, J., Rovensky, J. & Blank, M. (2002). Efficacy of IVIG affinity-purified anti-double-

stranded DNA anti-idiotypic antibodies in the treatment of an experimental murine model of systemic lupus erythematosus. *Int Immunol* **14**, 1303-11.

175. Viard, I., Wehrli, P., Bullani, R., Schneider, P., Holler, N., Salomon, D., Hunziker, T., Saurat, J. H., Tschopp, J. & French, L. E. (1998). Inhibition of toxic epidermal necrolysis by blockade of CD95 with human intravenous immunoglobulin. *Science* **282**, 490-3.

176. von Gunten, S., Schaub, A., Vogel, M., Stadler, B. M., Miescher, S. & Simon, H. U. (2006). Immunologic and functional evidence for anti-Siglec-9 autoantibodies in intravenous immunoglobulin preparations. *Blood* **108**, 4255-9.

177. Dietrich, G. & Kazatchkine, M. D. (1990). Normal immunoglobulin G (IgG) for therapeutic use (intravenous Ig) contain antiidiotypic specificities against an immunodominant, disease-associated, cross-reactive idiotype of human anti-thyroglobulin autoantibodies. *J Clin Invest* **85**, 620-5.

178. Rossi, F. & Kazatchkine, M. D. (1989). Antiidiotypes against autoantibodies in pooled normal human polyspecific Ig. *J Immunol* **143**, 4104-9.

179. Ballow, M. (2011). The IgG molecule as a biological immune response modifier: mechanisms of action of intravenous immune serum globulin in autoimmune and inflammatory disorders. *J Allergy Clin Immunol* **127**, 315-23; quiz 324-5.

180. Bayry, J., Lacroix-Desmazes, S., Carbonneil, C., Misra, N., Donkova, V., Pashov, A., Chevailler, A., Mouthon, L., Weill, B., Bruneval, P., Kazatchkine, M. D. & Kaveri, S. V. (2003). Inhibition of maturation and function of dendritic cells by intravenous immunoglobulin. *Blood* **101**, 758-65.

181. Nagata, S. (1999). Fas ligand-induced apoptosis. *Annu Rev Genet* **33**, 29-55.

182. Bayry, J., Bansal, K., Kazatchkine, M. D. & Kaveri, S. V. (2009). DC-SIGN and alpha2,6-sialylated IgG Fc interaction is dispensable for the anti-inflammatory activity of IVIg on human dendritic cells. *Proc Natl Acad Sci U S A* **106**, E24; author reply E25.

183. Ji, H., Ohmura, K., Mahmood, U., Lee, D. M., Hofhuis, F. M., Boackle, S. A., Takahashi, K., Holers, V. M., Walport, M., Gerard, C., Ezekowitz, A., Carroll, M. C., Brenner, M., Weissleder, R., Verbeek, J. S., Duchatelle, V., Degott, C., Benoist, C. & Mathis, D. (2002). Arthritis critically dependent on innate immune system players. *Immunity* **16**, 157-68.

184. Bruhns, P., Samuelsson, A., Pollard, J. W. & Ravetch, J. V. (2003). Colony-stimulating factor-1-dependent macrophages are responsible for IVIG protection in antibody-induced autoimmune disease. *Immunity* **18**, 573-81.

185. Clarkson, S. B., Bussel, J. B., Kimberly, R. P., Valinsky, J. E., Nachman, R. L. & Unkeless, J. C. (1986). Treatment of refractory immune thrombocytopenic purpura with an anti-Fc gamma-receptor antibody. *N Engl J Med* **314**, 1236-9.

186. Clarkson, S. B., Kimberly, R. P., Valinsky, J. E., Witmer, M. D., Bussel, J. B., Nachman, R. L. & Unkeless, J. C. (1986). Blockade of clearance of immune

complexes by an anti-Fc gamma receptor monoclonal antibody. *J Exp Med* **164**, 474-89.

187. Bazin, R., Lemieux, R. & Tremblay, T. (2006). Reversal of immune thrombocytopenia in mice by cross-linking human immunoglobulin G with a high-affinity monoclonal antibody. *Br J Haematol* **135**, 97-100.

188. Song, S., Crow, A. R., Freedman, J. & Lazarus, A. H. (2003). Monoclonal IgG can ameliorate immune thrombocytopenia in a murine model of ITP: an alternative to IVIG. *Blood* **101**, 3708-13.

189. Salama, A., Mueller-Eckhardt, C. & Kiefel, V. (1983). Effect of intravenous immunoglobulin in immune thrombocytopenia. *Lancet* **2**, 193-5.

190. Jain, A., Olsen, H. S., Vyzasatya, R., Burch, E., Sakoda, Y., Merigeon, E. Y., Cai, L., Lu, C., Tan, M., Tamada, K., Schulze, D., Block, D. S. & Strome, S. E. (2012). Fully recombinant IgG2a Fc multimers (stradomers) effectively treat collagen-induced arthritis and prevent idiopathic thrombocytopenic purpura in mice. *Arthritis Res Ther* **14**, R192.

191. Niknami, M., Wang, M. X., Nguyen, T. & Pollard, J. D. (2013). Beneficial effect of a multimerized immunoglobulin Fc in an animal model of inflammatory neuropathy (experimental autoimmune neuritis). *J Peripher Nerv Syst* **18**, 141-52.

192. Crow, A. R., Song, S., Freedman, J., Helgason, C. D., Humphries, R. K., Siminovitch, K. A. & Lazarus, A. H. (2003). IVIg-mediated amelioration of murine ITP via FcgammaRIIB is independent of SHIP1, SHP-1, and Btk activity. *Blood* **102**, 558-60.

193. Kaneko, Y., Nimmerjahn, F., Madaio, M. P. & Ravetch, J. V. (2006). Pathology and protection in nephrotoxic nephritis is determined by selective engagement of specific Fc receptors. *J Exp Med* **203**, 789-97.

194. Debre, M., Bonnet, M. C., Fridman, W. H., Carosella, E., Philippe, N., Reinert, P., Vilmer, E., Kaplan, C., Teillaud, J. L. & Griscelli, C. (1993). Infusion of Fc gamma fragments for treatment of children with acute immune thrombocytopenic purpura. *Lancet* **342**, 945-9.

195. Ramakrishna, C., Newo, A. N., Shen, Y. W. & Cantin, E. (2011). Passively administered pooled human immunoglobulins exert IL-10 dependent anti-inflammatory effects that protect against fatal HSV encephalitis. *PLoS Pathog* **7**, e1002071.

196. Schwab, I., Seeling, M., Biburger, M., Aschermann, S., Nitschke, L. & Nimmerjahn, F. (2012). B cells and CD22 are dispensable for the immediate antiinflammatory activity of intravenous immunoglobulins in vivo. *Eur J Immunol*.

197. Stadlmann, J., Weber, A., Pabst, M., Anderle, H., Kunert, R., Ehrlich, H. J., Peter Schwarz, H. & Altmann, F. (2009). A close look at human IgG sialylation and subclass distribution after lectin fractionation. *Proteomics* **9**, 4143-53.

198. Kasermann, F., Boerema, D. J., Ruegsegger, M., Hofmann, A., Wymann, S., Zuercher, A. W. & Miescher, S. (2012). Analysis and Functional Consequences of Increased

Fab-Sialylation of Intravenous Immunoglobulin (IVIG) after Lectin Fractionation. *PLoS One* **7**, e37243.

199. Guhr, T., Bloem, J., Derksen, N. I., Wuhrer, M., Koenderman, A. H., Aalberse, R. C. & Rispens, T. (2011). Enrichment of sialylated IgG by lectin fractionation does not enhance the efficacy of immunoglobulin G in a murine model of immune thrombocytopenia. *PLoS One* **6**, e21246.

200. Leontyev, D., Katsman, Y., Ma, X. Z., Miescher, S., Kasermann, F. & Branch, D. R. (2012). Sialylation-independent mechanism involved in the amelioration of murine immune thrombocytopenia using intravenous gammaglobulin. *Transfusion* **52**, 1799-805.

201. Leontyev, D., Katsman, Y. & Branch, D. R. (2012). Mouse background and IVIG dosage are critical in establishing the role of inhibitory Fcgamma receptor for the amelioration of experimental ITP. *Blood* **119**, 5261-4.

202. Schwab, I. & Nimmerjahn, F. (2013). Intravenous immunoglobulin therapy: how does IgG modulate the immune system? *Nat Rev Immunol* **13**, 176-89.

203. Hovius, J. W., de Jong, M. A., den Dunnen, J., Litjens, M., Fikrig, E., van der Poll, T., Gringhuis, S. I. & Geijtenbeek, T. B. (2008). Salp15 binding to DC-SIGN inhibits cytokine expression by impairing both nucleosome remodeling and mRNA stabilization. *PLoS Pathog* **4**, e31.

204. Shan, M., Klasse, P. J., Banerjee, K., Dey, A. K., Iyer, S. P., Dionisio, R., Charles, D., Campbell-Gardener, L., Olson, W. C., Sanders, R. W. & Moore, J. P. (2007). HIV-1 gp120 mannoses induce immunosuppressive responses from dendritic cells. *PLoS Pathog* **3**, e169.

205. Su, S. V., Hong, P., Baik, S., Negrete, O. A., Gurney, K. B. & Lee, B. (2004). DC-SIGN binds to HIV-1 glycoprotein 120 in a distinct but overlapping fashion compared with ICAM-2 and ICAM-3. *J Biol Chem* **279**, 19122-32.

206. Feinberg, H., Mitchell, D. A., Drickamer, K. & Weis, W. I. (2001). Structural basis for selective recognition of oligosaccharides by DC-SIGN and DC-SIGNR. *Science* **294**, 2163-6.

207. Mitchell, D. A., Fadden, A. J. & Drickamer, K. (2001). A novel mechanism of carbohydrate recognition by the C-type lectins DC-SIGN and DC-SIGNR. Subunit organization and binding to multivalent ligands. *J Biol Chem* **276**, 28939-45.

208. Guo, Y., Feinberg, H., Conroy, E., Mitchell, D. A., Alvarez, R., Blixt, O., Taylor, M. E., Weis, W. I. & Drickamer, K. (2004). Structural basis for distinct ligand-binding and targeting properties of the receptors DC-SIGN and DC-SIGNR. *Nat Struct Mol Biol* **11**, 591-8.

209. Holla, A. & Skerra, A. (2011). Comparative analysis reveals selective recognition of glycans by the dendritic cell receptors DC-SIGN and Langerin. *Protein Eng Des Sel* **24**, 659-69.

210. van Liempt, E., Bank, C. M., Mehta, P., Garcia-Vallejo, J. J., Kawar, Z. S., Geyer, R., Alvarez, R. A., Cummings, R. D., Kooyk, Y. & van Die, I. (2006). Specificity of DC-SIGN for mannose- and fucose-containing glycans. *FEBS Lett* **580**, 6123-31.

211. Anthony, R. M., Wermeling, F. & Ravetch, J. V. (2012). Novel roles for the IgG Fc glycan. *Ann N Y Acad Sci* **1253**, 170-80.

212. Tha-In, T., Bayry, J., Metselaar, H. J., Kaveri, S. V. & Kwekkeboom, J. (2008). Modulation of the cellular immune system by intravenous immunoglobulin. *Trends Immunol* **29**, 608-15.

213. Rhoades, C. J., Williams, M. A., Kelsey, S. M. & Newland, A. C. (2000). Monocyte-macrophage system as targets for immunomodulation by intravenous immunoglobulin. *Blood Rev* **14**, 14-30.

214. Steinman, R. M. (2012). Decisions about dendritic cells: past, present, and future. *Annu Rev Immunol* **30**, 1-22.

215. Siragam, V., Crow, A. R., Brinc, D., Song, S., Freedman, J. & Lazarus, A. H. (2006). Intravenous immunoglobulin ameliorates ITP via activating Fc gamma receptors on dendritic cells. *Nat Med* **12**, 688-92.

216. Huang, H. S., Sun, D. S., Lien, T. S. & Chang, H. H. (2010). Dendritic cells modulate platelet activity in IVIg-mediated amelioration of ITP in mice. *Blood* **116**, 5002-9.

217. Tha-In, T., Metselaar, H. J., Tilanus, H. W., Boor, P. P., Mancham, S., Kuipers, E. J., de Man, R. A. & Kwekkeboom, J. (2006). Superior immunomodulatory effects of intravenous immunoglobulins on human T-cells and dendritic cells: comparison to calcineurin inhibitors. *Transplantation* **81**, 1725-34.

218. Bayry, J., Lacroix-Desmazes, S., Delignat, S., Mouthon, L., Weill, B., Kazatchkine, M. D. & Kaveri, S. V. (2003). Intravenous immunoglobulin abrogates dendritic cell differentiation induced by interferon-alpha present in serum from patients with systemic lupus erythematosus. *Arthritis Rheum* **48**, 3497-502.

219. Smed-Sorensen, A., Moll, M., Cheng, T. Y., Lore, K., Norlin, A. C., Perbeck, L., Moody, D. B., Spetz, A. L. & Sandberg, J. K. (2008). IgG regulates the CD1 expression profile and lipid antigen-presenting function in human dendritic cells via FcgammaRIIa. *Blood* **111**, 5037-46.

220. Bayry, J., Lacroix-Desmazes, S., Donkova-Petrini, V., Carbonneil, C., Misra, N., Lepelletier, Y., Delignat, S., Varambally, S., Oksenhendler, E., Levy, Y., Debre, M., Kazatchkine, M. D., Hermine, O. & Kaveri, S. V. (2004). Natural antibodies sustain differentiation and maturation of human dendritic cells. *Proc Natl Acad Sci U S A* **101**, 14210-5.

221. Abe, J., Jibiki, T., Noma, S., Nakajima, T., Saito, H. & Terai, M. (2005). Gene expression profiling of the effect of high-dose intravenous Ig in patients with Kawasaki disease. *J Immunol* **174**, 5837-45.

222. Shimozato, T., Iwata, M., Kawada, H. & Tamura, N. (1991). Human immunoglobulin preparation for intravenous use induces elevation of cellular cyclic adenosine 3':5'-

monophosphate levels, resulting in suppression of tumour necrosis factor alpha and interleukin-1 production. *Immunology* **72**, 497-501.

223. Andersson, J. P. & Andersson, U. G. (1990). Human intravenous immunoglobulin modulates monokine production in vitro. *Immunology* **71**, 372-6.

224. von Gunten, S., Vogel, M., Schaub, A., Stadler, B. M., Miescher, S., Crocker, P. R. & Simon, H. U. (2007). Intravenous immunoglobulin preparations contain anti-Siglec-8 autoantibodies. *J Allergy Clin Immunol* **119**, 1005-11.

225. Chang, J., Shi, P. A., Chiang, E. Y. & Frenette, P. S. (2008). Intravenous immunoglobulins reverse acute vaso-occlusive crises in sickle cell mice through rapid inhibition of neutrophil adhesion. *Blood* **111**, 915-23.

226. Jarius, S., Eichhorn, P., Albert, M. H., Wagenpfeil, S., Wick, M., Belohradsky, B. H., Hohlfeld, R., Jenne, D. E. & Voltz, R. (2007). Intravenous immunoglobulins contain naturally occurring antibodies that mimic antineutrophil cytoplasmic antibodies and activate neutrophils in a TNFalpha-dependent and Fc-receptor-independent way. *Blood* **109**, 4376-82.

227. Bleeker, W. K., Teeling, J. L. & Hack, C. E. (2001). Accelerated autoantibody clearance by intravenous immunoglobulin therapy: studies in experimental models to determine the magnitude and time course of the effect. *Blood* **98**, 3136-42.

228. Martin, F. & Chan, A. C. (2006). B cell immunobiology in disease: evolving concepts from the clinic. *Annu Rev Immunol* **24**, 467-96.

229. Wehrens, E. J., Prakken, B. J. & van Wijk, F. (2012). T cells out of control-impaired immune regulation in the inflamed joint. *Nat Rev Rheumatol*.

230. Seite, J. F., Cornec, D., Renaudineau, Y., Youinou, P., Mageed, R. A. & Hillion, S. (2010). IVIg modulates BCR signaling through CD22 and promotes apoptosis in mature human B lymphocytes. *Blood* **116**, 1698-704.

231. Prasad, N. K., Papoff, G., Zeuner, A., Bonnin, E., Kazatchkine, M. D., Ruberti, G. & Kaveri, S. V. (1998). Therapeutic preparations of normal polyspecific IgG (IVIg) induce apoptosis in human lymphocytes and monocytes: a novel mechanism of action of IVIg involving the Fas apoptotic pathway. *J Immunol* **161**, 3781-90.

232. Toyoda, M., Pao, A., Petrosian, A. & Jordan, S. C. (2003). Pooled human gammaglobulin modulates surface molecule expression and induces apoptosis in human B cells. *Am J Transplant* **3**, 156-66.

233. de Grandmont, M. J., Racine, C., Roy, A., Lemieux, R. & Neron, S. (2003). Intravenous immunoglobulins induce the in vitro differentiation of human B lymphocytes and the secretion of IgG. *Blood* **101**, 3065-73.

234. Heidt, S., Roelen, D. L., Eijsink, C., Eikmans, M., Claas, F. H. & Mulder, A. (2009). Intravenous immunoglobulin preparations have no direct effect on B cell proliferation and immunoglobulin production. *Clin Exp Immunol* **158**, 99-105.

235. Achiron, A., Mor, F., Margalit, R., Cohen, I. R., Lider, O. & Miron, S. (2000). Suppression of experimental autoimmune encephalomyelitis by intravenously administered polyclonal immunoglobulins. *J Autoimmun* **15**, 323-30.

236. Amran, D., Renz, H., Lack, G., Bradley, K. & Gelfand, E. W. (1994). Suppression of cytokine-dependent human T-cell proliferation by intravenous immunoglobulin. *Clin Immunol Immunopathol* **73**, 180-6.

237. Tsurikisawa, N., Saito, H., Oshikata, C., Tsuburai, T. & Akiyama, K. (2012). High-dose intravenous immunoglobulin treatment increases regulatory T cells in patients with eosinophilic granulomatosis with polyangiitis. *J Rheumatol* **39**, 1019-25.

238. Ephrem, A., Chamat, S., Miquel, C., Fisson, S., Mouthon, L., Caligiuri, G., Delignat, S., Elluru, S., Bayry, J., Lacroix-Desmazes, S., Cohen, J. L., Salomon, B. L., Kazatchkine, M. D., Kaveri, S. V. & Misra, N. (2008). Expansion of CD4+CD25+ regulatory T cells by intravenous immunoglobulin: a critical factor in controlling experimental autoimmune encephalomyelitis. *Blood* **111**, 715-22.

239. Padet, L., St-Amour, I., Aubin, E. & Bazin, R. (2011). Neutralization of mitogenic lectins by intravenous immunoglobulin (IVIg) prevents T cell activation: does IVIg really have a direct effect on T cells? *Clin Exp Immunol* **166**, 352-60.

240. MacMillan, H. F., Lee, T. & Issekutz, A. C. (2009). Intravenous immunoglobulin G-mediated inhibition of T-cell proliferation reflects an endogenous mechanism by which IgG modulates T-cell activation. *Clin Immunol* **132**, 222-33.

241. Modiano, J. F., Amran, D., Lack, G., Bradley, K., Ball, C., Domenico, J. & Gelfand, E. W. (1997). Posttranscriptional regulation of T-cell IL-2 production by human pooled immunoglobin. *Clin Immunol Immunopathol* **83**, 77-85.

242. Caccavelli, L., Field, A. C., Betin, V., Dreillard, L., Belair, M. F., Bloch, M. F., Bruneval, P., Kazatchkine, M. & Bellon, B. (2001). Normal IgG protects against acute graft-versus-host disease by targeting CD4(+)CD134(+) donor alloreactive T cells. *Eur J Immunol* **31**, 2781-90.

243. Dunlop, D. C., Bonomelli, C., Mansab, F., Vasiljevic, S., Doores, K. J., Wormald, M. R., Palma, A. S., Feizi, T., Harvey, D. J., Dwek, R. A., Crispin, M. & Scanlan, C. N. (2010). Polysaccharide mimicry of the epitope of the broadly neutralizing anti-HIV antibody, 2G12, induces enhanced antibody responses to self oligomannose glycans. *Glycobiology* **20**, 812-23.

244. Ramasamy, V., Ramakrishnan, B., Boeggeman, E., Ratner, D. M., Seeberger, P. H. & Qasba, P. K. (2005). Oligosaccharide preferences of beta1,4-galactosyltransferase-I: crystal structures of Met340His mutant of human beta1,4-galactosyltransferase-I with a pentasaccharide and trisaccharides of the N-glycan moiety. *J Mol Biol* **353**, 53-67.

245. Reeves, P. J., Callewaert, N., Contreras, R. & Khorana, H. G. (2002). Structure and function in rhodopsin: high-level expression of rhodopsin with restricted and homogeneous N-glycosylation by a tetracycline-inducible N-acetylglucosaminyltransferase I-negative HEK293S stable mammalian cell line. *Proc Natl Acad Sci U S A* **99**, 13419-24.

246. Scanlan, C. N., Ritchie, G. E., Baruah, K., Crispin, M., Harvey, D. J., Singer, B. B., Lucka, L., Wormald, M. R., Wentworth, P., Jr., Zitzmann, N., Rudd, P. M., Burton, D. R. & Dwek, R. A. (2007). Inhibition of mammalian glycan biosynthesis produces non-self antigens for a broadly neutralising, HIV-1 specific antibody. *J Mol Biol* **372**, 16-22.

247. Kuster, B., Wheeler, S. F., Hunter, A. P., Dwek, R. A. & Harvey, D. J. (1997). Sequencing of N-linked oligosaccharides directly from protein gels: in-gel deglycosylation followed by matrix-assisted laser desorption/ionization mass spectrometry and normal-phase high-performance liquid chromatography. *Anal Biochem* **250**, 82-101.

248. Harvey, D. J., Royle, L., Radcliffe, C. M., Rudd, P. M. & Dwek, R. A. (2008). Structural and quantitative analysis of N-linked glycans by matrix-assisted laser desorption ionization and negative ion nanospray mass spectrometry. *Anal Biochem* **376**, 44-60.

249. Neville, D. C., Coquard, V., Priestman, D. A., te Vruchte, D. J., Sillence, D. J., Dwek, R. A., Platt, F. M. & Butters, T. D. (2004). Analysis of fluorescently labeled glycosphingolipid-derived oligosaccharides following ceramide glycanase digestion and anthranilic acid labeling. *Anal Biochem* **331**, 275-82.

250. Romani, N., Reider, D., Heuer, M., Ebner, S., Kampgen, E., Eibl, B., Niederwieser, D. & Schuler, G. (1996). Generation of mature dendritic cells from human blood. An improved method with special regard to clinical applicability. *J Immunol Methods* **196**, 137-51.

251. Aida, Y. & Pabst, M. J. (1990). Removal of endotoxin from protein solutions by phase separation using Triton X-114. *J Immunol Methods* **132**, 191-5.

252. Burton, D. R., Pyati, J., Koduri, R., Sharp, S. J., Thornton, G. B., Parren, P. W., Sawyer, L. S., Hendry, R. M., Dunlop, N., Nara, P. L. & et al. (1994). Efficient neutralization of primary isolates of HIV-1 by a recombinant human monoclonal antibody. *Science* **266**, 1024-7.

253. Hua, S., Jeong, H. N., Dimapasoc, L. M., Kang, I., Han, C., Choi, J. S., Lebrilla, C. B. & An, H. J. (2013). Isomer-Specific LC/MS and LC/MS/MS Profiling of the Mouse Serum N-Glycome Revealing a Number of Novel Sialylated N-Glycans. *Anal Chem*.

254. Lin, S. Y., Chen, Y. Y., Fan, Y. Y., Lin, C. W., Chen, S. T., Wang, A. H. & Khoo, K. H. (2008). Precise mapping of increased sialylation pattern and the expression of acute phase proteins accompanying murine tumor progression in BALB/c mouse by integrated sera proteomics and glycomics. *J Proteome Res* **7**, 3293-303.

255. Lai, J. C., Chan, W. W., Kien, F., Nicholls, J. M., Peiris, J. S. & Garcia, J. M. (2010). Formation of virus-like particles from human cell lines exclusively expressing influenza neuraminidase. *J Gen Virol* **91**, 2322-30.

256. Domon, B. & Costello, C. E. (1988). A systematic nomenclature for carbohydrate fragmentation in FAB-MS/MS spectra of glycoconjugates. *Glycoconj. J.* **5**, 397-409.

257. Barb, A. W., Meng, L., Gao, Z., Johnson, R. W., Moremen, K. W. & Prestegard, J. H. (2012). NMR characterization of immunoglobulin g fc glycan motion on enzymatic sialylation. *Biochemistry* **51**, 4618-26.

258. Bruhns, P., Iannascoli, B., England, P., Mancardi, D. A., Fernandez, N., Jorieux, S. & Daeron, M. (2009). Specificity and affinity of human Fcgamma receptors and their polymorphic variants for human IgG subclasses. *Blood* **113**, 3716-25.

259. Crispin, M., Harvey, D. J., Chang, V. T., Yu, C., Aricescu, A. R., Jones, E. Y., Davis, S. J., Dwek, R. A. & Rudd, P. M. (2006). Inhibition of hybrid- and complex-type glycosylation reveals the presence of the GlcNAc transferase I-independent fucosylation pathway. *Glycobiology* **16**, 748-56.

260. Horton, H. M., Bernett, M. J., Pong, E., Peipp, M., Karki, S., Chu, S. Y., Richards, J. O., Vostiar, I., Joyce, P. F., Repp, R., Desjarlais, J. R. & Zhukovsky, E. A. (2008). Potent in vitro and in vivo activity of an Fc-engineered anti-CD19 monoclonal antibody against lymphoma and leukemia. *Cancer Res* **68**, 8049-57.

261. Crocker, P. R. (2005). Siglecs in innate immunity. *Curr Opin Pharmacol* **5**, 431-7.

262. Bonomelli, C., Doores, K. J., Dunlop, D. C., Thaney, V., Dwek, R. A., Burton, D. R., Crispin, M. & Scanlan, C. N. (2011). The glycan shield of HIV is predominantly oligomannose independently of production system or viral clade. *PLoS One* **6**, e23521.

263. Doores, K. J., Bonomelli, C., Harvey, D. J., Vasiljevic, S., Dwek, R. A., Burton, D. R., Crispin, M. & Scanlan, C. N. (2010). Envelope glycans of immunodeficiency virions are almost entirely oligomannose antigens. *Proc Natl Acad Sci U S A* **107**, 13800-5.

264. Elbein, A. D., Tropea, J. E., Mitchell, M. & Kaushal, G. P. (1990). Kifunensine, a potent inhibitor of the glycoprotein processing mannosidase I. *J Biol Chem* **265**, 15599-605.

265. Dhaliwal, B., Yuan, D., Pang, M. O., Henry, A. J., Cain, K., Oxbrow, A., Fabiane, S. M., Beavil, A. J., McDonnell, J. M., Gould, H. J. & Sutton, B. J. (2012). Crystal structure of IgE bound to its B-cell receptor CD23 reveals a mechanism of reciprocal allosteric inhibition with high affinity receptor FcepsilonRI. *Proc Natl Acad Sci U S A* **109**, 12686-91.

266. Ulyanova, T., Blasioli, J., Woodford-Thomas, T. A. & Thomas, M. L. (1999). The sialoadhesin CD33 is a myeloid-specific inhibitory receptor. *Eur J Immunol* **29**, 3440-9.

267. Bandala-Sanchez, E., Zhang, Y., Reinwald, S., Dromey, J. A., Lee, B. H., Qian, J., Bohmer, R. M. & Harrison, L. C. (2013). T cell regulation mediated by interaction of soluble CD52 with the inhibitory receptor Siglec-10. *Nat Immunol* **14**, 741-8.

268. von Gunten, S. & Bochner, B. S. (2008). Basic and clinical immunology of Siglecs. *Ann N Y Acad Sci* **1143**, 61-82.

269. Zou, Z., Chastain, A., Moir, S., Ford, J., Trandem, K., Martinelli, E., Cicala, C., Crocker, P., Arthos, J. & Sun, P. D. (2011). Siglecs facilitate HIV-1 infection of macrophages through adhesion with viral sialic acids. *PLoS One* **6**, e24559.

270. Ballow, M. & Allen, C. (2011). Intravenous immunoglobulin modulates the maturation of TLR 4-primed peripheral blood monocytes. *Clin Immunol* **139**, 208-14.

271. Kaisho, T. & Akira, S. (2003). Regulation of dendritic cell function through Toll-like receptors. *Curr Mol Med* **3**, 373-85.

272. Steinman, R. M. (1991). The dendritic cell system and its role in immunogenicity. *Annu Rev Immunol* **9**, 271-96.

273. Winzler, C., Rovere, P., Rescigno, M., Granucci, F., Penna, G., Adorini, L., Zimmermann, V. S., Davoust, J. & Ricciardi-Castagnoli, P. (1997). Maturation stages of mouse dendritic cells in growth factor-dependent long-term cultures. *J Exp Med* **185**, 317-28.

274. Zanoni, I., Ostuni, R., Capuano, G., Collini, M., Caccia, M., Ronchi, A. E., Rocchetti, M., Mingozzi, F., Foti, M., Chirico, G., Costa, B., Zaza, A., Ricciardi-Castagnoli, P. & Granucci, F. (2009). CD14 regulates the dendritic cell life cycle after LPS exposure through NFAT activation. *Nature* **460**, 264-8.

275. Singh-Jasuja, H., Thiolat, A., Ribon, M., Boissier, M. C., Bessis, N., Rammensee, H. G. & Decker, P. (2013). The mouse dendritic cell marker CD11c is down-regulated upon cell activation through Toll-like receptor triggering. *Immunobiology* **218**, 28-39.

276. Jin, P., Han, T. H., Ren, J., Saunders, S., Wang, E., Marincola, F. M. & Stroncek, D. F. (2010). Molecular signatures of maturing dendritic cells: implications for testing the quality of dendritic cell therapies. *J Transl Med* **8**, 4.

277. Ohta, M., Ishida, A., Toda, M., Akita, K., Inoue, M., Yamashita, K., Watanabe, M., Murata, T., Usui, T. & Nakada, H. (2010). Immunomodulation of monocyte-derived dendritic cells through ligation of tumor-produced mucins to Siglec-9. *Biochem Biophys Res Commun* **402**, 663-9.

278. Lock, K., Zhang, J., Lu, J., Lee, S. H. & Crocker, P. R. (2004). Expression of CD33-related siglecs on human mononuclear phagocytes, monocyte-derived dendritic cells and plasmacytoid dendritic cells. *Immunobiology* **209**, 199-207.

279. Wysocka, M., Robertson, S., Riemann, H., Caamano, J., Hunter, C., Mackiewicz, A., Montaner, L. J., Trinchieri, G. & Karp, C. L. (2001). IL-12 suppression during experimental endotoxin tolerance: dendritic cell loss and macrophage hyporesponsiveness. *J Immunol* **166**, 7504-13.

280. Karp, C. L., Wysocka, M., Ma, X., Marovich, M., Factor, R. E., Nutman, T., Armant, M., Wahl, L., Cuomo, P. & Trinchieri, G. (1998). Potent suppression of IL-12 production from monocytes and dendritic cells during endotoxin tolerance. *Eur J Immunol* **28**, 3128-36.

281. Cooper, N., Heddle, N. M., Haas, M., Reid, M. E., Lesser, M. L., Fleit, H. B., Woloski, B. M. & Bussel, J. B. (2004). Intravenous (IV) anti-D and IV immunoglobulin achieve acute platelet increases by different mechanisms: modulation of cytokine and platelet responses to IV anti-D by FcgammaRIIa and FcgammaRIIIa polymorphisms. *Br J Haematol* **124**, 511-8.

282. Meyer, O., Winter, O. & Salama, A. (2012). Influence of Intravenous Immunoglobulin Treatment on Thrombopoiesis. *Transfus Med Hemother* **39**, 217-220.

283. Aukrust, P., Froland, S. S., Liabakk, N. B., Muller, F., Nordoy, I., Haug, C. & Espevik, T. (1994). Release of cytokines, soluble cytokine receptors, and interleukin-1 receptor antagonist after intravenous immunoglobulin administration in vivo. *Blood* **84**, 2136-43.

284. Gupta, M., Noel, G. J., Schaefer, M., Friedman, D., Bussel, J. & Johann-Liang, R. (2001). Cytokine modulation with immune gamma-globulin in peripheral blood of normal children and its implications in Kawasaki disease treatment. *J Clin Immunol* **21**, 193-9.

285. Allhorn, M., Olin, A. I., Nimmerjahn, F. & Collin, M. (2008). Human IgG/Fc gamma R interactions are modulated by streptococcal IgG glycan hydrolysis. *PLoS One* **3**, e1413.

286. Bar-Or, D., Thomas, G. W., Bar-Or, R., Rael, L. T., Scarborough, K., Rao, N. & Shimonkevitz, R. (2006). Commercial human albumin preparations for clinical use are immunosuppressive in vitro. *Crit Care Med* **34**, 1707-12.

287. Taverna, M., Marie, A. L., Mira, J. P. & Guidet, B. (2013). Specific antioxidant properties of human serum albumin. *Ann Intensive Care* **3**, 4.

288. Shimonkevitz, R., Thomas, G., Slone, D. S., Craun, M., Mains, C. & Bar-Or, D. (2008). A diketopiperazine fragment of human serum albumin modulates T-lymphocyte cytokine production through rap1. *J Trauma* **64**, 35-41.